Advances in Polymer Science 270

Philipp Vana *Editor*

Controlled Radical Polymerization at and from Solid Surfaces

Springer

270
Advances in Polymer Science

Aims and Scope

The series Advances in Polymer Science presents critical reviews of the present and future trends in polymer and biopolymer science. It covers all areas of research in polymer and biopolymer science including chemistry, physical chemistry, physics, material science.

The thematic volumes are addressed to scientists, whether at universities or in industry, who wish to keep abreast of the important advances in the covered topics.

Advances in Polymer Science enjoys a longstanding tradition and good reputation in its community. Each volume is dedicated to a current topic, and each review critically surveys one aspect of that topic, to place it within the context of the volume. The volumes typically summarize the significant developments of the last 5 to 10 years and discuss them critically, presenting selected examples, explaining and illustrating the important principles, and bringing together many important references of primary literature. On that basis, future research directions in the area can be discussed. Advances in Polymer Science volumes thus are important references for every polymer scientist, as well as for other scientists interested in polymer science - as an introduction to a neighboring field, or as a compilation of detailed information for the specialist.

Review articles for the individual volumes are invited by the volume editors. Single contributions can be specially commissioned.

Readership: Polymer scientists, or scientists in related fields interested in polymer and biopolymer science, at universities or in industry, graduate students.

Special offer:
For all clients with a standing order we offer the electronic form of Advances in Polymer Science free of charge.

More information about this series at http://www.springer.com/series/12

Philipp Vana
Editor

Controlled Radical Polymerization at and from Solid Surfaces

With contributions by

E. Bourgeat-Lami · F. D'Agosto · D. Gigmes · A. Goto · J. Jestin · H. Jo · A. Khabibullin · M. Lansalot · E. Mastan · K. Matyjaszewski · S. Perrier · T.N.T. Phan · C. Rossner · P. Theato · Y. Tsujii · P. Vana · Y. Zhao · S. Zhu

Springer

Editor
Philipp Vana
Makromolekulare Chemie
Institut für Physikalische Chemie
Georg-August-Universität Göttingen
Germany

ISSN 0065-3195 ISSN 1436-5030 (electronic)
Advances in Polymer Science
ISBN 978-3-319-22137-3 ISBN 978-3-319-22138-0 (eBook)
DOI 10.1007/978-3-319-22138-0

Library of Congress Control Number: 2015945965

Springer Cham Heidelberg New York Dordrecht London

Printed on acid-free paper

Springer International Publishing AG Switzerland is part of Springer Science+Business Media (www.springer.com)

Preface

The tailoring of well-defined polymer structures upon the surfaces of solid materials constitutes the molecular basis for advanced functional surfaces. The recent advent of a multitude of controlled radical polymerization methods (also called reversible deactivation radical polymerization according to IUPAC), which greatly outperform conventional radical polymerization processes with respect to topological control, has had a major impact on this field. These methods allow for the confinement of polymerizations at surfaces, which may lead to polymer brushes and other surface-bound polymer arrangements. They also provide macromolecular architectures of stunning complexity with relative ease, which were far beyond the wildest dreams of polymer chemists just short time ago. These polymers may have tailored functionalities that can be used for controlling the interface regime between the solid material and the soft polymer coverage. The functionality may also be used to arrange polymer chains and particles in a predetermined manner so that complicated nano-composites emerge. The polymer and its functionality may finally be used to modulate surface functions. All these benefits are currently fully exploited for new surface structures for applications in energy conversion, e.g., solar cells; nanomedicine, e.g., drug delivery and tagging; and materials science, where they are used for the design of functional, responsive, or high mechanical performance nano-composite materials.

This book presents state-of-the art knowledge about all aspects that are important when considering controlled radical polymerization and surfaces. It is intended to guide the interested polymer chemist through the constantly increasing number of scientific studies and should help to apply this knowledge for tailoring novel surfaces. The book starts with four chapters which are dedicated to the four major controlled radical polymerization methods, namely NMP, ATRP, RAFT and RTCP. In the second part of the book, a chapter deals with the specific situations in heterogeneous aqueous media, followed by a contribution about post-modifications of the polymers formed upon surfaces. The book ends with a chapter about how tailored polymer from controlled radical polymerization can be used to fabricate nano-composites. All chapters of this book are by leading scientists in the

respective fields and I express my sincerest gratitude to them that they have contributed in this excellent way to this fine book. I am confident that this issue of APS will help to make further progress in this fascinating field and will help to stimulate the development of new applications both in the field of polymer chemistry and materials science. I am looking forward to these new exciting steps forward.

Göttingen, Germany Philipp Vana

Contents

Adv Polym Sci (2016) 270: 1–28
DOI: 10.1007/12_2015_317

Published online: 23 June 2015

Nitroxide-Mediated Polymerization from Surfaces

Trang N.T. Phan, Jacques Jestin, and Didier Gigmes

Abstract The current chapter gives a general overview on surface-initiated nitroxide-mediated polymerization (SI-NMP). More particularly, the developed strategies to perform an SI-NMP process, the various type of substrates including inorganic and organic supports, and the potential of SI-NMP to prepared advanced materials are discussed. Based on a selected number of literature examples it appears that SI-NMP is a versatile and powerful approach to introduce polymer brushes on surfaces and/or tune polymer surface properties.

Keywords Grafted or brush polymers • Nitroxide-mediated polymerization • Planar, spherical, and porous surfaces

Contents

T.N.T. Phan and D. Gigmes (✉)
Aix-Marseille Université, CNRS, Institut de Chimie Radicalaire, UMR7273, 13397 Marseille cedex 20, France
e-mail: didier.gigmes@univ-amu.fr

J. Jestin
Laboratoire Léon Brillouin, CEA Saclay, 91191 Gif-sur-Yvette Cedex, France

Abbreviations

3-MPS	3-Methacryloxyproyltrimethoxysilane
AFM	Atomic force microscopy
AIBN	Azobisisobutyronitrile
APTES	3-Aminopropryl triethoxysilane
ATRP	Atom transfer radical polymerization
BlocBuilder MA	2-Methyl-2-[*N*-*tert*-butyl-*N*-(1-diethoxyphosphoryl-2,2-dimethylpropyl)aminoxy]propionic acid
BPO	Benzoyl peroxide
CNT	Carbon nanotube
DLS	Dynamic light scattering
DMAc	Dimethylacetamide
DMF	*N*,*N*-Dimethylformamide
DPPC	L-Adipalmytoyl-phosphatidylcholine
HEMA	2-Hydroxyethyl methacrylate
LB	Langmuir–Blodgett
MAMA-NHS	2-Methyl-2-[*N*-*tert*-butyl-*N*-(1-diethoxyphosphoryl-2,2-dimethylpropyl)aminoxy]-*N*-propionyloxysuccinimide
MMA	Methyl methacrylate
MMT	Montmorillonite
MWNT	Multiwalled carbon nanotube
NEXAFS	Near-edge X-ray absorption fine structure
NMP	Nitroxide-mediated polymerization
OMS	Ordered mesoporous silica
P3VP	Poly(3-vinylpyridine)
P4VP	Poly(4-vinylpyridine)
PAA	Poly(acrylic acid)
PBA	Poly(*n*-butyl acrylate)
P*t*BA	Poly(*tert*-butyl acrylate)
PDMAEA	Poly(2-dimethylamino ethyl acrylate)
PHPMA	Poly(2-hydroxypropyl methacrylamide)
PNIPAM	Poly(*N*-isopropylacrylamide)
PPTEA	Poly[2-phenyl-2-(2,2,6,6-tetramethylpiperidin-1-yloxy)ethyl acrylate]
PS	Polystyrene
PS-*b*-PCL	Polystyrene-*block*-polycaprolactone
PSMA	Poly[styrene-*co*-(maleic anhydride)]
RAFT	Reversible–addition fragmentation chain transfer
SANS	Small-angle neutron scattering
SAXS	Small-angle X-ray scattering
SG1	*N*-*tert*-Butyl-*N*-[1-diethylphosphono-(2-2-dimethylpropyl) nitroxide]
SI-NMP	Surface-initiated nitroxide-mediated polymerization
SWNT	Single-walled carbon nanotube

TEM	Transmission electron microscopy
TEMPO	2,2,6,6-Tetramethylpiperidinyl-1-oxy
TEMPO-Br	1-Oxo-2,2,6,6-tetramethylpiperidinium bromide
TIPNO	2,2,5-Trimethyl-4-phenyl-3-azahexane-3-oxyl
TSPMA	3-(Trimethoxysilyl)propyl methacrylate
VBC	4-Vinylbenzyl chloride
XPS	X-ray photoelectron spectroscopy

1 Introduction

Surface modification with thin polymer films is considered one of the most attractive ways of obtaining "smart" surfaces in response to external stimuli such as solvent, temperature, pH, and ions. This modification imparts new surface properties such as wettability, biocompatibility, corrosion resistance, and friction. Thin polymer films can either be prepared by spin-coating with a polymeric solution or by covalent attachment of one end of a polymer chain to the surface. The latter technique gives rise to polymer brushes [1]. The "grafting-from" approach is one of two strategies commonly used to attach polymers to a substrate surface. This approach has been largely developed thanks to controlled or "living" polymerization techniques (CLRP), because they allow accurate control over polymer thickness, density, composition, and architecture [2]. Polymerizations can be performed on substrates exhibiting different topologies, such as planar wafers, spherical particles, or a confined environment, and are compatible with a broad range of monomers. Different controlled radical polymerization (CRP) techniques such as atom transfer radical polymerization (ATRP), reversible–addition fragmentation chain transfer (RAFT), and nitroxide-mediated polymerization (NMP) have been used for the preparation of functionalized surfaces [2–4]. However compared with other CRP techniques, NMP is underexploited and has so far been the subject of only a few review articles. Indeed, initially, NMP was limited to a small range of polymerizable monomers (i.e., only styrene and its derivatives). Meanwhile, the development of more potent nitroxides has greatly expanded the number of monomers (acrylates and acrylamides) compatible with the NMP process [5]. An important advantage of surface-initiated NMP (SI-NMP) is that no further addition of metals or metal complexes is necessary. Hence, no extra purification steps are required and the likelihood of introducing impurities is also strongly limited. This specific feature is particularly attractive for applications where the purity of polymer-based materials is of high importance, such as in biomedical and electronic fields.

NMP is controlled by the persistent radical effect (PRE) [6] that can be described as follows: If we consider a diamagnetic compound (RY) that decomposes homolytically to generate two radical species at both the same time and the same rate, the PRE occurs when one of the radical species ($Y^{\cdot}$) is more persistent than the other ($R^{\cdot}$). Typically, at the early stages of the reaction, the concentrations of the

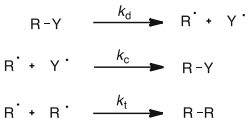

Scheme 1 Homolytic decomposition of a diamagnetic compound RY, with R· being transient and Y· persistent

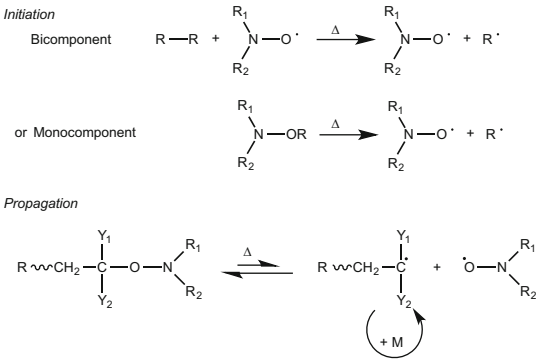

Scheme 2 Mechanism of nitroxide-mediated polymerization

two radical species are strictly equivalent. However, after a short period of time some self-termination reactions of the transient radical (R·) are unavoidable, leading to a decrease in its concentration relative to that of the more persistent radical species. Therefore, recombination of the transient and persistent radicals becomes progressively favored, rather than self-reaction of the transient radical (Scheme 1). This specific feature of the PRE explains many highly selective radical cross-coupling processes, including the NMP process.

Hence, NMP is grounded on a reversible termination equilibrium between the propagating (macro)radical and the nitroxide (Scheme 2) [5]. Typically, the nitroxide plays the role of controlling agent and, thanks to the PRE, the growing polymer chains mainly have a (macro)alkoxyamine-based chemical structure. These (macro)alkoxyamines (the so-called dormant species) are able to cleave homolytically to yield the propagating radical and the nitroxide once again. Interestingly, this equilibrium is only ruled by a thermal process.

Initially, NMP was conducted using a bicomponent initiating system (i.e., a conventional radical initiator in the presence of a nitroxide). Obviously, this system is attractive from an economic and practical point of view. However, with a bicomponent initiating system, the polymerization kinetics and the molecular weight of the polymer chains are difficult to control. Indeed, with conventional radical initiators it is difficult to exactly determine the number of generated radicals. Moreover, compared with the radical initiator concentration, a large excess of nitroxide decreases the polymerization rate by shifting the equilibrium

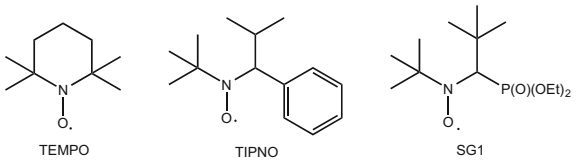

Fig. 1 Structure of nitroxides frequently used for SI-NMP. *TEMPO* 2,2,6,6-tetramethylpiperidinyl-1-oxy; *TIPNO* 2,2,5-trimethyl-4-phenyl-3-azahexane-3-oxyl; and *SG1 N-tert*-butyl-*N*-[1-diethylphosphono-(2,2-dimethylpropyl)] nitroxide

of the propagating step towards the dormant species. To overcome these drawbacks, the use of a monocomponent initiating system is preferred. This approach consists in using an alkoxyamine that decomposes homolytically, under heating, to afford the corresponding alkyl radical as initiator and nitroxide as controller. The dissociation rate constant of the alkoxyamine is of major importance in ensuring efficient establishment of the PRE and, therefore, an efficient CRP process [5].

Typically, surface-initiated NMP is achieved by following one of two main strategies. As an example of the first strategy, a conventional radical initiator is anchored to the surface and then the polymerization reaction is performed in the presence of free nitroxide, which allows the in situ formation of (macro) alkoxyamine. In the second strategy, a preformed alkoxyamine is first attached to surface; in this case, the initiation and polymerization control proceeds from a monocomponent system. Depending on the chemical nature of the surface substrate, various strategies can be envisioned for grafting the initiator to the surface. For instance, initiator anchoring can be achieved using covalent bonding, electrostatic interaction, or even hydrogen bonding. The nitroxides frequently used for SI-NMP are TEMPO, TIPNO, and SG1 (see Fig. 1 for structures).

This review focuses on NMP initiated from the surface of different substrates such as silicon, metal oxide, carbon, and polymer. The possible architecture and composition of polymer chains grown from the surface is also discussed. Application of surfaces modified with polymer films prepared by NMP is briefly described.

2 Variation of Substrates

SI-NMP has proven efficient for the growing of polymer chains from various substrates. To reach this goal, the surface is usually modified with a suitable initiator or mediator, introduced in either a single step or via a multistep procedure.

In this section, the preparation of grafted polymer via SI-NMP from different substrates such as silicon oxide, metal oxide, metal and semiconductor, mineral clay, carbon-based materials, and polymer surfaces is discussed. For each class of substrate, the discussion focuses on the surface chemistry available for introducing functional groups that allow SI-NMP.

2.1 NMP from Silicon Oxide Surfaces

Silicon oxide is probably one of the most studied substrates used to graft polymer chains via NMP. Typically, silicon wafers, glass, quartz slides, porous and non-porous particles, as well as membranes are used in the SI-NMP process. To introduce a functional group that can initiate or mediate SI-NMP from silicon oxide surfaces, organosilane is often used. Prior to the grafting step, silicon oxide materials are first treated with a H_2SO_4/H_2O_2 mixture or oxygen plasma to clean the surface and optimize the number of silanol groups involved in further reaction. In this case, a thin layer of water is formed on the silicon oxide surface. The introduction of organosilane onto this surface is obtained after surface adsorption, hydration, and salinization steps. In this procedure, the silanol functions (Si–OH) present at the silicon oxide surface are able to undergo a condensation reaction with different types of organosilane reagents, such as R-$SiMe_2Cl$, R-$SiCl_3$, or R-Si$(OMe)_3$, and R-Si$(OEt)_3$, leading to siloxane bonds Si–O–Si [7].

2.1.1 NMP from Silicon Oxide Planar Surfaces

The first example of polymer synthesis from SI-NMP was reported by Hawker's group [8]. The authors immobilized a TEMPO-based alkoxyamine on the surface of an oxidized silicon wafer via the reaction of chlorosilane groups present on the alkoxyamine with the silanol groups of the oxidized silicon wafer in the presence of triethylamine as catalyst. Then, polystyrene (PS) brushes were obtained from NMP of styrene. For planar substrates with low specific surface areas, such as silicon wafer in this example, the concentration of persistent radicals in the reaction medium is low because of the limited number of initiator molecules on the wafer surface. To overcome this drawback, a predetermined amount of free alkoxyamine (called sacrificial initiator) can be added to the reaction mixture to control the polymerization process (Scheme 3). Addition of this sacrificial alkoxyamine provides a sufficiently high concentration of free nitroxide in the polymerization mixture, which controls the polymer chain growth of both immobilized and soluble initiators. However, the addition of free alkoxyamine leads to the formation of non-surface-attached polymers, which have to be removed from the resulting polymer brushes. The authors found that the number-average molecular weight (M_n) and the dispersity of the grafted PS were similar to those of the free polymer chains in solution. Following this strategy, homopolymer and random copolymers grafted on surfaces were prepared with control of molar mass or thickness of the brushes (up to 80 nm), while maintaining low dispersities. The living nature of the polymerization was demonstrated by re-initiation of the end-capped chains to form the corresponding block copolymer brushes.

Following this strategy, Hawker and coworkers [9] successfully initiated the polymerization of *tert*-butyl acrylate from the surface of oxidized silicon wafer functionalized with **1** in the presence of the TIPNO-based alkoxyamine **2** and TIPNO (Scheme 4) [10]. The rapid exchange of free nitroxide between bound

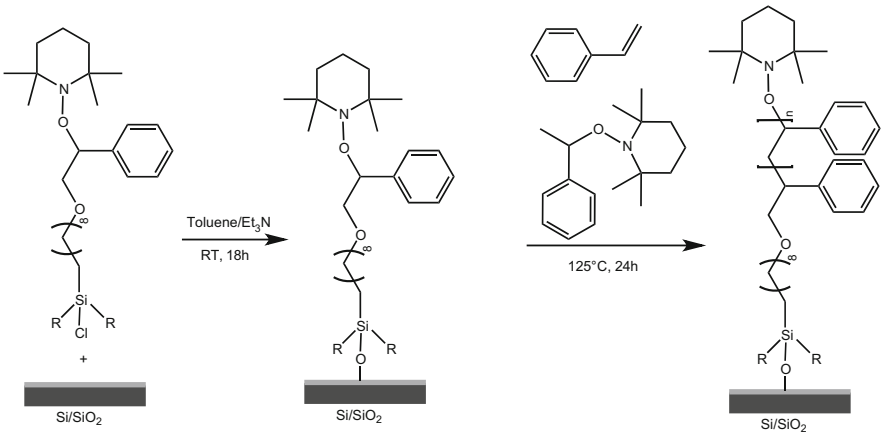

Scheme 3 Styrene SI-NMP from silicon wafer grafted with a TEMPO-based alkxoyamine

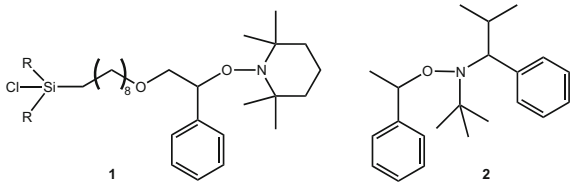

Scheme 4 Structure of alkoxyamines used for SI-NMP of *tert*-butyl acrylate on oxidized silicon wafer. Reported by Hawker and coworkers [9]

macroalkoxyamines on the surface and nitroxide in solution allowed the controlled formation of poly(*tert*-butyl acrylate) (P*t*BA) chains from surfaces. The thickness of polymer brushes (100–200 nm) could be controlled by varying the molar ratio of *tert*-butyl acrylate and alkoxyamine **2**. The P*t*BA brushes were then patterned using photolithographic techniques to yield original patterned poly(acrylic acid) chains, leading to discrete hydrophobic and hydrophilic domains.

TEMPO-functionalized silicon wafers or glass slides were also used to prepare SI-NMP-made polymer brushes on surfaces [11–19]. Chapel and colleagues employed a similar system, using an ester instead of ether linkage and triethoxysilane as reactive anchor group on a C_{11} spacer [11, 17]. With this reactive system, molecules spread on water gradually become amphiphilic when triethoxysilane end groups are converted to trihydroxy groups. Taking advantage of this amphiphilic character, stable monolayers of various densities can be deposited by the Langmuir–Blodgett (LB) technique onto silicon wafers. Hydrolysis and/or condensation of the triethoxysilane end groups allows formation of a Si–O–Si covalent bond with the oxidized silicon wafer. Surface-initiated styrene polymerization was performed on a system with different initiator densities. In addition, immobilization of alkoxyamine initiators and subsequent surface-initiated styrene polymerization was performed on an atomic force microscopy (AFM) tip by LB transfer [12].

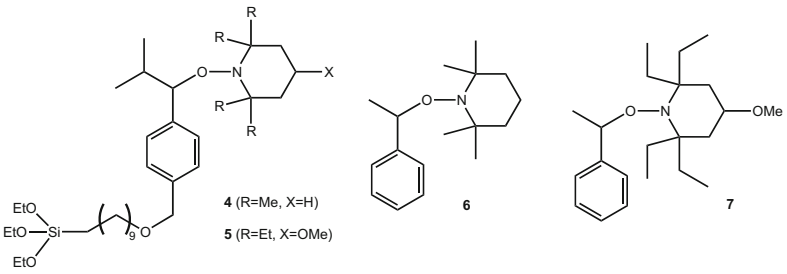

Scheme 5 Alkoxyamines and nitroxide used for SI-NMP of *tert*-butyl acrylate on oxidized silicon wafer. Reported by Studer and coworkers [16]

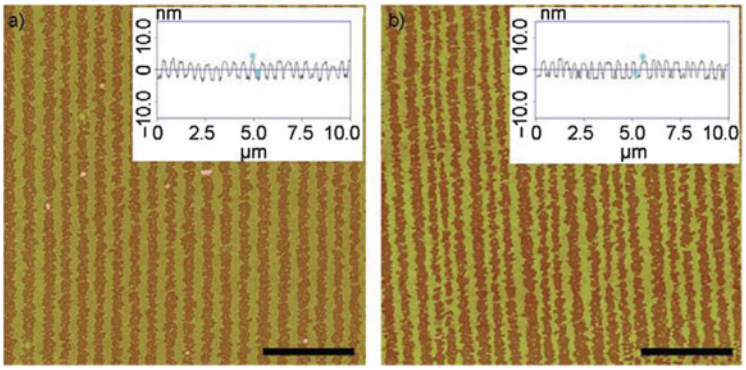

Scheme 6 (**a**) AFM image of surface after SI-NMP of styrene with **5**. (**b**) AFM image of surface after SI-NMPP of *n*-butyl acrylate with **5** (*insets* show cross-sections; *scale bars*: 2.5 µm). Reproduced from Brinks et al. [16] with permission from Wiley

LB lithography for spatially controlled attachment of initiator to form regular stripes of PS and poly(*n*-butyl-acrylate) (PBA) brushes was reported by Studer and coworkers [16]. Mixed monolayers of L-adipalmytoyl-phosphatidylcholine (DPPC) and TEMPO-derived alkoxyamines **4** or **5** (Scheme 5) were transferred by the LB technique onto oxidized silicon wafer in regular stripes with submicrometer lateral dimensions. Physisorbed DPPC was removed by washing, and NMP of styrene from the surface of silicon wafer covalently bonded to **4** was performed at 125°C for 24 h in the presence of **6** as sacrificial polymerization regulator. NMP of *n*-butyl acrylate was conducted with a surface modified with **5** in the presence of **7** at 105°C for 24 h. Polymer stripe width was controlled by the concentration of alkoxyamine in the mixed phase and adjusted from about 0.2 to 1.3 µm. The height of the stripes increased to 8 ± 0.2 nm for PS and 4.7 ± 0.2 nm for PBA (Scheme 6).

LB reactive deposition was also employed for anchoring of triethoxysilyl alkoxyamine derivatives of TEMPO **8**, SG1 **9**, and TIPNO **10** nitroxides to silicon substrates (Scheme 7) [17]. The nitroxide polarity and, therefore, the behavior of the corresponding alkoxyamine at the air–water interface of the LB trough had a

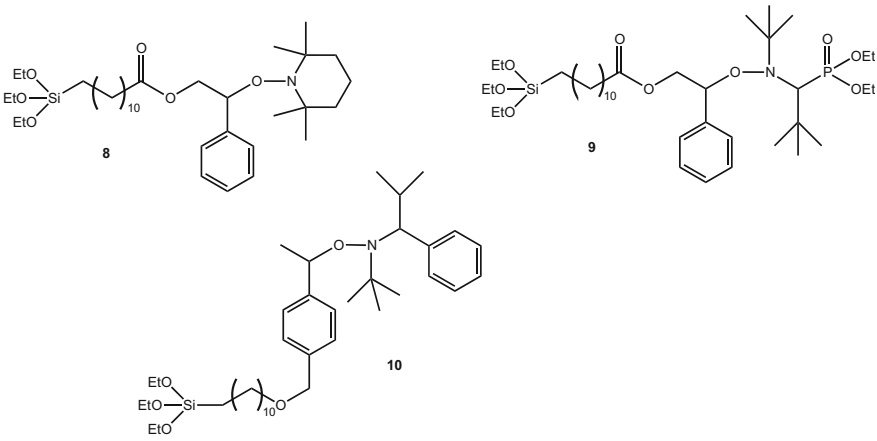

Scheme 7 Triethoxysilyl alkoxyamines derivatives of TEMPO **8**, SG1 **9**, and TIPNO **10** nitroxides

strong influence on the grafting density and the stretching of the resulting PS brushes. The TEMPO- and TIPNO-based alkoxyamines yielded relatively dense PS brushes, whereas the SG1-based alkoxyamine yielded brushes with low grafting densities and stretching as a consequence of the polar phosphorylated group.

Surface-tethered styrene-based homopolymer and diblock copolymers brushes bearing fluorinated alkyl side groups or ethylene glycol oligomers were produced with controlled chemical architecture and high coverage using SI-NMP on planar oxidized silicon surfaces [14, 15]. The silicon oxide surfaces were first modified with a chlorosilyl-functionalized TEMPO derivative (Scheme 8). In the case of diblock copolymer brushes, the second block was always detected at the polymer–air interface, as shown by angle-resolved X-ray photoelectron spectroscopy (XPS) and water contact angle measurements. Near-edge X-ray absorption fine structure (NEXAFS) analysis revealed an orientation of fluorinated side chains that could be correlated with surface stability upon exposure to water. Surface grafted with oligo (ethylene glycol)-containing polymer brushes possessed a superior ability to inhibit protein and cell adhesion compared with surface assemblies with deposited oligo (ethylene glycol).

Tethered alkoxyamines were also obtained in situ following a two-step procedure. First, 3-(trimethoxysilyl)propyl methacrylate (TSPMA) was attached to the surface. Then, the methacrylate function was allowed to react, under heating, with AIBN in the presence of TEMPO to afford the corresponding alkoxyamines. From this alkoxyamine-coated silicon, PS and poly(2-hydroxyethyl methacrylate) (HEMA) were then successfully prepared [20]. The novelty of this report is that micropatterning of the silicon surface was controlled by a combination of SI-NMP and SI-ATRP. The ATRP initiator was covalently immobilized via UV-induced hydrosilylation of 4-vinylbenzyl chloride (VBC) with the (hydrofluoric acid-etched) hydrogen-terminated silicon (Si–H) microdomains to produce a micropatterned and Si–C bonded VBC monolayer.

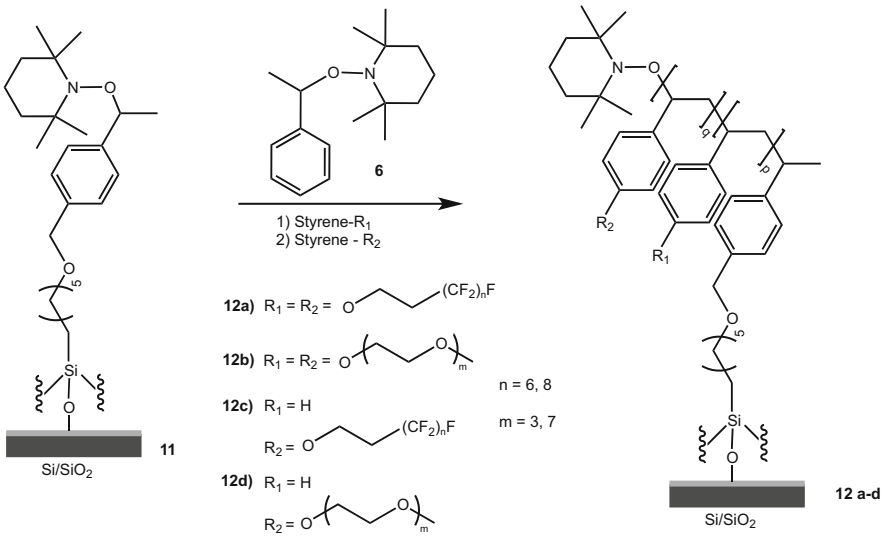

Scheme 8 Synthesis of surface-grown styrene-based homopolymer and diblock copolymer brushes bearing fluorinated alkyl side group and ethylene glycol oligomer

Recently, Studer and coworkers [19] prepared polymer brushes bearing α-hydroxyalkylphenylketone moieties as photoreactive polymer backbone using SI-NMP with **11**. Photoreactive polymer brushes (with thickness up to 60 nm) can undergo Norrish type I photoreaction upon irradiation to give surface-bound acyl radicals, which are trapped with functionalized nitroxides to give the corresponding acylalkoxyamines. This post-polymerization modification provided functionalized polymer brushes bearing cyano, poly(ethylene glycol), perfluoroalkyl, and biotin moieties.

Vapor phase polymerization from SI-NMP of various vinylic monomers resulted in polymer brushes with greater thicknesses than those formed by the solution phase process [21]. To explain this result, the authors supposed a more efficient reaction on the surface as a result of prolongation of the mean path of vaporized monomers in a vacuum, higher thermal energy of the monomer, and the possibility of adjusting the reaction parameters independently. Thin films of PS grafted polymer, poly (acrylic acid) (PAA), poly(2-hydroxypropyl methacrylamide) (PHPMA), and poly(*N*-isopropylacrylamide) (PNIPAM) were prepared with thicknesses of a few nanometers to submicrometers. This process was also used for the preparation of block copolymers (e.g., PS-*b*-PAA and PAA-*b*-PS-PHPMA). It is important to mention that solution phase polymerization of AA, HPMA, and NIPAM is impossible with TEMPO-based alkoxyamines.

SI-NMP can also be carried out using an initiator/nitroxide bimolecular system [22]. In this strategy, an azo-based initiator functionalized with chlorosilyl groups was first attached to the silicon wafer after immersion of the substrates in a toluene solution containing the azo derivatives. The formation of PBA brushes with thickness of 4–14 nm using two different azo initiators (AMCl and ATCl) was performed

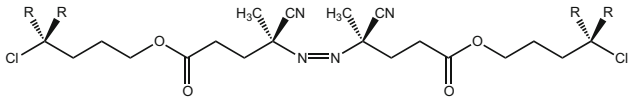

Scheme 9 Chemical structure of the chlorosilyl derivatives of azo initiators ATCl (R=Cl) and AMCl ($R=CH_3$)

in the presence of SG1 as controlling agent (Scheme 9). Elaboration of block copolymers by re-initiation of PBA growth from macromolecular chains grafted on a flat substrate with different monomers was also achieved.

Recently, SI-NMP using a bimolecular system was applied to the preparation of PS brushes. In this study, the initiator sites were generated from the silicon wafer surfaces by treating the latter with hydrogen plasma at atmospheric pressure [18]. According to the authors, the dissociation of molecular hydrogen in gas phase collisions produces hydrogen plasma, which can react with surface sites and surface-adsorbed water to form surface-activated sites. Precise control of plasma treatment time and radio frequency power allows a dense surface coverage of radical initiators to be obtained, from which vinyl monomers can combine to form surface-grafted polymer chains. Growth of PS film was thus achieved in the presence of TEMPO and exhibited a linear increase with respect to time, resulting in a polymer layer thickness of 28 nm.

2.1.2 NMP from Silicon Oxide Particle Surfaces

Synthesis

SI-NMP from silicon oxide surfaces has not been confined to planar surfaces, but has also been extended to colloidal supports as well as particle surfaces. As with silicon oxide planar surfaces, the most convenient strategy for introducing initiator onto the SiO_2 particle surfaces is to first graft functional alkoxyamines on their surfaces and then perform the polymerization reaction. A number of TEMPO, TEMPO-derivative, TIPNO, or SG1-based alkoxyamines bearing trichlorosilane ($–SiCl_3$), trimethoxysilane [$–Si(OMe)_3$], and triethoxysilane [$–Si(OEt)_3$] as the functional group have been prepared. A complete review of SI-NMP from SiO_2 particle surfaces has been recently published [5]. Chain conformation is a crucial factor in determining the macroscopic properties (solution, gel, composite, thin film, etc.) of the final grafted nanoparticle system. NMP enables the preparation of well-defined grafted silica nanoparticles. Therefore, control of polymerization opens the way to probe the conformation of the grafted chains at the surface of the nanoparticles and to analyze whether this conformation is affected by grafting as a function of various parameters such as the molecular mass of the grafted chains, grafting density, solvent quality, nature and shape of the surface (surface curvature), and interactions of nanoparticles in solution.

Conformation of Grafted Polymer Chains

Numerous works have been carried out on spherical grafted brushes to predict the conformation of grafted chains using theory [23, 24] and/or numerical simulations [25, 26]. Experimental validation is limited to a small number of techniques for evaluating the typical size of the grafted chain: rheology for the viscosimetric radius R_η, dynamic light scattering (DLS) for the hydrodynamic radius R_h [27, 28], and small angle X-ray or neutron scattering (SAXS or SANS) for the radius of gyration R_g. Viscosimetric or DLS measurements give a total value (including the nanoparticle size) that can be affected by nanoparticle concentration or nanoparticle aggregation and/or percolation. The accuracy of such determinations can be improved using SANS combined with neutron contrast variation, enabling direct determination of the radius of gyration of the grafted chains by matching the scattering of the core particles while controlling the colloidal stability of the solution by determination of interparticle structure factors. In solution, contrast variation is simply performed by adjusting the ratio of hydrogenated and deuterated solvent to obtain the desired values of neutron scattering length density for both the particle and the grafted polymer. This was first described by Chevigny et al. [29] for silica nanoparticles grafted with PS chains. The efficiency of the polymerization was improved by adding free initiator at the beginning of the reaction. At the final stage, free polymer chains were removed by ultrafiltration. The grafted brushes were finely characterized by fitting the SANS curves with different models (core–shell and Gaussian chain mode) to extract the physical parameters of the grafted brushes: number of chains per particle, molecular mass, and radius of gyration of the grafted chains. An example of such a curve is given in Scheme 10a.

A significant feature of the curve is the decrease in intensity as a function of scattering vector (Q^{-2}) for the high Q region, indicating that the grafted chains are still Gaussian. The extension of the grafted layer $h = 2R_{g\ \text{grafted}}$ was ~1.30 times larger than the corresponding Gaussian chain in theta solvent ($2R_{g\ \text{bulk}}$, with $R_{g\ \text{bulk}} = 0.275\, M_w{}^{0.5}$), as determined by size-exclusion chromatography (SEC) after the cleaving process. This indicates stretching of the chain at the surface of the particle. Such a stretching, which can be explained by excluded volume interactions with lateral neighboring chains, has been described by Alexander in terms of scaling laws of the grafting density [24]. For a layer grafted on a planar surface, the extension of the grafted layer is expected to be $h = a_0 N^{1/3}$ for a good solvent and $h = a_0 N^{1/2}$ for a theta solvent, where a_0 is the monomer length and N the number of monomers. In addition, the effect of surface curvature $r_0{}^{2/5}$ has to be taken into account; it reduces the extension of the grafted layer to $h = N^{1/2}\sigma^{1/2} r_0{}^{2/5}$ for the case of theta solvent [26]. Replacing free initiator by controller (SG1) in the reaction enables variation of the molecular mass of the grafted chain in the range 5–50 kg. mol-1 [32]. Whatever the N value, a systematic agreement is found between the extension of the grafted brush deduced from the fitting analysis $h = 2R_{g\ \text{grafted}}$ and the theoretical prediction derived from the scaling law $h = N^{1/2}\sigma^{1/2} r_0{}^{2/5}$. Genevaz and colleagues (unpublished results) have recently adapted the previous NMP protocol to the grafting of a diblock copolymer P*t*BA-*b*-PS at the surface of silica

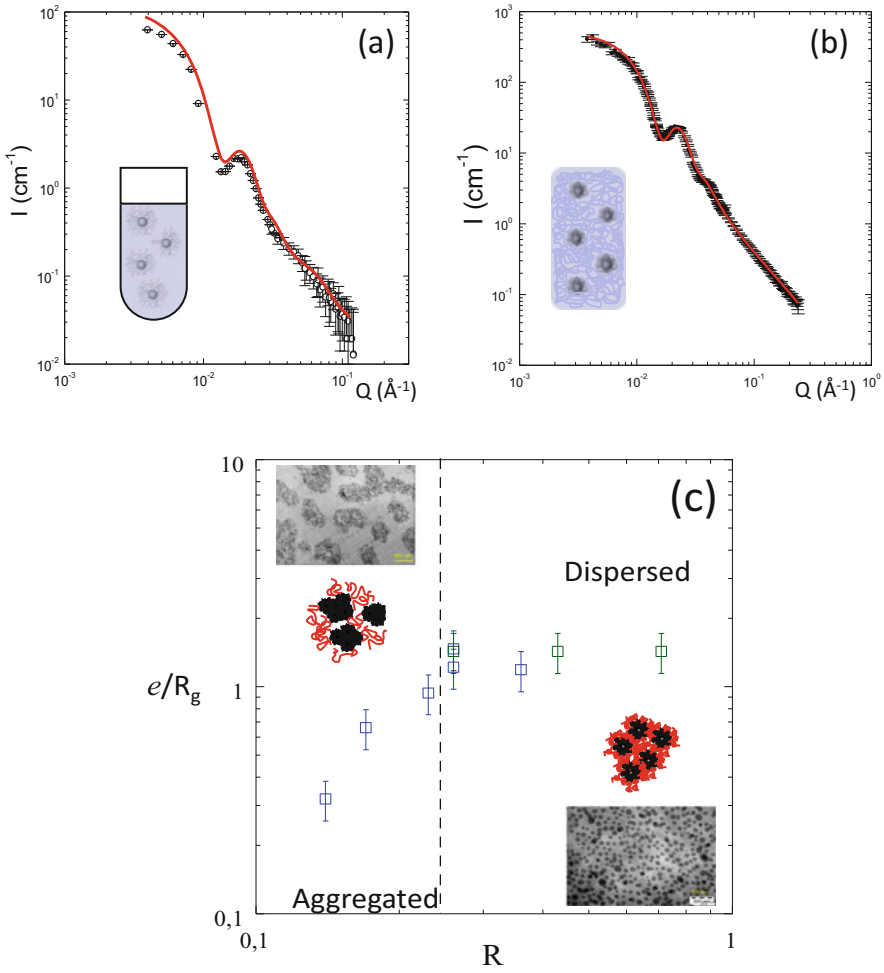

Scheme 10 (**a**) SANS curve of silica nanoparticles with PS-grafted brush in solution (*black dots*) and the corresponding fitting calculation (*red line*). From Chevigny et al. [29]. (**b**) SANS curve of silica nanoparticles with PS-grafted brush in melt (*black dots*) and the corresponding fitting calculation (*red line*). From Chevigny et al. [30]. (**c**) Variation of the grafted brush conformation as a function of the nanoparticle dispersion in the host polymer matrix. From Chevigny et al. [31]

particles by associating dynamic light scattering (DLS) and SANS. The motivation of this work was to make spherical brushes with an interface of tunable dynamics using a combination of a block (P*t*BA) with low glass transition temperature (T_g) and a block (PS) with high T_g. They showed that the diblock conformation behaved in the same way as the homopolymer chain and that the grafting had no influence on the chain extension when the chain is close to the Kuhn length. Robbes et al. [33] grafted PS chains on magnetic nanoparticles (maghemites, γ-Fe_2O_3) using NMP. In contrast to the silica "single sphere" particles, in solution maghemites form linear

clusters of three to four primary particles from which the PS chains grow under controlled polymerization. It is possible to directly probe the influence of surface curvature on the extension of the grafted chains for a given grafting density and under theta solvent conditions; indeed, the extension of the grafted chain ($h = 18$ nm) was found to be intermediate between the pure spherical case ($h = 11$ nm) and the pure plan geometry ($h = 44$ nm). Regarding the question of the conformation of grafted chains in solution, it is interesting to look at the corresponding conformation in nanocomposites when spherical brushes are mixed with identical free chains. This was probed by Chevigny et al. [30] using a statistical hydrogenated–deuterated PS matrix that matched the particle scattering in SANS experiments; the silica becomes invisible to neutrons in the matrix, and only the deuterated corona contributes to the signal. The resulting curve (presented in Scheme 10b) was perfectly fitted by a Gaussian model and showed partial collapse of the grafted brushes from solution (12 nm) to film (6 nm), corresponding to a wet–dry transition driven by entropy mixing between the grafted and free chains. By varying the dispersion state of the nanoparticles inside the matrix, the same authors [31] demonstrated a second transition from partial to complete collapse of the spherical brushes, associated with the formation of compact aggregates inside the film (Scheme 10c).

2.1.3 NMP from Porous Silicon Oxide

In comparison with colloidal particles such as silica or planar surfaces such as silicon wafer, SI-NMP from ordered mesoporous silica (OMS) has been much less investigated. Alongside the usual issues of SI-CRP from dense substrates, such as initiator and deactivator concentration or initiator efficiency, the porous nature of OMS (high specific surface area, high porous volume, pore morphology, pore diameter, and pore connectivity) brings to the system new complexity, such as diffusion of reactants in a confined space. The first SI-NMP from OMS was performed by Lenarda et al. at the inner surface of MCM-41 mesoporous silica [34]. Typically, the MCM-41 silica was modified following a three-step grafting procedure: first, reaction with 3-aminopropyltriethoxysilane, then terephthaloyl chloride, and finally 1-hydroxy-2-phenyl-2-TEMPO-ethane. The styrene polymerization was shown to occur inside the mesoporous silica channels. It should be mentioned that partial filling of the pores decreased the surface area of the MCM-41 silica without destroying its structural and morphological characteristics. More recently, the SI-NMP of styrene was performed from various types of ordered mesoporous silica particles with different morphologies and pore sizes, using an SG1-based alkoxyamine derived from BlocBuilder MA initiator [35]. Whatever the pore morphology and pore size, the polymerization kinetics were similar in all cases, but with important differences in the molar mass distribution. The authors showed that for good diffusion of the reactants, large pore sizes of 5 nm were adequate and that the porous morphology of the particles is of high importance, particularly pore connectivity.

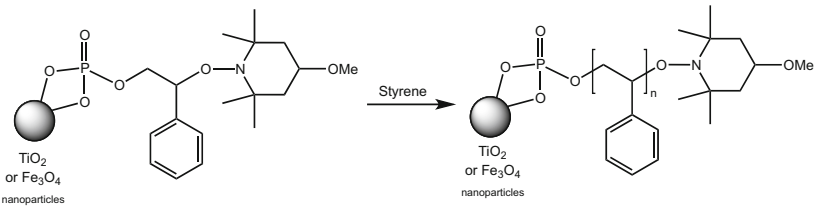

Scheme 11 Polymerization of styrene on metal oxide nanoparticles

2.2 NMP from Metal Oxide Surfaces

SI-NMP from metal oxide surfaces is mainly performed from previously modified titanium or iron oxide substrates. Titanium oxide (TiO_2, $d = 15$ nm) and magnetite (Fe_3O_4, $d = 10$ nm) nanoparticles chemically modified with 4-methoxy-TEMPO-based alkoxyamine by a phosphonic acid group were utilized by Takahara and coworkers for the preparation of PS (Scheme 11) and poly(3-vinylpyridine) (P3VP) brushes [36–40]. The grafting densities of PS chains on TiO_2 particles were estimated to be 0.04–0.28 chains nm^{-2} whereas those on Fe_3O_4 particles were 0.12–0.2 chains nm^{-2}. Functionalized nanoparticles showed stable dispersibility in good solvents of PS without losing their physical properties. In the case of P3VP-modified magnetite, the particles gave a stable dispersion in good solvents thanks to pyridinium formation through either protonation of the pyridine rings with an acidic solution or quaternization with an aqueous solution of iodomethane [40].

In a similar procedure, Binder et al. used a TIPNO-based alkoxyamine bearing a 1,2-diol function for its attachment onto iron oxide. This system was used for the preparation of core–shell Fe_2O_3 nanoparticles with a well-defined PNIPAM shell (Scheme 12) [41]. The polymerization reaction was performed in *N*,*N*-dimethylformamide (DMF) at 150°C. Under these conditions, monomer conversion reached 90% and experimental M_n was 5,600 g mol^{-1}. Poly (4-vinylpyridine) (P4VP) brushes were prepared by SI-NMP on the surface of 3-methacryloxyproyltrimethoxysilane (3-MPS)-modified magnetite nanoparticles with an average diameter of 30 nm. The NMP-made P4VP polymer brushes were obtained at 130°C using 4-hydroxyl-TEMPO free radical as controlling agent and benzoyl peroxide (BPO) as initiator [42].

Recently, an efficient three-step grafting-from procedure was developed to obtain well-controlled PS grafted magnetic γ-Fe_2O_3 nanoparticles [33]. In the first step, after modification of the surface charge of the nanoparticles and then replacement of H_2O by dimethylacetamide (DMAc), 3-aminopropryl trethoxysilane (APTES) was allowed to react with the surface. The corresponding amino-modified nanoparticles were then reacted with MAMA-NHS alkoxyamine (Scheme 13) to afford nanoparticles functionalized with SG1-based alkoxyamine. In the last step, polymerization of styrene was performed from the previously modified nanoparticles. The grafting-from strategy was also used to graft poly [styrene-*co*-(maleic anhydride)] (PSMA) chains from the Fe_3O_4 nanoparticle

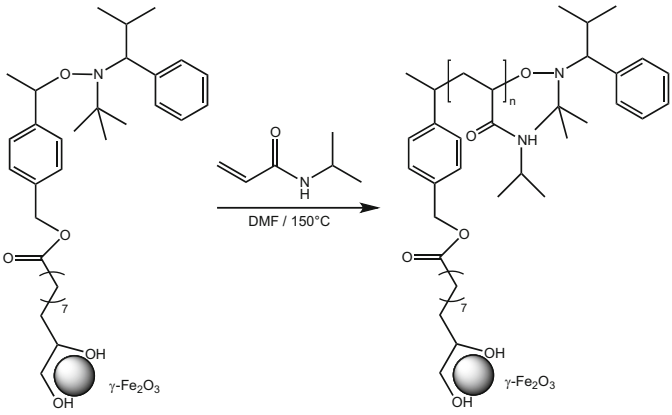

Scheme 12 Grafting-from of *N*-isopropyl acrylamide from the surface of γ-Fe_2O_3 nanoparticles attached to TIPNO-based alkoxyamine bearing a 1,2-diol

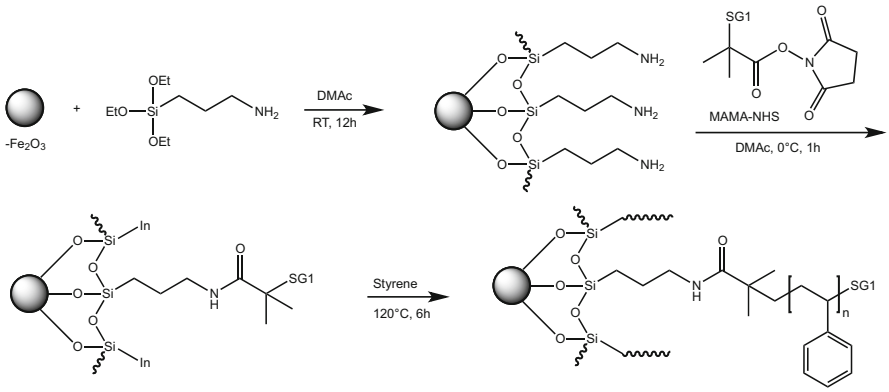

Scheme 13 Grafting-from strategy for preparation of well-defined PS-grafted magnetic γ-Fe_2O_3 nanoparticles

surface with TEMPO moieties [43]. For this, TEMPO was first immobilized onto Fe_3O_4 nanoparticles by the nucleophilic substitution reaction between 1-oxo-2,2,6,6-tetramethylpiperidinium bromide (TEMPO-Br) and hydroxyl groups on the Fe_3O_4 surfaces. In the second stage, PSMA-Fe_3O_4 was synthesized using TEMPO-immobilized Fe_3O_4 in the presence of styrene and maleic anhydride. Free TEMPO was also present in the system to enhance control of polymerization.

There has been only one report describing SI-NMP from a metal oxide other than those of titanium and iron, namely from a copper oxide surface [44]. In this study, poly(ionic liquid) was grafted onto micro/nanoscale CuO/Cu surfaces by bimolecular-initiated polymerization with TEMPO nitroxide. For this purpose, the peroxide groups were first introduced onto micro/nanoscale CuO surfaces by reaction of 3-chloropropyltrimethoxysilane (immobilized on the CuO surface) with

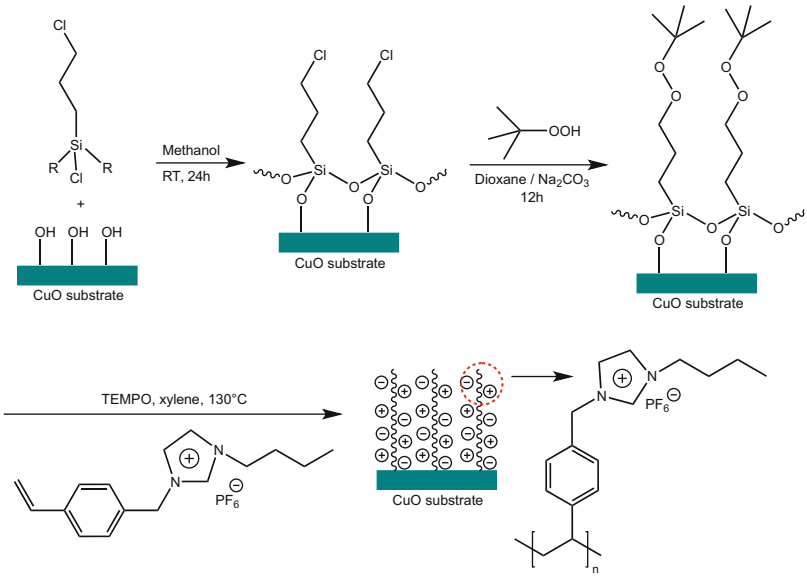

Scheme 14 Process of poly(ionic liquid) growth at CuO surface

tert-butyl hydroperoxide. Polymerization of 1-(4-vinylbenzyl)-3-butylimidazoliumhexafluorophosphate, an ionic liquid monomer, from the peroxide-activated CuO surface in the presence of TEMPO led to the formation of polymer brushes (Scheme 14).

2.3 NMP from Clay Mineral Surfaces

The main approach for immobilization of functional groups that can initiate or mediate SI-NMP on clay mineral surfaces is based on noncovalent electrostatic interactions. Indeed, clay minerals present the ability to exchange cations in the interlayer spacing with other ionic species present in solution. Sogah and coworkers were the first to report an efficient approach for the direct synthesis of dispersed SI-NMP-made silicate nanocomposites. Typically, they performed an intergallery polymerization via a montmorillonite (MMT)-anchored TEMPO-based alkoxyamine initiator bearing a benzyltrimethylammonium **13** (Scheme 15) moiety [45]. Other alkoxyamines bearing cationic groups were also attached on MMT surfaces. A cationic alkoxyamine **14** based on 2,6-diethyl-2,3,6-trimethyl-piperidine-4-hydroxy-*N*-oxyl nitroxide was directly intercalated into MMT layers. PBA chains were then grown, exhibiting tunable M_n in the 1,000–14,000 g mol^{-1} range and a dispersity of 1.5, allowing facile re-dispersion of the resulting composite in apolar solvents [46]. In another example, a three-step procedure was proposed by Shen et al. for grafting PS chains on the surface of MMT [47]. The first step

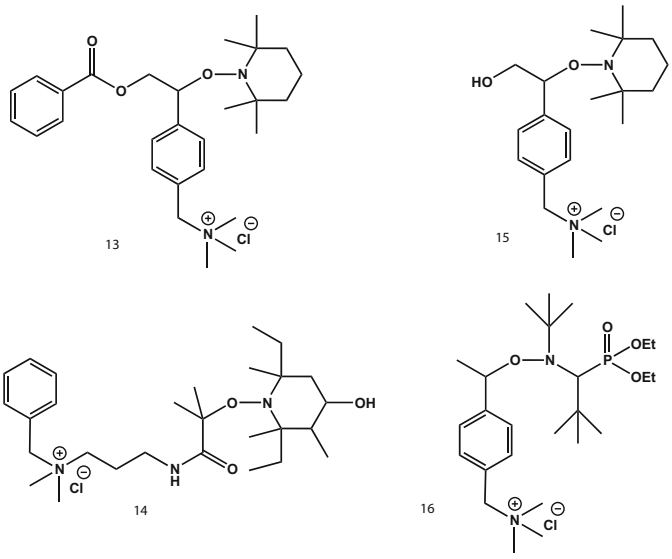

Scheme 15 Structure of cationic alkoxyamines used for SI-NMP from clay surfaces

consisted in attaching 2-methacryloyloxy ethyl trimethylammonium chloride to the surface of MMT by an ion-exchange reaction. Then, the alkoxyamine-functionalized MMT was reacted with the previously introduced methacrylate function in the presence of BPO and TEMPO at 90°C. PS chains with controlled M_n and low dispersity were then successfully grown from the MMT surface by SI-NMP. Polystyrene-*block*-polycaprolactone (PS-*b*-PCL) diblock copolymers were also grafted to MMT surfaces in one-step in situ living polymerization from a silicate-anchored bifunctional initiator based on TEMPO **15** (Scheme 15) via divergent chain growth [48]. Recently, Paulis et al. performed SI-NMP of methyl methacrylate (MMA)/butyl acrylate using modified MMT macroinitiator [49]. The macroinitiator was synthesized by NMP of vinylbenzyl trimethylammonium chloride, MMA, and styrene at 90°C using Blocbuilder MA as alkoxyamine. The obtained macroinitiator of 1,000 g mol^{-1} was exchanged with the sodium cations of MMT to yield surface-modified reactive MMT. SI-NMP of MMA/butyl acrylate from reactive MMT surfaces allowed exfoliation of the clay. The composite was then used as master batch in the mini-emulsion polymerization of MMA/butyl acrylate.

A similar strategy has been used to allow SI-NMP from other clay minerals such as laponite [50] and saponite [51]. In the case of laponite, a SG1-based alkoxyamine bearing an ammonium group **16** (Scheme 15) was first immobilized by cation exchange (Scheme 16) [50]. Then, PS chains were obtained from its surface in the presence of a sacrificial alkoxyamine initiator to afford composites exhibiting improved colloidal stability in inorganic solvent. Transmission electron

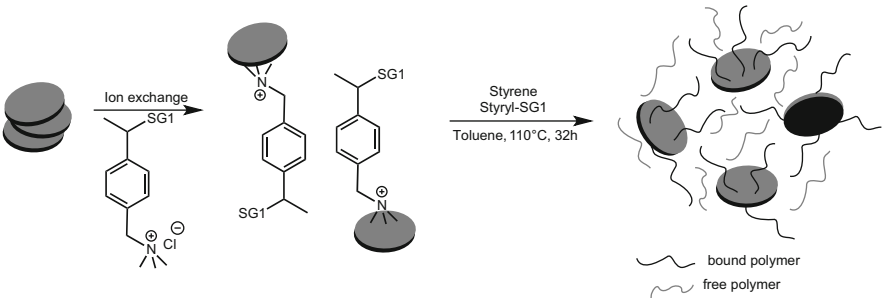

Scheme 16 SI-NMP of styrene from laponite clay platelets

microscopy (TEM) performed on these samples demonstrated a completely exfoliated structure of the clay tactoids within the polymer matrix.

Alternatively, different reports describe the immobilization of free-radical initiators carrying cationic groups on mineral clay surfaces for subsequent SI-NMP of vinylic monomers performed in the presence of an efficient nitroxide mediator [52–55]. For example, Mittal reported the immobilization of 4,4-azobis(4-cyanovaleric acid)-based initiator bearing long alkyl chains and two cationic groups for subsequent SI-NMP of lauryl methacrylate in the presence of SG1 [52]. The same approach was employed by Billon and coworkers for the preparation of (co) polymer/mica composites [53–55]. Mica SI-NMP proceeds in two steps: (1) mica surface modification via ion exchange of 2,2-azobis(isobutyramidine hydrochloride) as a free-radical initiator bearing a cationic moiety, and (2) SI-NMP of butyl acrylate performed from the initiator-bound mica in the presence of free SG1 nitroxide. In the case of copolymer/mica composites, polymerization of butyl acrylate followed by polymerization of a mixture of styrene and a modified alizarin dye monomer were performed. Although control was lost during the polymerization of the second block, colored diblock copolymer/mica composites were indeed obtained [54]. Interestingly, the colors of poly(styrene-*co*-alizarin)/mica composites were strongly related to both the adsorption density of macromolecular chains on the mica surface and the dye content [55].

Besides noncovalent interactions, covalent immobilization has also been used to link TEMPO-based alkoxyamine bearing a trichlorosilane group onto a magadiite interlayer surface [56]. SI-NMP of styrene from the radical initiator immobilized on magadiite occurred in a controlled manner. Moreover, the fine dispersion state of magadiite in the PS matrix contributed to an increase in the thermal stability of PS.

2.4 NMP from Metal and Semiconductor Surfaces

As a result of their conduction properties, metallic surfaces are particularly attractive materials. Jérôme and coworkers reported a two-step procedure to

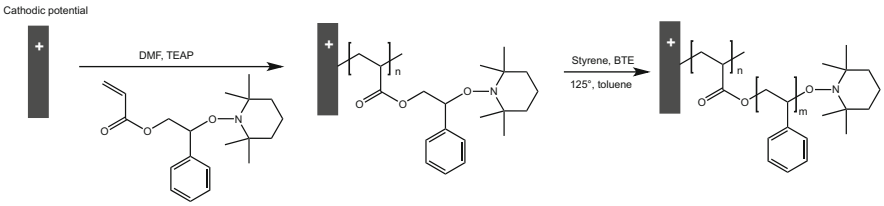

Scheme 17 Two-step grafting-from strategy using electrochemistry

functionalize steel with polymer brushes [57]. The electrografting of an inimer to an acrylate bearing a TEMPO-based alkoxyamine moiety on the ester group was used for the preparation of polyacrylate brushes. After the electrografting process, SI-NMP of styrene was performed in the presence of a free-radical initiator (Scheme 17). Grafted PS chains were removed from the surface under acidic hydrolysis. The restored metal substrate was then used for further electrochemical reactions. A similar procedure was also applied to stainless steel surfaces [58]. To this end, the electrografting of poly[2-phenyl-2-(2,2,6,6-tetramethylpiperidin-1-yloxy)-ethyl acrylate] (PPTEA) onto stainless steel was first carried out and then followed by the NMP of 2-(dimethylamino ethyl)acrylate and styrene or *n*-butyl acrylate, initiated from the electrografted polyacrylate chains in the presence of a TIPNO-based alkoxyamine. In order to impart antibacterial properties to the obtained materials, quaternization of the grafted copolymers was then performed. Jérôme and coworkers also reported an electrochemical approach based on the simultaneous electrodeposition of silver and the electrografting of polymer chains grafted onto stainless steel and used as a cathode [59]. This strategy allowed the synthesis of poly(ethyl acrylate), PPTEA, and poly(8-quinolinyl acrylate). Hence, silver-immobilized polymer films having antibacterial properties were efficiently prepared in a single step.

A colored polymer/aluminum hybrid pigment was synthesized by NMP initiated from the surface of aluminum flakes [60]. The latter were coated with a thin silica layer. In this case, the chemical grafting of the initiator was performed through silylation reactions. The initiator used was an SG1-based alkoxyamine functionalized with an alkoxysilane moiety. This compound was previously prepared from the intermolecular radical 1,2-addition of Blocbuilder MA in the presence of 3-(trimethoxysilyl)propyl acrylate. Styrene or *n*-butyl acrylate were then copolymerized with vinyl dye monomer in a controlled manner.

Many reports related to SI-CRP on metal describe the use of gold nanoparticles and mainly from SI-ATRP. We note only one report describing the modification of gold nanoparticles with SI-NMP. In this report, the NMP initiator was a TEMPO-derivative functionalized with disulfide as ligand for the synthesis of gold nanoparticles [61]. Two populations of gold nanoparticles, of 1.5 and 5.5 nm diameter, covered with PS of 10,000 g mol^{-1} were prepared.

Similarly, CdSe nanoparticles have been functionalized using ligand exchange reactions [62]. The nanoparticles were stabilized by the tri-*n*-octylphosphine oxide

ligand. TEMPO-based alkoxyamines containing phosphine groups were introduced to CdSe nanoparticles following a ligand-exchange strategy. First, the tri-*n*-octylphosphine oxide ligand was replaced with pyridine, followed by exchange with the appropriate alkoxyamine. From the surface of functionalized CdSe nanoparticles, PS and poly(styrene-*co*-MMA) copolymers were efficiently obtained.

2.5 NMP from Carbon Surfaces

Carbon-based materials have attracted wide interest in the materials science community for decades. These materials are extremely light and versatile. Indeed, depending on the local bonding of the constituting carbon atoms, their properties can be easily tuned. Diamond, carbon black, and graphite are well-known examples of carbon-based materials; more recently discovered allotropes are fullerenes, carbon nanotubes (CNTs), and graphene. Of these carbon-based materials, CNTs are particularly studied because of their unique electronic, mechanical, thermal, and chemical properties. To target specific applications, a number of experiments have focused on the chemical modification of CNTs [63], including the use of CRP techniques [64]. SI-NMP involves first attaching either an alkoxyamine moiety or a nitroxide to the CNT surfaces, or the in situ synthesis of an alkoxyamine.

In order to facilitate anchoring of an initiator at the surface of CNTs (and carbon in general), these substrates first need to be treated. For instance, carboxylic acid groups can be introduced to single-walled nanotubes (SWNTs) and multiwalled carbon nanotubes (MWNTs) by oxidation of the pristine nanotubes in the presence of HNO_3 or H_2SO_4/HNO_3. The corresponding acid chloride derivatives are then obtained by action of thionyl chloride in the presence of carboxylic acid-functionalized CNTs. Introduction of the initiator/controller agent is finally performed by esterification of 4-hydroxy TEMPO [65] or TEMPO-based alkoxyamine bearing a hydroxyl group with acid chloride-functionalized CNTs [66–68] (Scheme 18). Conventional radical polymerization of styrene, initiated by AIBN or simple heating, in the presence of nitroxide-carrying CNTs provided CNT–PS conjugates [65]. CNTs functionalized with TEMPO-based alkoxyamine **17** were used to perform SI-NMP of different monomers such as styrene, 4-vinylpyridine, and styrene sulfonate (SS). The resulting MWCNT–PS and MWCNT–PS-*b*-P4VP exhibited relatively good dispersibility in various organic solvents [66], whereas MWCNT–P4VP presented good dispersibility in acidic aqueous solutions. MWCNT–PSS composites afforded stable dispersions in aqueous solutions over a large pH range [67]. In addition, SI-NMP of butyl acrylate and *N*,*N*-dimethylacetoacetamide (DMAAm) were also successfully performed from CNTs [69].

In addition to the modification of oxidized CNTs, another strategy consists in performing radical addition reactions onto the carbon–carbon double bond of CNTs, allowing introduction of specific groups able to initiate or mediate

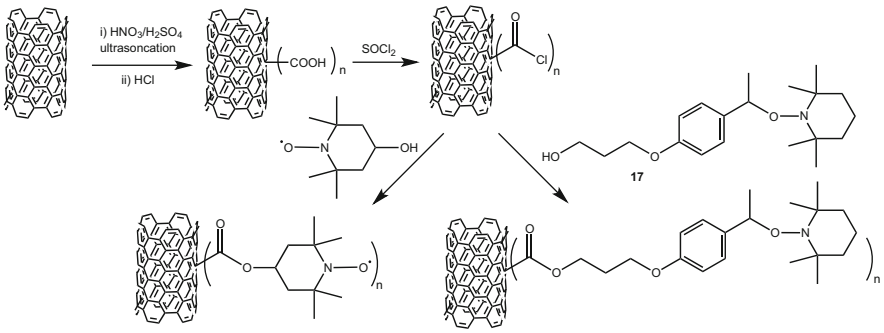

Scheme 18 Synthesis of carbon-nanotube-supported TEMPO nitroxide or TEMPO-based alkoxyamine initiator

SI-NMP [70, 71]. For instance, heating of nitrogen-doped CNTs in the presence of both dibenzoyl peroxide and TEMPO afforded the corresponding alkoxyamine-modified CNTs. The SI-NMP of styrene then provided PS brushes [70].

Graphene is considered one of the most important materials of the next 20 years. Indeed, this material combines several outstanding properties never observed before in a single material, such as remarkably high electron mobility at room temperature [72], tunable band gap [73], high strength [74], and transparency [75]. Because of these features, even unmodified graphene is a good candidate for several applications. The incorporation of graphene into polymers has attracted attention not only as a route to original materials exhibiting structural and functional properties superior to those of the pure components, but also to previous nanocomposite systems obtained with other nanofillers. Modification of graphene with grafted polymer chains was recently reviewed by Salavagione et al. [76] and Layek and Nandi [77]. Only one report describes SI-NMP from a graphene surface [78]. In this study, graphene oxide-*g*-polystyrene and graphene oxide-*g*-polyisoprene were synthesized using a two-step procedure involving (1) application of an oxoammonium salt (TEMPO-Br) to modify the surface of graphene oxide with TEMPO, and (2) styrene or isoprene graft polymerization from the TEMPO-functionalized graphene oxide surface (Scheme 19).

2.6 NMP from Polymer Surfaces

Synthetic and natural polymers are also used as substrates for SI-NMP. The two principal strategies used to modify polymer substrates are (1) direct attachment of initiators to a polymer surface bearing suitable functional groups, and (2) in the case of inert polymers, appropriate treatment or activation to introduce functional groups prior to anchoring of the initiator.

Merrifield polymer resins are often used as substrates for polymer brush synthesis using NMP. To achieve this, TEMPO is reduced with sodium ascorbate,

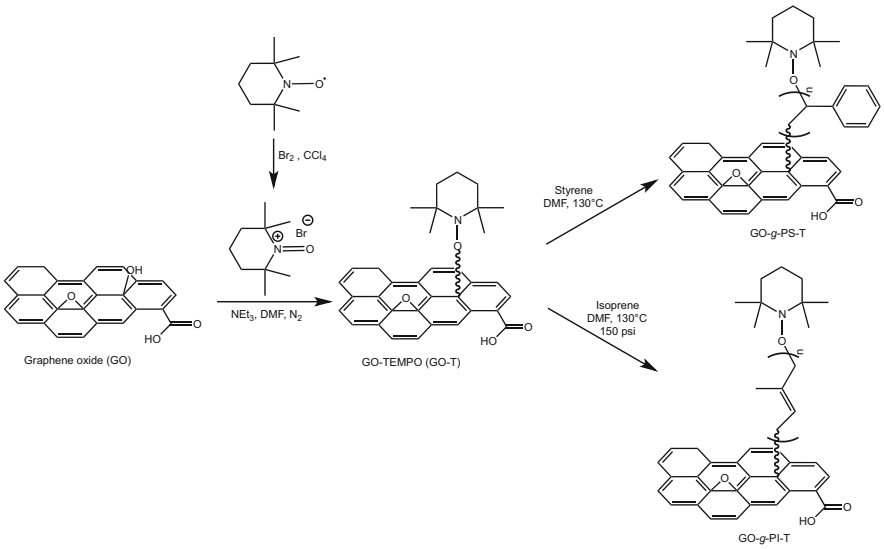

Scheme 19 Preparation of TEMPO-Br and subsequent functionalization of graphene oxide (GO) to graphene oxide-TEMPO (GO-T) and graft polymerization of styrene and isoprene from GO-T

deprotonated, and then allowed to react with the benzyl chlorides of the resin to covalently bind TEMPO via an ether linkage [79]. The immobilized alkoxyamine can then be used for preparation of PS-based polymer brushes [80–82].

SG1 nitroxide was attached to latex particles made of poly(styrene-*co*-chloromethylstyrene) of 60 nm diameter previously prepared via atom transfer radical addition [83]. Microspheres grafted with the homopolymer poly (2-dimethylamino ethyl acrylate) (PDMAEA), as well as block copolymers poly (styrene-*b*-DMAEA) and poly(butyl acrylate-*b*-DMAEA) were prepared by SI-NMP in DMF at 112°C, with the initial addition of free SG1 to ensure polymerization control.

The N-terminus of peptide sequences obtained from solid phase synthesis was transformed into a carboxylic acid group by the action of glutaric anhydride. NMP initiator tethered to the N-terminus of the peptide was then introduced via reaction of the benzylic amine of a fluorine-labeled alkoxyamine with the previously modified peptide. The peptide-supported initiator was then used to create block copolymers, under conditions that promote sequential NMP of *tert*-butyl acrylate and methyl acrylate [84].

Natural polymers such as cellulose and natural rubber were also subjected to SI-NMP. NMP was the first living radical polymerization method to be used in cellulose grafting. Daly et al. [85] reported the first use of nitroxide-mediated, controlled radical grafting from cellulose and cellulose derivatives. Controlled radical grafting from hydroxypropyl cellulose (HPC) was performed using TEMPO monoadducts, formed from the HPC–Barton carbonate derivative

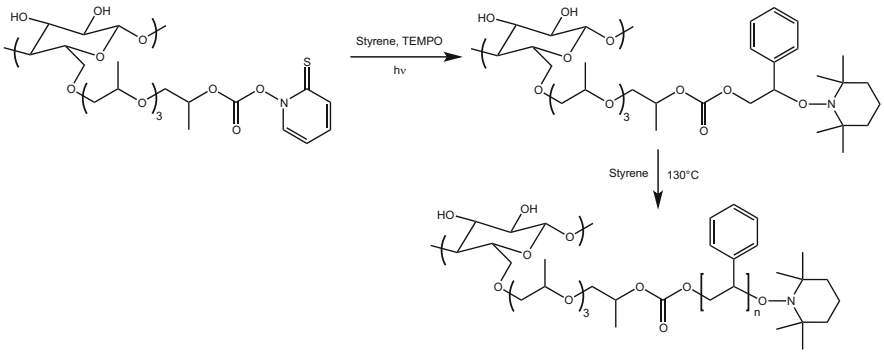

Scheme 20 NMP-mediated controlled radical grafting from hydroxypropyl cellulose

(carbonates of *N*-hydroxypyridine-2-thione) (Scheme 20). Photolysis of this derivative in the presence of styrene and TEMPO provided an adduct. Heating the macroinitiator at 130°C provided styrene–HPC graft copolymers. An increase in grafted polymeric chain length with increasing polymerization time was observed. The dispersity of the PS grafts ranged from 1.3 to 1.5.

Natural rubber (NR) in the form of a solid film was modified by grafting with PS using TEMPO as nitroxide mediator in an SI-NMP process [86]. The attachment of TEMPO on the NR substrate was carried out in a two-step process (Scheme 21). The first step was to introduce active functional groups for transformation into radical species. For this, hydroxylation of the NR substrate by thermal decomposition of potassium persulfate was chosen. In the second step, the hydroxyl group of the hydroxylated NR was dissociated with the aid of ceric ions and transformed into an active alkoxy radical, which reacted with styrene and then TEMPO. The resulting rubber was a TEMPO-modified NR, which was then used for PS grafting from the NR surface (Scheme 21). The authors showed that by using either the "optical slicing" or "*z*-scanning" approach, a "homogeneous grafting" of about 30 mol% PS occurred inside the bulk NR substrate.

3 Conclusion

Many results in the literature demonstrate that SI-NMP is a powerful way to control chain length, distribution, and composition of a large range of polymers grafted onto various organic and inorganic surfaces. Thanks to this approach, a wide variety of materials finding application in fields of major importance such as coatings, compatibilizing agents, electronics, and biomaterials have been successfully prepared. The main advantage of SI-NMP is that this technique does not require any addition of metal or metal salt. However, despite the development of efficient strategies to obtain NMP-grafted polymer on surfaces, there is still room to improve the SI-NMP process. Indeed, the synthetic procedures used to anchor alkoxyamine

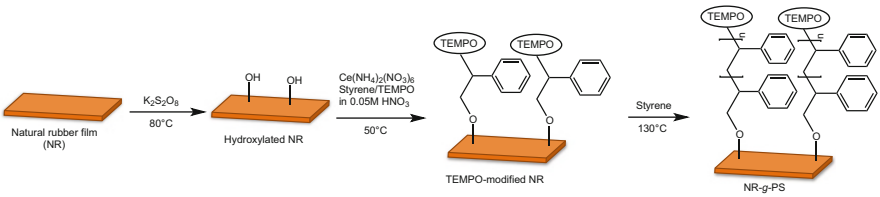

Scheme 21 Synthesis of polystyrene grafted onto the surface of natural rubber using SI-NMP

on the surface often require multistep pathways. Moreover, in order to reach a good level of control, polymerization reactions have to be performed in the presence of free alkoxyamine as sacrificial initiator. These points will have to be addressed in order to push further the development of SI-NMP. In the future, SI-NMP initiated photochemically could also be an attractive way of grafting polymer chains onto surfaces.

References

1. Zhao B, Brittain WJ (2000) Prog Polym Sci 25:677
2. Barbey R, Lavanant L, Paripovic D, Schüwer N, Sugnaux C, Tugulu S, Klok H-A (2009) Chem Rev 109:5437
3. Edmondson S, Osborne VL, Husk WTS (2004) Chem Soc Rev 33:14
4. Olivier A, Meyer F, Raquez J-M, Damman P, Dubois P (2012) Prog Polym Sci 37:157
5. Nicolas J, Guillaneuf Y, Lefay C, Bertin D, Gigmes D, Charleux B (2013) Prog Polym Sci 38:63
6. Fischer H (2001) Chem Rev 101:3581
7. Schwartz DK (2001) Annu Rev Phys Chem 52:107
8. Husseman M, Malmström EE, McNamara M, Mate M, Mecerreyes D, Benoit DG, Hedrick JL, Mansky P, Huang E, Russell TP (1999) Macromolecules 32:1424
9. Husemann M, Morrison M, Benoit D, Frommer J, Mate CM, Hinsberg WD, Hedrick JL, Hawker CJ (2000) J Am Chem Soc 122:1844
10. Hawker CJ, Barclay GG, Dao J (1996) J Am Chem Soc 118:11467
11. Devaux C, Chapel JP, Chaumont P (2002) Eur Phys J E 7:345
12. Devaux C, Chapel J-P (2003) Eur Phys J E 10:77
13. Mulfort KL, Ryu J, Zhou Q (2003) Polymer 44:3185
14. Andruzzi L, Hexemer A, Li X, Ober CK, Kramer EJ, Galli G, Chiellini E, Fischer DA (2004) Langmuir 20:10498
15. Andruzzi L, Senaratne W, Hexemer A, Sheets ED, Ilic B, Kramer EJ, Baird B, Ober CK (2005) Langmuir 21:2495
16. Brinks MK, Hirtz M, Chi L, Fuchs H, Studer A (2007) Angew Chem Int Ed 46:5231
17. Ostaci R-V, Celle C, Seytre G, Beyou E, Chapel J-P, Drockenmuller E (2008) J Polym Sci A Polym Chem 46:3367
18. Lewis GT, Cohen Y (2008) Langmuir 24:13102
19. Mardyukov A, Li Y, Dickschat A, Schaefer AH, Studer A (2013) Langmuir 29:6369
20. Xu FJ, Song Y, Cheng ZP, Zhu XL, Zhu CX, Kang ET, Neoh KG (2005) Macromolecules 38:6254
21. Li J, Chen X, Chang Y-C (2005) Langmuir 21:9562
22. Parvole J, Laruelle G, Billon L (2005) Macromol Chem Phys 206:372

23. De Gennes PG (1980) Macromolecules 13:1069
24. Alexander S (1977) J Phys 38:983
25. Verso FL, Yelash L, Egorov SA, Binder K (2012) Soft Matter 8:4185
26. Egorov S, Binder K (2012) J Chem Phys 137:094901
27. Tande BM, Wagner NJ, Mackay ME, Hawker CJ, Jeong M (2001) Macromolecules 34:8580
28. Dukes D, Li Y, Lewis S, Benicewicz B, Schadler L, Kumar SK (2010) Macromolecules 43:1564
29. Chevigny C, Gigmes D, Bertin D, Jestin J, Boue F (2009) Soft Matter 5:3741
30. Chevigny C, Jestin J, Gigmes D, Schweins R, Di-Cola E, Dalmas F, Bertin D, Boue F (2010) Macromolecules 43:4833
31. Chevigny C, Dalmas F, Di Cola E, Gigmes D, Bertin D, Boué F, Jestin J (2010) Macromolecules 44:122
32. Chevigny C, Gigmes D, Bertin D, Schweins R, Jestin J, Boué F (2011) Polym Chem 2:567
33. Robbes AS, Cousin F, Meneau F, Chevigny C, Gigmes D, Fresnais J, Schweins R, Jestin J (2012) Soft Matter 8:3407
34. Lenarda M, Chessa G, Moretti E, Polizzi S, Storaro L, Talon A (2006) J Mater Sci 41:6305
35. Blas H, Save M, Boissière C, Sanchez C, Charleux B (2011) Macromolecules 44:2577
36. Matsuno R, Otsuka H, Takahara A (2005) Trans Mater Res Soc Jap 30:723
37. Kobayashi M, Matsuno R, Otsuka H, Takahara A (2006) Sci Technol Adv Mater 7:617
38. Matsuno R, Otsuka H, Takahara A (2006) Soft Matter 2:415
39. Matsuno R, Yamamoto K, Otsuka H, Takahara A (2003) Chem Mater 15:3
40. Matsuno R, Yamamoto K, Otsuka H, Takahara A (2004) Macromolecules 37:2203
41. Binder WH, Gloger D, Weinstabl H, Allmaier G, Pittenauer E (2007) Macromolecules 40:3097
42. Chen Z, Yang Q, Peng K, Guo Y (2011) J Appl Polym Sci 119:3582
43. Chen F, Cai Z, Huang Y, Luo W, Chen J (2013) Polym Eng Sci 53:956
44. Long S, Wan F, Yang W, Guo H, He X, Ren J, Gao J (2013) J Appl Polym Sci 128:2687
45. Weimer MW, Chen H, Giannelis EP, Sogah DY (1999) J Am Chem Soc 121:1615
46. Mühlebach A, Nesvadba P, Rime F, Bugnon L (2008) Chimia 62:799
47. Shen Y, Wang Y, Chen J, Li H, Li Z, Li C (2010) J Appl Polym Sci 118:1198
48. Di J, Sogah DY (2006) Macromolecules 39:5052
49. Micusik M, Bonnefond A, Paulis M, Leiza JR (2012) Eur Polym J 48:896
50. Konn C, Morel F, Beyou E, Chaumont P, Bourgeat-Lami E (2007) Macromolecules 40:7464
51. Röben C, Studer A, Hemme WL, Eckert H (2010) Synlett 2010(7):1110. doi: 10.1055/s-0029-1219587
52. Mittal V (2007) J Colloid Interface Sci 314:141
53. Ghannam L, Bacou M, Garay H, Shanahan ME, François J, Billon L (2004) Polymer 45:7035
54. Ghannam L, Garay H, Shanahan MER, François J, Billon L (2005) Chem Mater 17:3837
55. Ghannam L, Garay H, Billon L (2008) Macromolecules 41:7374
56. Yukutake H, Kobayashi M, Otsuka H, Takahara A (2009) Polym J 41:555
57. Voccia S, Jérôme C, Detrembleur C, Leclere P, Gouttebaron R, Hecq M, Gilbert B, Lazzaroni R, Jérôme R (2003) Chem Mater 15:923
58. Ignatova M, Voccia S, Gilbert B, Markova N, Mercuri PS, Moreno Galleni M, Sciannamea V, Lenoir S, Cossement D, Gouttebaron R, Jérôme R, Jérôme C (2004) Langmuir 20:10718
59. Voccia S, Ignatova M, Jérôme R, Jérôme C (2006) Langmuir 22:255
60. Joubert M, Khoukh A, Tranchant J-F, Morvan F, Billon L (2009) Macromol Chem Phys 210:1544
61. Zawada K, Tomaszewski W, Megiel E (2014) RSC Adv 4:23876
62. Sill K, Emrick T (2004) Chem Mater 16:1240
63. Karousis N, Tagmatarchis N, Tasis D (2010) Chem Rev 110:5366
64. Yingkui Y, Shengqiang Q, Xianbao W, Xiaolin X (2010) Prog Chem 22:684
65. Fan D-Q, He J-P, Tang W, Xu J-T, Yang Y-L (2007) Eur Polym J 43:26

66. Zhao X-D, Fan X-H, Chen X-F, Chai C-P, Zhou Q-F (2006) J Polym Sci A Polym Chem 44:4656
67. Zhao X, Lin W, Song N, Chen X, Fan X, Zhou Q (2006) J Mater Chem 16:4619
68. Chang JH, Lee YW, Kim BG, Kim H-K, Choi IS, Paik H-J (2007) Compos Interfaces 14:493
69. Ramirez SM, Sogah DY (2006) Polymer Prepr 47:95
70. Dehonor M, Varlot-Masenelli K, Gonzalez-Montiel A, Gauthier C, Cavaille JY, Terrones H, Terrones M (2005) Chem Commun 2005(42):5349. doi: 10.1039/B510471H
71. Dehonor M, Masenelli-Varlot K, Gonzalez-Montiel A, Gauthier C, Cavaillé J-Y, Terrones M (2007) J Nanosci Nanotechnol 7:3450
72. Geim AK, Novoselov KS (2007) Nat Mater 6:183
73. Zhang Y, Tang T-T, Girit C, Hao Z, Martin MC, Zettl A, Crommie MF, Shen YR, Wang F (2009) Nature 459:820
74. Lee C, Wei X, Kysar JW, Hone J (2008) Science 321:385
75. Blake P, Brimicombe PD, Nair RR, Booth TJ, Jiang D, Schedin F, Ponomarenko LA, Morozov SV, Gleeson HF, Hill EW (2008) Nano Lett 8:1704
76. Salavagione HJ, Martinez G, Ellis G (2011) Macromol Rapid Commun 32:1771
77. Layek RK, Nandi AK (2013) Polymer 54:5087
78. García-Valdez O, Ledezma-Rodríguez R, Saldívar-Guerra E, Yate L, Moya S, Ziolo RF (2014) Polymer 55:2347
79. Hodges JC, Harikrishnan LS, Ault-Justus S (2000) J Comb Chem 2:80
80. McAlpine SR, Lindsley CW, Hodges JC, Leonard DM, Filzen GF (2001) J Comb Chem 3:1
81. Lindsley CW, Hodges JC, Filzen GF, Watson BM, Geyer AG (2000) J Comb Chem 2:550
82. Bian K, Cunningham MF (2005) J Polym Sci A Polym Chem 43:2145
83. Bian K, Cunningham M (2006) Polymer 47:5744
84. Becker ML, Liu J, Wooley KL (2003) Chem Commun 2003(2):180. doi: 10.1039/B209557B
85. Daly WH, Evenson TS, Iacono ST, Jones RW (2001) Recent developments in cellulose grafting chemistry utilizing Barton ester intermediates and nitroxide mediation. Macromol Symp 174:155–164
86. Prakanrat S, Phinyocheep P, Daniel P (2009) Appl Spectrosc 63:233

Adv Polym Sci (2016) 270: 29–76
DOI: 10.1007/12_2015_311

Published online: 20 May 2015

Surface-Initiated Atom Transfer Radical Polymerization

Amir Khabibullin, Erlita Mastan, Krzysztof Matyjaszewski, and Shiping Zhu

Abstract This review covers the basic principles of surface-initiated atom transfer radical polymerization (SI-ATRP). SI-ATRP is a robust and versatile method for preparation of various hybrid materials with controlled molecular characteristics of the tethered polymer chains, such as polymer composition and architecture. Various aspects of SI-ATRP, such as polymer brush grafting density, surface geometry, and reaction conditions, including structure of initiator, ligand, and catalyst, are important for engineering the structure and properties of the hybrid polymer materials. Elementary reactions, such as initiation, propagation, termination, transfer, and activation/deactivation equilibria as well as factors affecting these processes are discussed. The properties of materials prepared by SI-ATRP are illustrated through several selected examples.

Keywords Controlled radical polymerization · Elementary reactions · Mechanism · Grafting density · Surface geometry

Contents

A. Khabibullin and K. Matyjaszewski (✉)
Department of Chemistry, Carnegie Mellon University, Pittsburgh, PA 15213, USA
e-mail: km3b@andrew.cmu.edu

E. Mastan and S. Zhu (✉)
Department of Chemical Engineering, McMaster University, 1280 Main Street West, Hamilton, ON, Canada, L8S 4L7
e-mail: zhuship@mcmaster.ca

1 ATRP Fundamentals

Controlled radical polymerization (CRP, also termed reversible-deactivation radical polymerization, RDRP) is a versatile method for the preparation of well-defined polymers [1]. Unlike conventional radical polymerization with its slow continuous initiation, fast propagation, and inevitable radical termination, CRP creates and exploits a dynamic equilibrium between growing radicals and dormant species [2]. In this system, the active radicals are deactivated after adding one or several monomer units and converted back to the dormant state. This approach allows preparation of polymers with precise control over molecular weight (MW), molecular weight distribution (MWD), polymer composition, topology, and functionality.

Atom transfer radical polymerization (ATRP) is one of the most robust and widely used CRP techniques for polymerization of a broad range of commercially available functional monomers [3–5]. It is attractive because of the simple experimental setup, with readily available initiators and catalysts that can be used in a range of solvents under a broad spectrum of reaction conditions, allowing precise control over final polymer MW and architecture [6].

In ATRP, the dormant species are either low MW initiating alkyl halides or a macromolecular species (P_n-X). The dormant species intermittently react with activators and deactivators. Activators are, typically, ligand-stabilized transition metal complexes in their lower oxidation states (M^m/L), that react with the dormant species to form active radicals ($P_n^{\bullet}$). Deactivators are usually transition metal complexes in their higher oxidation state, coordinated with the transferred halide ligands (X-M^{m+1}/L). After adding a few monomer units, the growing radical then reacts with a deactivator to re-form a dormant species and regenerate the activator. Radicals also terminate, as in any radical polymerization. Scheme 1 illustrates a typical ATRP equilibrium.

Scheme 1 ATRP equilibrium

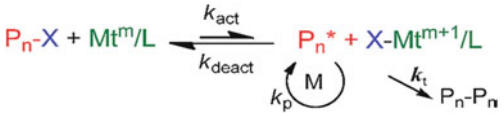

The rate of ATRP (R_p) depends on the propagation rate constant (k_p) and on the concentrations of monomer and growing radical. The concentration of the growing radical depends on the ATRP equilibrium constant, as well as on the concentrations of the dormant species, activators, and deactivators, as shown in the ATRP rate equation given below. The equilibrium constant K_{ATRP} is equal to k_{act}/k_{deact} and depends on the strength of both the C–X and the Cu^{II}–X bonds. The equilibrium constant increases with the strength of the Cu^{II}–X bonds, or the halogenophilicity of the Cu^{I} complex, and decreases with the strength of the C–X bonds.

$$R_p = k_p[M]\left[P_n^*\right] = k_p K_{ATRP}\left(\frac{[P_nX][Cu^IL][M]}{[X\text{-}Cu^{II}L]}\right) \quad \text{(ATRP equation)}$$

ATRP is a catalytic process and can be mediated by many redox-active transition metal complexes. The most frequently used metal is Cu; however, ATRP has also been successfully carried out using Ru, Fe, Mo, Os, etc. [7]. The key limitation of "normal" ATRP (as it was initially defined) is the large amount of catalyst loading (up to ca. 1 mol%) compared with monomer. This residual metal creates difficulties in purification of the final product [8]. Also, in ATRP, as in any radical process, radical termination occurs but involves only about 1–10% of all chains. Radical termination leads to irreversible transformation of a fraction of the activator to deactivator, leading to a decrease in the reaction rate.

However, according to the equation given above, the ATRP rate does not depend on the absolute catalyst concentration, but rather on the ratio of the concentrations of activator and deactivator. Several novel ATRP techniques have been developed exploiting this feature, eliminating the problem of high catalyst loading and a slowdown in the rate of polymerization as a result of radical termination [9]. These novel low catalyst concentration procedures include activators regenerated by electron transfer (ARGET)-ATRP [10], initiators for continuous activator regeneration (ICAR)-ATRP [11], supplemental activator and reducing agent (SARA)-ATRP [12–14], photochemically mediated ATRP [15–19], and eATRP, where the activator/deactivator ratio is controlled electrochemically [20–22]. These recent developments are summarized in Scheme 2, which also summarizes the possibilities for engineering macromolecular architecture provided by ATRP, as well as a few of the targeted applications for the resulting materials [23].

The appropriate choice of initiator and ligand and their amounts are important for preparation of the desired product in a controlled manner [24–26]. The selected alkyl halide initiators should possess sufficient reactivity for efficient initiation of polymerization of the selected monomers, which correspondingly depends on the structure of the alkyl group and the transferable halogen or pseudohalogen [27]. The reactivities of the halides follow the order tertiary > secondary > primary carbon atom, according to the change in bond dissociation energy needed for

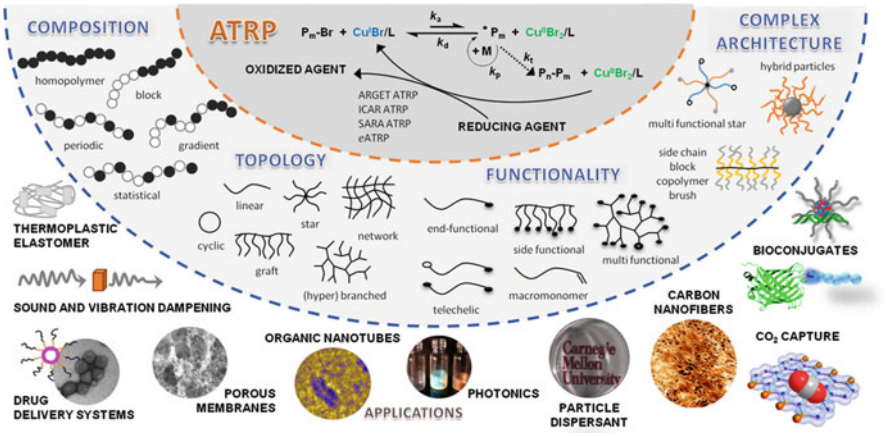

Scheme 2 Overview of recent advances in ATRP that allow a reduction in catalyst loading, down to part per million levels, and engineering of macromolecular architecture. Applications for some of the resulting materials are shown. Reprinted with permission from Matyjaszewski and Tsarevsky [23]

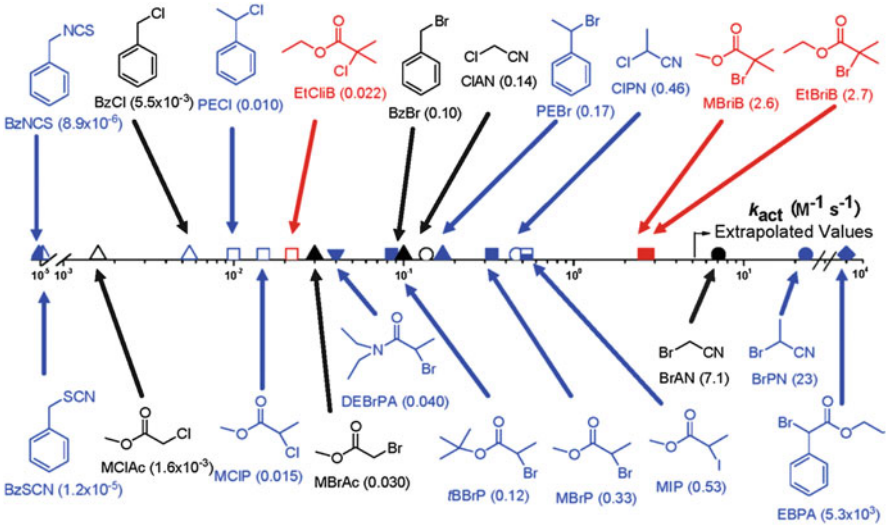

Scheme 3 ATRP activation rate constants for various initiators with $Cu^{I}X$/PMDETA (where X=Br or Cl) in MeCN at 35°C. 3° initiators are in *red*; 2° *blue*; 1° *black*; with isothiocyanate/thiocyanate *half-filled triangle*; chloride *open symbols*; bromide *filled symbols*; iodide *half-filled square*; amide ▼; benzyl ▲; ester □; nitrile ○; phenyl ester ◇. Reprinted with permission from Tang and Matyjaszewski [27]

homolytic bond cleavage. Also, the reactivities of alkyl halides follow the order I ~ Br > Cl and are higher than the reactivity of alkyl pseudohalides. The ATRP activation rate constants for various initiators are shown in Scheme 3

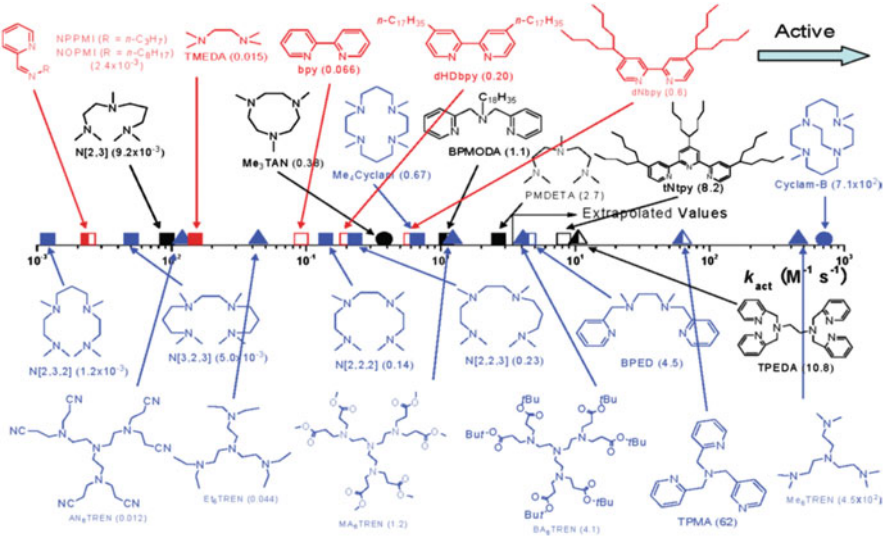

Scheme 4 ATRP activation rate constants for various ligands with EtBriB in the presence of CuIBr in MeCN at 35°C. Compounds with two nitrogen atoms (N2) *red*; N3 *black*; N4 *blue*; amine/imine *filled symbols*; pyridine *open symbols*; mixed *left-half filled symbols*; linear □; branched ▲; cyclic ○. Reprinted with permission from Tang and Matyjaszewski [29]

The effect of the selected ligand on the ATRP rate constant is profound, and the range of activity of the formed copper-based ATRP catalyst complexes covers six orders of magnitude [26, 28, 29]. Generally, Cu complex activity in ATRP for ligands follows the order tetradentate (cyclic-bridged) > tetradentate (branched) > tetradentate (cyclic) > tridentate > tetradentate (linear) > bidentate. The activity of ligands for ATRP also depends on the nature of the nitrogen atom and follows the order aliphatic amine > imine > aromatic amine. Steric effects are also very important. The ATRP activation rate constants for Cu complexes with various ligands are shown in Scheme 4.

There are several other factors in ATRP that affect polymerization control and properties of the final product in addition to choice of initiator and ligand. The polymerization media plays a significant role in the process. ATRP can be conducted in bulk, solution, or in a variety of heterogeneous media including microemulsions, miniemulsions, emulsions, suspensions, dispersions, and inverse miniemulsions. The choice of media primarily depends on solubility or heat transfer considerations; for example, conditions have to be selected so that the catalyst complex and the product are at least partially soluble in the reaction medium. ATRP is strongly accelerated in the presence of more polar solvents [30], and at higher temperatures [31] and pressures [32].

Surface-initiated ATRP (SI-ATRP) follows the same mechanism and is controlled by the same factors as a regular ATRP; however, there are several unique requirements, which are discussed in detail in Sect. 4.

2 Hybrid Materials

Hybrid materials consist of two or more disparate components connected at molecular level, most often by covalent bonds. Typical hybrid systems are formed by attaching organic polymers to an inorganic substrate (organic/inorganic hybrids), linking synthetic polymers to natural products, or combining polymer fragments prepared by different polymerization techniques. Hybrid materials represent a rapidly growing area of molecularly designed materials, and ATRP has contributed significantly to its development. Polymers synthesized using ATRP can provide important desired properties to hybrid materials, including solubility in different phases of a biphasic system, responsiveness to stimuli, functionality, and mechanical strength.

The three widely used methods used to create hybrid materials containing polymer segments are grafting-from, grafting-onto, and grafting-through. Another method for hybrid material synthesis was introduced recently, the template approach.

2.1 "Grafting From" Approach

The grafting-from approach provides a versatile and efficient tool for creating functional hybrid materials. It includes surface-initiated CRP (SI-CRP) and, particularly, SI-ATRP, which is widely used to graft polymers from substrate surfaces [33, 34]. The advantages of the grafting-from approach using ATRP include a high level of control over polymer graft architecture and grafting density, as well its applicability to various substrate surface geometries (flat surfaces, nanoparticles, inside the pores, etc.) and compositions, including metals and metal oxides, silicon, organic polymers, and natural products. Ultimately, (co)polymers with a very high graft density form polymeric brushes [35].

The key requirement for the grafting-from approach is the presence of polymerization initiators that are covalently attached and evenly distributed throughout the substrate surface. The polymer chains are then grown from the surface of the substrate. The initiator can either be an inherent part of the substrate (e.g., some polymers carrying functional groups) or can be introduced to the substrate surface via an additional surface functionalization reaction. One can precisely control the grafting density and, if desired, introduce densely grafted brushes to the surface. Scheme 5 illustrates the grafting-from approach using SI-ATRP.

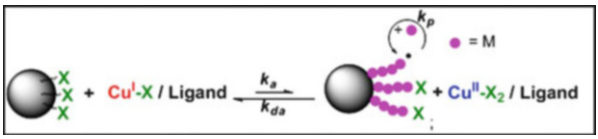

Scheme 5 Grafting-from approach employed to introduce polymer brushes onto the surface of a nanoparticle via SI-ATRP

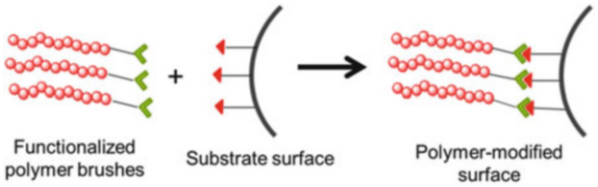

Scheme 6 Grafting-onto approach using "click" chemistry

2.2 *"Grafting-Onto" Approach*

In this method, one needs to prepare polymer chains with end-functional groups and then covalently link the polymer chains to the substrate surface. The substrate surface should have corresponding complementary functional groups, which can either be an inherent part of the substrate, for instance, the hydroxyl groups on the surface of metal oxides, or can be introduced separately. However, this method is often limited by steric hindrance and slow diffusion of bulk polymer chains to the substrate surface [36]. Although this high-yield grafting-onto method gained increased attention with the development of "click" chemistry, which allows fast and quantitative linking of functionalized chains to corresponding surface functional groups via Cu-catalyzed reaction between alkynes and azides [37, 38], the grafting density is much lower than that attained in grafting-from procedures as a result of steric crowding and entropic effects.

Scheme 6 illustrates the grafting-onto approach using click chemistry.

2.3 *"Grafting-Through" Approach*

In order to utilize the grafting-through approach, the substrate first needs to be modified with a polymerizable monomer unit, thus becoming a hybrid "macromonomer." The macromonomer is then copolymerized with low molecular weight monomers to form a polymer chain with "sewed" substrate moieties. This method is illustrated in Scheme 7.

This method permits preparation of hybrid materials using macromonomers that can be inorganic, natural products, or other polymers, either prepared by CRP or any other polymerization technique. The grafting density and number of grafted chains depend on the ratio of the concentrations of monomer and macromonomer

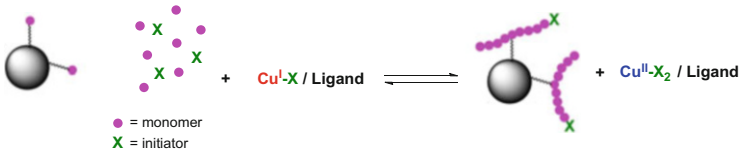

Scheme 7 Grafting-through approach for introduction of polymer brushes to the surface of nanoparticles using ATRP

but are generally much lower than obtained using grafting-onto or grafting-from procedures.

2.4 Templated Approach

Inorganic particles (spheres and cylinders) are often prepared using surfactants that form templating micelles [39–42]. Polymer chemistry provides an easy approach for preparation of unimolecular micelles of predefined structure such as molecular brushes [43–45] or stars [46, 47], which can serve as templates for the preparation of silica [39, 40], titania [48, 49], or gold [41, 42] nanoparticles. The polymer templating approach can also be used for preparation of ordered honeycomb structures of Pd and other heavy metals [50]. The emerging templating techniques use core–shell brushes [40] or star-like block copolymers [51] as nanoreactors, providing facile and versatile tools for synthesis of well-defined nanocrystals with uniform controlled size, composition, and architecture.

For example, Scheme 8 summarizes the strategy for the preparation of silica nanowires using a polymer brush template approach. First, a poly (3-acryloylpropyltrimethoxysilane) (APTS) block was grafted from linear multifunctional initiator, that is, a linear polymer backbone carrying ATRP initiating sites. Each APTS block was then chain-extended with an oligo(ethylene glycol) methacrylate (OEGMA) block, thus creating a cylindrical polymer brush with a cylindrical APTS core and an OEGMA shell. The APTS core block was then crosslinked, forming a hybrid organo-silica nanowire. The hybrid nanowire can be further transformed to a fully inorganic silica nanowire via pyrolysis of the organic segment at 700°C.

The star-polymer template approach allows preparation of spherical nanocrystals. In the initial step, a star-like block copolymer nanoreactor was prepared, with a polyacrylic acid (PAA) inner block and an outer block of polystyrene. Then, the inner PAA block was infiltrated with the precursor for preparation of the desired nanoparticles. Finally, the precursor is transformed into the nanoparticle inside the star-polymer template, resulting in formation of uniform well-defined nanocrystals. By using a star-like triblock copolymer template, core–shell and hollow nanocrystals can be prepared following similar strategies (Scheme 9).

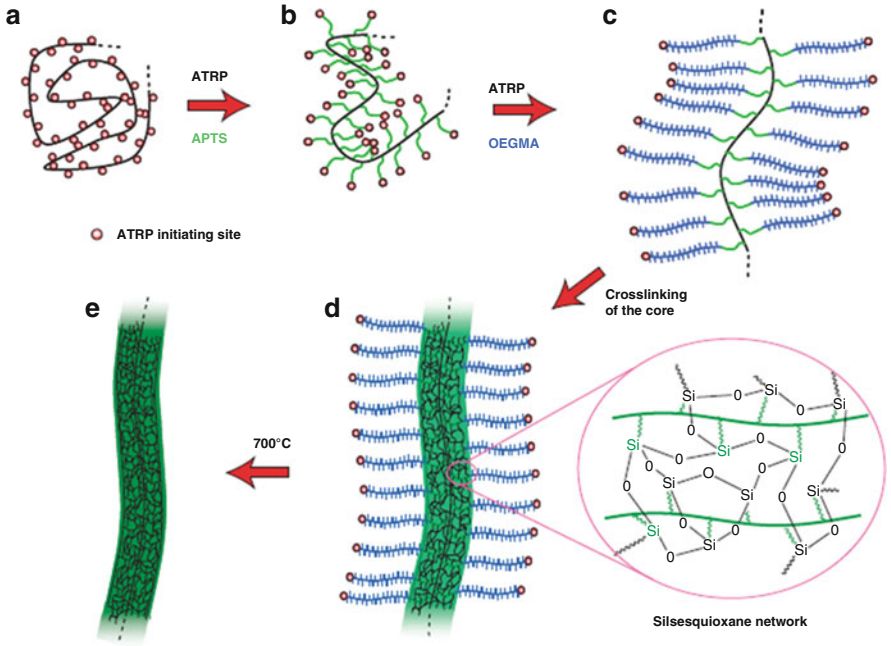

Scheme 8 Synthesis of a silica nanowire using the polymer brush template approach. (**a**) ATRP multi-initiator poly[2-(2-bromoisobutyryloxy)ethyl methacrylate] (PBIEM) with degree of polymerization of 3,200; (**b**) cylindrical polymer brush (CPB) with side chains of 20 APTS units; (**c**) core–shell CPB with an additional 57 OEGMA units; (**d**) soluble organo-silica hybrid nanowires with a crosslinked silsesquioxane network in the core; (**e**) inorganic silica nanowires after pyrolysis. Reprinted with permission from Yuan et al. [40]

Depending on the precursor used, the resulting nanocrystals can provide different functionalities (e.g., they can be metallic, magnetic, semiconductor, or fluorescent).

3 SI-ATRP

3.1 Selection of Surface Geometry

SI-ATRP can be carried out on wide variety of surfaces, including flat surfaces, nanoparticles, cylindrical surfaces, or on the surface inside nanopores. The presence of ATRP initiator is the only requirement for successful introduction of polymer brushes via SI-ATRP. However, the choice of surface geometry can influence the parameters controlling the architecture of the grafted polymer brushes. For example, the grafting density for polymer brushes on a flat surface is usually below 0.5 chain/nm^2, whereas convex systems, such as functionalized nanoparticles, can have a significantly higher grafting density, approaching 1 chain/nm^2. However,

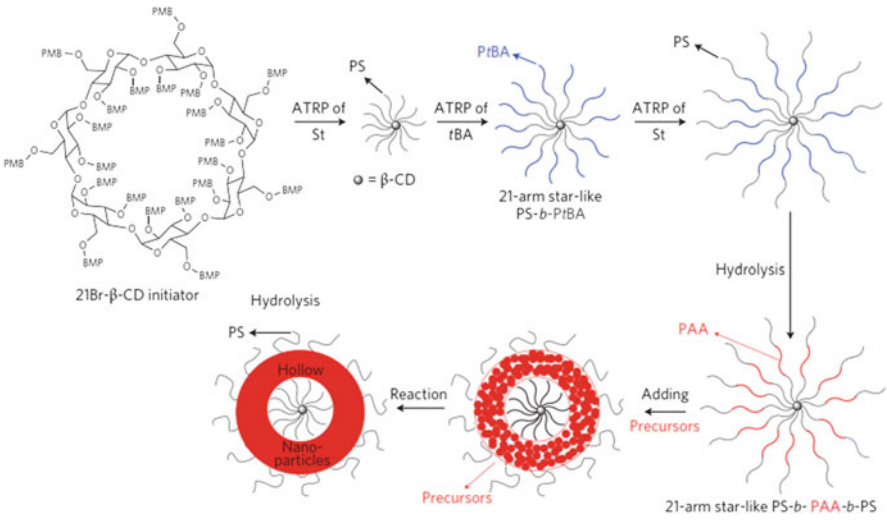

Scheme 9 Synthesis of hollow hybrid nanoparticles using the star-polymer template approach. Reprinted with permission from Pang et al. [51]

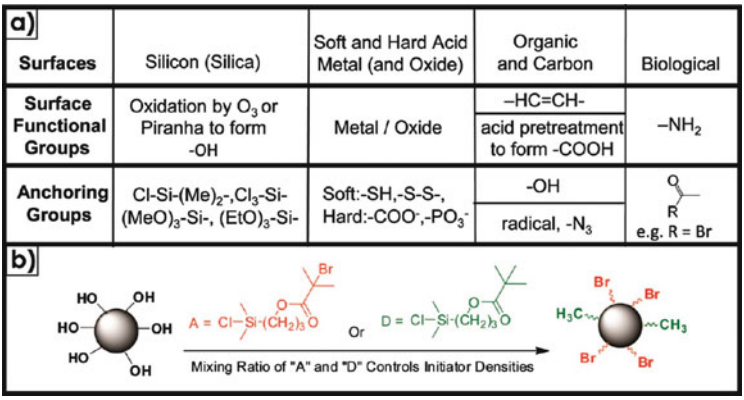

Scheme 10 (**a**) Examples of functional groups for modification of various surfaces. (**b**) Strategy for controlling grafting density using the active/inactive initiator approach. Reprinted with permission from Hui et al. [34]

such systems are prone to macroscopic gelation, even at only 0.1% of interparticle radical termination. In concave systems (e.g., inside cylindrical or spherical pores), steric hindrance plays a significant role, reducing the level of control over polymer brush MW and MWD. However, in some systems good control was reported [52]. Details of the effect of surface geometry on grafting polymers via SI-ATRP are discussed further in Sect. 4.

3.2 Selection of Substrate

A suitable substrate material can be selected depending on the desired application of the final functional material. SI-ATRP allows growth of polymer chains from the surface of metals, metal oxides, silicon, quantum dots, and a variety of organic polymers and biological species. The only requirement is that the initiator moieties are covalently attached to each substrate via the corresponding anchoring groups. Scheme 10a shows examples of anchoring groups for different substrate materials.

3.3 Advantages of SI-ATRP

The versatility of SI-ATRP as a method for grafting polymer brushes from the selected surface arises from the ability to precisely control and modulate the structure and properties of prepared hybrid material.

Control over grafting density is essential for regulation of the number of polymer brushes on the surface. This can be achieved by using a mixture of active and inactive ("dummy") initiators to functionalize the substrate surface. The number of active ATRP initiators, and thus the number of polymer chains on the surface, is varied by controlling the corresponding fraction of active initiators in the mixture. Scheme 10b illustrates this strategy.

Another approach for controlling grafting density is partial removal of tethered initiators from the surface by specific treatment (UV light, temperature, chemical).

The ability to control the chain topology and composition of polymer brushes is a major tool for engineering the structure and properties of the resulting hybrid materials prepared using SI-ATRP. This technique allows the grafting of (co) polymer, block, gradient, and statistical copolymer brushes from the surface of various substrates [33, 34]. The brushes can have different topologies, including linear, branched, hyperbranched, and crosslinked chains [53, 54]. Miktoarm hybrid systems can be created by introducing two different polymer chains to the substrate surface using SI-ATRP [55–57] or SI-ATRP combined with other polymerization techniques [58]. These materials are responsive to solvent change and can be turned into Janus nanoparticles by variation of solvent composition [56].

The polymer brush MWD can be controlled by varying the ratio of activator to deactivator. ATRP allows preparation of polymers with very low dispersity; however, sometimes a broad MWD or even bimodal distribution of polymer brushes is desired [59].

SI-ATRP facilitates preparation of functional polymer brushes. Functional groups can either be an inherent part of the monomer molecule, thus being present along the polymer backbone, or can be introduced to previously prepared polymer chains. Chain-end functional groups can be converted into other functional groups and provide an opportunity for conducting click chemistry to the brush end.

Functional polymer brushes can provide stimuli-responsive properties, as well as providing transport and targeting properties, ion conductivity, etc.

4 Reactions in SI-ATRP

In this section, the basic reactions involved in SI-ATRP are discussed, namely initiation, propagation, termination, transfer, equilibrium, and other reactions. Most of the section is further divided on the basis of the curvature of the substrate.

4.1 Initiation

The surface properties introduced by the grafted layer depend on how long the chains are and how crowded the surface is (i.e., the polymer chain length and its grafting density). Grafted chain length can be easily controlled using ATRP. On the other hand, predicting and tailoring the surface to possess a certain grafting density remains one of the major challenges in SI-ATRP. This is because all of the factors affecting grafting density are not fully understood.

On a flat substrate, the measurement of grafting density is challenging because of the limited amount of grafted polymers. In order to estimate the grafting density, it is either assumed that grafted chains have the same properties as free chains when polymerization is conducted simultaneously in both phases [55, 60–63], or that an accurate relationship between swollen and dry thicknesses of polymer layer is known [64]. For systems having large surface-to-volume ratios (e.g., nanoparticles), polymers can be cleaved from the substrate and characterized to give an estimate of grafting density, after the experiments are conducted.

The polymer grafting density is strongly related to the initiator density, which can be controlled by varying the initiator concentration and immobilization time, or by introducing an inert analog along with the initiator species [65–72]. The inert molecules, or spacers, are usually chosen to have a structure similar to the initiator moieties, but do not possess the transferable group for initiating ATRP. The similar chemical structure of spacer and initiator allows the assumption of similar chemical reactivity with the surface of the substrate. Therefore, the fraction of initiator spacer used during immobilization is generally assumed to be the same as the fraction immobilized on the substrate. However, prediction of how many immobilized initiators grow into polymer chains (i.e., grafting efficiency) still cannot be made.

The terms “grafting efficiency” and “initiation efficiency” are used interchangeably in the literature, mainly referring to how many of the tethered initiator sites successfully grow into polymer chains. There are two ways to calculate the initiation efficiency from experimental data. The first is by directly considering the ratio of the polymer grafting density to the initiator density [73–76]. The second is by comparing the theoretical molecular weight to the molecular weight measured from cleaved polymer chains [77–79]. These two methods should theoretically represent

the same value. Lower initiation efficiency is usually obtained at high initiator density, but increases with reduced initiator density up to the point where the efficiency becomes independent of the initiator density [65–67, 76]. This is because steric hindrance dictates the maximum concentration of polymer chains that can be grafted onto a substrate.

Apart from the initiator density, the types of monomer and initiator can affect initiation efficiency [63, 80, 81]. The type of catalyst could indirectly affect the initiation efficiency, as shown by a study of aqueous SI-ATRP of methyl methacrylate (MMA) [74]. The SI-ATRP system with CuCl as catalyst showed slower polymerization rate but better controllability and higher initiator efficiency than the system with CuBr. The difference in initiation efficiency observed was thought to be caused by the difference in polymerization rate, whereby faster polymerization leads to a decrease in initiator efficiency. In addition, a difference in polymerization rate as a result of a difference in catalyst-to-deactivator ratio has also been shown to affect the resulting grafting density [82]. Solvent type is another factor that could influence the grafting density. When SI-ATRP of OEGMA is conducted in a more polar solvent, the resulting grafting density is lower because of the bulkier tethered polymer coils in that system, which imposed steric hindrance for the other initiation sites [61].

The length and phobicity of the link between the initiator and solid surface can also affect the initiation efficiency, as studied by Green and coworkers for SI-ATRP of MMA and of styrene from silica nanoparticles [74, 75]. In the MMA system, their experimental results showed a monotonous increase in grafting density and initiation efficiency with longer initiator linkers, as a result of the increased hydrophobicity of the longer spacer. On the other hand, the system utilizing styrene as monomer showed little difference between shortest and longest linker, as each led to a similar grafting density of 0.7–0.8 chains/nm^2, with an initiation efficiency of 26–35%. However, the system with the middle-length link resulted in a much lower grafting density of 0.2 chains/nm^2, with initiation efficiency around 10%. This difference was postulated to be caused by conformational change, in which the Br end group is hidden in the case of middle-length linker. Comparison of the initiation efficiency between the two studies is shown in Fig. 1.

Surface curvature plays an important role in determining initiation efficiency. The initiation efficiency of SI-ATRP from a flat substrate has been estimated to be around 10% [83–85]. On the other hand, the initiation efficiency that could be obtained from a convex substrate is close to, or even more than, 30% [73–76, 79, 86]. Even higher initiation efficiency values of approximately 80% for particles have also been reported in several studies [77, 78, 87]. In particle systems, some studies have reported a constant increase in initiation efficiency with time [73, 75], whereas others reported it to increase as polymerization progresses to higher conversion [77, 78, 86]. This again shows the uncertainty in predicting initiation efficiency.

Some studies have reported an initiation efficiency of 3–8.5% for concave substrates within ordered mesoporous silica nanoparticles, with mesopore diameter ranging from 1.8 to 2.3 nm [88, 89]. Another study reported 22–37% initiation efficiency when SI-ATRP was conducted in ordered mesoporous silica with 15 nm

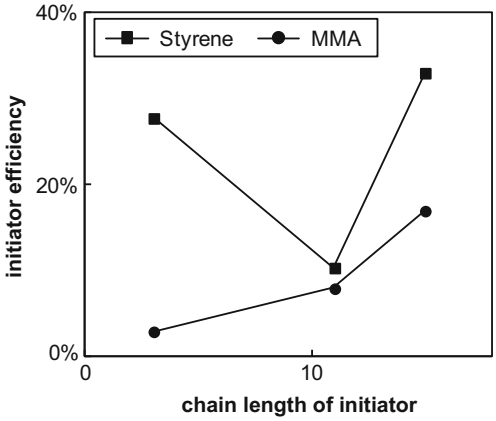

Fig. 1 Effect of initiator spacer length on the initiation efficiency of SI-ATRP of styrene and MMA with CuBr. Detailed experimental conditions can be found in the original publications [74, 75]

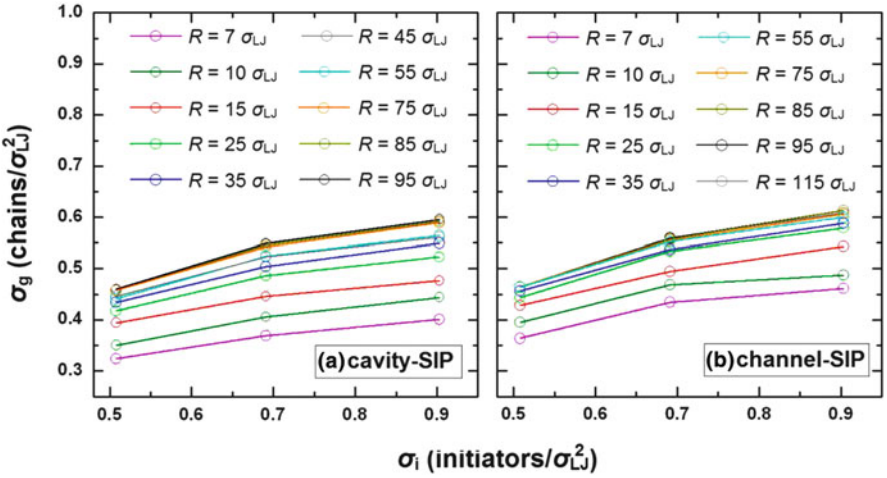

Fig. 2 Effect of confinement on grafting efficiency (σ_g/σ_i), as simulated for surface-initiated polymerization within a spherical cavity or channel with various curvatures; R radius of the cavity. Reprinted with permission from Liu et al. [90]

cylindrical pores [52]. These experimental results point to the conclusion that concave systems, with more severe confinement effects, exhibit lower initiation efficiency. This comparison might of course be influenced by the other factors mentioned above, because they are collected from experiments conducted under different conditions. However, similar findings have been reported in a simulation study of grafting from concave substrate with a "perfectly living" polymerization [90]. As shown in Fig. 2, the simulation results predicted lower grafting density, σ_g, in systems with higher curvature (smaller R), for the same initiator density, σ_i.

It should be noted that in an experimental setting, the dependence of initiator density on the curvature and the influence of termination reactions may further complicate the actual result.

4.2 Propagation

Despite the numerous studies conducted using SI-ATRP, there are several fundamental points that still cannot be definitively answered. For example, what causes the grafted layer to stop growing, even when there is an abundance of monomer in the solution phase? Another fundamental question is related to the validity of assuming grafted and free chains to have comparable properties [68, 91–93]. This assumption is especially important as it is commonly made for graft polymerization on flat substrates, because it allows estimation of the grafting density of the polymer chains even when the amount of polymer collected from flat substrates is not enough for further characterization.

On the other hand, nanoparticle systems have a much larger surface-to-volume ratio than flat systems, allowing a sufficient amount of polymer to be collected for further characterization. Therefore, the assumption can be experimentally verified for these systems. As a matter of fact, much of the data on polymers obtained from SI-ATRP conducted on particle systems show an excellent agreement with the properties of polymers formed in the solution phase [36]. However, this does not guarantee the same trend for polymers grown from flat substrates, because the degree of confinement on polymer chains grown from a convex substrate is less severe than that on a flat substrate. Owing to its positive curvature, polymers grown on convex substrates experience less and less confinement as the chain grows longer and the initiation site is farther away from the surface.

In SI-ATRP from a flat surface, one end of each individual polymer chain is fixed onto a substrate. This forces the polymer chains to grow in close proximity to one another, creating crowding of polymer chains and forcing them to assume a chain-extended brush conformation. The brush conformation is evident from the greater thickness of the grafted polymer layer on a flat substrate than the radius of gyration of the free polymer. The calculation of grafting density shows that each polymer chain occupies a smaller projected area than that predicted by its radius of gyration, further confirming the chain-extended brush conformation.

The steric crowding of polymer chains gives rise to unique properties not seen in grafted polymers with lower grafting density [36, 94]. However, the crowding of surface polymer chains can also lead to starvation of monomer, or earlier formation of a glassy state, which in turn hinders the propagation of additional surface chains. Moreover, some of the surface chains could have their active ends buried inside the dense polymer layer, thereby reducing the available monomer concentration for that radical to propagate. This is one of the two theories often used to explain many experimental trends in the literature, often referred to as the “school of propagation” because of the decrease in propagation rate. The other school of thought, referred to

as the "school of termination," is discussed in Sect.4.3. A recent publication has collected experiment data and compared predictions based on these two schools of thought [95]. The result is inconclusive, as no model can fully explain the various contradicting experimental trends reported in the literature.

Based on the reduced rate of propagation, one could explain the slowing down of the growth rate for grafted chains at negligible monomer conversion. This school of thought could also shed light on when the assumption of equal properties of free and grafted chains can be considered valid. As a result of the difference in the availability of monomer for the chains solution and for the tethered surface chains, the chain length and dispersity of the two polymer populations may not be comparable. The reduction in the concentration of available monomers for the grafted chains is expected to result in chains that are shorter than the free chains in solution.

Recent simulation studies based on the understanding of the school of propagation have shown that the assumption of equal properties of grafted and free polymers is often invalid in a perfectly living polymerization [92, 93]. Simulation results show that the grafted polymers are always shorter and have broader distribution than their solution counterparts when polymerization is conducted simultaneously from a surface and in solution. The difference depends on the fraction of polymers present as grafted chains, η, and on the grafting density, σ, as shown by Fig. 3. Higher grafting density leads to more confinement and reduced propagation rate as a result of monomer limitations, resulting in shorter grafted chains. On the other hand, a lower fraction of congested surface chains leads to less difference in properties between surface and free chains. Therefore, the assumption of surface chains having similar properties to free chains is true only when the surface chains exhibit low grafting density, which is not usually the case in experimental settings. However, it should be noted that some experimental studies of SI-ATRP on flat surfaces have reported controlled growth to a very thick polymer brush, for example, 700 nm of poly(hydroxyethyl methacrylate) (PHEMA) brush on a gold surface [96] and 700 nm of poly(dimethylaminoethyl methacrylate) (PDMAEMA) on a silicon surface [97].

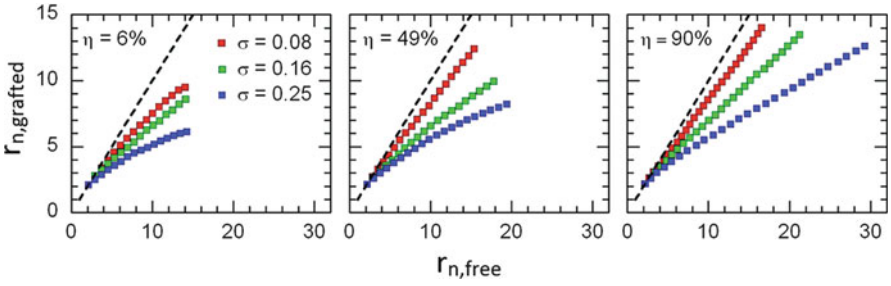

Fig. 3 Model predictions of the chain length of grafted and free polymers in simultaneous surface-initiated polymerization with various grafting densities (σ) and fractions of grafted polymer (η). Reprinted with permission from Turgman-Cohen and Genzer [93]

For systems with concave substrates, the effect of confinement is expected to be even more severe than that for flat substrates. A theoretical study based on molecular dynamics simulations has systematically investigated surface-initiated living polymerization on concave substrates for polymerization occurring strictly on the surface [90]. The simulation results verified the confinement effect on the grafted polymer: shorter chains are obtained in systems with higher degrees of confinement (i.e., smaller surface radius). However, the results are counter-intuitive for the dispersity, where the resulting grafted polymers have narrower distribution with increasing confinement for the same amount of reaction time or at the same monomer conversion. This trend is attributed to the slower polymerization rate in a more confined system, which leads to more uniform growth. It should be noted that the simulation was conducted in the absence of termination reactions, which could significantly affect the resulting dispersity in an experimental setting.

4.3 Termination

Termination is unavoidable in ATRP systems because of the very nature of radicals. Termination in SI-ATRP is highly dependent on the geometry of the substrates. For example, the confined environment of concave substrate leads to closer proximity of polymer chains, which could lead to higher possibility of termination. On flat or convex substrates, the termination could occur via multiple modes. The modes of termination and experimental data supporting the role of termination in kinetics of SI-ATRP are discussed in the following sections.

4.3.1 Termination on Flat Substrates

The termination of living chains during SI-ATRP could offer an explanation for some of the experimentally observed phenomena. For example, termination provides plausible explanation for the experimentally observed decrease in the growth rate of the grafted polymer layer, even when no significant monomer depletion is expected in the bulk contacting solution. This experimental trend has been repeatedly reported in the literature for various types of substrates and monomers [60, 98–100], and has also been supported by an experimentally measured decrease in the concentration of halide groups on the surface [101].

On flat substrates, the possible termination modes depend on the polymerization locus. For SI-ATRP accompanied by simultaneous polymerization in the contacting solution, termination could occur between two surface radicals, two solution radicals, or between a surface and a solution radical. On the other hand, the termination could only occur between two surface radicals for surface-confined SI-ATRP. These possible termination modes are illustrated in Fig. 4.

Termination modes between two solution radicals and between solution and surface radicals are easily imaginable, because at least one of the participants is a mobile free chain. On the other hand, it is harder to picture how two randomly

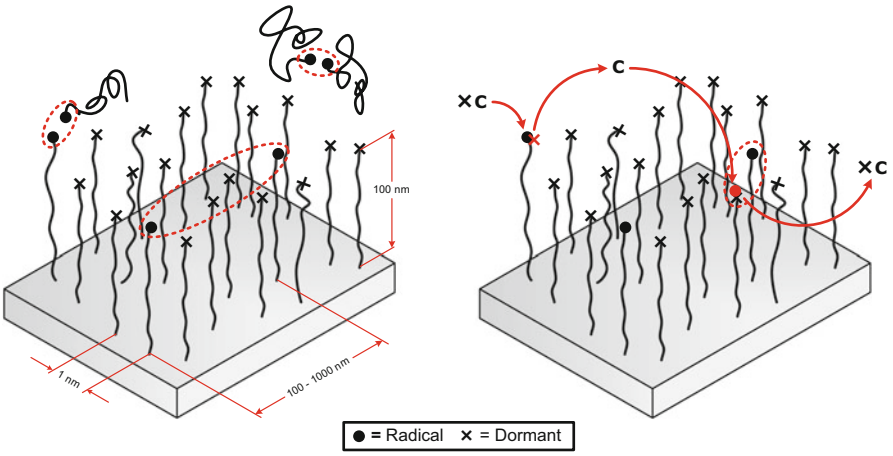

Fig. 4 *Left*: Possible termination modes involved in SI-ATRP on a flat substrate. The estimated distances shown are calculated based on the assumption of high grafting density (1 chain/nm^2), a typical ratio of radical to dormant chains in ATRP ([P$^\bullet$]/[PX] = 10^{-4} to 10^{-6}), and typical brush thickness of 100 nm. *Right*: Migration of surface radicals through activation/deactivation in SI-ATRP promotes termination between surface radicals. Reprinted with permission from Zhou et al. [102]

formed radicals that are fixed to a substrate can reach each other to undergo termination, especially if they are located far from one another. As discussed in the section on propagation (Sect. 4.2), with one end of the polymer chain fixed onto a substrate, the polymer chain cannot move as freely as chains in solution, even though the local concentration of polymer chains is much higher as a result of crowding. Only a very small portion of the chains have active ends at any instant, with most of the chains being capped and dormant. In fact, as demonstrated by Zhou et al., estimation of the distance between radicals on a highly grafted flat substrate indicates that termination between two surface radicals is highly improbable, as denoted in Fig. 4a [102]. It is hard to picture how two surface-constrained radicals can reach each other for termination to occur.

Gao and colleagues proposed a mechanism by which two radical centers that are originally present on surface chains that are far apart could have a high probability of "hopping" to other fixed chains on the substrate [91, 102]. Although the chains do not move because of their attachment to the surface, the active (radical) ends could move as a result of the activation/deactivation involved in the basic ATRP mechanism. Faster migration of active centers from one chain to another, resulting from more frequent activation/deactivation of surface chains, could increase the probability of two radicals being adjacent to one another, as illustrated in Fig. 4b. Therefore, the termination rate is proposed to be proportional to the migration rate, which in turn depends on the rate of activation/deactivation, as shown by Eq. (1) [102].

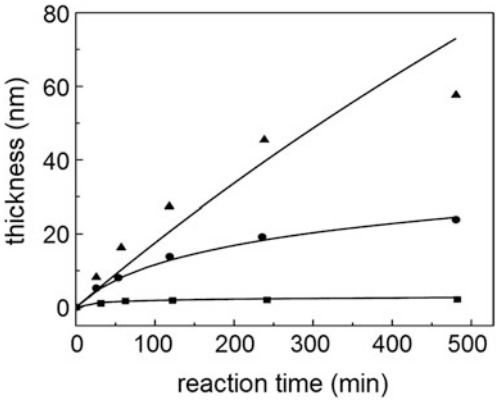

Fig. 5 Growth kinetics of grafted polymer for different catalyst concentrations in SI-ATRP of methyl acrylate (MA) from gold substrate, with [MA] = 2 M and [$CuBr_2$/Me6TREN]/[CuCl/Me_6TREN] = 0.3. *Lines* show the predicted result from the model. *Data points* were experimentally obtained: *squares* 40 mM, *circles* 2 mM, *triangles* 0.1 mM [102, 103]

$$k_t \propto \text{migration rate} \propto [C]_{sol} \tag{1}$$

For SI-ATRP, a constant ratio of catalyst to deactivator is supposed to imply a constant polymerization rate. This is because only a small amount of polymer chains are present on the surface and therefore do not affect the catalyst-to-deactivator ratio throughout the polymerization medium. However, experimental data have shown that an increase in catalyst concentration can result in a faster leveling-off of the growth rate [103]. This concept of migration-assisted termination has been used to explain the experimental data, where a decrease in growth rate of surface chains is observed with increasing catalyst concentration at a constant ratio of catalyst to deactivator, as shown in Fig. 5.

Another possible explanation for the trend observed in Fig. 5 is the recently proposed mechanism of catalytic radical termination in solution ATRP [104]. The proposed termination mechanism for solution ATRP might also be applicable for SI-ATRP. According to that mechanism, the presence of catalyst can increase the amount of termination, which contributes to the observed decrease in growth rate. Another factor to be considered is the possibility that the resulting grafting density is affected by different concentrations of catalyst. However, as mentioned previously, the grafting density is not known a priori, nor can it be measured accurately for a flat substrate.

The termination rate constant has also been proposed to depend on the grafting density (σ) according to Eq. (2), from comparison of the model-predicted thickness with experimental data [102]. The exponential decrease in termination rate constant (k_t) as grafting density increases could be a result of conformational change of the polymer chains.

$$k_t \propto \exp(-\gamma\sigma) \tag{2}$$

Based on the school of termination philosophy, two expressions, Eqs. (3) and (4), have been developed by two different groups to predict the thickness growth profile [101, 102]. These two equations were derived from kinetic equations using

quasi-steady state assumption (QSSA) $k_{act}[PX][C] = k_{deact}[P^{\bullet}][XC]$, and are applicable for cases with negligible conversion. The first group applied QSSA to the mass balance of radicals to obtain an expression for the dry grafted layer thickness, δ, as shown in Eq. (3). On the other hand, the second expression, shown by Eq. (4), was obtained by applying QSSA to the balance of dead chains. Both equations predict the growth rate of the grafted layer thickness to decrease with polymerization time, which offers an explanation for the tapering off observed in the growth kinetics of the grafted layer in experiments.

$$\delta \propto \frac{k_p[M]_0[P^{\bullet}]_0 t}{1 + k_t[P^{\bullet}]_0 t} \tag{3}$$

$$\delta \propto \ln\left(1 + \sigma k_t \left(\frac{k_a[C]}{k_d[XC]}\right)^2 t\right) \tag{4}$$

Although data is scarce, some studies have reported the properties of grafted chains formed by SI-ATRP after cleaving the polymer brush grown on large or multiple planar substrates [65, 68, 83, 105–107]. Unfortunately, such a comparison of grafted chain properties with those of free polymers is very limited, because some of these studies conducted polymerization strictly on the surface [65, 83, 107]. Other studies have reported that collected grafted chains are longer than the free chains produced during simultaneous polymerization [68, 105, 106]. Similar findings have also been reported when surface-initiated nitroxide-mediated polymerization was employed instead of SI-ATRP [108, 109]. A different trend was reported by Yamago et al., who found free and grafted chains to possess similar properties when using surface-initiated organotellurium-mediated living radical polymerization (SI-TERP) [110].

One way to confirm negligible termination has been reported by Kang et al. [107]. The authors conducted a SI-ATRP of styrene on a silicon wafer from a photo-cleavable initiator. The molecular weight of the cleaved polymers was used to calculate the grafting density. For their polystyrene system, which mainly terminates via coupling, constant grafting density implies negligible termination. It should be noted that this method is not valid for other monomers that terminate via disproportionation, since disproportionation would not affect the grafting density value calculated using this method.

4.3.2 Termination on Nanoparticles

In SI-ATRP involving nanoparticles, there are two possible modes for termination between two surface radicals: interparticle and intraparticle termination. Intraparticle termination is basically similar to termination between two surface radicals observed on flat substrates, with the additional limitation of a curvature effect. On the other hand, interparticle termination occurs between chains that are

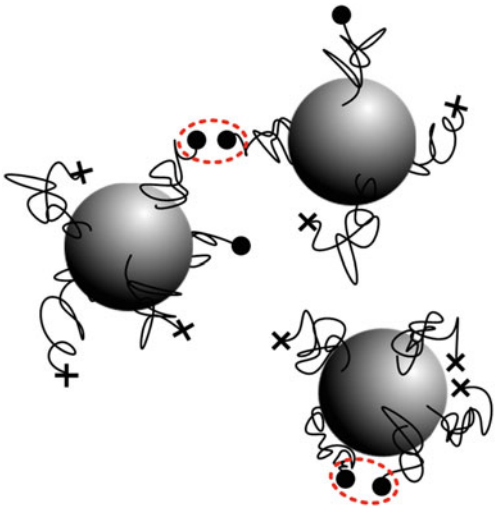

Fig. 6 Interparticle and intraparticle termination modes between two surface radicals in SI-ATRP on nanoparticles

fixed on two different nanoparticles. The termination modes in such a particle system are illustrated in Fig. 6.

A problem that often arises in conducting SI-ATRP on particles is macroscopic gelation, which occurs as a result of interparticle termination via coupling or combination. This can result in an increase in viscosity, leading to diffusion-controlled reactions and loss of polymerization control. The large number of initiation sites on one particle makes it faster for the system to gel as compared with a solution polymerization system. By assuming approximately 1,600 initiation sites per particle, the gelation point can be estimated using Flory's gelation theory as occurring when only 0.125% of the chains undergo interparticle coupling termination [87]. Therefore, macroscopic gelation has been reported even when no bimodality is reported in the MWD of the cleaved grafted chains [77].

Several ways have been proposed for reducing the macroscopic gelation, including using a dilute concentration of particles, or stopping the reaction at low monomer conversion [77, 78, 86]. Free initiator in the solution is also often added to the reaction to form free polymers and prevent network formation [111, 112]. However, both of these methods can increase the cost of synthesizing pure polymer-grafted nanoparticles. Bombalski et al. have shown that macroscopic gelation can be avoided by conducting SI-ATRP in a miniemulsion system as a result of radical compartmentalization, as illustrated in Fig. 7 [87].

Another strategy that is effective for avoiding macroscopic gelation is conducting the polymerization in a high pressure system [76]. When SI-ATRP is conducted under high pressure the polymerization occurs with an increase in propagation rate, whereas the termination rate is suppressed. This leads to a faster polymerization with better living characteristics. Successful synthesis of PMMA grafted chains, with molecular weight above 1 million and low dispersity (<1.3), on silica nanoparticles has been reported using miniemulsion AGET-ATRP in a vessel

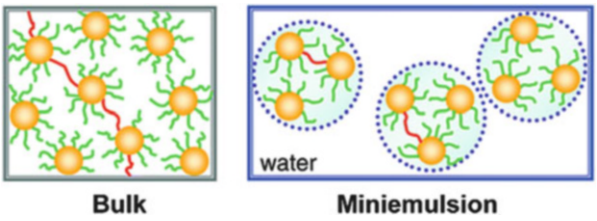

Fig. 7 Interparticle coupling in SI-ATRP on nanoparticles for bulk and miniemulsion systems. The compartmentalization of particles in a miniemulsion prevents macroscopic gelation from occurring. Reprinted with permission from Bombalski et al. [87]

pressurized to 6 kbar [76]. The livingness of the tethered chains, or retention of high chain-end functionality, was confirmed by conducting SI-ATRP of methyl acrylate using the PMMA-grafted nanoparticles as surface initiator.

Chakkalakal et al. have observed bimodality in the MWD of grafted polymer on silica nanoparticles at higher conversion (above 25%) [86]. However, the bimodal distribution was attributed to intraparticle coupling and/or to the coupling termination between surface and solution radicals. The termination occurring via interparticle coupling was considered negligible in their study, based on dynamic light scattering (DLS) results. They also observed that more termination occurred for smaller nanoparticles than for larger particles, as suggested by earlier broadening and bimodality of the MWD.

4.3.3 Termination on Concave Substrates

In the case of systems involving concave substrates, such as porous particles or cylindrical channels, the confinement effect is expected to be much more severe than that for flat substrates. In addition to the obvious mass transport issue that results from a more confined space, the probability of termination could also increase. Therefore, a less living and less controlled polymerization is expected in systems involving concave substrates.

Multiple studies have reported a population of shorter grafted polymer chains with broader distribution in comparison with free/solution polymer chains [88, 89, 113]. Gorman et al. conducted SI-ATRP from a silicon wafer, porous silicon, and anodically etched aluminum oxide. The results were compared with those of ATRP conducted in solution under similar conditions. The grafted polymer chains from a flat substrate were shown to be shorter than the free chains formed in the parallel solution polymerization. The polymers obtained from concave substrates have an even lower molecular weight and broader distribution.

The Charleux group has conducted several studies of SI-ATRP in mesoporous silica nanoparticles [88, 89]. Instead of conducting parallel polymerizations, they conducted simultaneous polymerization in solution and from the surface. Their findings were similar to those of Gorman et al., showing grafted chains to have

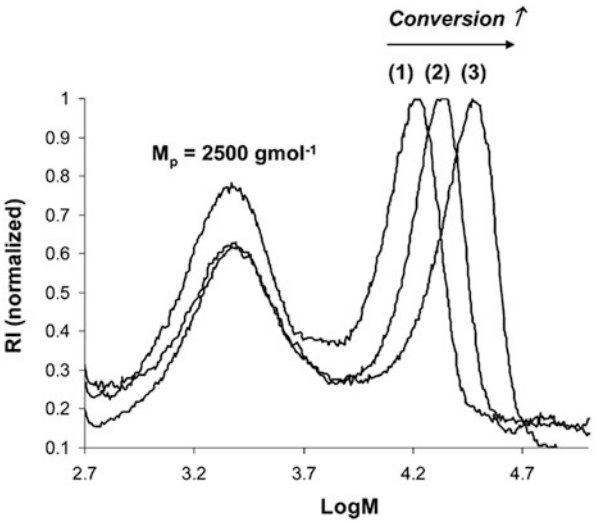

Fig. 8 Molecular weight distributions of grafted chains for SI-ATRP of MMA from a concave substrate. Detailed experimental conditions are provided in the original literature. $M_{p,l}$ indicates the molar mass at the peak for the living chains. (*1*) 50%, $M_{p,l} = 16{,}320$ g/mol; (*2*) 62%, $M_{p,l} = 21{,}880$ g/mol; (*3*) 91%, $M_{p,l} = 30{,}020$ g/mol. The lower peak ($M_p = 2500$ g/mol) indicates the presence of dead chains. Reprinted with permission from Pasetto et al. [89]

significantly lower molecular weight with broader distribution than the chains formed in solution. Moreover, for some of the experiments, the grafted chains were shown to display multimodal distribution, as characterized using gel permeation chromatography (GPC) (see Fig. 8). The lower molecular weight peak observed in the distribution did not shift, even at higher conversion, indicating the presence of dead chains. From this GPC curve, they estimated that approximately 50% of the chains had been terminated. Characterization of the grafted chains using mass spectroscopy also provided proof that some of the grafted chains had undergone termination by disproportionation.

Simulation of polymerization from a concave substrate could prove to be a challenging task because of the complexity of the system. However, Liu et al. used coarse-grained molecular dynamic simulation to investigate the effect of curvature on polymer growth and dispersity [90]. Unfortunately, the polymerization was considered to be a perfectly living polymerization (i.e., in the absence of termination and other side reactions), thus it does not help in elucidating the role of termination in SI-ATRP.

4.4 Exchange

At the beginning of normal ATRP, only catalyst and initiator are present in the solution. As the polymerization progresses, some of the chains undergo bimolecular termination, resulting in accumulation of the deactivator. The accumulation of deactivator, termed the persistent radical effect [114], is important in reaching an equilibrium between dormant and active chains. Indeed, control in ATRP systems relies on creating an equilibrium between dormant and active chains, as they

reversibly react with catalyst and deactivator, respectively. The broadness of the MWD (i.e., dispersity) is often used as an indicator of how controlled the polymerization is. For cases with negligible termination and high degrees of polymerization, the dispersity ($Đ$) of polymer chains synthesized through ATRP as a function of conversion (conv) follows Eq. (5), with the polymerization rate (R_p) shown by Eq. (6) [115, 116]. Based on Eq. (5), in order to obtain a high degree of control over the polymerization (low dispersity), there must be a sufficient concentration of deactivator (XC) present in the system. However, it is clear from Eq. (6) that there is a trade-off between the polymerization rate and degree of control:

$$Đ = 1 + \frac{k_p[\mathrm{PX}]_0}{k_d[\mathrm{XC}]}\left(\frac{2}{\mathrm{conv}} - 1\right) \tag{5}$$

$$R_p = k_p[\mathrm{M}][\mathrm{PX}]\left(\frac{k_a[\mathrm{C}]}{k_d[\mathrm{XC}]}\right) \tag{6}$$

In SI-ATRP from a flat substrate, the amount of initiator present on the surface is not nearly enough to provide sufficient accumulation of deactivator in the contacting system. This leads to an uncontrolled polymerization. Two procedures are commonly used to mitigate the uncontrolled SI-ATRP from flat substrates: the addition of free initiator [117] and the addition of deactivator [99]. The presence of free initiator provides solution chains that do terminate and, hence, accumulate enough deactivator to control the polymerization. For this reason, the free initiator is also often referred to as "sacrificial" initiator. Other than for maintaining control of the polymerization process, free initiator is also added to systems with flat substrates to provide an estimate of the properties of grafted chains. The validity of this estimation has been discussed in previous sections. On the other hand, the addition of deactivator can provide enough deactivator to control the polymerization without requiring surface chains to undergo termination. However, the addition of too much extra deactivator could result in retardation of the polymerization rate (Eq. 6).

One of the main differences between SI-ATRP from flat substrates involving addition of free initiator and addition of extra deactivator lies in the formation of free polymer. The free chains in solution greatly affect the polymerization kinetics of both chain populations. Because of the small amount of surface chains, the monomer conversion in SI-ATRP with extra deactivator is negligible. However, free initiator in solution can consume significant amounts of monomer and cause monomer depletion. For this reason, a thicker polymer layer is usually obtained when the polymerization is conducted using SI-ATRP with added deactivator [118, 119]. Figure 9 shows a comparison between the growth profiles obtained from these two methods.

As noted above, in SI-ATRP with addition of deactivator, the consumption of monomer is negligible; therefore, the growth profile of the polymer layer with time is expected to be linear in an ideal case (no crowding or termination effects). On the other hand, monomer conversion in SI-ATRP with free initiator is not negligible.

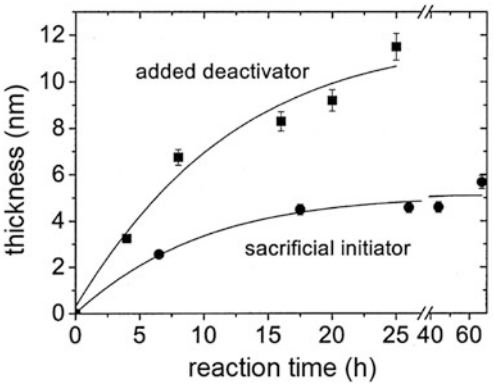

Fig. 9 Growth profiles of grafted polystyrene on a silicon wafer with addition of sacrificial initiator (*circles*) or deactivator (*squares*). Reprinted with permission from Jeyaprakash et al. [118]

Hence, the growth profile of the polymer layer with conversion is expected to be linear in an ideal case, where the polymerization rates of solution and surface chains are the same. Deviation from linearity in the growth profile with time or with conversion (added deactivator or sacrificial initiator, respectively) could be explained by applying the philosophy of either the school of propagation or school of termination, as previously discussed.

In particle systems, as a result of the large surface-to-volume ratio, a sufficient number of surface initiators might be present to generate the required concentration of deactivator in the solution. However, free initiator and/or excess deactivator are still often added to this system. Free initiator is often added for SI-ATRP of particles for multiple reasons. One reason is to provide better control over the polymerization, another is to prevent macroscopic gelation resulting from interparticle coupling.

The type of catalyst has also been shown to affect the equilibrium in SI-ATRP. Huang et al. compared the use of CuBr with CuCl for SI-ATRP of MMA from silica nanoparticles [74]. The grafted chains on the nanoparticles were cleaved and their dispersity used as an indicator of polymerization controllability. They found that CuBr resulted in faster polymerization but produced a less uniform polymer layer and higher dispersity. Several researchers have attributed poorer control to differences in the local concentrations of catalyst and deactivator, which can affect the equilibrium experienced by the surface chains. According to experimental results from Behling et al., surface-initiated polymerization occurs faster than solution polymerization [68]. The difference in polymerization rate was attributed to deviation of the ratio of local concentrations of catalyst and deactivator available to the surface chains, as shown in Fig. 10. They postulated that in the "viscous front" (shaded area in Fig. 10) the local concentration of catalyst (C) is higher than that in the bulk, whereas the opposite is true for the local concentration of deactivator (XC). Because of the reduced deactivation rate in the viscous front, the surface radical concentration increases, which results in a faster propagation rate for surface-tethered chains than for chains present in the contacting solution.

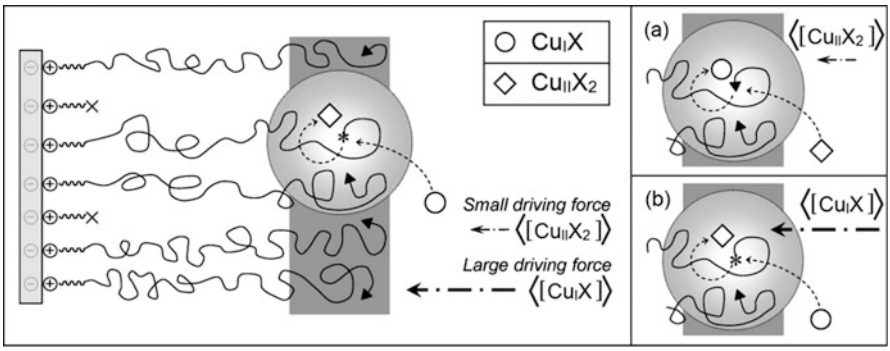

Fig. 10 The growing viscous front for SI-ATRP postulated by Behling et al. [68]. The local concentration of catalyst in the *shaded area* is higher than that in the bulk solution, whereas the local concentration of deactivator is lower than that in the bulk. (**a**) conversion of catalyst (◇) to deactivator (○) (**b**) conversion of deactivator to catalyst. Reproduced with permission from Behling et al. [68]

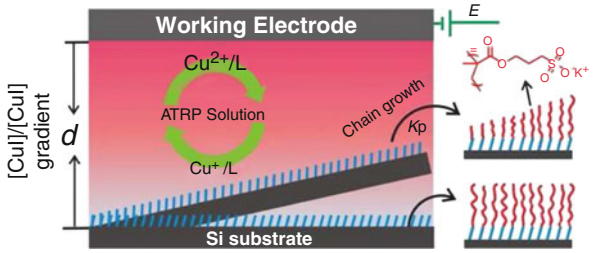

Fig. 11 Generation of a gradient of catalyst-to-deactivator concentration ratio induced by adjusting the distance between the surface and the electrode, resulting in a gradient in the thickness of the grafted polymer layer. Reproduced with permission from Li et al. [120]

Li et al. investigated the effect of catalyst-to-deactivator concentration ratio on the growth of a polymer layer on a flat substrate [120]. They induced a gradient of the concentration ratio of activator to deactivator by using electrochemically mediated ATRP (eATRP) and tilting the substrate toward the electrode (as illustrated in Fig. 11). In eATRP, the catalyst is regenerated electrochemically from the deactivator [20]. By adjusting the distance, the surface closer to the electrode experiences a higher concentration ratio of catalyst to deactivator, thereby experiencing a faster polymerization, as indicated by the thickness gradient in the grafted polymer layer.

4.5 Transfer

Several studies have investigated the importance of chain transfer reactions in solution ATRP. The importance of chain transfer to ligand was reported by

Matyjaszewski and coworkers for ATRP of *n*-butyl acrylate [121]. This chain transfer reaction was proposed to be the cause of the deviation observed in the first-order kinetic plot when excess ligand (pentamethyldiethylenetriamine, PMDETA) was used in the polymerization recipe. The mechanism of the chain transfer reaction to PMDETA was further investigated by Sharma et al. [122]. Chain transfer to PMDETA has been proposed to induce a higher degree of control for SI-ATRP systems containing acrylate monomers [123]. This was achieved by conducting the SI-ATRP at a higher ratio of ligand to catalyst, [PMDETA]/[CuBr] = 3, in the absence of excess deactivator and free initiator. Other SI-ATRP studies have also used similar polymerization recipes, with elevated levels of PMDETA for a *N*-isopropylacrylamide (NIPAM) system showing great success [64, 124–126].

The extent of chain transfer reactions in SI-ATRP could affect the polymerization kinetics and the resulting grafting density of polymers. However, further studies need to be conducted in order to fully understand the role of chain transfer reactions in the SI-ATRP mechanism.

4.6 Other Side Reactions

For some monomers (e.g., styrene) thermal self-initiation is unavoidable. This results in simultaneous polymerization in solution and on the surface, even in the absence of added free ATRP initiator. The presence of free polymers might not be desirable, as they can alter the properties of the bulk nanoparticle system, hence requiring further separation steps. Moreover, the presence of free polymer chains affects the characterization of grafted polymer properties, including the estimation of grafting density, potentially generating large errors [79, 127]. Therefore, when seeking to determine the properties of a hybrid system, the presence of free polymer chains must be quantified to account for their effect on the system, or to ensure that they have been fully separated from the system. Figure 12 illustrates how even the presence of a small amount of free polymer chains can bridge the voids between grafted nanoparticles at certain particle size/graft chain molecular weight, thereby altering the material properties.

In nanoparticle systems, the separation of free polymers and grafted nanoparticles can be tricky and time-consuming. Therefore, it is necessary to understand factors affecting thermal self-initiation in order to control its rate. Tchoul and coworkers used size exclusion chromatography (SEC) to quantify the amount of free polystyrene chains formed during the SI-ATRP of styrene from nanoparticles (shown in Fig. 13) [79]. They demonstrated the accuracy of using SEC to quantify the small amount of free polymer chains. They have also shown that interparticle distance is greatly affected by the presence of free polymer chains, as indicated by the results of their TEM studies [127]. By quantifying the formation of free polystyrene, they optimized the reaction conditions to suppress the thermal self-initiation of styrene. Using the dependence of thermal self-initiation rate on

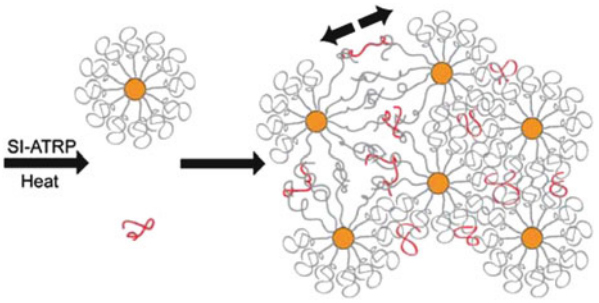

Fig. 12 Presence of free polymer chains in a grafted nanoparticles system. The free chains act as bridges for the grafted nanoparticles to form a network. Reproduced with permission from Hui et al. [127]

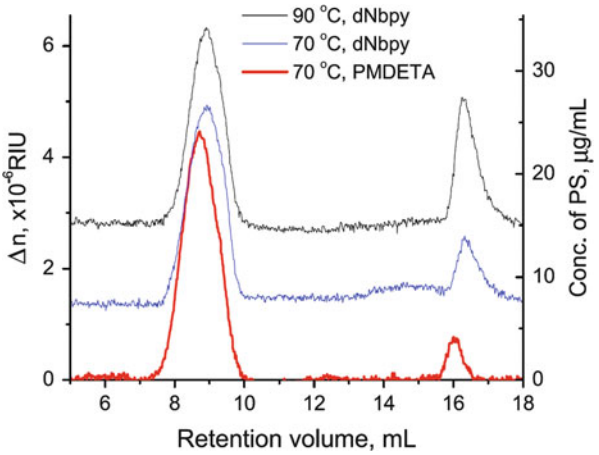

Fig. 13 SEC results for polystyrene grafted from silica nanoparticles with different polymerization recipes. The *concentration axis* on the *right* is only applicable to the peaks at 16–17 mL. Reprinted with permission from Tchoul et al. [79]

time and temperature the authors minimized the rate by using a lower reaction temperature combined with the use of a more active catalyst system [79, 127].

Chakkalakal et al. conducted SI-ATRP of MMA and styrene from silica nanoparticles, and their GPC curves showed a bimodality in the MWD of grafted polystyrene on silica nanoparticles at high conversion [86]. The SI-ATRP was conducted at an elevated temperature, with free polymers formed by thermal self-initiation of styrene at 90°C. Even though there was significant bimolecular termination occurring via a coupling mechanism, as indicated by the bimodal MWD, the DLS result did not show evidence of interparticle termination. Therefore, the coupling could occur only by intraparticle coupling or by coupling of a surface radical with solution radical.

Mu et al. demonstrated the formation of polymer nanocapsules using SI-ATRP to grow a polymer brush from particles, crosslinking of the tethered polymer brush, followed by etching of the particles [128]. Silica nanoparticles can work as a template for the preparation of polymeric nanocapsules. In an extension of this concept, formation of nanonetwork polymers was demonstrated by Matyjaszewski and coworkers, as shown in Fig. 14 [129]. In addition to forming a nanocapsule by etching the silica particles after crosslinking, the authors also showed that a

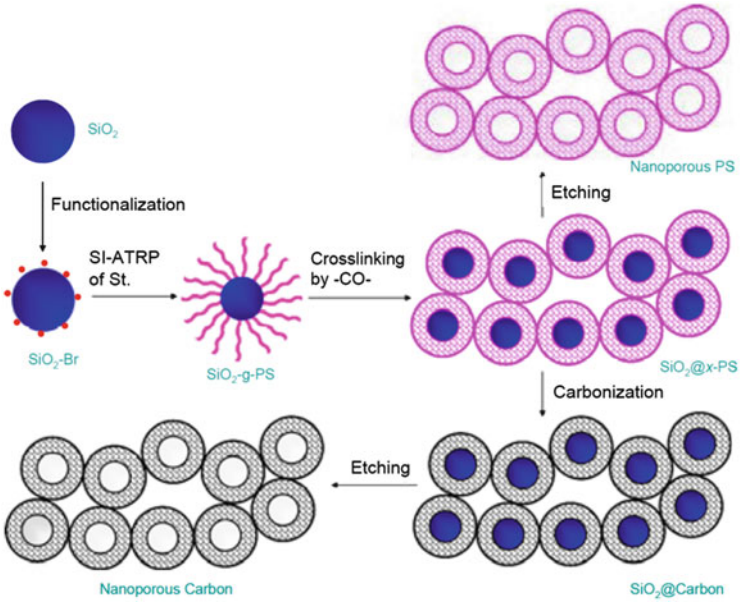

Fig. 14 Formation of nanonetwork polymers and carbon materials using SI-ATRP from silica nanoparticles [129]

nanonetwork of carbon materials can be obtained by carbonizing the polymer prior to etching the core of the nanoparticles. The resulting material was a core–shell system with a mesoporous core from the silica template and a microporous shell from the intraparticle crosslinking of the tethered carbon precursor polymer brush.

5 Materials

Grafting of polymers on material substrates to impart various surface properties is advantageous if one desires to govern the interactions between the material and its surroundings, without compromising its bulk properties. Different surface properties can be obtained, depending on the type of polymers grafted from the surface. For example, regarding the increasing trend to use stimuli-responsive polymers, responsive and switchable surface properties can be obtained by selective grafting of a polymer brush from a surface. The properties imparted by the grafted polymer layer depend not only on the type of polymer chemistry, but also on the uniformity, grafting density, and thickness of the grafted polymer layer. A major advantage of using SI-ATRP for grafting polymers from a surface is that it allows preparation of more complex polymer chain microstructures and topologies and better control over polymer brush properties, which means that more precise surface properties can be generated. Moreover, the grafting density that can be obtained by SI-ATRP

is higher than attained by the grafting-to method or by free radical polymerization. It has been shown that grafted polymers with moderate to high grafting densities give different properties from those observed for low grafting density [130, 131].

5.1 Flat Substrates

SI-ATRP can be used to synthesize complex polymer brush structures that range from block copolymer brushes, to linear chains with gradient composition and gradient molecular weight brushes, to binary brush types, which allows preparation of hybrid substrates with highly tunable and unique properties [55]. Therefore, SI-ATRP is a popular method for the preparation of surfaces for biomedical applications, with numerous papers being published every year on the synthesis of materials having surface properties required for such applications (antifouling, antimicrobial, etc.) [132–138]. For biomaterial applications as such as biosensors, implants, etc., where the material comes in contact with various proteins in a complex biological environment, it must possess antifouling surface properties. The antifouling properties improve the performance of biomaterials by reducing the amount of adsorbed proteins on the surface. These properties can be introduced by grafting biocompatible polymer brushes via SI-ATRP from the surface, for example, by grafting hydrophilic neutral or zwitterionic polymers. The group of Zhu and Brash investigated the biocompatibility of silicon [61, 100, 139–149], gold [150], and polymeric [151–154] surfaces grafted with hydrophilic and zwitterionic polymer brushes. Feng and coworkers from the same group compared the protein resistance of silicon surfaces grafted with poly(2-methacryloyloxyethyl phosphorylcholine) (PMPC) or POEGMA, having various grafting densities and chain lengths [146–149]. They reported lower fibrinogen adsorption and platelet adhesion for surfaces with higher grafting density and longer chain length, but the results were similar for both types of polymer brushes. This result suggests that a water barrier created in the presence of both brushes plays a major role in improving resistance to protein adsorption.

In addition to the antifouling properties, some biomaterials should also possess antimicrobial properties to prevent bacterial infection. The grafted polymer brushes can suppress bacterial growth by reducing bacterial adhesion or by acting as a tethered biocide and killing the bacteria by cellular disruption. The polymers that are used to impart antifouling properties also generally reduce the adhesion of bacteria on the surface to a certain degree. Chang's group grafted a zwitterionic polymer brush onto titanium and stainless steel via SI-ATRP and prepared surfaces with high resistance to cell, bacterial, and protein adhesion [155, 156]. They reported at least 95% reduction in bacterial adhesion on the grafted surfaces compared with reference unmodified surfaces, showing the great potential of poly (sulfobetaine methacrylate) (PSBMA) for the preparation of biocompatible implants. Matyjaszewski's group has demonstrated that the introduction of quaternary ammonium groups into the backbone of polymer brushes can kill bacteria

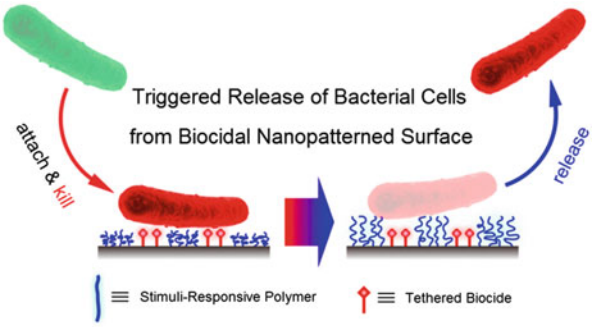

Fig. 15 Self-cleaning, antimicrobial surface prepared by utilizing PNIPAM and a quaternary ammonium salt. Reproduced with permission from Yu et al. [159]

[157, 158]. Using SI-ATRP, they grafted PDMAEMA from glass, filter paper, or a polypropylene slide, followed by quaternization of the tertiary amino groups. The modified surfaces exhibited significant antimicrobial properties. The group also showed that the killing efficiency depends on the polymer brush chain length, with longer chains showing higher killing efficiency. Yu et al. combined a thermo-responsive polymer (PNIPAM) with a quaternary ammonium salt and prepared self-cleaning antimicrobial surfaces, as illustrated in Fig. 15 [159]. The thermally responsive behavior of PNIPAM allowed the surface to expel the dead bacteria when PNIPAM switched to its extended conformation, resulting in self-cleaning properties that could be controlled simply by adjusting the temperature in the contacting environment.

PMPC has also been grafted onto a surface to improve the surface lubrication properties [160–162], because some applications, such as biological surfaces in artificial joints, require extremely low friction properties. Kobayashi et al. studied the friction behavior of PMPC brushes synthesized by SI-ATRP compared with other polyelectrolyte brushes [160, 161]. They found that higher humidity resulted in generation of lower friction properties for the surface, which was attributed to the presence of adsorbed water molecules in the polymer brush. In other words, the lubrication properties induced by polymer brushes depend heavily on the surrounding environment. A similar finding was reported by Nomura et al., who investigated the dependence of lubrication on the swelling characteristics of a polystyrene brush (controlled by the solvent composition), and by Bielecki et al. who studied the tribological properties of surfaces grafted with various alkyl methacrylates [163, 164]. Nomura and coworkers proposed that the lubrication properties of densely grafted polymer brushes followed two mechanisms, namely boundary lubrication and hydrodynamic lubrication.

Grafting of stimuli-responsive polymers broadens the applicability of grafted surfaces. Depending on the polymer grafted, the surface can reversibly switch its properties in response to different stimuli. Kumar et al. grafted various diblock copolymers, with the outer block being a stimuli-responsive polymer, as shown in Fig. 16 [165]. The inner block acted as a reservoir for small molecules, which were released when the outer block assumed a chain-extended conformation after external stimulus was applied. The same research group also grafted a CO_2-responsive polymer, PDEAEMA, onto silicon- and gold-coated substrates [166]. The modified

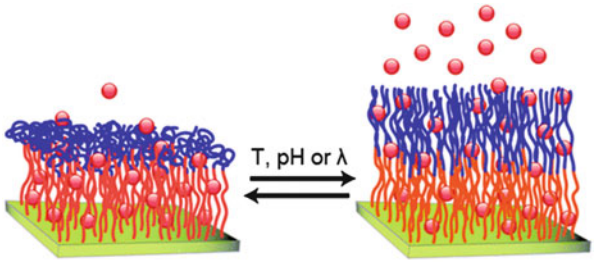

Fig. 16 Diblock copolymers with stimuli-responsive outer block grafted onto a substrate to release dye molecules when an external stimulus (temperature, pH, or light) is applied. Reproduced with permission from Kumar et al. [165]

surfaces underwent reversible adsorption and release of proteins simply by bubbling carbon dioxide into the contacting medium. There are also many studies using thermoresponsive polymers for the preparation of smart biosurfaces. By grafting OEGMA on gold surfaces, Wischerhoff et al. obtained surfaces with temperature-switchable cell adhesion/antifouling properties [167]. Liu et al. showed how stimuli-responsive polymer brushes of PNIPAM and PDMAEMA could be used to prepare surfaces with switchable adhesive properties and demonstrated how the mobility of water droplets on the surface was controlled by changing the temperature or pH [126].

Another interesting feature that can be introduced to a surface using SI-ATRP is the property of self-healing. Takahara and colleagues demonstrated reversible nanoscale adhesion/separation of two substrates by grafting a polyelectrolyte having a positive charge on one surface and a negative charge on the other using SI-ATRP [168]. The electrostatic attraction between polymer brushes on these two surfaces created a strong adhesion, which could be reversibly released by adding a salt solution. However, adhesion of the two oppositely charged polyelectrolytes released salt into the solution, which affected the resulting adhesion. To counter this problem, the same research group grafted zwitterionic polymer brushes onto both substrates to achieve a similar reversible adhesion/separation feature through dipole–dipole interactions [169]. The adhesion reversibility of the surfaces grafted with zwitterionic polymer brushes was found to be better than that of surfaces with oppositely charged polyelectrolyte brushes. Moreover, the de-bonding reaction was achieved simply by placing the substrate in water at an elevated temperature of 50°C.

SI-ATRP can also be used to modify the surface properties of metals. Several types of acrylic monomers have been grafted on metal surfaces, such as iron, steel, nickel, copper, and stainless steel [170–173]. The grafted surfaces showed significant improvement in corrosion resistances compared with the unmodified surface [171]. Moreover, some researchers have found an iron catalyst to be more efficient than copper in controlling SI-ATRP on these surfaces [171, 172]. SI-ATRP is also an excellent tool for producing patterned polymer brushes by immobilizing the initiator moieties in desired patterns, through methods such as microcontact printing [84], polymer pen lithography [174], and many others [175, 176]. A review by Chen et al. discussed various synthesis methods and applications of patterned polymer brushes [177]. Recent studies of patterned polymer brushes via SI-ATRP have focused on the preparation of large surfaces [174, 176].

5.2 Concave Substrates

SI-ATRP can be employed to graft polymers from porous materials. The thickness of grafted polymer can be precisely controlled, eliminating possible blockage of small pores in membranes or other porous materials. Indeed SI-ATRP has been used to modify the surface of membrane pores for various purposes, such as to impart antifouling properties [178], improve biocompatibility, and/or to introduce surface responsiveness to external stimuli. The use of SI-ATRP also ensures no significant change in the pore size distribution after grafting. In one example, PNIPAM was grafted from ultrafiltration membranes (pore diameter 110 nm) and gave the surface thermoresponsive properties [179]. The pore diameter of the membrane could be changed by changing the temperature to above or below the lower critical solution temperature of PNIPAM. Chen et al. synthesized a membrane that responded to four different stimuli, namely temperature, pH, salt concentration, and type of anion [180]. The multistimuli-responsiveness was achieved by grafting a diblock copolymer brush of PNIPAM and poly(methyl acrylate) (PMA) from the membrane pores using SI-ATRP. By changing the copolymer composition ratio, the gating behavior of the membrane in response to an external stimulus could be altered as desired (see Fig. 17). A recent review by Ran et al. summarized various studies of functionalization of membranes using SI-ATRP [181].

Ordered mesoporous silica nanoparticles have shown significant potential for use as biomedical devices, such as drug delivery carriers [182]. In one example, a thermoresponsive polymer, PNIPAM, was grafted onto porous substrates, which allowed formation of surface-responsive properties in the pores [183]. The conformation change of PNIPAM brushes with temperature was used to initiate the

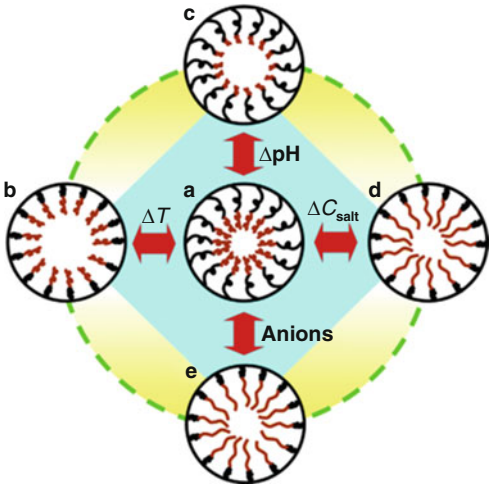

Fig. 17 Quadri-stimuli-responsive properties of PNIPAM-b-poly (methacrylic acid)-grafted gating membrane responding to temperature, anion type, pH, and salt concentration. *Black lines* show the responsive nature of the PNIPAM segment and *red lines* show the responsive nature of the poly(methacrylic acid) segment of the polymer brush. Reproduced with permission from Chen et al. [180]

release of drugs contained inside the pores. Through this approach, drug release can be triggered by various external stimuli, such as temperature and pH.

Shen et al. used SI-ATRP to modify the surface of a polymeric monolith with grafted PDMAEMA to impart pH and salt-responsive properties. Because of the controlled and living characteristic of SI-ATRP, the surface hydrophobicity could be controlled by varying the polymerization time. The responsive monolithic surface was used to prepare materials for an HPLC column to control the retention of steroids [184]. Filter paper is another popular concave substrate that can be modified using SI-ATRP. As previously mentioned, Matyjaszewski's group used SI-ATRP to graft PDMAEMA onto filter paper, which was subsequently modified to form quaternized ammonium units, which act as a biocidal agent [157]. Jiang's group recently reported the synthesis of a highly sensitive, low fouling, glucose sensor by grafting poly(carboxy betaine methacrylate) (PCBMA) onto cellulose filter paper [185]. As a result of the hydrophilic properties of the polymer brushes, the grafted filter paper exhibited a fast response in detecting the presence of glucose in complex media.

Carbon black is another type of inexpensive material with excellent bulk properties. However, it possesses surface properties that are incompatible with many other materials. Consequently, a suspension of carbon black in a matrix material is often unstable. Modification of carbon black surface via SI-ATRP has been reported by Matyjaszewski's group [186]. The dispersibility of the modified carbon black was significantly improved. In addition, various other functional groups have also been successfully introduced onto the surface.

5.3 Convex Substrates

There are a variety of reasons for surface modification of nanoparticles through grafting including, but not limited to, improving colloidal stability, generating smart properties through the use of stimuli-responsive polymers, and altering the surface properties of a particle for specific applications. The resulting properties depend not only on the grafting density and the average length of the chains grafted from the particles, but also on the uniformity of the polymer layer. These polymer chain properties affect the polymer brush conformations and can be precisely tailored by using SI-ATRP. For example, the dependence of the ordered/disordered formation on the chain length and particle size of nanoparticles has been investigated, as qualitatively shown in Fig. 18 [187]. In addition, the effect of polymer architecture on the final properties, such as mechanical and thermal properties, of the resulting materials has been systematically studied [188, 189]. It is also possible to graft polymer brushes onto nanoparticles to obtain particles with a prespecified average refractive index value, which can be used as fillers [190]. By tuning the refractive index of the final particles, by taking into consideration the refractive index of the inorganic core and the polymer shell along with the thickness of the shell, a core–shell particle can be prepared with a refractive index that matches the

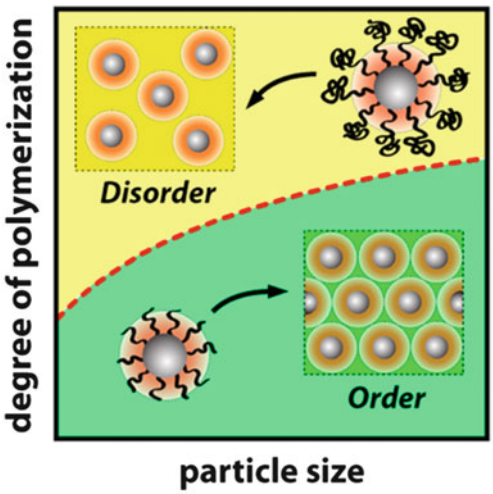

Fig. 18 Dependence of order formation on the degree of polymerization and the particle size. Reproduced with permission from Choi et al. [187]

targeted matrix material and, thus, a transparent nanofilled reinforced composite can be obtained. This allows all the benefits of using nanofillers without compromising the optical quality of the material.

Polymer-coated magnetite nanoparticles are gaining popularity due to their wide applicability. These particles combine the magnetic properties of the core with the functional groups of the polymer brush shell [191]. Bull et al. reported a method for preparation of multigram magnetite nanoparticles using a polymeric surfactant, which was synthesized via ATRP [192]. Another method often utilized to synthesize magnetic nanoparticles with a polymer coating is through surface-initiated polymerization. The use of SI-ATRP to introduce a polymer layer onto these nanoparticles has been investigated for various purposes. Polymer brushes can be introduced to provide better dispersion [193–196]. Another potential application demonstrated for polymer-coated magnetite nanoparticles is for oil–water separation, as shown in Fig. 19 [197]. The negatively charged grafted polymer allows the nanoparticles to absorb water, which can be separated from the oil phase by applying an external magnetic field. The magnetic properties of the original particles are retained in the grafted particles, making it easy to separate the particles from the oil phase.

Dong et al. used SI-ATRP to prepare recyclable antimicrobial substrates from magnetite nanoparticles [198]. They grew PDMAEMA brushes from magnetite nanoparticles, followed by further reaction to form quaternary ammonium groups. The resulting nanoparticles exhibited antimicrobial properties and excellent recyclability as a result of the presence of quaternary ammonium groups and the magnetic properties of the cores. Stark's group proposed a method for producing magnetic inks, which can be used for greener paper recycling processes, via SI-ATRP [194, 199]. The magnetic inks consisted of carbon-coated magnetite nanoparticles, which were grafted with polymer brushes to improve their stability in water. The use of magnetic inks allowed easy de-inking of papers, reducing the

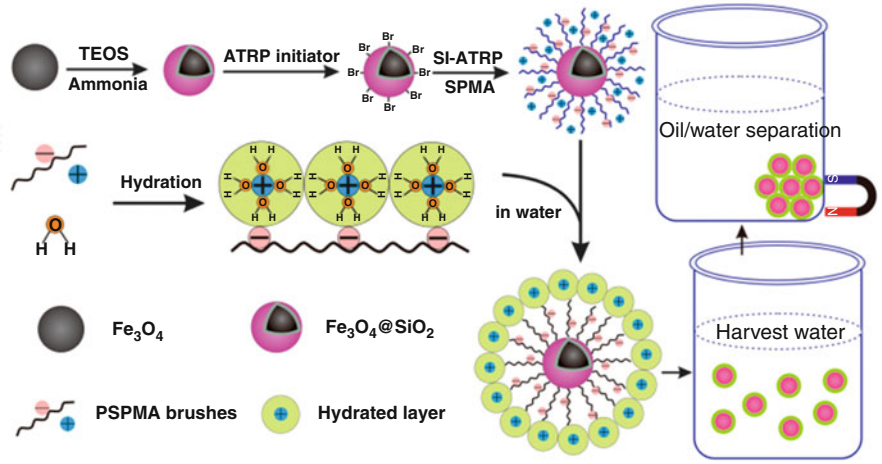

Fig. 19 Zwitterionic polymer brushes on magnetite nanoparticles as a tool for separating oil and water. Reprinted with permission from Liu [197]

use of toxic chemicals needed for bleaching the papers. Moreover, magnetic inks from the recycling process could be recovered for subsequent reuse. Gu et al. prepared magnetic nanoparticles grafted with block copolymer of polyhedral oligomeric silsesquioxanes (POSS) and PMMA using SI-ATRP [196]. These nanoparticles can be used as smart fillers, as their location in the solution can be controlled using a magnetic field, allowing localization of fillers. The localization of fillers is beneficial in minimizing the amount of filler required to achieve the same surface properties. The resulting PMMA film containing these fillers exhibited 30% improvement in the indentation microhardness compared with film without fillers.

Post-grafting modification of nanoparticles allows even more variation in the attainable polymeric architectures. By crosslinking the polymer brushes on nanoparticles after SI-ATRP, polymeric nanocapsules can be obtained by etching the nanoparticles [128]. Carbonization prior to etching allows formation of nanonetwork carbon materials [129]. The polymer brush can also be acidified to form an acidic brush layer, which can be used as a reusable catalyst in the dehydration of fructose [200].

SI-ATRP has also been used to modify the surface of quantum dots in order to improve the dispersibility and stability of these nanoparticles. Farmer and Patten demonstrated the use of SI-ATRP to graft PMMA from CdS/SiO_2 core–shell nanoparticles [201]. A film formed from the resulting grafted nanoparticles exhibited the same luminescence properties as the CdS core, with the inorganic cores uniformly distributed throughout the polymer matrix. Esteves et al. reported grafting of poly(*n*-butyl acrylate) from CdS quantum dots via miniemulsion ATRP [202]. Characterization of the nanocomposites demonstrated an even dispersion of CdS cores in the polymer matrix.

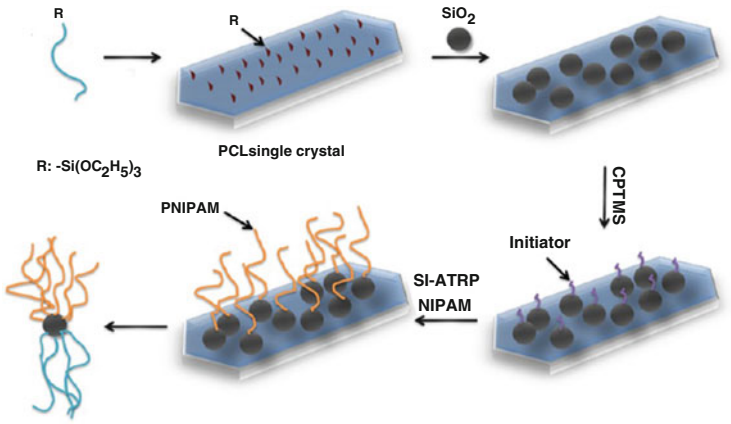

Fig. 20 Synthesis of Janus nanoparticles using a combination of polymer single-crystal templating with SI-ATRP. Reprinted with permission from Zhou et al. [205]

Janus particles have attracted increasing research interest because of the unique properties imparted by their asymmetric structure [39]. One way to synthesize Janus particles is by introducing different polymers onto each side of the particle, thus introducing asymmetric surface properties. Berger et al. used a two-step process involving SI-ATRP followed by a grafting-to approach to immobilize oppositely charged polyelectrolyte brushes on opposite sides of the particles (PAA on one side, poly (2-vinyl pyridine) on the other) [203]. As a result of the pH-responsive nature of the polymer brushes, the resulting Janus particles exhibited pH-responsive aggregation. Liu et al. reported the synthesis of Janus particles via biphasic SI-ATRP at a Pickering emulsion interface [204]. Zhou et al. synthesized Janus particles, with poly(ε-caprolactone) and PNIPAM, through a combination of polymer single-crystal templating and SI-ATRP, as illustrated in Fig. 20 [205].

6 Conclusions

SI-ATRP is a very rapidly developing area of the polymer and materials sciences. The scope of the procedure is constantly evolving, benefiting from new advances in ATRP, such as new catalysts and new initiating techniques, but also from seeking to meet an increasing demand for new advanced nanostructured materials. New ATRP techniques such as eATRP and photoATRP that are mediated by external stimuli have been successfully applied for modification and patterning of surfaces. The modified surfaces can provide extraordinary properties in terms of adhesion, lubrication, antifouling, and antimicrobial behavior. As described in this review, modification of flat, concave, and convex surfaces with polymeric brushes dramatically alters the surface properties of the substrates and provides good dispersibility of

nanoparticles, creates responsiveness in membranes, and provides other properties to composite materials. Although the general polymerization kinetics and mechanisms of homogeneous ATRP and SI-ATRP are similar, there are some peculiarities that can alter the molecular properties of the tethered polymer chains. These differences are based on the specific distribution of active centers anchored to surfaces, diffusion, congestion, and other phenomena. SI-ATRP sometimes resembles other CRP systems but also carries some specific behavior associated with the activator/deactivator nature of ATRP catalysts. Better understanding of such mechanistic features will help in the design and synthesis of new and more efficient hybrid materials.

Acknowledgements Financial supports from NSF (DMR 09 69301), BSF 2012074, DE-EE0006702, and NSERC Discovery Grant (RGPIN/170128-2009) are gratefully acknowledged.

References

1. Braunecker WA, Matyjaszewski K (2007) Controlled/living radical polymerization: features, developments, and perspectives. Prog Polym Sci 32(1):93–146
2. Matyjaszewski K, Davis TP (2002) Handbook of radical polymerization. Wiley-Interscience, Hoboken
3. Matyjaszewski K, Xia JH (2001) Atom transfer radical polymerization. Chem Rev 101(9): 2921–2990
4. Wang JS, Matyjaszewski K (1995) Controlled living radical polymerization – atom-transfer radical polymerization in the presence of transition-metal complexes. J Am Chem Soc 117(20):5614–5615
5. Kamigaito M, Ando T, Sawamoto M (2001) Metal-catalyzed living radical polymerization. Chem Rev 101:3689
6. Matyjaszewski K, Tsarevsky NV (2009) Nanostructured functional materials prepared by atom transfer radical polymerization. Nat Chem 1(4):276–288
7. di Lena F, Matyjaszewski K (2010) Transition metal catalysts for controlled radical polymerization. Prog Polym Sci 35(8):959–1021
8. Shen Y, Tang H, Ding S (2004) Catalyst separation in atom transfer radical polymerization. Prog Polym Sci 29(10):1053–1078
9. Tsarevsky NV, Matyjaszewski K (2007) "Green" atom transfer radical polymerization: from process design to preparation of well-defined environmentally-friendly polymeric materials. Chem Rev 107:2270–2299
10. Jakubowski W, Matyjaszewski K (2006) Activators regenerated by electron transfer for atom-transfer radical polymerization of (meth)acrylates and related block copolymers. Angew Chem Int Ed Engl 45(27):4482–4486
11. Matyjaszewski K, Jakubowski W, Min K, Tang W, Huang JY, Braunecker WA, Tsarevsky NV (2006) Diminishing catalyst concentration in atom transfer radical polymerization with reducing agents. Proc Natl Acad Sci USA 103(42):15309–15314
12. Konkolewicz D, Krys P, Gois JR, Mendonca PV, Zhong M, Wang Y, Gennaro A, Isse AA, Fantin M, Matyjaszewski K (2014) Aqueous RDRP in the presence of Cu0: the exceptional activity of CuI confirms the SARA ATRP mechanism. Macromolecules 47(2):560–570
13. Konkolewicz D, Wang Y, Zhong M, Krys P, Isse AA, Gennaro A, Matyjaszewski K (2013) Reversible-deactivation radical polymerization in the presence of metallic copper.

A critical assessment of the SARA ATRP and SET-LRP mechanisms. Macromolecules 46(22):8749–8772
14. Konkolewicz D, Wang Y, Krys P, Zhong M, Isse AA, Gennaro A, Matyjaszewski K (2014) SARA ATRP or SET-LRP. End of controversy? Polym Chem 5(15):4396–4417
15. Konkolewicz D, Schroder K, Buback J, Bernhard S, Matyjaszewski K (2012) Visible light and sunlight photoinduced ATRP with ppm of Cu catalyst. ACS Macro Lett 1(10):1219–1223
16. Ribelli TG, Konkolewicz D, Bernhard S, Matyjaszewski K (2014) How are radicals (re) generated in photochemical ATRP? J Am Chem Soc 136:13303–13312
17. Fors BP, Hawker CJ (2012) Control of a living radical polymerization of methacrylates by light. Angew Chem Int Ed 51:8850–8853
18. Mosnáček J, Ilčíková M (2012) Photochemically mediated atom transfer radical polymerization of methyl methacrylate using ppm amounts of catalyst. Macromolecules 45(15): 5859–5865
19. Tasdelen MA, Uygun M, Yagci Y (2011) Photoinduced controlled radical polymerization. Macromol Rapid Commun 32(1):58–62
20. Magenau AJD, Strandwitz NC, Gennaro A, Matyjaszewski K (2011) Electrochemically mediated atom transfer radical polymerization. Science 332(6025):81–84
21. Bortolamei N, Isse AA, Magenau AJD, Gennaro A, Matyjaszewski K (2011) Controlled aqueous atom transfer radical polymerization with electrochemical generation of the active catalyst. Angew Chem Int Ed 50(48):11391–11394
22. Magenau AJD, Bortolamei N, Frick E, Park S, Gennaro A, Matyjaszewski K (2013) Investigation of electrochemically mediated atom transfer radical polymerization. Macromolecules 46(11):4346–4353
23. Matyjaszewski K, Tsarevsky NV (2014) Macromolecular engineering by atom transfer radical polymerization. J Am Chem Soc 136:6513–6533
24. Matyjaszewski K (2012) Atom transfer radical polymerization: from mechanisms to applications. Isr J Chem 52(3–4):206–220
25. Matyjaszewski K (2012) Atom transfer radical polymerization (ATRP): current status and future perspectives. Macromolecules 45(10):4015–4039
26. Goto A, Fukuda T (2004) Kinetics of living radical polymerization. Prog Polym Sci 29(4): 329–385
27. Tang W, Matyjaszewski K (2007) Effects of initiator structure on activation rate constants in ATRP. Macromolecules 40(6):1858–1863
28. Tang W, Kwak Y, Braunecker W, Tsarevsky NV, Coote ML, Matyjaszewski K (2008) Understanding atom transfer radical polymerization: effect of ligand and initiator structures on the equilibrium constants. J Am Chem Soc 130(32):10702–10713
29. Tang W, Matyjaszewski K (2006) Effect of ligand structure on activation rate constants in ATRP. Macromolecules 39(15):4953–4959
30. Braunecker WA, Tsarevsky NV, Gennaro A, Matyjaszewski K (2009) Thermodynamic components of the atom transfer radical polymerization equilibrium: quantifying solvent effects. Macromolecules 42(17):6348–6360
31. Seeliger F, Matyjaszewski K (2009) Temperature effect on activation rate constants in ATRP: new mechanistic insights into the activation process. Macromolecules 42(16): 6050–6055
32. Kwiatkowski P, Jurczak J, Pietrasik J, Jakubowski W, Mueller L, Matyjaszewski K (2008) High molecular weight polymethacrylates by AGET ATRP under high pressure. Macromolecules 41(4):1067–1069
33. Pyun J, Matyjaszewski K (2001) Synthesis of nanocomposite organic/inorganic hybrid materials using controlled/"living" radical polymerization. Chem Mater 13(10):3436–3448
34. Hui CM, Pietrasik J, Schmitt M, Mahoney C, Choi J, Bockstaller MR, Matyjaszewski K (2014) Surface-initiated polymerization as an enabling tool for multifunctional (nano-) engineered hybrid materials. Chem Mater 26(1):745–762

35. de Gennes PG (1987) Polymers at an interface: a simplified view. Adv Colloid Interface Sci 27(3–4):189–209
36. Tsujii Y, Ohno K, Yamamoto S, Goto A, Fukuda T (2006) Structure and properties of high-density polymer brushes prepared by surface-initiated living radical polymerization. In: Jordan R (ed) Surface-initiated polymerization I, vol 197. Springer, Berlin/Heidelberg, pp 1–45
37. Kolb HC, Finn MG, Sharpless KB (2001) Click chemistry: diverse chemical function from a few good reactions. Angew Chem Int Ed 40:2004–2021
38. Golas PL, Matyjaszewski K (2010) Marrying click chemistry with polymerization: expanding the scope of polymeric materials. Chem Soc Rev 39(4):1338–1354
39. Walther A, Müller AHE (2013) Janus particles: synthesis, self-assembly, physical properties, and applications. Chem Rev 113(7):5194–5261
40. Yuan J, Xu Y, Walther A, Bolisetty S, Schumacher M, Schmalz H, Ballauff M, Müller AHE (2008) Water-soluble organo-silica hybrid nanowires. Nat Mater 7:718–722
41. Djalali R, Hugenberg N, Fischer K, Schmidt M (1999) Amphipolar core-shell cylindrical brushes. Macromol Rapid Commun 20(8):444–449
42. Djalali R, Li S-Y, Schmidt M (2002) Amphipolar core – shell cylindrical brushes as templates for the formation of gold clusters and nanowires. Macromolecules 35(11):4282–4288
43. Lee H, Jakubowski W, Matyjaszewski K, Yu S, Sheiko SS (2006) Cylindrical core-shell brushes prepared by a combination of ROP and ATRP. Macromolecules 39(15):4983–4989
44. Lee H-I, Pietrasik J, Sheiko SS, Matyjaszewski K (2010) Stimuli-responsive molecular brushes. Prog Polym Sci 35(1–2):24–44
45. Sheiko SS, Sumerlin BS, Matyjaszewski K (2008) Cylindrical molecular brushes: synthesis, characterization, and properties. Prog Polym Sci 33(7):759–785
46. Gao H, Ohno S, Matyjaszewski K (2006) Low polydispersity star polymers via cross-linking macromonomers by ATRP. J Am Chem Soc 128(47):15111–15113
47. Gao H, Matyjaszewski K (2009) Synthesis of functional polymers with controlled architecture by CRP of monomers in the presence of cross-linkers: from stars to gels. Prog Polym Sci 34(4):317–350
48. Müllner M, Lunkenbein T, Schieder M, Gröschel AH, Miyajima N, Förtsch M, Breu J, Caruso F, Müller AHE (2012) Template-directed mild synthesis of anatase hybrid nanotubes within cylindrical core–shell–corona polymer brushes. Macromolecules 45(17):6981–6988
49. Müllner M, Lunkenbein T, Miyajima N, Breu J, Müller AHE (2012) A facile polymer templating route toward high-aspect-ratio crystalline titania nanostructures. Small 8(17): 2636–2640
50. Connal LA, Franks GV, Qiao GG (2010) Photochromic, metal-absorbing honeycomb structures. Langmuir 26(13):10397–10400
51. Pang X, Zhao L, Han W, Xin X, Lin Z (2013) A general and robust strategy for the synthesis of nearly monodisperse colloidal nanocrystals. Nat Nano 8(6):426–431
52. Kruk M, Dufour B, Celer EB, Kowalewski T, Jaroniec M, Matyjaszewski K (2008) Grafting monodisperse polymer chains from concave surfaces of ordered mesoporous silicas. Macromolecules 41(22):8584–8591
53. Mori H, Seng DC, Zhang M, Mueller AHE (2002) Hybrid nanoparticles with hyperbranched polymer shells via self-condensing atom transfer radical polymerization from silica surfaces. Langmuir 18(9):3682–3693
54. Dong H, Zhu M, Yoon JA, Gao H, Jin R, Matyjaszewski K (2008) One-pot synthesis of robust core/shell gold nanoparticles. J Am Chem Soc 130(39):12852–12853
55. Ye P, Dong H, Zhong M, Matyjaszewski K (2011) Synthesis of binary polymer brushes via two-step reverse atom transfer radical polymerization. Macromolecules 44(7):2253–2260
56. Luzinov I, Minko S, Tsukruk VV (2004) Adaptive and responsive surfaces through controlled reorganization of interfacial polymer layers. Prog Polym Sci 29(7):635–698
57. Julthongpiput D, Lin Y-H, Teng J, Zubarev ER, Tsukruk VV (2003) Y-shaped polymer brushes: nanoscale switchable surfaces. Langmuir 19(19):7832–7836

58. Zhao B, He T (2003) Synthesis of well-defined mixed poly(methyl methacrylate)/polystyrene brushes from an asymmetric difunctional initiator-terminated self-assembled monolayer. Macromolecules 36(23):8599–8602
59. Li Y, Tao P, Viswanath A, Benicewicz BC, Schadler LS (2012) Bimodal surface ligand engineering: the key to tunable nanocomposites. Langmuir 29(4):1211–1220
60. Chen R, Feng W, Zhu S, Botton G, Ong B, Wu Y (2006) Surface-initiated atom transfer radical polymerization grafting of poly(2,2,2-trifluoroethyl methacrylate) from flat silicon wafer surfaces. J Polym Sci A Polym Chem 44(3):1252–1262
61. Feng W, Chen R, Brash JL, Zhu S (2005) Surface-initiated atom transfer radical polymerization of oligo(ethylene glycol) methacrylate: effect of solvent on graft density. Macromol Rapid Commun 26(17):1383–1388
62. Ell JR, Mulder DE, Faller R, Patten TE, Kuhl TL (2009) Structural determination of high density, ATRP grown polystyrene brushes by neutron reflectivity. Macromolecules 42(24):9523–9527
63. Tomlinson MR, Efimenko K, Genzer J (2006) Study of kinetics and macroinitiator efficiency in surface-initiated atom-transfer radical polymerization. Macromolecules 39(26):9049–9056
64. Wang S, Zhu Y (2009) Facile method to prepare smooth and homogeneous polymer brush surfaces of varied brush thickness and grafting density. Langmuir 25(23):13448–13455
65. Jones DM, Brown AA, Huck WTS (2002) Surface-initiated polymerizations in aqueous media: effect of initiator density. Langmuir 18(4):1265–1269
66. Bao Z, Bruening ML, Baker GL (2006) Control of the density of polymer brushes prepared by surface-initiated atom transfer radical polymerization. Macromolecules 39(16):5251–5258
67. Jia H, Wildes A, Titmuss S (2012) Structure of pH-responsive polymer brushes grown at the gold–water interface: dependence on grafting density and temperature. Macromolecules 45(1):305–312
68. Behling RE, Williams BA, Staade BL, Wolf LM, Cochran EW (2009) Influence of graft density on kinetics of surface-initiated ATRP of polystyrene from montmorillonite. Macromolecules 42(6):1867–1872
69. Lego B, François M, Skene WG, Giasson S (2009) Polymer brush covalently attached to OH-functionalized mica surface via surface-initiated ATRP: control of grafting density and polymer chain length. Langmuir 25(9):5313–5321
70. Wu T, Efimenko K, Vlček P, Šubr V, Genzer J (2003) Formation and properties of anchored polymers with a gradual variation of grafting densities on flat substrates. Macromolecules 36(7):2448–2453
71. Lilge I, Steuber M, Tranchida D, Sperotto E, Schönherr H (2013) Tailored (Bio)interfaces via surface initiated polymerization: control of grafting density and new responsive diblock copolymer brushes. Macromol Symp 328(1):64–72
72. Coad BR, Styan KE, Meagher L (2014) One step ATRP initiator immobilization on surfaces leading to gradient-grafted polymer brushes. ACS Appl Mater Interfaces 6(10):7782–7789
73. Ohno K, Morinaga T, Koh K, Tsujii Y, Fukuda T (2005) Synthesis of monodisperse silica particles coated with well-defined, high-density polymer brushes by surface-initiated atom transfer radical polymerization. Macromolecules 38(6):2137–2142
74. Huang C, Tassone T, Woodberry K, Sunday D, Green DL (2009) Impact of ATRP initiator spacer length on grafting poly(methyl methacrylate) from silica nanoparticles. Langmuir 25(23):13351–13360
75. Sunday D, Curras-Medina S, Green DL (2010) Impact of initiator spacer length on grafting polystyrene from silica nanoparticles. Macromolecules 43(11):4871–4878
76. Pietrasik J, Hui CM, Chaladaj W, Dong H, Choi J, Jurczak J, Bockstaller MR, Matyjaszewski K (2011) Silica-polymethacrylate hybrid particles synthesized using high-pressure atom transfer radical polymerization. Macromol Rapid Commun 32(3):295–301
77. Pyun J, Jia S, Kowalewski T, Patterson GD, Matyjaszewski K (2003) Synthesis and characterization of organic/inorganic hybrid nanoparticles: kinetics of surface-initiated

atom transfer radical polymerization and morphology of hybrid nanoparticle ultrathin films. Macromolecules 36(14):5094–5104
78. El Harrak A, Carrot G, Oberdisse J, Eychenne-Baron C, Boué F (2004) Surface−atom transfer radical polymerization from silica nanoparticles with controlled colloidal stability. Macromolecules 37(17):6376–6384
79. Tchoul MN, Dalton M, Tan L-S, Dong H, Hui CM, Matyjaszewski K, Vaia RA (2012) Enhancing the fraction of grafted polystyrene on silica hybrid nanoparticles. Polymer 53(1): 79–86
80. Averick SE, Bazewicz CG, Woodman BF, Simakova A, Mehl RA, Matyjaszewski K (2013) Protein–polymer hybrids: conducting ARGET ATRP from a genetically encoded cleavable ATRP initiator. Eur Polym J 49(10):2919–2924
81. Sugnaux C, Lavanant L, Klok H-A (2013) Aqueous fabrication of pH-gated, polymer-brush-modified alumina hybrid membranes. Langmuir 29(24):7325–7333
82. Cheng N, Azzaroni O, Moya S, Huck WTS (2006) The effect of [CuI]/[CuII] ratio on the kinetics and conformation of polyelectrolyte brushes by atom transfer radical polymerization. Macromol Rapid Commun 27(19):1632–1636
83. Kim J-B, Bruening ML, Baker GL (2000) Surface-initiated atom transfer radical polymerization on gold at ambient temperature. J Am Chem Soc 122(31):7616–7617
84. Shah RR, Merreceyes D, Husemann M, Rees I, Abbott NL, Hawker CJ, Hedrick JL (2000) Using atom transfer radical polymerization to amplify monolayers of initiators patterned by microcontact printing into polymer brushes for pattern transfer. Macromolecules 33(2): 597–605
85. Hou J, Shi Q, Stagnaro P, Ye W, Jin J, Conzatti L, Yin J (2013) Aqueous-based immobilization of initiator and surface-initiated ATRP to construct hemocompatible surface of poly (styrene-b-(ethylene-co-butylene)-b-styrene) elastomer. Colloids Surf B Biointerfaces 111:333–341
86. Chakkalakal GL, Alexandre M, Abetz C, Boschetti-de-Fierro A, Abetz V (2012) Surface-initiated controlled radical polymerization from silica nanoparticles with high initiator density. Macromol Chem Phys 213(5):513–528
87. Bombalski L, Min K, Dong H, Tang C, Matyjaszewski K (2007) Preparation of well-defined hybrid materials by ATRP in miniemulsion. Macromolecules 40(21):7429–7432
88. Audouin F, Blas H, Pasetto P, Beaunier P, Boissière C, Sanchez C, Save M, Charleux B (2008) Structured hybrid nanoparticles via surface-initiated ATRP of methyl methacrylate from ordered mesoporous silica. Macromol Rapid Commun 29(11):914–921
89. Pasetto P, Blas H, Audouin F, Boissière C, Sanchez C, Save M, Charleux B (2009) Mechanistic insight into surface-initiated polymerization of methyl methacrylate and styrene via ATRP from ordered mesoporous silica particles. Macromolecules 42(16):5983–5995
90. Liu H, Zhu Y-L, Zhang J, Lu Z-Y, Sun Z-Y (2012) Influence of grafting surface curvature on chain polydispersity and molecular weight in concave surface-initiated polymerization. ACS Macro Lett 1(11):1249–1253
91. Gao X, Feng W, Zhu S, Sheardown H, Brash JL (2010) Kinetic modeling of surface-initiated atom transfer radical polymerization. Macromol React Eng 4(3–4):235–250
92. Turgman-Cohen S, Genzer J (2011) Simultaneous bulk- and surface-initiated controlled radical polymerization from planar substrates. J Am Chem Soc 133(44):17567–17569
93. Turgman-Cohen S, Genzer J (2012) Computer simulation of concurrent bulk- and surface-initiated living polymerization. Macromolecules 45(4):2128–2137
94. Schneider D, Schmitt M, Hui CM, Sainidou R, Rembert P, Matyjaszewski K, Bockstaller MR, Fytas G (2014) Role of polymer graft architecture on the acoustic eigenmode formation in densely polymer-tethered colloidal particles. ACS Macro Lett 3(10):1059–1063
95. Mastan E, Xi L, Zhu S (2015) What limits the chain growth from flat surfaces in surface-initiated ATRP: propagation, termination or both? Macromol Theor Simulat 24(2):89–99. doi:10.1002/mats.201400085

96. Huang W, Kim J-B, Bruening ML, Baker GL (2002) Functionalization of surfaces by water-accelerated atom-transfer radical polymerization of hydroxyethyl methacrylate and subsequent derivatization. Macromolecules 35(4):1175–1179
97. Dunderdale GJ, Urata C, Miranda DF, Hozumi A (2014) Large-scale and environmentally friendly synthesis of pH-responsive oil-repellent polymer brush surfaces under ambient conditions. ACS Appl Mater Interfaces 6(15):11864–11868
98. Jain P, Dai J, Baker GL, Bruening ML (2008) Rapid synthesis of functional polymer brushes by surface-initiated atom transfer radical polymerization of an acidic monomer. Macromolecules 41(22):8413–8417
99. Matyjaszewski K, Miller PJ, Shukla N, Immaraporn B, Gelman A, Luokala BB, Siclovan TM, Kickelbick G, Vallant T, Hoffmann H, Pakula T (1999) Polymers at interfaces: using atom transfer radical polymerization in the controlled growth of homopolymers and block copolymers from silicon surfaces in the absence of untethered sacrificial initiator. Macromolecules 32(26):8716–8724
100. Feng W, Brash J, Zhu S (2004) Atom-transfer radical grafting polymerization of 2-methacryloyloxyethyl phosphorylcholine from silicon wafer surfaces. J Polym Sci A Polym Chem 42(12):2931–2942
101. Xiao D, Wirth MJ (2002) Kinetics of surface-initiated atom transfer radical polymerization of acrylamide on silica. Macromolecules 35(8):2919–2925
102. Zhou D, Gao X, Wang W-J, Zhu S (2012) Termination of surface radicals and kinetic modeling of ATRP grafting from flat surfaces by addition of deactivator. Macromolecules 45(3):1198–1207
103. Kim J-B, Huang W, Miller MD, Baker GL, Bruening ML (2003) Kinetics of surface-initiated atom transfer radical polymerization. J Polym Sci A Polym Chem 41(3):386–394
104. Wang Y, Soerensen N, Zhong M, Schroeder H, Buback M, Matyjaszewski K (2013) Improving the "livingness" of ATRP by reducing Cu catalyst concentration. Macromolecules 46(3):683–691
105. Koylu D, Carter KR (2009) Stimuli-responsive surfaces utilizing cleavable polymer brush layers. Macromolecules 42(22):8655–8660
106. Yamamoto K, Miwa Y, Tanaka H, Sakaguchi M, Shimada S (2002) Living radical graft polymerization of methyl methacrylate to polyethylene film with typical and reverse atom transfer radical polymerization. J Polym Sci A Polym Chem 40(20):3350–3359
107. Kang C, Crockett RM, Spencer ND (2014) Molecular-weight determination of polymer brushes generated by SI-ATRP on flat surfaces. Macromolecules 47(1):269–275
108. Devaux C, Chapel JP, Beyou E, Chaumont P (2002) Controlled structure and density of "living" polystyrene brushes on flat silica surfaces. Eur Phys J E 7:345–352
109. Miwa Y, Yamamoto K, Sakaguchi M, Shimada S (2001) Well-defined polystyrene grafted to polypropylene backbone by "living" radical polymerization with TEMPO. Macromolecules 34(7):2089–2094
110. Yamago S, Yahata Y, Nakanishi K, Konishi S, Kayahara E, Nomura A, Goto A, Tsujii Y (2013) Synthesis of concentrated polymer brushes via surface-initiated organotellurium-mediated living radical polymerization. Macromolecules 46(17):6777–6785
111. Ohno K, Akashi T, Huang Y, Tsujii Y (2010) Surface-initiated living radical polymerization from narrowly size-distributed silica nanoparticles of diameters less than 100 nm. Macromolecules 43(21):8805–8812
112. Ohno K, Tabata H, Tsujii Y (2013) Surface-initiated living radical polymerization from silica particles functionalized with poly(ethylene glycol)-carrying initiator. Colloid Polym Sci 291(1):127–135
113. Gorman CB, Petrie RJ, Genzer J (2008) Effect of substrate geometry on polymer molecular weight and polydispersity during surface-initiated polymerization. Macromolecules 41(13): 4856–4865
114. Fischer H (1997) The persistent radical effect in "living" radical polymerization. Macromolecules 30(19):5666–5672

115. Matyjaszewski K (1997) Mechanistic and synthetic aspects of atom transfer radical polymerization. J Macromol Sci A Pure Appl Chem 34(10):1785–1801
116. Fukuda T, Goto A (1997) Gel permeation chromatographic determination of activation rate constants in nitroxide-controlled free radical polymerization, 2. Analysis of evolution of polydispersities. Macromol Rapid Commun 18(8):683–688
117. Ejaz M, Yamamoto S, Ohno K, Tsujii Y, Fukuda T (1998) Controlled graft polymerization of methyl methacrylate on silicon substrate by the combined use of the langmuir−blodgett and atom transfer radical polymerization techniques. Macromolecules 31(17):5934–5936
118. Jeyaprakash JD, Samuel S, Dhamodharan R, Rühe J (2002) Polymer brushes via ATRP: role of activator and deactivator in the surface-initiated ATRP of styrene on planar substrates. Macromol Rapid Commun 23(4):277–281
119. Chen R, Feng W, Zhu S, Botton G, Ong B, Wu Y (2006) Surface-initiated atom transfer radical polymerization of polyhedral oligomeric silsesquioxane (POSS) methacrylate from flat silicon wafer. Polymer 47(4):1119–1123
120. Li B, Yu B, Huck WTS, Liu W, Zhou F (2013) Electrochemically mediated atom transfer radical polymerization on nonconducting substrates: controlled brush growth through catalyst diffusion. J Am Chem Soc 135(5):1708–1710
121. Huang J, Pintauer T, Matyjaszewski K (2004) Effect of variation of [PMDETA]0/[Cu(I)Br] 0 ratio on atom transfer radical polymerization ofn-butyl acrylate. J Polym Sci A Polym Chem 42(13):3285–3292
122. Sharma R, Goyal A, Caruthers JM, Won Y-Y (2006) Inhibitive chain transfer to ligand in the ATRP of *n*-butyl acrylate. Macromolecules 39(14):4680–4689
123. Yu Q, Zhang Y, Chen H, Wu Z, Huang H, Cheng C (2010) Protein adsorption on poly (N-isopropylacrylamide)-modified silicon surfaces: effects of grafted layer thickness and protein size. Colloids Surf B Biointerfaces 76(2):468–474
124. Wang XJ, Bohn PW (2007) Spatiotemporally controlled formation of two-component counter-propagating lateral graft density gradients of mixed polymer brushes on planar Au surfaces. Adv Mater 19(4):515–520
125. Xue C, Yonet-Tanyeri N, Brouette N, Sferrazza M, Braun PV, Leckband DE (2011) Protein adsorption on poly(N-isopropylacrylamide) brushes: dependence on grafting density and chain collapse. Langmuir 27(14):8810–8818
126. Liu X, Ye Q, Yu B, Liang Y, Liu W, Zhou F (2010) Switching water droplet adhesion using responsive polymer brushes. Langmuir 26(14):12377–12382
127. Hui CM, Dang A, Chen B, Yan J, Konkolewicz D, He H, Ferebee R, Bockstaller MR, Matyjaszewski K (2014) Effect of thermal self-initiation on the synthesis, composition, and properties of particle brush materials. Macromolecules 47(16):5501–5508
128. Mu B, Shen R, Liu P (2009) Crosslinked polymeric nanocapsules from polymer brushes grafted silica nanoparticles via surface-initiated atom transfer radical polymerization. Colloids Surf B Biointerfaces 74(2):511–515
129. Wu D, Hui CM, Dong H, Pietrasik J, He H, Ryu HJ, Li Z, Zhong M, Jaroniec M, Kowalewski T, Matyjaszewski K (2011) Nanonetwork-structured polystyrene and carbon materials with core-shell nanosphere network unit. Polym Preprints 52(2):693–694
130. Yamamoto S, Ejaz M, Tsujii Y, Fukuda T (2000) Surface interaction forces of well-defined, high-density polymer brushes studied by atomic force microscopy. 2. Effect of graft density. Macromolecules 33(15):5608–5612
131. Liao W-P, Elliott IG, Faller R, Kuhl TL (2013) Normal and shear interactions between high grafting density polymer brushes grown by atom transfer radical polymerization. Soft Matter 9(24):5753–5761
132. Xu FJ, Neoh KG, Kang ET (2009) Bioactive surfaces and biomaterials via atom transfer radical polymerization. Prog Polym Sci 34(8):719–761
133. Krishnamoorthy M, Hakobyan S, Ramstedt M, Gautrot JE (2014) Surface-initiated polymer brushes in the biomedical field: applications in membrane science, biosensing, cell culture, regenerative medicine and antibacterial coatings. Chem Rev 114(21):10976–11026

134. Jiang H, Xu F-J (2013) Biomolecule-functionalized polymer brushes. Chem Soc Rev 42(8): 3394
135. Barbey R, Lavanant L, Paripovic D, Schüwer N, Sugnaux C, Tugulu S, Klok H-A (2009) Polymer brushes via surface-initiated controlled radical polymerization: synthesis, characterization, properties, and applications. Chem Rev 109(11):5437–5527
136. Siegwart DJ, Oh JK, Matyjaszewski K (2012) ATRP in the design of functional materials for biomedical applications. Prog Polym Sci 37(1):18–37
137. Yu K, Mei Y, Hadjesfandiari N, Kizhakkedathu JN (2014) Engineering biomaterials surfaces to modulate the host response. Colloids Surf B Biointerfaces 124:69–79
138. Zhang L, Ning C, Zhou T, Liu X, Yeung KWK, Zhang T, Xu Z, Wang X, Wu S, Chu PK (2014) Polymeric nanoarchitectures on Ti-based implants for antibacterial applications. ACS Appl Mater Interfaces 6(20):17323–17345
139. Feng W, Brash JL, Zhu S (2006) Non-biofouling materials prepared by atom transfer radical polymerization grafting of 2-methacryloloxyethyl phosphorylcholine: separate effects of graft density and chain length on protein repulsion. Biomaterials 27(6):847–855
140. Feng W, Zhu S, Ishihara K, Brash JL (2005) Adsorption of fibrinogen and lysozyme on silicon grafted with poly(2-methacryloyloxyethyl phosphorylcholine) via surface-initiated atom transfer radical polymerization. Langmuir 21(13):5980–5987
141. Gao X, Feng W, Zhu S, Sheardown H, Brash JL (2008) A facile method of forming nanoscale patterns on poly(ethylene glycol)-based surfaces by self-assembly of randomly grafted block copolymer brushes. Langmuir 24(15):8303–8308
142. Gao X, Kučerka N, Nieh M-P, Katsaras J, Zhu S, Brash JL, Sheardown H (2009) Chain conformation of a new class of PEG-based thermoresponsive polymer brushes grafted on silicon as determined by neutron reflectometry. Langmuir 25(17):10271–10278
143. Feng W, Zhu S, Brash JL (2005) Preparation of biocompatible surfaces by atom transfer radical polymerization grafting and evaluation of protein adsorption. Polym Preprints 46(2): 1278
144. Gao X, Zhu S, Sheardown H, Brash JL (2010) Nanoscale patterning through self-assembly of hydrophilic block copolymers with one chain end constrained to surface. Polymer 51(8): 1771–1778
145. Feng W, Brash JL, Zhu S (2005) Atom transfer radical polymerization grafting of 2-methacryloyloxyethyl phosphorylcholine for non-biofouling surfaces. Polym Preprints 46(2):154
146. Feng W, Gao X, McClung G, Zhu S, Ishihara K, Brash JL (2011) Methacrylate polymer layers bearing poly(ethylene oxide) and phosphorylcholine side chains as non-fouling surfaces: in vitro interactions with plasma proteins and platelets. Acta Biomater 7(10): 3692–3699
147. Feng W, Zhu S, Ishihara K, Brash JL (2006) Protein resistant surfaces: comparison of acrylate graft polymers bearing oligo-ethylene oxide and phosphorylcholine side chains. Biointerphases 1(1):50
148. Zhu S, Brash JL, Feng W (2007) Atom transfer radical polymerization grafting for surface modification-high grafting density and controlled molecular weight. In: Proceedings 2007 annual meeting of the American Institute of Chemical Engineers (07AIChE). AIChE, Salt Lake City. Paper ID 101135
149. Feng W, Nieh M-P, Zhu S, Harroun TA, Katsaras J, Brash JL (2007) Characterization of protein resistant, grafted methacrylate polymer layers bearing oligo(ethylene glycol) and phosphorylcholine side chains by neutron reflectometry. Biointerphases 2(1):34
150. Jin Z, Brash JL, Zhu S (2010) ATRP grafting of oligo(ethylene glycol) methacrylates from gold surface — effect of monomer size on grafted chain and EO unit densities. Can J Chem 88(5):411–417
151. Jin Z, Feng W, Beisser K, Zhu S, Sheardown H, Brash JL (2009) Protein-resistant polyurethane prepared by surface-initiated atom transfer radical graft polymerization (ATRgP) of

water-soluble polymers: effects of main chain and side chain lengths of grafts. Colloids Surf B Biointerfaces 70(1):53–59
152. Jin Z, Feng W, Zhu S, Sheardown H, Brash JL (2009) Protein-resistant polyurethane via surface-initiated atom transfer radical polymerization of oligo(ethylene glycol) methacrylate. J Biomed Mater Res A 91A(4):1189–1201
153. Jin Z, Feng W, Zhu S, Sheardown H, Brash JL (2010) Protein-resistant polyurethane by sequential grafting of poly(2-hydroxyethyl methacrylate) and poly(oligo(ethylene glycol) methacrylate) via surface-initiated ATRP. J Biomed Mater Res A 95(4):1223–1232
154. Jin Z, Feng W, Zhu S, Sheardown H, Brash JL (2010) Protein-resistant materials via surface-initiated atom transfer radical polymerization of 2-methacryloyloxyethyl phosphorylcholine. J Biomater Sci Polym Ed 21(10):1331–1344
155. Yu B-Y, Zheng J, Chang Y, Sin M-C, Chang C-H, Higuchi A, Sun Y-M (2014) Surface zwitterionization of titanium for a general Bio-inert control of plasma proteins, blood cells, tissue cells, and bacteria. Langmuir 30(25):7502–7512
156. Sin M-C, Sun Y-M, Chang Y (2014) Zwitterionic-based stainless steel with well-defined polysulfobetaine brushes for general bioadhesive control. ACS Appl Mater Interfaces 6(2): 861–873
157. Lee SB, Koepsel RR, Morley SW, Matyjaszewski K, Sun Y, Russell AJ (2004) Permanent, nonleaching antibacterial surfaces. 1. Synthesis by atom transfer radical polymerization. Biomacromolecules 5(3):877–882
158. Huang J, Murata H, Koepsel RR, Russell AJ, Matyjaszewski K (2007) Antibacterial polypropylene via surface-initiated atom transfer radical polymerization. Biomacromolecules 8(5):1396–1399
159. Yu Q, Cho J, Shivapooja P, Ista LK, López GP (2013) Nanopatterned smart polymer surfaces for controlled attachment, killing, and release of bacteria. ACS Appl Mater Interfaces 5(19): 9295–9304
160. Kobayashi M, Terada M, Takahara A (2012) Polyelectrolyte brushes: a novel stable lubrication system in aqueous conditions. Faraday Discuss 156:403
161. Kobayashi M, Terayama Y, Hosaka N, Kaido M, Suzuki A, Yamada N, Torikai N, Ishihara K, Takahara A (2007) Friction behavior of high-density poly(2-methacryloyloxyethyl phosphorylcholine) brush in aqueous media. Soft Matter 3(6):740
162. Chen M, Briscoe WH, Armes SP, Klein J (2009) Lubrication at physiological pressures by polyzwitterionic brushes. Science 323(5922):1698–1701
163. Nomura A, Okayasu K, Ohno K, Fukuda T, Tsujii Y (2011) Lubrication mechanism of concentrated polymer brushes in solvents: effect of solvent quality and thereby swelling state. Macromolecules 44(12):5013–5019
164. Bielecki RM, Benetti EM, Kumar D, Spencer ND (2012) Lubrication with oil-compatible polymer brushes. Tribol Lett 45(3):477–487
165. Kumar S, Dory YL, Lepage M, Zhao Y (2011) Surface-grafted stimuli-responsive block copolymer brushes for the thermo-, photo- and pH-sensitive release of dye molecules. Macromolecules 44(18):7385–7393
166. Kumar S, Tong X, Dory YL, Lepage M, Zhao Y (2013) A CO2-switchable polymer brush for reversible capture and release of proteins. Chem Commun 49(1):90–92
167. Wischerhoff E, Uhlig K, Lankenau A, Börner HG, Laschewsky A, Duschl C, Lutz JF (2008) Controlled cell adhesion on PEG-based switchable surfaces. Angew Chem Int Ed 47(30): 5666–5668
168. Kobayashi M, Terada M, Takahara A (2011) Reversible adhesive-free nanoscale adhesion utilizing oppositely charged polyelectrolyte brushes. Soft Matter 7(12):5717
169. Kobayashi M, Takahara A (2013) Environmentally friendly repeatable adhesion using a sulfobetaine-type polyzwitterion brush. Polym Chem 4(18):4987
170. Matrab T, Save M, Charleux B, Pinson J, Cabet-deliry E, Adenier A, Chehimi MM, Delamar M (2007) Grafting densely-packed poly(n-butyl methacrylate) chains from an iron substrate by aryl diazonium surface-initiated ATRP: XPS monitoring. Surf Sci 601(11):2357–2366

171. Gong R, Maclaughlin S, Zhu S (2008) Surface modification of active metals through atom transfer radical polymerization grafting of acrylics. Appl Surf Sci 254(21):6802–6809
172. Chen R, Zhu S, Maclaughlin S (2008) Grafting acrylic polymers from flat nickel and copper surfaces by surface-initiated atom transfer radical polymerization. Langmuir 24(13): 6889–6896
173. Lu G, Li Y-M, Lu C-H, Xu Z-Z (2010) Corrosion protection of iron surface modified by poly(methyl methacrylate) using surface-initiated atom transfer radical polymerization (SI-ATRP). Colloid Polym Sci 288(14–15):1445–1455
174. Xie Z, Chen C, Zhou X, Gao T, Liu D, Miao Q, Zheng Z (2014) Massively parallel patterning of complex 2D and 3D functional polymer brushes by polymer pen lithography. ACS Appl Mater Interfaces 6(15):11955–11964
175. Ohno K, Kayama Y, Ladmiral V, Fukuda T, Tsujii Y (2010) A versatile method of initiator fixation for surface-initiated living radical polymerization on polymeric substrates. Macromolecules 43(13):5569–5574
176. Sweat DP, Kim M, Yu X, Schmitt SK, Han E, Choi JW, Gopalan P (2013) A dual functional layer for block copolymer self-assembly and the growth of nanopatterned polymer brushes. Langmuir 29(41):12858–12865
177. Chen T, Amin I, Jordan R (2012) Patterned polymer brushes. Chem Soc Rev 41(8):3280
178. Yue W-W, Li H-J, Xiang T, Qin H, Sun S-D, Zhao C-S (2013) Grafting of zwitterion from polysulfone membrane via surface-initiated ATRP with enhanced antifouling property and biocompatibility. J Membr Sci 446:79–91
179. Frost S, Ulbricht M (2013) Thermoresponsive ultrafiltration membranes for the switchable permeation and fractionation of nanoparticles. J Membr Sci 448:1–11
180. Chen Y-C, Xie R, Chu L-Y (2013) Stimuli-responsive gating membranes responding to temperature, pH, salt concentration and anion species. J Membr Sci 442:206–215
181. Ran J, Wu L, Zhang Z, Xu T (2014) Atom transfer radical polymerization (ATRP): a versatile and forceful tool for functional membranes. Prog Polym Sci 39(1):124–144
182. Slowing II, Trewyn BG, Giri S, Lin VSY (2007) Mesoporous silica nanoparticles for drug delivery and biosensing applications. Adv Funct Mater 17(8):1225–1236
183. Zhou Z, Zhu S, Zhang D (2007) Grafting of thermo-responsive polymer inside mesoporous silica with large pore size using ATRP and investigation of its use in drug release. J Mater Chem 17(23):2428–2433
184. Shen Y, Qi L, Wei X, Zhang R, Mao L (2011) Preparation of well-defined environmentally responsive polymer brushes on monolithic surface by two-step atom transfer radical polymerization method for HPLC. Polymer 52(17):3725–3731
185. Zhu Y, Xu X, Brault ND, Keefe AJ, Han X, Deng Y, Xu J, Yu Q, Jiang S (2014) Cellulose paper sensors modified with zwitterionic poly(carboxybetaine) for sensing and detection in complex media. Anal Chem 86(6):2871–2875
186. He H, Zhong M, Konkolewicz D, Yacatto K, Rappold T, Sugar G, David NE, Matyjaszewski K (2013) Carbon black functionalized with hyperbranched polymers: synthesis, characterization, and application in reversible CO_2 capture. J Mater Chem A 1(23):6810
187. Choi J, Hui CM, Schmitt M, Pietrasik J, Margel S, Matyjazsewski K, Bockstaller MR (2013) Effect of polymer-graft modification on the order formation in particle assembly structures. Langmuir 29(21):6452–6459
188. Choi J, Hui CM, Pietrasik J, Dong H, Matyjaszewski K, Bockstaller MR (2012) Toughening fragile matter: mechanical properties of particle solids assembled from polymer-grafted hybrid particles synthesized by ATRP. Soft Matter 8(15):4072–4082
189. Dang A, Hui CM, Ferebee R, Kubiak J, Li T, Matyjaszewski K, Bockstaller MR (2013) Thermal properties of particle brush materials: effect of polymer graft architecture on the glass transition temperature in polymer-grafted colloidal systems. Macromol Symp 331–332 (1):9–16

190. Dang A, Ojha SS, Hui CM, Mahoney C, Matyjaszewski K, Bockstaller MR (2014) High transparency polymer nanocomposites enabled by polymer graft modification of particle fillers. Langmuir 30(48):14434–14442
191. Pyun J (2007) Nanocomposite materials from functional polymers and magnetic colloids. Polym Rev 47(2):231–263
192. Bull MM, Chung WJ, Anderson SR, Kim S-J, Shim I-B, Paik H-J, Pyun J (2010) Synthesis of ferromagnetic polymer coated nanoparticles on multi-gram scale with tunable particle size. J Mater Chem 20(29):6023
193. Marutani E, Yamamoto S, Ninjbadgar T, Tsujii Y, Fukuda T, Takano M (2004) Surface-initiated atom transfer radical polymerization of methyl methacrylate on magnetite nanoparticles. Polymer 45(7):2231–2235
194. Zeltner M, Grass RN, Schaetz A, Bubenhofer SB, Luechinger NA, Stark WJ (2012) Stable dispersions of ferromagnetic carbon-coated metal nanoparticles: preparation via surface initiated atom transfer radical polymerization. J Mater Chem 22(24):12064
195. Chen R, Maclaughlin S, Botton G, Zhu S (2009) Preparation of Ni-g-polymer core–shell nanoparticles by surface-initiated atom transfer radical polymerization. Polymer 50(18): 4293–4298
196. Gu H, Faucher S, Zhu S (2012) Magnetic organosilica nanoparticles for localized polymer surface modification. Macromol Mater Eng 297(3):263–271
197. Liu G, Cai M, Wang X, Zhou F, Liu W (2014) Core–shell–corona-structured polyelectrolyte brushes-grafting magnetic nanoparticles for water harvesting. ACS Appl Mater Interfaces 6(14):11625–11632
198. Dong H, Huang J, Koepsel RR, Ye P, Russell AJ, Matyjaszewski K (2011) Recyclable antibacterial magnetic nanoparticles grafted with quaternized poly(2-(dimethylamino)ethyl methacrylate) brushes. Biomacromolecules 12(4):1305–1311
199. Zeltner M, Toedtli LM, Hild N, Fuhrer R, Rossier M, Gerber LC, Raso RA, Grass RN, Stark WJ (2013) Ferromagnetic inks facilitate large scale paper recycling and reduce bleach chemical consumption. Langmuir 29(16):5093–5098
200. Tian C, Bao C, Binder A, Zhu Z, Hu B, Guo Y, Zhao B, Dai S (2013) An efficient and reusable "hairy" particle acid catalyst for the synthesis of 5-hydroxymethylfurfural from dehydration of fructose in water. Chem Commun 49(77):8668–8670
201. Farmer SC, Patten TE (2001) Photoluminescent polymer/quantum dot composite nanoparticles. Chem Mater 13(11):3920–3926
202. Esteves ACC, Bombalski L, Trindade T, Matyjaszewski K, Barros-Timmons A (2007) Polymer grafting from CdS quantum dots via AGET ATRP in miniemulsion. Small 3(7): 1230–1236
203. Berger S, Synytska A, Ionov L, Eichhorn K-J, Stamm M (2008) Stimuli-responsive bi-component polymer janus particles by "grafting from"/"grafting to" approaches. Macromolecules 41(24):9669–9676
204. Liu B, Wei W, Qu X, Yang Z (2008) Janus colloids formed by biphasic grafting at a pickering emulsion interface. Angew Chem Int Ed 47(21):3973–3975
205. Zhou T, Wang B, Dong B, Li CY (2012) Thermoresponsive amphiphilic janus silica nanoparticles via combining "polymer single-crystal templating" and "grafting-from" methods. Macromolecules 45(21):8780–8789

Adv Polym Sci (2016) 270: 77–106
DOI: 10.1007/12_2015_316

Published online: 17 May 2015

Reversible Addition-Fragmentation Chain Transfer Polymerization from Surfaces

Youliang Zhao and Sébastien Perrier

Abstract Reversible addition–fragmentation chain transfer (RAFT) polymerization-based surface modification has emerged as a powerful tool for preparation of well-defined polymers grafted solid substrates. Combination of the RAFT process with highly efficient ligation reactions involving click chemistry can further extend its application in controlled synthesis of functional hybrid and composite materials. This review highlights some basic features of this method and describes synthesis of polymer-grafted solid surfaces such as silica particles, metal oxide, gold nanoparticles, cellulose, and graphene oxide. Applications of such functional materials, including their use in functional additives, bioactive surfaces and biomaterials, stationary phases for chromatographic applications, and preparation of hollow capsules and molecularly imprinted polymer films, are also summarized.

Keywords Click chemistry • Graft reaction • Hybrid material • Post-polymerization modification • RAFT polymerization • Surface modification

Contents

Y. Zhao (✉)
Suzhou Key Laboratory of Macromolecular Design and Precision Synthesis, Jiangsu Key Laboratory of Advanced Functional Polymer Design and Application, College of Chemistry, Chemical Engineering and Materials Science, Soochow University, Suzhou, 215123, China
e-mail: ylzhao@suda.edu.cn

S. Perrier
Department of Chemistry, The University of Warwick, Gibbet Hill, Coventry CV4 7AL, UK

Faculty of Pharmacy and Pharmaceutical Sciences, Monash University, 381 Royal Parade, Parkville, VIC 3052, Australia
e-mail: s.perrier@warwick.ac.uk

1 Introduction to the RAFT Process

Reversible addition–fragmentation chain transfer (RAFT) polymerization [1, 2] proceeds by a degenerative chain transfer mechanism in which a thiocarbonylthio group is exchanged between growing polymeric chains. The RAFT process was developed independently by Moad, Rizzardo, and Thang from the Commonwealth Scientific Research Organisation (CSIRO) group [3] and Zard and coworkers in collaboration with Rhodia [4]. The technique developed by Zard and coworkers, although mechanistically identical to that developed by the CSIRO group, used xanthates as the transfer agent and was coined "macromolecular design via the interchange of xanthates" (MADIX). Because these techniques only differ in the nature of the chain transfer agent (CTA), both are referred to here as RAFT for clarity.

The reactivity and, hence, suitability of a RAFT agent (CTA) for polymerizing different monomers is determined by the nature of the R and Z substituents. The Z-group influences both the activity of the thiocarbonyl group for radical addition and the stability of the resulting radical species, whereas the R-group initiates the growth of new polymeric chains. RAFT polymerization consists of the addition of a small amount of thiocarbonyl thio-based CTA to a conventional free radical polymerization system. The mechanism is thought to occur as described in Scheme 1. This mechanism comprises an initiation step (I) in which radicals are produced, for instance from thermal decomposition of a radical initiator (e.g., AIBN). These radicals then react with monomer, forming oligomers, before reacting with the RAFT agent (II). As the reactivity of the thiocarbonyl thio group is higher than that of the monomer, most of the RAFT agent is consumed to form oligomeric adducts before propagation occurs. This adduct can then fragment back to the oligomer and original RAFT agent, or form an oligomeric RAFT agent and R-group radical that can then reinitiate (III). To ensure that the

(I) Initiation

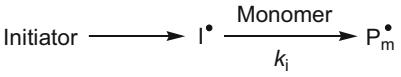

(II) Chain transfer

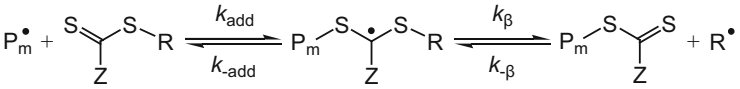

(III) Reinitiation/Propagation

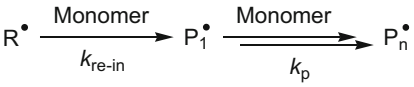

(IV) Chain equilibration

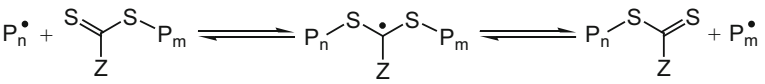

(V) Termination

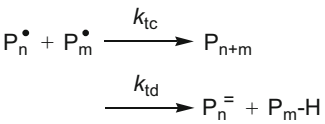

Scheme 1 Generally accepted mechanism for RAFT polymerization, showing stages *I–V*. Adapted from Perrier and Takolpuckdee [2]

reaction is controlled, the R-group must fragment from the RAFT agent at least as fast as the monomer or initiator, and reinitiate polymerization effectively. After this initial step, the reaction proceeds under equilibrated conditions, with radicals propagating and regularly transferring to the RAFT agent (IV). The kinetics of RAFT polymerization is close to that of conventional free radical polymerization, and is typically governed by the monomer concentration, with termination events determined by the amount of initiator that has decomposed. This is a feature of the RAFT process; unlike other types of living radical polymerizations, the number of dead chains in a RAFT system is exactly known because it corresponds to the number of initiating radicals (assuming no side decomposition reactions of the CTA) [5]. Therefore, optimal control in short reaction times is obtained when the ratio of CTA to initiator is kept as low as possible (typically 100), and monomer concentration is maintained around 2–3 M [6–8].

The reactivity of the RAFT agent is a crucial factor in achieving controlled polymerization [9]. In addition to the R-group, which ensures effective chain transfer and reinitiation, the Z-group must be of appropriate activity for the monomer being polymerized. The Z-group both activates the thiocarbonyl bond,

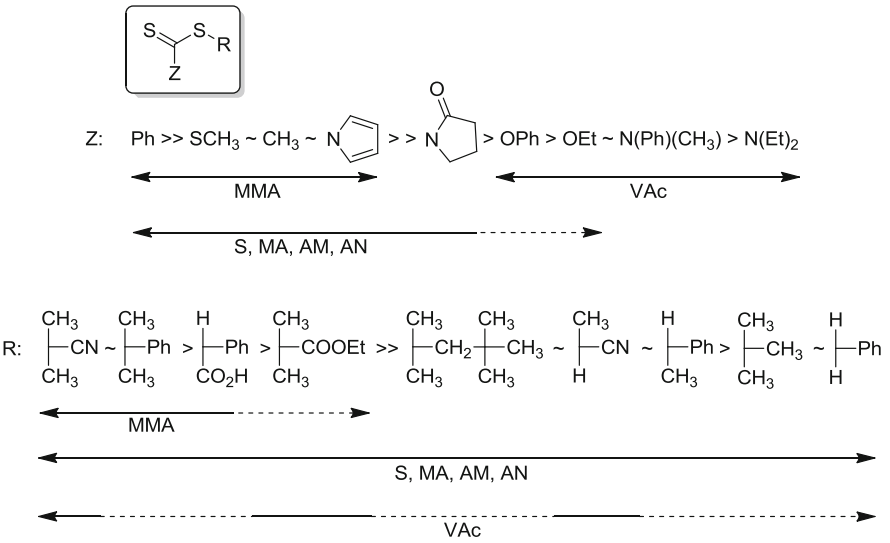

Fig. 1 Guidelines for the selection of Z-groups and R-groups for the polymerization of methyl methacrylate (*MMA*), styrene (*S*), methyl acrylate (*MA*), acrylamide (*AM*), acrylonitrile (*AN*) and vinyl acetate (*VAc*). For Z, addition rate decreases and fragmentation rate increases from *left* to *right*. For R, fragmentation rates decrease from *left* to *right*. *Dashed line* indicates partial control. Adapted from Moad et al. [9]

thus controlling the rate of addition, and stabilizes the intermediate radical, which controls the fragmentation step. The rates of addition and fragmentation required depend on the nature of the monomer being polymerized. Figure 1 shows a range of R- and Z-groups and their suitability for the polymerization of a selection of common monomers.

2 Synthetic Strategies for Surface-Grafted RAFT Polymerization

Surface-grafted RAFT polymerization differs from other techniques by the type of possible tethering points for attaching polymeric chains to the substrate surface. Grafting can occur by attaching the RAFT agent to the substrate either via its R-group (Scheme 2a) or its Z-group (Scheme 2b). Attaching the RAFT agent by its R-group is defined as a "grafting-from" approach. Using the Z-group as tethering point is often acknowledged as a "grafting-to" approach, because the chains grow away from the substrate before reacting back onto the tethered RAFT agent. Alternatively, chains can be grafted by attaching the free radical initiator to the substrate (typically a thermal initiator).

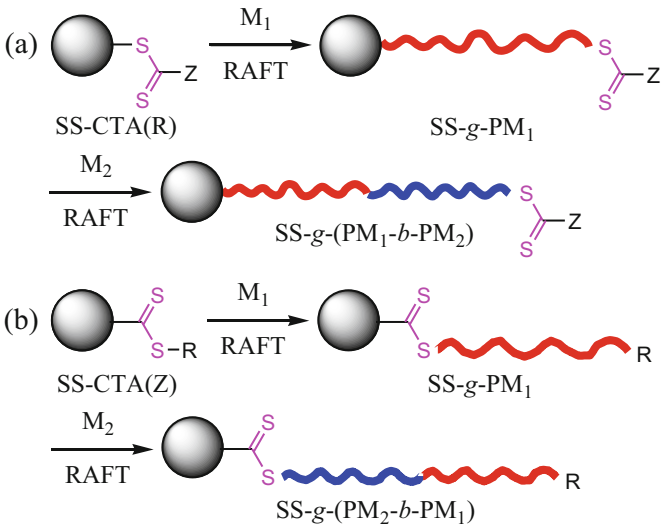

Scheme 2 Synthetic routes to diblock copolymer-grafted solid substrates (*SS*) via the R-group approach (**a**) or Z-group approach (**b**)

Tsujii et al. first described a silica-supported R-group RAFT agent prepared by transforming the bromide group of a polystyrene (PS) chain grafted onto silica by atom transfer radical polymerization (ATRP) into a dithiobenzoate. The authors then used these particles to mediate the RAFT polymerization of styrene [10]. Li and Benicewicz proposed a more direct approach to surface-initiated RAFT (SI-RAFT) polymerization by directly attaching a dithiobenzoate RAFT agent to the surface of silica particles [11, 12]. This approach is now more widely adopted, and improved control over the polymerization is obtained by introducing a free RAFT agent, which favors rapid exchange between surface-bound radicals and free chains. The free polymeric chains obtained in such a process provide a good indication of the molecular weight and polydispersity of the grafted chains [10, 13, 14]. However, at high surface density of RAFT agent, the tethered chains could have a higher molecular weight than the free chains, because slow diffusion of species leads to grafted chains growing via an uncontrolled radical process. Typically, excellent control over the polymerization is achieved, although reactions have to be kept at low monomer conversion (<20%) [14].

The ability to graft polymeric chains by tethering the RAFT agent via its Z-group is a unique feature of the RAFT process. In this approach, a propagating polymeric chain diffuses to the surface of the particle to undergo the degenerative transfer, a process closer to the grafting-to approach than the grafting-from approach. The first example of this synthetic route was provided by Perrier and Zhao, who functionalized Merrifield resin and silica particles by attaching a Z-supported RAFT agent to mediate polymerization [15–18]. The same concept

was extended to the use of xanthate, to mediate polymerization of vinyl acetate from a Wang resin [19]. A noteworthy feature of the Z-group approach is that it produces "pure" living polymeric chains, as each polymer chain bound to the particle is end-functionalized by the Z-group of the RAFT agent and can therefore be purified from dead chains, which remain in solution. This synthetic route, however, suffers from the typical drawback of the grafting-to approach: steric hindrance of the chains diffusing to the surface-anchored Z-group leads to low grafting density. Zhao et al. exploited this aspect of the reaction by reacting azide-functionalized silica particles with alkyne Z-functionalized RAFT agents in a parallel copper(I)-mediated azide–alkyne cycloaddition (CuAAC)/RAFT approach [20]. The silica–polymer core–shell nanoparticles obtained by this process were only partially grafted with polymer chains, by reaction with some azide groups. The polymer grafts were subsequently cleaved from the particles and the remaining unreacted azide groups were employed for further RAFT/CuAAC reactions. This process permits use of the silica particles as a reusable solid support to generate pure living polymers.

A very interesting study by Ranjan and Brittain compared the R- and Z-group approaches by attaching an alkyne-functionalized RAFT agent to azide-functionalized silica particles via either the R- or Z-group using CuAAC. The authors showed that a much higher grafting density could be obtained via the R-group approach than via the Z-group method [21–23]. An elegant synthesis by Rotzoll and Vana confirmed these observations: the authors grafted PMA loops to silica surfaces by employing a bifunctional RAFT agent anchored by both its R- and Z-groups [24, 25]. The polymeric chains grafted by the RAFT agent Z-group exhibited higher molecular weights than the chains obtained from an R-group-tethered RAFT agent. The authors proposed that larger propagating polymer chains were capable of reacting with the RAFT agents tethered by their Z-group as a result of the lower steric hindrance caused by low grafting densities.

In addition to Z-supported RAFT graft polymerization, some other grafting-to strategies have been developed for preparation of hybrid and composite materials. These protocols are usually based on efficient ligation reactions in which "as-prepared" RAFT polymers are attached to surface-functionalized solid substrates. Such reactions include CuAAC, thiol-based click chemistry, ligand exchange [26–29], esterification and carbodiimide chemistry [30], alkoxylsilane–hydroxyl coupling, Diels–Alder reactions [31, 32], and functional RAFT polymers as precursors or templates for formation of metal oxide nanoparticles [33, 34]. For instance, Kaupp et al. synthesized novel photosensitive RAFT agents based on *ortho*-quinodimethane (photoenol) chemistry for advanced microparticle design, in which the photoenol group reacted with dieneophiles under mild irradiation ($\lambda_{max} = 320$ nm) and ambient conditions [31]. With the aid of a light-induced grafting reaction, RAFT polymers could be grafted onto porous poly(glycidyl methacrylate) (PGMA) microspheres, and Janus microspheres could be prepared by employing a Pickering emulsion approach. Meanwhile, Kaupp et al. also reported photo-induced functionalization of spherical and planar surfaces via

caged thioaldehyde end-functionalized RAFT polymers, in which the terminal photogenerated thioaldehyde could undergo hetero Diels–Alder reactions with dienes as well as reactions with nucleophiles [32]. The terminal photoreactive polymers were photografted to porous diene-reactive polymeric microspheres to form core–shell objects with grafting densities of up to 0.10 molecules/nm^2. In addition, the versatility of the thioaldehyde ligation was evidenced by spatially resolved grafting of PS onto nucleophilic groups present in polydopamine-coated glass slides and silicon wafers via two-photon direct laser writing imaged by time-of-flight secondary ion mass spectrometry (ToF-SIMS). As an alternative to traditional polymer–metal nanoparticle hybrids prepared by ligand exchange with thiol-terminated polymers [26–29], Liu and coworkers reported an alternative approach to the size-selective and template-free synthesis of asymmetrically functionalized ultrasmall (<4 nm) gold nanoparticles (AuNPs), stably functionalized with a single amphiphilic triblock copolymer chain per nanoparticle [35]. The RAFT-synthesized copolymer had poly(ethylene oxide) (PEO) and PS outer blocks and a 1,2-dithiolane-functionalized AuNP-binding middle block, poly[lipoic acid 2-hydroxy-3-(methacryloyloxy)propyl ester-*co*-glycidyl methacrylate]. Directed nanoparticle self-assembly was used to afford organic–inorganic hybrid micelles, vesicles, rods, and large compound micelles by taking advantage of the rich microphase separation behavior of the as-synthesized AuNP hybrid amphiphilic triblock copolymers.

The use of free radical initiator tethered to a surface is an alternative approach to surface-grafted RAFT polymerization. Baum and Brittain were the first to report RAFT polymerization using a silica-functionalized free radical initiator, azoundecylchlorosilane [36]. The polymerization was mediated by a free cumyldithiobenzoate RAFT agent in solution, and yielded a mixture of free and grafted chains. Rotzoll and Vana proposed an interesting alternative method that involved attaching both a free radical initiator and a RAFT agent onto a silica particle; this strategy led to grafted particles with no observable free chains in solution [37]. More recently, Le-Masurier et al. proposed an original approach to grafting polymeric chains from silica particles coated with polydopamine [38]. The authors used a RAFT agent bearing a latent isocyanate functionality (azide carbonyl) on its R-group [39] to mediate polymerization. The carbonyl azide of the RAFT agent was converted into an isocyanate group as the R-group fragmented from the CTA, followed by rapid addition of the isocyanate onto the amine and hydroxyl groups of the polydopamine substrate. In this system, the mechanism is a hybrid between grafting-to and grafting-from in the early steps of the polymerization, but rapid addition of the isocyanate group formed in situ to the substrate ensures that the polymerization rapidly follows the traditional grafting-from route. This approach is versatile because it does not require prefunctionalization of the particles with a CTA. The approach also enables fine-tuning of the grafting density, thanks to the selectivity of the isocyanate reaction with amine (no catalyst required) and hydroxyl (catalyst required) groups.

3 Synthesis of Polymer-Grafted Solid Substrates via the RAFT Process

3.1 Polymer-Grafted Silica Particles

Silica–polymer hybrids have attracted much attention recently because of their wide range of applications in adhesion, biomaterials, coatings, composites, microelectronics, and thin films [40–45]. Thus far, silicon-based surfaces such as silica particles, silicon wafers, and polyhedral oligomeric silsesquioxanes (POSS) have been subjected to covalent modification with polymers to generate the target hybrids. Of these, silica (nano)particles have some advantages, including high mechanical strength, permeability, thermal and chemical stability, relatively low refractive index, and high surface area. They are usually chosen as ideal solid substrates for surface modification.

If polymerizable vinyl bonds are tethered to the surface of silica particles, subsequent copolymerization can be readily used to achieve silica–polymer hybrids. Guo et al. reported the synthesis of well-defined lactose-containing polymer grafted onto silica particles, in which poly(2-*O*-methacryloyloxyethoxyl-(2,3,4,6-tetra-*O*-acetyl-*β*-D-galactopyranosyl)-(1-4)-2,3,6-tri-*O*-acetyl-*β*-D-glucopyranoside) (PMAEL) obtained by cumyl dithiobenzoate (CDB)-mediated RAFT polymerization was grafted onto *γ*-methacryloxypropyltrimethoxy-modified silica particles and then deprotected to generate lactose-carrying polymer-grafted silica [46]. Chinthamanipeta et al. reported the preparation of poly(methyl methacrylate) (PMMA)–silica nanocomposites via the "grafting-through" approach, in which 3-methacryloxypropyldimethylchlorosilane was used to attach methacryl groups to the silica surface, and RAFT polymerization produced the target nanocomposites with controlled molecular weight up to 100 kDa [47]. Yang et al. synthesized silica–PS core–shell particles by SI-RAFT, in which poly(*γ*-methacryloxypropyltrimetboxysilane)-based macro-RAFT agents were immobilized onto the silica surface via a silane coupling. Subsequent grafting of polymer onto silica formed core–shell nanostructures showing a sharp contrast between silica core and polymer shell in the phase composition [48]. More recently, aerogel–PS nanocomposites with mixed free and aerogel-attached PS chains were synthesized by Sobani et al. via a grafting-through approach using 3-methacryloxypropyldimethylchlorosilane as an aerogel modifier [49].

Using Z-supported RAFT graft polymerization, Zhao and Perrier synthesized a series of homopolymer- and diblock copolymer-grafted silica particles and fumed silica. The grafted chains comprising poly(methyl acrylate) (PMA), poly(butyl acrylate) (PBA), poly(*N*,*N*-dimethylacrylamide) (PDMA), poly(*N*-isopropylacrylamide) (PNIPAM), PMMA, and PS segments usually had controlled chain length and relatively low polydispersity [16–18]. Stenzel and coworkers prepared stimuli-responsive glycopolymer brushes composed of poly(*N*-acryloyl glucosamine) (PAGA) and PNIPAM, in which the RAFT agent was immobilized on the surface of a treated silicon wafer. PAGA and PNIPAM brushes generated by

Z-supported RAFT polymerization showed a linear increase in brush thickness with the consumption of monomer in solution [50]. In addition to enhanced brush thickness after chain-extension polymerization, the suggested mechanism (whereby the second monomer NIPAM was incorporated between the first layer and the silicon surface) was further confirmed by contact angle measurements. Zhao and colleagues demonstrated that radical-induced addition–fragmentation processes between Z-supported silica and RAFT-generated polymers could be efficiently utilized for surface modification of fumed silica, and that Z-supported solid CTAs could be reused in the presence of excess sacrificial thermal initiator [51]. Nguyen and Vana performed RAFT polymerizations of styrene and MMA in bulk, mediated by fumed silica-supported CDB, in which increasing molecular weight with monomer conversion and absence of conventional polymerization activity in the interstitial solution phase were observed [52]. More recently, Vana and coworkers found that the immobilization of CTAs on silica for SI-RAFT via the Z-group approach was strongly dependent on the functionality of the RAFT-agent anchor group. Monoalkoxy-, dialkoxy-, and trialkoxy silyl ether groups were incorporated into trithiocarbonates and bound to planar silica surfaces and silica nanoparticles. It was found that the immobilization efficiency and the structure of the bound RAFT-agent film varied strongly according to the solvent used and the anchor group functionality [53]. SI-RAFT based on silica nanoparticles revealed that grafted oligomers were not formed within the crosslinked structures that originated from the immobilization. Furthermore, RAFT-agent films with less aggregation during the immobilization were more efficient during SI-RAFT in terms of polymer grafting density.

Using R-supported RAFT graft polymerization, a wide range of polymers have been grafted onto the surface of silica particles. Because this method is similar to the grafting-from approach, it allows synthesis of silica–polymer hybrids with grafting densities higher than those obtained by the Z-supported graft reaction. Benicewicz and coworkers reported the synthesis of well-defined silica nanoparticles grafted with PS, PBA, PS-*b*-PBA [11], PMMA [12], and dye-labeled poly(methacrylic acid) (PMAA) [54]. Dye-labeled PMAA-grafted nanoparticles with grafting density of up to 0.65 chains/nm^2 provided a platform to bind biomolecules and to track the movement of the nanoparticles in biological systems. On the basis of homopolymerization of styrene and alternating copolymerization of styrene and maleic anhydride (MAh), Liu and Pan prepared PS [55], P(S-*alt*-MAh), and P[S-*alt*-(MAh-*g*-PEO)] [56]. Liu et al. developed a universal route for preparation of silica-supported organic–inorganic hybrid noble metal nanomaterials, in which polymer-encapsulated gold or silver nanoparticles were synthesized and sterically stabilized by a shell layer of poly(4-vinylpyridine) (P4VP) grafted onto silica nanoparticles [57]. Using 6-(triethoxysilyl) 2-([(methylthio)carbonothioyl]thio)-2-phenylacetate, Ohno et al. synthesized monodisperse silica particles grafted with PS, PMMA, PNIPAM, and PBA [13]. As a result of the exceptionally high uniformity and perfect dispersibility, these hybrid particles could form interesting two- and three-dimensionally ordered arrays at the air–water interface and in suspension, respectively. Perrier and coworkers used the same approach to synthesize well-defined poly(4-vinylbenzyl

chloride)-grafted nanoparticles [58]. Using a grafting-from strategy, Choi et al. prepared reactive polymer brushes via surface RAFT polymerization of pentafluorophenyl acrylate, in which the reactive ester moieties were reacted with amino-spiropyrans to form reversible light-responsive polymer brush films. This was followed by a lithography technique to obtain a patterned surface of polymer brushes [59]. Conversion of the patterned polymer brushes with 5-[(2-aminoethyl) amino]naphthalene-1-sulfonic acid resulted in patterned fluorescent polymer brush films. More recently, Maleki et al. used SI-RAFT to synthesize mechanically reinforced silica aerogels with PS and PBA grafts. The aerogels exhibited a low density of 0.13–0.17 g/cm^3, high thermal insulation performance of 0.03–0.04 W/(m · K), and a high specific surface area of 350–780 m^2/g, with approximately one order of magnitude improvement in the compression strength compared with the nonreinforced aerogels [60]. It should be mentioned that hollow micro- and nanoobjects can be readily obtained if surface-grafted polymers are subjected to crosslinking and subsequent etching to remove the silica substrates. These objects have promising potential in materials science. For example, robust and narrowly distributed polymeric nanocapsules with size of 450 nm and a wall thickness of 10 nm were prepared by Huang et al. by combination of RAFT graft polymerization, photocrosslinking, and etching [61].

The combination of RAFT polymerization and highly efficient linking reaction can further extend the types of silica–polymer hybrids (Scheme 3). For instance, the coupling reaction between alkoxysilane and surface-bound hydroxyl moieties can lead not only to functional groups tethered to silica, but also to silica–polymer hybrids when alkoxysilane-functionalized polymers are used for the surface modification. Zhao and coworkers developed a combinatorial approach based on RAFT polymerization and alkoxylsilane–hydroxyl coupling to prepare silica particles grafted with well-defined homopolymers and di-, tri-, and tetrablock copolymers [62]. With *S*-methoxycarbonylphenylmethyl *S*-trimethoxysilylpropyltrithiocarbonate as RAFT agent, RAFT and chain-extension polymerization of vinyl monomers such as MA,

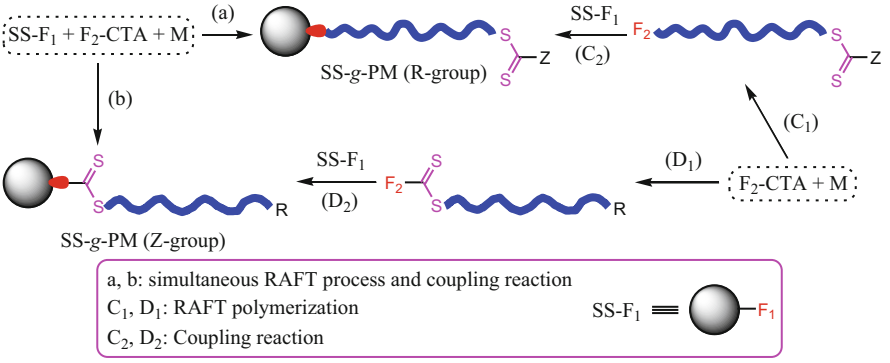

Scheme 3 Tandem (*a*, *b*) and successive (*C*, *D*) syntheses of polymer-grafted solid substrates, in which F_1–F_2 functionalities can, in theory, be any couplable moieties such as OH–$(RO)_3$Si, epoxy–COOH, azide–alkyne, and SH–en/exoxy or their precursors

BA, DMA, NIPAM, *N*-acrylomorpholine (NAM), MMA, and styrene were used to generate functional polymers, followed by a coupling reaction to synthesize the target hybrids. The grafted polymeric chains were cleaved from the surface of silica by aminolysis. Gel permeation chromatography revealed that all the grafted polymers possessed low polydispersity (typically less than 1.2) and molecular weights similar to those of the "as-prepared" polymers. Furthermore, the solid-supported polymeric chains were almost 100% living, as evident from the highly efficient chain-extension polymerization used to prepare well-defined block copolymers grafted onto silica particles. More recently, Zhao and colleagues synthesized silica nanoparticles grafted with some quaternized linear, comblike, and toothbrushlike copolymers via two-step individual reactions comprising a alkoxysilane–hydroxyl coupling reaction, quaternization, and RAFT polymerization (Scheme 4). This provides a versatile method for constructing quaternized brushes grafted onto hydroxyl-rich solid substrates [63]. Silica nanoparticles grafted with poly(*N*,*N*-dimethylaminoethyl methacrylate) (PDMAEMA) were initially prepared via tandem linking reaction and RAFT polymerization, and could act as a versatile platform for generation of three types of ion-bearing topological copolymer-grafted silica. On this basis, bromide-functionalized agents and polymers were grafted onto a surface-tethered PDMAEMA backbone to form quaternized random and comblike copolymer-grafted silica. Concurrent quaternization and RAFT polymerization were performed to generate silica nanoparticles grafted with toothbrushlike copolymers comprising PMMA, PS,

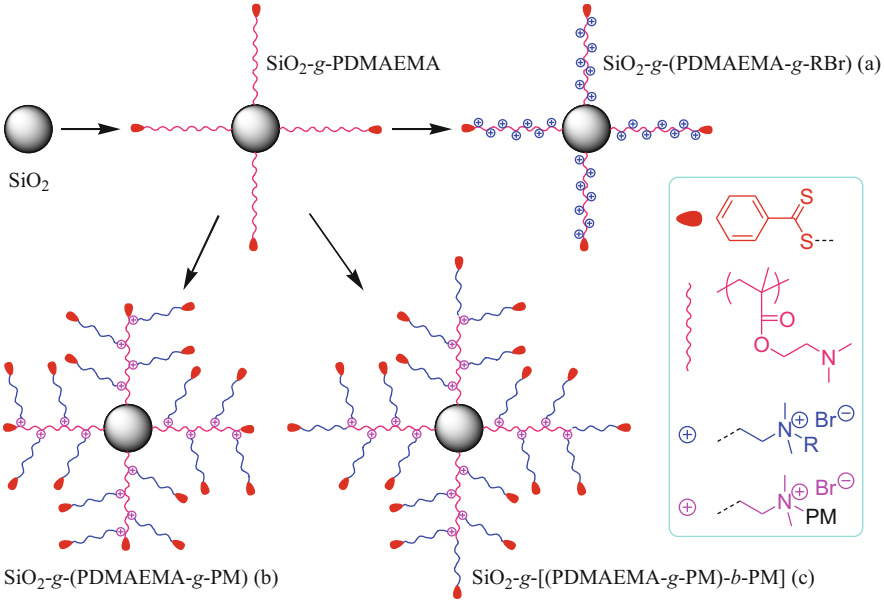

Scheme 4 Versatile synthesis of silica nanoparticles grafted with quaternized random (*a*), comblike (*b*), and toothbrushlike (*c*) copolymers via two-step reactions. Adapted from Guo et al. [63]

PNIPAM, and poly(*tert*-butyl acrylate) (P*t*BA) segments. Free polymers and grafted side chains obtained by the tandem approach usually had similar chain length and low polydispersity, and the quaternization efficiency of graft reactions was in the range 34–79% (for attaching small molecules) and 3.8–7.4% (for grafting polymeric chains). Preliminary results revealed that the surface wettability of hybrid films was dependent on factors such as macromolecular architecture, quaternization degree, chemical composition, and temperature.

An alternative approach is the use of click reactions, such as CuAAC [64–66] and thiol-based reactions [67–71], to generate silica–polymer hybrids. In their pioneering research, Ranjan and Brittain developed tandem and stepwise RAFT polymerization and click chemistry to prepare PS, PAM, and PS-*b*-PMA brushes grafted to silica nanoparticles; a wide range of grafting densities was possible [21–23]. Using the RAFT process and CuAAC, silica particles grafted with PNIPAM were prepared by Chen et al. [72]. Li and Benicewicz synthesized silica nanoparticles grafted with poly(6-azidohexyl methacrylate) and introduced various functionalities by subsequent postfunctionalization using functional alkynes via click reactions [73]. In a more recent study, Zhao and colleagues extended this method, using click chemistry to achieve highly pure block copolymers with polymeric segments such as PS, polyacrylamides, and polyacrylates [20, 74]. Tandem RAFT polymerization and CuAAC were used to prepare silica particles grafted with well-defined living block copolymers with molecular weights of up to 26,300 g/mol. Subsequent de-grafting /postmodification generated highly pure block copolymers with terminal functionalities such as thiol, methyldithio, carboxyl, hydroxyl, and halogen and also recovered surface-clickable silica particles (Scheme 5). The cycles of grafting and de-grafting reactions could be applied many times until all surface-bound clickable functionalities vanished. Kotsuchibashi

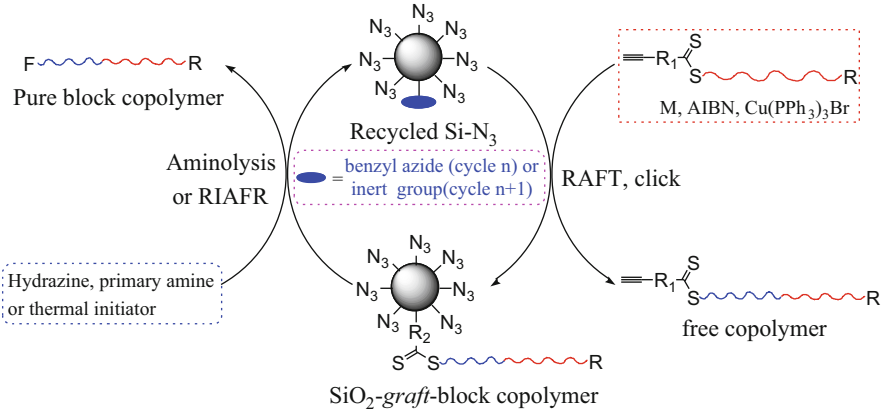

Scheme 5 Synthesis of highly pure block copolymers by combination of RAFT polymerization, azide–alkyne click reaction, and de-grafting, in which cleavage of grafted chains from a silica surface can be achieved by either aminolysis or radical-induced addition–fragmentation reactions (*RIAFR*). Adapted from Zhao et al. [20]

et al. reported preparation of temperature- and pH-responsive silica nanoparticles via simple thiol–ene click chemistry [75]. RAFT-generated PDEAEMA and PNIPAM were reduced to generate a thiol group at the chain end to react with vinyl groups on the surface of silica nanoparticles. The hybrids showed both pH- and temperature-responsive behavior and the solution properties were dependent on the ratio of the two polymers on the surface. Chen et al. reported grafting of poly (lauryl acrylate) onto nanosilica via a thiol–ene reaction, in which the trithioester terminal group of the RAFT polymer was converted to thiol and grafted onto nanosilica modified with 3-(methacryloxy)propyl-trimethoxysilane. The hybrid material has potential application in coatings or composites [76]. Peng et al. reported a facile method for combining the sol–gel reaction, RAFT process, and thiol–ene click reaction to prepare monodisperse silica–poly(*N*-vinylimidazole) core–shell microspheres of 200 nm average diameter [77]. Han et al. reported preparation of surfaces that were dual-switchable between hydrophobic and superhydrophobic by combination of RAFT and thiol–NCO chemistry, in which poly(7-[6-(acryloyloxy)hexyloxy]coumarin)-*b*-PNIPAM was grafted onto the surface of SiO_2 modified by toluene diisocyanate [78]. The static contact angle of the surface of hybrid film switched from 98° to 137° by adjusting the temperature, the contact angle also oscillated between 137° and 157° upon UV irradiation at 365 and 254 nm, respectively, revealing dual-switchable surface wettability.

3.2 *Polymer-Grafted Metal Oxide*

As a result of the strong tendency of nanoparticles such as metal oxides to agglomerate, homogeneous dispersion of these materials in a polymeric matrix is extremely important. Surfaces modified via the RAFT process have been efficiently used to prepare functional hybrids or composites, in order to avoid aggregation of nanoparticles and to enhance the filler–polymer interaction. This approach has been applied to a range of metal oxides, and examples are detailed below.

TiO_2 Hojjati et al. reported synthesis of TiO_2–PAA nanocomposites by RAFT polymerization using a bifunctional RAFT agent, 2-(butylsulfanylcarbonothioylsulfanyl) propanoic acid, with an available carboxyl group to anchor onto TiO_2 nanoparticles. Subsequent RAFT polymerization of acrylic acid (AA) formed the desired nanocomposites [79]. Ngo et al. synthesized hybrid TiO_2 nanoparticles with well-defined PMMA and poly(*tert*-butyldimethylsilyl methacrylate), in which the surface of titania nanoparticles was first modified by a coupling agent, 3-(trimethoxysilyl)propyl methacrylate (MPS), to form polymerizable particles. Then, the immobilized vinyl bond on the surface was subjected to radical polymerization in the presence of RAFT agent 2-cyanoprop-2-yl dithiobenzoate to form nanocomposites [80]. Hojjati and Charpentier reported synthesis of TiO_2–PMMA nanocomposites in supercritical CO_2 via RAFT polymerization, in which 4-cyano-4-(dodecylsulfanylthiocarbonylsulfanyl)pentanoic acid was first coordinated to the TiO_2 surface. A subsequent

RAFT process formed the target nanocomposites [81]. Crippa et al. reported preparation of high dielectric constant rutile–PS composite with an enhanced percolative threshold, in which hydrothermally synthesized TiO_2 nanocrystals were coated with PS grown by RAFT polymerization and then dispersed into a PS matrix at various concentrations [82]. It was found that the polymer molecules attached to the surfaces of nanoparticles existed in a brush regime, and that the rutile nanoparticles self-assembled into chestnut-burr aggregates whose number increased with increasing filler amount. With increasing filler concentration, the composites displayed a higher dielectric constant as a result of the self-assembly of rutile nanoparticles into chestnut-burr aggregates, where rutile crystals could share lateral faces and form capacitive microstructures.

Quantum Dots The polymeric functionalization of quantum dots (QDs) via ligand exchange is a robust method for the preparation of stable fluorescent particles with high quantum yields. For most biological applications of QDs, water solubility is a key requirement. To achieve biocompatibility, polymeric ligand systems that can provide water solubility as well as effective anchoring groups are advantageous. Viswanath et al. prepared multiply binding histamine ligands for the robust functionalization of QDs, in which histamine functional polymers bearing poly (ethylene glycol) (PEG) side chains were coated onto the surface of oleate-capped CdSe/$Cd_xZn_{1-x}S$ QDs via ligand exchange [83]. Esteves et al. reported synthesis of QD–polymer nanocomposites by RAFT polymerization in miniemulsion using a grafting-from approach, in which the surfaces of CdS and CdSe QDs were modified by PS and PS-*b*-PBA grafts [84]. Liu et al. presented some polymeric ligands for QD water solubilization to yield biocompatible and derivatizable QDs with compact size, high quantum yields (>50%), excellent stability across a large pH range (pH 5–10.5), and low nonspecific binding [85]. Das and Claverie developed a simple route for the preparation of PbS QDs embedded into polymeric nanospheres by emulsion polymerization, in which QDs were first dispersed in an aqueous solution containing a statistical oligomer with butyl acrylate and acrylic acid units, and then an emulsion polymerization process was performed to obtain core–shell nanoparticles [86]. Dilag et al. reported controlled fabrication of CdS/PDMA, CdS/poly(DMA-*co*-MMA), and CdS/poly(DMA-*co*-styrene) fluorescent QD nanocomposites for use as latent fingermark developing agents on nonporous surfaces [87]. The intrinsic optical properties of CdS QDs were retained throughout the synthetic pathways, which allowed for the successful one-step application and fluorescent visualization of latent fingermarks (fresh and aged) on aluminum foil and glass substrates under UV illumination.

Magnetic Nanoparticles Boyer et al. prepared antifouling magnetic nanoparticles (MNPs) for siRNA delivery by coating iron oxide nanoparticles (diameter of 8 nm) with poly[oligo(ethylene glycol) methyl ether acrylate] and poly(dimethylaminoethyl acrylate) (PDMAEA) [88]. Li et al. reported shape-controlled synthesis of glycopolymer-coated iron oxide nanoparticles, in which RAFT-synthesized glycopolymers were conjugated to spindle and cube-like iron oxide nanoparticles coated with dopamine methacrylamide. The resultant glyco-nanoparticles with

variable shapes had shape-dependent cell uptake behavior and enhanced activity towards specific lectins [89]. Sahoo et al. prepared thermo- and pH-responsive polymer-tethered multifunctional MNPs for targeted delivery of anticancer drugs [90]. MNPs were first surface-modified by introducing amine groups using 3-aminopropyl-triethoxysilane; then, RAFT-synthesized dual-responsive PNIPAM-*b*-PAA was attached to the amine-functionalized MNPs via the EDC/NHS method. Folic acid was tethered to the surface to accomplish cancer-specific targeting properties, and rhodamine B isothiocyanate was conjugated to endow the MNPs with fluorescence for cellular imaging applications. These nanoparticles were capable of target-specific release of loaded anticancer drug doxorubicin in response to pH and temperature and, hence, could serve as potential drug carriers for in vivo applications. More recently, Wang et al. reported a new combination of recyclable MNPs, polymers, and antibiotics that showed increased effectiveness in combating bacterial infections [91]. The strategy of direct co-precipitation of iron salts was used to generate superparamagnetic nanoparticles with a saturation magnetization of 59.5 emu/g. A silica coating was applied and used to stabilize the MNPs and create a convenient platform for further functionalization, followed by SI-RAFT to graft a variety of PMAA brushes of different lengths and at different densities. The polymer-grafted MNPs were removed from aqueous solution after antimicrobial testing using a magnet to avoid nano-based pollution of the environment. The bioactivity of an antibiotic (penicillin-G) against bacteria (*Staphylococcus aureus* and *Escherichia coli*) was significantly enhanced when physically bound to the PMAA-grafted MNPs. The inhibition activity of the penicillin–nanoparticle complex was retained using recycled MNPs that had been reloaded with penicillin-G.

3.3 Polymer-Grafted Gold Nanoparticles

The grafting of polymers onto AuNPs has attracted much attention because of the multiple applications of the resulting materials, in applications ranging from materials to medicine and biology. Sumerlin et al. reported modification of gold surfaces with water-soluble (co)polymers prepared via aqueous RAFT polymerization, which enabled the immobilization of poly(sodium 4-styrenesulfonate), poly[(4-vinylbenzyl) trimethylammonium chloride], PDMA, and poly(3-[2-(*N*-methylacrylamido)ethyldimethyl ammonio]propane sulfonate-*b*-*N*,*N*-dimethylacrylamide) onto gold films [92]. Rossner and Vana reported ordered planet–satellite nanostructures using RAFT star polymers. Preparation was based on star polymers decorated with surface-tethered trithiocarbonate groups and thus provided the polymer with the ability to connect larger AuNP planets to smaller AuNP satellites [93]. This strategy offers a straightforward way to prepare AuNP scaffolds with multiple reactive functionalities at defined distances from the central core. Glycopolymer-coated AuNPs can be used as anticancer agents [94–96] and for biomolecular recognition [97]. Kirkland-York et al. reported tailored design of

AuNP-siRNA carriers utilizing RAFT polymers [98]. Duong et al. extended the application of functional AuNPs to storage and controlled release of nitric oxide using poly[oligo(ethylene glycol) methyl ether methacrylate]-*b*-poly(vinyl benzyl chloride) as precursor [99]. Thus far, a series of functional polymers have been coated on the surface of AuNPs or acted as scaffolds to stabilize AuNPs, and these polymers primarily comprise glycopolymers [100–102], PEG-bearing poly(meth) acrylates [103–105], PS [106], poly(4-vinylpyridine) (P4VP) [107], PNIPAM [108–110], poly(*N*-vinyl caprolactam) [111, 112], poly[(3-acrylamidopropyl) trimethyl ammonium chloride [113], poly(pentafluorophenyl methacrylate) [114], PDMAEMA [115, 116], and branched poly[(*S*-4-vinylbenzyl *S*′-propyl-trithiocarbonate)-*co*-PEGMA] [117].

3.4 Polymer-Grafted Cellulose

Cellulose is a highly interesting material as a result of its materials properties, abundance, renewability and low cost. The heterogeneous grafting of cellulose fibers through controlled radical polymerization methods allows preparation of fibers with tailorable properties and built-in functionalities that can act as promising materials for advanced applications [118–121].

Carlsson revealed that modification of cellulose surfaces by cationic polymer latexes could be accomplished by RAFT-mediated surfactant-free emulsion polymerization [122]. Using radiation-induced RAFT polymerization, PS [123] and PGMA [124] were grafted onto cellulose substrates. Poly(isobornyl acrylate) was grafted onto a solid cellulose substrate by combination of RAFT polymerization and hetero Diels–Alder cycloaddition [125]. Demirci et al. performed surface modification of electrospun cellulose acetate nanofibers via RAFT polymerization and found that surface-tethered poly[(4-vinylbenzyl)trimethylammonium chloride] (PVBTAC) brushes were suitable membrane materials for filtration, purification, and/or separation of DNA [126]. Perrier and coworkers synthesized PDMAEMA-grafted cellulose and showed that its antibacterial activity was dependent on the alkyl chain length and on the degree of quaternization of graft polymers [127–129]. The PDMAEMA-grafted cellulose fiber with the highest degree of quaternization and quaternized with the shortest alkyl chains was found to exhibit particularly high activity against *E. coli*. A tailor-made conjunct of methyl cellulose and poly(vinyl acetate) (PVAc) was synthesized through the combination of RAFT polymerization and a thiol–ene click reaction [130]. Yuan et al. prepared zwitterionic polysulfobetaine brushes grafted to cellulose membranes (CMs) to improve hemocompatibility and antibiofouling properties [131]. The composites had excellent hemocompatibility, featuring lower platelet adhesion and protein adsorption properties without causing hemolysis. *E. coli* and HeLa cell adhesion tests showed that grafted CMs had superior antibacterial adhesion properties and long-term cell adhesion resistance for up to 4 days, revealing their great potential for use in biomedical applications. In addition, other homopolymers and block copolymers

such as PS [132], poly(sodium 4-styrenesulfonate) [133], PMA [134], poly(2,2,2-trifluoroethyl methacrylate) [135], poly(*N*-acryloyl-L-amino acid) [136], poly (hydroxyethyl methacrylate) (PHEMA) [137], PAM [138], poly(*N*,*N*-diethyl-acrylamide) [139], PNIPAM, PAA, and their copolymers [140] were also covalently grafted onto the surface of cellulose.

3.5 Polymer-Grafted Graphene and Graphene Oxide

Graphene nanosheets possess a range of extraordinary physical and electrical properties and have enormous potential for applications in microelectronics, photonic devices, and nanocomposite materials [141–145]. However, single graphene platelets tend to undergo agglomeration as a result of strong π–π and van der Waals interactions, which significantly compromises the final material properties. One of the strategies to overcome this problem and increase graphene compatibility with a receiving polymer host matrix is to modify graphene or graphene oxide (GO) with polymer brushes. Research to date can be grouped into approaches involving grafting-from and grafting-to techniques, and into approaches relying on covalent or noncovalent attachment of polymer chains to the suitably modified graphene or GO [146–148].

Li et al. reported a GO-based molecularly imprinted polymer (MIP) platform for detecting endocrine-disrupting chemicals. The GO–MIP hybrids showed outstanding affinity towards 2,4-dichlorophenol in aqueous solution [149]. Layek et al. synthesized amphiphilic poly(*N*-vinyl pyrrolidone)-grafted graphene by RAFT polymerization for the reinforcement of PVAc films [150]. Ye et al. developed versatile grafting approaches for functionalizing individually dispersed graphene nanosheets using RAFT polymerization and CuAAC [151]. Various types of polymer chains have been covalently tethered to graphene nanosheets using these two approaches, producing various molecular brushes with multifunctional arms, resulting in water-soluble, oil-soluble, acidic, basic, polar, apolar, and variously functionalized polymers. Peeters et al. reported thermal detection of histamine with a GO-based MIP platform prepared by RAFT polymerization [152], in which MIP–GO hybrids were able to measure histamine in buffer solutions by thermal detection. Using methacrylic acid as a hydrophilic monomer, Liu et al. synthesized hydrophilic surface ion-imprinted polymers based on GO for removal of strontium from aqueous solution [153]. Thus far, a wide range of polymers such as PS [154–156], PDMAEA, PAA [157, 158], PMMA, P*t*BA and PNIPAM [159], poly[*N*-(2-hydroxypropyl) methacrylamide] [160], poly(*N*-vinylcarbazole) [161, 162] and their copolymers have been efficiently grafted onto the surface of GO and reduced GO.

In addition to SI-RAFT and click chemistry, other linking reactions such as alkoxysilane–hydroxyl coupling reactions and carboxyl–epoxy ring-opening reactions can also be efficiently used to generate well-defined polymer-grafted graphene and GO. Zhao and coworkers reported synthesis of V-shaped copolymers grafted to

GO via a combinatorial approach [163]. Starting from a monomethoxy poly(ethylene glycol) (MPEG)-based macro chain transfer agent, three kinds of triblock copolymers with epoxy, carboxyl, or methoxysilane functionalities in the central short block were synthesized via RAFT processes. Subsequent carboxyl–epoxy and hydroxyl–methoxysilane coupling reactions were used to synthesize the target V-shaped copolymer–GO nanocomposites (Scheme 6). Owing to satisfactory control over molecular weight and polydispersity of the RAFT process, the resulting triblock copolymer MPEG-*b*-PM_1'-*b*-PM_2 possessed predetermined molecular weight, low polydispersity (1.04–1.19) and precise chemical structure; PM_1' represents poly[3-(trimethoxysilyl)propyl methacrylate] (PMPS), PGMA, or PAA obtained by hydrolysis of P*t*BA; PM_2 represents PPEGMA ($M_n = 300$), PS, PNIPAM, PDMA, or PMA. By assuming that GO nanosheets have the same specific surface area as graphene (about 2,630 m^2/g), the grafting density of V-shaped grafted copolymer on each side of GO was estimated to be within 0.025–0.162 chains/nm^2. With the aid of ultrasonic treatment, V-shaped copolymer-grafted GO could be efficiently dispersed in a wide range of solvents involving hexane and toluene. The film wettability and surface morphology of GO–copolymer nanocomposites obtained were tunable by control over factors such as temperature, solvent, and amphiphilicity of grafted chains, allowing potential applications in biomaterials, nanoscience, and nanotechnology. Meanwhile, Zhao and colleagues also synthesized homopolymer- and diblock copolymer-grafted GO by simultaneous coupling reaction and RAFT process, in which a series of polymers were covalently grafted onto GO surfaces via either grafting-to or grafting-from approaches using Z-functionalized *S*-methoxycarbonylphenylmethyl *S*′-3-(trimethoxysilyl)propyltrithiocarbonate (MPTT) and R-functionalized *S*-4-(trimethoxysilyl)benzyl *S*′-propyltrithiocarbonate (TBPT) as functional RAFT

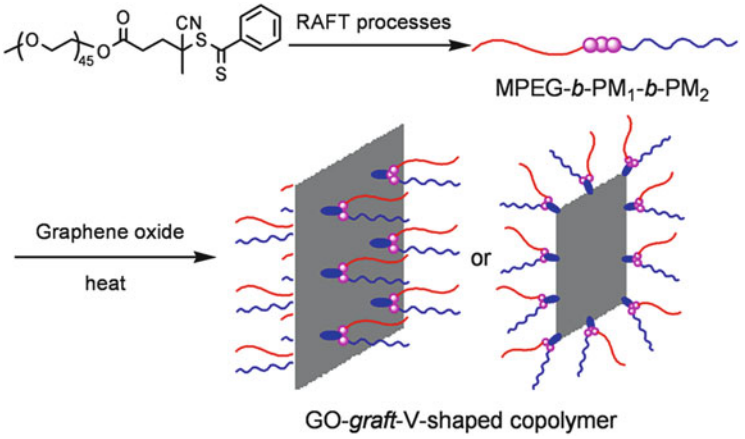

Scheme 6 Versatile syntheses of V-shaped copolymer-grafted GO. *Spherical symbols* denote monomer units with epoxy, carboxyl, or methoxysilane functionalities. Adapted from Zhang et al. [163]

agents [164]. The improved solubility and dispersibility of GO–polymer composites in various solvents, including hexane and water, confirmed their amphiphilicity. Surface morphologies involving nanosheets, nanoparticles, and nanorods were observed as the composites were dispersed in different solvents with the aid of sonication treatment, demonstrating that the grafting process can offer the opportunity to alter GO morphology.

4 Applications of Polymer-Grafted Solid Substrates

4.1 Additives to Improve Physicochemical Properties

Although silica–polymer composites can be prepared by mixing organic and inorganic components, it is difficult to obtain a homogeneous mixture [165]. To improve the compatibility between silica and polymer matrix, a popular method is to modify the silica surface using coupling agents, which not only improve the compatibility between organic and inorganic phases but also enhance the interaction between the components at the interface level. An alternative approach uses high energy plasma lasers, whereby the energetic ions from the plasma laser break the Si–C and Si–O bonds in the silane surface groups and create active sites that can react with the surrounding polymer matrix [166]. Incorporation of silica nanoparticles in the polymeric matrices gives hybrid polymer films with increased tensile strength and impact resistance, without decreasing the flexural properties of the polymer matrix. In addition to combining the flexibility and easy processing of polymers with the hardness of nanoparticles, functional hybrids can also incorporate other features by using the versatility of the solid substrate to carry catalysts, dyes, and drugs. Thus, they have a wide range of applications in hydrophobic, anticorrosion, conductive, antireflective, and photoactive materials. The utilization of polymer-coated silica nanoparticles can reduce particle aggregation in the films and achieve more homogeneous distribution of the inorganic components, resulting in better physicochemical properties.

Guo et al. synthesized a series of block-type amphiphilic copolymers via copolymerization of methacrylate end-capped oligo-urethane and MPS via the sol–gel process [167]. After hydrolysis and condensation of the copolymer precursors (self-assembled in the form of spherical micelles), polyurethane–silica hybrid materials with excellent thermal stability and mechanical properties were obtained. Etmimi et al. synthesized PS–GO nanocomposites via surface RAFT-mediated miniemulsion polymerization [155]. The molar mass and dispersity of PS in the nanocomposites were dependent on the amount of RAFT-grafted GO in the system. The PS–GO nanocomposites were of exfoliated morphology, and their thermal stability and mechanical properties were dependent on the modified GO content and better than those of neat PS polymer. Salami-Kalajahi et al. studied the effect of pristine nanoparticle loading on the properties of PMMA–silica nanocomposites prepared

via RAFT polymerization and found that the introduction of modified nanoparticles could result in better thermal and mechanical properties than those of pristine nanoparticles [168]. Surface modification and an increasing content of silica nanoparticles resulted in changes in the thermal degradation behavior of the nanocomposites. The best improvement in mechanical and thermophysical properties was achieved for nanocomposites containing 7 wt% silica nanoparticles. More recently, mechanically reinforced polymer–silica aerogels with PS and PBA segments were prepared by SI-RAFT, whereby well-defined polymers were grown on the silica surface to improve the mechanical strength compared with that of native aerogels [60]. The aerogel composites exhibited a low density of 0.13–0.17 g/cm^3, high thermal insulation performance of 0.03–0.04 W/(m · K), and a high specific surface area of 350–780 m^2/g, with approximately one order of magnitude improvement in the compression strength compared with the nonreinforced aerogels.

4.2 Bioactive Surfaces and Biomaterials

Polymer-grafted solid substrates with biocompatible or antibacterial polymers bound onto the surface can act as promising bioactive materials. Zhu et al. reported the preparation and properties of polyethersulfone (PES) ultrafiltration membranes with PHEMA-grafted silica nanoparticles as the blending additive [169]. Organic–inorganic hybrid membranes of PES with hybrid nanoparticles were fabricated via the traditional nonsolvent-induced phase separation (NIPS) process. The membrane surface porosity was increased and the surface hydrophilicity was enhanced after modification. Furthermore, the water permeability, solute rejection, and antifouling ability of PES membranes were also improved significantly. In contrast to traditional neat inorganic nanoparticle additives, the organic–inorganic hybrids could be held in/on PES membranes for a long period of time as a result of the intertwisting of polymer chains. Zhu et al. developed antifouling and antibacterial PES membranes by the addition of PDMAEMA-grafted silica nanoparticles and further postquaternization [170]. PES/SiO_2-*g*-PDMAEMA hybrid ultrafiltration membranes were prepared from the blending solutions via the NIPS process. The PDMAEMA chains incorporated into the PES membranes were further quaternized by reacting with 1,3-propane sultone and methyl iodide, respectively. The zwitterionic PES membranes exhibited excellent hydrophilicity, water permeability, solute rejection, and protein antifouling properties. The cationic membranes obtained from CH_3I treatment showed strong antibacterial activity against *E. coli* and *S. aureus* Rosenbach. Zhi et al. reported preparation of polyacrylonitrile (PAN)-based composite membranes by immersion precipitation using PDMAEMA-grafted silica nanoparticles as hydrophilic additive [171]. The synthesized nanoparticles had a typical core–shell structure, and the prepared PAN-based composite membranes had higher porosity and water permeation flux than the pure PAN membranes. As a result of the good hydrophilicity of the hybrid

nanoparticles, the membranes also showed high rejection (≥90%) of bovine serum albumin and high flux recovery ratio (≥90%) to water permeation.

Functional hybrid samples with tunable pores and stimuli-responsive grafts are promising as carriers for drug and gene delivery. A wide range of functional polymers such as PDMAEMA [172–174], PNIPAM [175], PAA [176], poly [2-(diethylamino)ethyl methacrylate]-*b*-poly[oligo(ethylene glycol) methacrylate] [177], and PAA-*b*-poly[poly(ethylene glycol) acrylate] [178] have been successfully grafted onto solid substrates for drug and gene delivery applications. The introduction of functional dyes and fluorescent molecules also allows hybrid materials to be used for therapeutic and diagnostic imaging applications[179–182].

4.3 Stationary Phases for Chromatographic Applications

Polymer-grafted silica has been widely utilized as a stationary phase in high performance liquid chromatography and shows satisfactory separation efficiency. These materials exhibit unique advantages such as high stability in extreme pH environments and sufficient retention for a variety of chemicals. As a result of heterogeneous structures and high mass-transfer resistance, polymer-grafted stationary phases normally exhibit lower column efficiency than traditional octadecyl-bonded silica. Controlled radical polymerization offers an efficient route to address this limitation as a result of its ability to provide more homogeneous structures and evenly distributed thin polymeric layers [183, 184]. PNIPAM-grafted silica can provide a thermoresponsive stationary phase in chromatography, and thus the separation can be adjusted by changing the temperature instead of changing the composition of the mobile phase [185, 186]. In addition to preparing a PS-bound chromatographic stationary phase [187, 188], Ali et al. also immobilized styrene-acrylamide copolymer on porous partially sub-2 μm silica monolith particles and the inner surface of fused silica capillary tubes (50 μm internal diameter and 28 cm length) to result in stationary phases for micro liquid chromatography (μLC) and capillary electrochromatography (CEC), respectively, for the separation of anomeric D-glucose derivatives [189]. RAFT polymerization was used to induce surface polymerization, and acrylamide was employed to incorporate amide functionality in the stationary phase. The resultant stationary phases were able to separate isomers of D-glucose derivatives with high selectivity and efficiency. The CEC stationary phase also gave good separation of other saccharides such as maltotriose and Dextran 1500 (molecular weight of about 1,500) with good separation efficiency (number of theoretical plates was about 300,000/m). Zhang and coworkers developed a tandem RAFT/click chemistry method for preparation of amide-polystyrene-silica (NHCO-PS-silica) stationary phase [190]. Styrene was immobilized on the amino-silica surface via an azide-functionalized RAFT agent in a one-pot procedure. The resultant NHCO-PS-silica column demonstrated better performance for shielding of residue silanols than traditional octadecylsilyl

columns, which was ascertained by Engelhardt, Tanaka, Galushko, and Walters tests. The NHCO-PS-silica was suitable for the separation of basic compounds, and this column also showed excellent stability with pure water as mobile phase.

4.4 Preparation of Hollow Capsules

Some methods such as layer-by-layer self-assembly [191], distillation precipitation polymerization [192–199], and surface-initiated polymerization [61, 200–202] have been developed for preparation of functional core–shell hybrids and composites. Using polymer-grafted solid substrates as precursors, functional hollow objects with multipurpose applications can be obtained by chemical postmodification such as etching and dissolving to remove the cores. Huang et al. reported controlled synthesis of photocrosslinked polymeric nanocapsules by SI-RAFT [61]. Narrowly distributed hollow polymeric nanocapsules (P*t*BMA-*co*-PDMIPM-*b*-PHPMA) of 450 or 900 nm diameter were prepared by exploiting silica nanoparticles as sacrificial templates and 2,3-dimethylmaleic imidopropyl methacrylate (DMIPM) as a photocrosslinker. A wall thickness of 10 nm could be achieved by using grafted block copolymer with molecular weight of 19,500 g/mol. Rahman and Elaissari developed a versatile method employing emulsion polymerization and precipitation polymerization to prepare rigid submicron-sized hollow capsules with a temperature-responsive shell [201]. After dissolving the inner magnetic core, PDVB@P(NIPAM-*co*-AEMA) hollow microcapsules with submicron size, narrow size distribution, cationic surface charge, and volume phase transition above the lower critical solution temperature (LCST) of the shell were obtained. The volume phase transition behavior of the outer shell layer can be utilized as an on/off switch to control the permeability of biomolecules or drugs into/out of the hollow capsules. Panahian reported the synthesis of dual thermo- and pH-sensitive hollow nanospheres based on poly(AA-*b*-HEMA) using an atom transfer reversible addition–fragmentation radical process [202]. A surface-attached ATRP initiator was converted to a RAFT agent, and acrylic acid and HEMA were polymerized via grafting-from RAFT polymerization. The PAA block was partially crosslinked via an esterification reaction, and hollow nanospheres were obtained by etching the silica cores with aqueous hydrofuran solution. These hollow nanospheres exhibited dual pH-sensitive and thermosensitive properties. One LCST of the particles was noted at low contents, whereas two LCSTs were observed at higher contents.

4.5 Molecularly Imprinted Polymer Films

Molecularly imprinted polymer (MIP) films are tailor-made synthetic polymers with a predetermined selectivity for a given analyte or group of structurally related

compounds, and they are usually obtained by polymerization in the presence of molecular templates [203]. MIPs contain binding sites for target molecules, with affinities and specificities on a par with those of natural receptors involving antibodies, hormone receptors, and enzymes. Thus, they can act as ideal materials for applications in areas such as CEC [204], detection of low molecular mass analytes [205], inducing protein crystallization [206], ion recognition [207], electro-analysis [208], solid-phase micro-extraction [209], and chemical sensors [210–213]. Recent advances in MIPs films prepared via RAFT-based techniques are listed below.

Titirici and Sellergren reported MIP thin films in which mesoporous silica beads modified with an azo initiator were used for grafting of crosslinked MIPs via a RAFT process [214]. Graft copolymerization of methacrylic acid and ethylene glycol dimethacrylate (EGDMA) mediated by 2-phenylprop-2-yl-dithiobenzoate in the presence of L-phenylalanine anilide as the template led to imprinted thin film composite beads. The resulting materials proved to be highly selective chiral stationary phases, resulting in baseline separation of the template racemate and structurally analogous racemates within a few minutes. These results were comparable with those obtained for materials prepared in the absence of RAFT mediation, with a notable difference being the absence of detectable solution gelation using RAFT. Lu et al. presented a general protocol for preparation of surface-imprinted core–shell nanoparticles via SI-RAFT [215]. The grafting copolymerization of 4-vinylpyridine and EGDMA in the presence of 2,4-dichlorophenoxyacetic acid as the template led to the formation of the target nanoparticles. Their potential use as the recognition element in the competitive fluorescent binding assay for 2,4-dichlorophenoxyacetic acid was also demonstrated. Li et al. reported preparation of MIP-grafted silica gel particles via SI-RAFT. The grafting copolymerization of methacrylic acid and divinyl benzene in the presence of template theophylline led to silica gel coated with a thin MIP film of about 1.98 nm thickness (MIP-silica) [216]. The measured binding kinetics for theophylline to the MIP-silica and for MIPs prepared by conventional bulk polymerization demonstrated that MIP-silica had improved mass-transfer properties. In addition, the theophylline-imprinted MIP-silica was used as the sorbent in solid-phase extraction to determine theophylline in blood serum, with satisfactory recovery higher than 90%. Nonspecific adsorption of interfering compounds could be eliminated by simple elution with acetonitrile, without sacrificing the selective binding of theophylline. Xu et al. developed an effective method for preparation of uniform surface-imprinted core–shell nanoparticles for determination of trace atrazine [217]. As a result of the advantages of controlled/living polymerization and surface-imprinting technology, the resultant RAFT surface-imprinted nanosized polymers (RAFT-SINPs) were spherically shaped particles with excellent monodispersity and demonstrated improved imprinting efficiency and mass transfer in comparison with MIPs prepared by traditional precipitation polymerization. Recoveries of 93.4% and 79.8% were achieved by one-step extraction when RAFT-SINPs were used for the pre-concentration and selective separation of atrazine in spiked corn and lettuce samples, respectively. These results enabled the separation and enrichment of

atrazine from complicated matrices using RAFT-SINPs. Halhalli et al. developed an improved grafting technique for production of thin film composite beads, whereby MIP films were grafted from porous silica using immobilized azoinitiators in the absence or presence of RAFT-mediated control or by controlled radical polymerization using immobilized iniferters (compounds that act as initiator, transfer agent, and terminator) [218]. Composites prepared by exhaustive polymerization under dilute conditions using high RAFT/initiator ratios displayed strongly enhanced chromatographic performance in terms of retentivity and enantioselectivity. Halhalli et al. developed a two-step route to address the classical deficiencies of MIPs, such as low binding capacity and nonuniform binding sites [219]. The thin-walled beads were produced in two steps by first grafting thin MIP films from porous silica beads under controlled (RAFT) or noncontrolled conditions, and then removing the silica supports from the composites by etching. This method led to beads with nanometer-thin walls with structure, morphology, and recognition properties that strongly depended on the grafting chemistry (RAFT or non-RAFT), monomer dilution, and film thickness of the original composite. The beads prepared under RAFT control showed a further enhanced saturation capacity, significantly exceeding that of the reference material. The reduced hydrophobic character of the thin-walled materials indicated the existence of two separate pore systems with different pore wettabilities.

5 Conclusions and Outlook

The high versatility of RAFT polymerization has made it a method of choice for surface modification. The latest advances in surface-initiated polymerization have enabled synthesis of target hybrids and (nano)composites with well-controlled molecular weight and topology, relatively low polydispersity, and tunable structural parameters such as grafting density, hydrophobic/hydrophilic ratio, and thickness of polymeric shell. With the introduction of functional polymers, the resultant hybrid/composite samples have found multipurpose applications in various fields, including bioscience and nanotechnology, and they hold great promise for smart surface and interface materials.

In our opinion, the following three aspects will attract increasing attention in both polymer and material sciences in the near future. First, the utilization of facile and controlled synthetic methods, especially tandem or one-pot approaches, holds great promise in advanced synthesis of target hybrids for materials science and engineering because of their simplicity in terms of process and because they favor large-scale production. Second, the introduction of smart moieties and cleavable linkages into grafted chains imparts increasing functionality and application, a hot topic in next-generation hybrid materials. Third, solid substrates grafted with complex macromolecular architectures with tunable compositions and molecular parameters will be an enduring topic in polymer science, materials science, and the biosciences. Design and synthesis of novel topological polymers not only allows

rapid construction of functional hybrids and composites but also promotes progress in related disciplines such as physics, materials science, and biotechnology. Solid substrates grafted with more complex topological polymers such as V-shaped, hyperbranched, cyclic, comb-on-comb, miktobrush, and miktoarm star copolymers will attract increasing attention as the role of polymeric graft architecture on the relation between structure, property, and application is established.

Acknowledgment Y.Z. acknowledges the financial support from the National Natural Science Foundation of China (Grants 20844001, 20874067 and 21074081) and the Project Funded by the Priority Academic Program Development of Jiangsu Higher Education Institutions. S.P. acknowledges the Royal Society Wolfson Merit Award (WM130055) and the Monash-Warwick Alliance for financial support.

References

1. Moad G, Rizzardo E, Thang SH (2012) Aust J Chem 65(8):985–1076
2. Perrier S, Takolpuckdee P (2005) J Polym Sci A Polym Chem 43(22):5347–5393
3. Chiefari J, Chong YK, Ercole F, Krstina J, Jeffery J, Le TPT, Mayadunne RTA, Meijs GF, Moad CL, Moad G, Rizzardo E, Thang SH (1998) Macromolecules 31(16):5559–5562
4. Corpart P, Charmot D, Biadatti T, Zard SZ, Michelet D (1998) Patent application WO 9858974
5. Gody G, Maschmeyer T, Zetterlund PB, Perrier S (2013) Nat Commun 4:2505 doi: 10.1038/ncomms3505
6. Gody G, Maschmeyer T, Zetterlund PB, Perrier S (2014) Macromolecules 47(2):639–649
7. Gody G, Maschmeyer T, Zetterlund PB, Perrier S (2014) Macromolecules 47(10):3451–3460
8. Zetterlund PB, Gody G, Perrier S (2014) Macromol Theory Simul 23(5):331–339
9. Moad G, Rizzardo E, Thang SH (2005) Aust J Chem 58(6):379–410
10. Tsujii Y, Ejaz M, Sato K, Goto A, Fukuda T (2001) Macromolecules 34(26):8872–8878
11. Li CZ, Benicewicz BC (2005) Macromolecules 38(14):5929–5936
12. Li C, Han J, Ryu CY, Benicewicz BC (2006) Macromolecules 39(9):3175–3183
13. Ohno K, Ma Y, Huang Y, Mori C, Yahata Y, Tsujii Y, Maschmeyer T, Moraes J, Perrier S (2011) Macromolecules 44:8944–8953
14. Cash BM, Wang L, Benicewicz BC (2012) J Polym Sci A Polym Chem 50(13):2533–2540
15. Perrier S, Takolpuckdee P, Mars CA (2005) Macromolecules 38(16):6770–6774
16. Zhao YL, Perrier S (2006) Macromolecules 39(25):8603–8608
17. Zhao YL, Perrier S (2007) Macromolecules 40(25):9116–9124
18. Zhao YL, Perrier S (2007) Macromol Symp 248(1):94–103
19. Nguyen DH, Wood MR, Zhao YL, Perrier S, Vana P (2008) Macromolecules 41(19):7071–7078
20. Zhao GD, Zhang PP, Zhang CB, Zhao YL (2012) Polym Chem 3(7):1803–1812
21. Ranjan R, Brittain WJ (2007) Macromol Rapid Commun 28(21):2084–2089
22. Ranjan R, Brittain WJ (2007) Macromolecules 40(17):6217–6223
23. Ranjan R, Brittain WJ (2008) Macromol Rapid Commun 29(12-13):1104–1110
24. Rotzoll R, Vana P (2008) J Polym Sci A Polym Chem 46(23):7656–7666
25. Rotzoll R, Nguyen DH, Vana P (2009) Macromol Symp 275–276(1):1–12
26. Zhu MQ, Wang LQ, Exarhos GJ, Li ADQ (2004) J Am Chem Soc 126(9):2656–2657
27. Liu FY, Agarwal S (2015) Macromol Chem Phys 216(4):460–465
28. Williams PE, Jones ST, Walsh Z, Appel EA, Abo-Hamed EK, Scherman OA (2015) ACS Macro Lett 4(2):255–259

29. Oschmann B, Tahir MN, Mueller F, Bresser D, Lieberwirth I, Tremel W, Passerini S, Zentel R (2015) Macromol Rapid Commun. doi:10.1002/marc.201400647
30. Ebara M, Hoffman JM, Hoffman AS, Stayton PS, Lai JJ (2013) Langmuir 29(18):5388–5393
31. Kaupp M, Tischer T, Hirschbiel AF, Vogt AP, Geckle U, Trouillet V, Hofe T, Stenzel MH, Barner-Kowollik C (2013) Macromolecules 46(17):6858–6872
32. Kaupp M, Quick AS, Rodriguez-Emmenegger C, Welle A, Trouillet V, Pop-Georgievski O, Wegener M, Barner-Kowollik C (2014) Adv Funct Mater 24(36):5649–5661
33. Kos T, Anžlovar A, Pahovnik D, Žagar E, Orel ZC, Žigon M (2013) Macromolecules 46(17): 6942–6948
34. Ning Y, Fielding LA, Andrews TS, Growney DJ, Armes SP (2015) Nanoscale 7:6691–6702
35. Hu JM, Wu T, Zhang GY, Liu SY (2012) J Am Chem Soc 134(18):7624–7627
36. Baum M, Brittain WJ (2002) Macromolecules 35(3):610–615
37. Rotzoll R, Vana P (2009) Aust J Chem 62(11):1473–1478
38. Le-Masurier SP, Gody G, Perrier S, Granville AM (2014) Polym Chem 5(8):2816–2823
39. Gody G, Rossner C, Moraes J, Vana P, Maschmeyer T, Perrier S (2012) J Am Chem Soc 134(30):12596–12603
40. Santoyo-Gonzalez F, Hernandez-Mateo F (2009) Chem Soc Rev 38(12):3449–3462
41. de Soler-Illia GJ, Sanchez C, Lebeau B, Patarin J (2002) Chem Rev 102(11):4093–4138
42. Kickelbick G (2003) Prog Polym Sci 28(1):83–114
43. Radhakrishnan B, Ranjan R, Brittain WJ (2006) Soft Mater 2(5):386–396
44. Tsujii Y, Ohno K, Yamamoto S, Goto A, Fukuda T (2006) Adv Polym Sci 197:1–45
45. Barbey R, Lavanant L, Paripovic D, Schüwer N, Sugnaux C, Tugulu S, Klok HA (2009) Chem Rev 109(11):5437–5527
46. Guo TY, Liu P, Zhu JW, Song MD, Zhang BH (2006) Biomacromolecules 7(4):1196–1202
47. Chinthamanipeta PS, Kobukata S, Nakata H, Shipp DA (2008) Polymer 49(26):5636–5642
48. Yang YK, Yang ZF, Zhao Q, Cheng XJ, Tjong SC, Li RKY, Wan XT, Xie XL (2009) J Polym Sci A Polym Chem 47(2):467–484
49. Sobani M, Haddadi-Asl V, Salami-Kalajahi M, Roghani-Mamaqani H, Mirshafiei-Langari SA, Khezri K (2013) J Solgel Sci Technol 66(2):337–344
50. Stenzel MH, Zhang L, Huck WTS (2006) Macromol Rapid Commun 27(14):1121–1126
51. Hou TT, Zhang PP, Zhou XD, Cao XQ, Zhao YL (2010) Chem Commun 46(39):7397–7399
52. Nguyen DH, Vana P (2006) Polym Adv Technol 17(9-10):625–633
53. Huebner D, Koch V, Ebeling B, Mechau J, Steinhoff JE, Vana P (2015) J Polym Sci A Polym Chem 53(1):103–113
54. Wang L, Benicewicz BC (2013) ACS Macro Lett 2(2):173–176
55. Liu CH, Pan CY (2007) Polymer 48(13):3679–3685
56. Liu CH, Pan CY (2008) Chem J Chin Univ 29(2):404–408
57. Liu JL, Zhang LF, Shi SP, Chen SA, Zhou NC, Zhang ZB, Cheng ZP, Zhu XL (2010) Langmuir 26(18):14806–14813
58. Moraes J, Ohno K, Gody G, Maschmeyer T, Perrier S (2013) Beilstein J Org Chem 9: 1226–1234
59. Choi J, Schattling P, Jochum FD, Pyun J, Char K, Theato P (2012) J Polym Sci A Polym Chem 50(19):4010–4018
60. Maleki H, Duraes L, Portugal A (2015) J Mater Chem A 3(4):1594–1600
61. Huang X, Appelhans D, Formanek P, Simon F, Voit B (2011) Macromolecules 44(21): 8351–8360
62. Huang YK, Liu Q, Zhou XD, Perrier S, Zhao YL (2009) Macromolecules 42(15):5509–5517
63. Guo YF, Liu HH, Tang DD, Li CX, Zhao YL (2015) Polym Chem 6:2647–2658
64. Kolb HC, Finn MG, Sharpless KB (2001) Angew Chem Int Ed 40(11):2004–2021
65. Hein JE, Fokin VV (2010) Chem Soc Rev 39(4):1302–1315
66. Tunca U (2014) J Polym Sci A Polym Chem 52(22):3147–3165
67. Kade MJ, Burke DJ, Hawker CJ (2010) J Polym Sci A Polym Chem 48(4):743–750
68. Hoyle CE, Bowman CN (2010) Angew Chem Int Ed 49(9):1540–1573

69. Lowe AB (2014) Polym Chem 5(17):4820–4870
70. Hoyle CE, Lowe AB, Bowman CN (2010) Chem Soc Rev 39(4):1355–1387
71. Yang ZL, Xu XL, Zhao YX (2014) Prog Chem 26(6):996–1004
72. Chen JC, Liu MZ, Chen C, Gong HH, Gao CM (2011) ACS Appl Mater Interfaces 3(8): 3215–3223
73. Li Y, Benicewicz BC (2008) Macromolecules 41(21):7986–7992
74. Huang YK, Hou TT, Cao XQ, Perrier S, Zhao YL (2010) Polym Chem 1(10):1615–1623
75. Kotsuchibashi Y, Ebara M, Aoyagi T, Narain R (2012) Polym Chem 3(9):2545–2550
76. Chen KL, Zhao YH, Yuan XY (2014) Chem Res Chin Univ 30(2):339–342
77. Peng C, Pan W, Bao L, Chen S, Chen Y, Han MS, Xiong YQ, Xu WJ (2014) Polym Adv Technol 25(6):684–688
78. Han MS, Zhang XY, Li L, Peng C, Bao L, Ou EC, Xiaong YQ, Xu WJ (2014) Express Polym Lett 8(7):528–542
79. Hojjati B, Sui RH, Charpentier PA (2007) Polymer 48(20):5850–5858
80. Ngo VG, Bressy C, Leroux C, Margaillan A (2009) Polymer 50(14):3095–3102
81. Hojjati B, Charpentier PA (2010) Polymer 51(23):5345–5351
82. Crippa M, Bianchi A, Cristofori D, D'Arienzo M, Merletti F, Morazzoni F, Scotti R, Simonutti R (2013) J Mater Chem C 1(3):484–492
83. Viswanath A, Shen Y, Green AN, Tan R, Greytak AB, Benicewicz BC (2014) Macromolecules 47(23):8137–8144
84. Esteves ACC, Hodge P, Trindade T, Barros-Timmons AMMV (2009) J Polym Sci A Polym Chem 47(20):5367–5377
85. Liu WH, Greytak AB, Lee J, Wong CR, Park J, Marshall LF, Jiang W, Curtin PN, Ting AY, Nocera DG (2010) J Am Chem Soc 132(2):472–483
86. Das P, Claverie JP (2012) J Polym Sci A Polym Chem 50(14):2802–2808
87. Dilag J, Kobus H, Ellis AV (2013) Forensic Sci Int 228(1-3):105–114
88. Boyer C, Priyanto P, Davis TP, Pissuwan D, Bulmus V, Kavallaris M, Teoh WY, Amal R, Carroll M, Woodward R (2010) J Mater Chem 20(2):255–265
89. Li X, Bao MM, Weng YY, Yang K, Zhang WD, Chen GJ (2014) J Mater Chem B 2(34): 5569–5575
90. Sahoo B, Devi KSP, Banerjee R, Maiti TK, Pramanik P, Dhara D (2013) ACS Appl Mater Interfaces 5(9):3884–3893
91. Wang L, Cole M, Li JT, Zheng Y, Chen YP, Miller KP, Decho AW, Benicewicz BC (2015) Polym Chem 6(2):248–255
92. Sumerlin BS, Lowe AB, Stroud PA, Zhang P, Urban MW, McCormick CL (2003) Langmuir 19(14):5559–5562
93. Rossner C, Vana P (2014) Angew Chem Int Ed 53(46):12639–12642
94. Adokoh CK, Quan S, Hitt M, Darkwa J, Kumar P, Narain R (2014) Biomacromolecules 15(10):3802–3810
95. Ahmed M, Mamba S, Yang XH, Darkwa J, Kumar P, Narain R (2013) Bioconjug Chem 24(6):979–986
96. Parry AL, Clamson NA, Ellis J, Bernhard SSR, Davis BG, Cameron NR (2013) J Am Chem Soc 135(25):9362–9365
97. Jiang XZ, Housni A, Gody G, Boullanger P, Charreyre MT, Delair T, Narain R (2010) Bioconjug Chem 21(3):521–530
98. Kirkland-York S, Zhang YL, Smith AE, York AW, Huang FQ, McCormick CL (2010) Biomacromolecules 11(4):1052–1059
99. Duong HTT, Adnan NNM, Barraud N, Basuki JS, Kutty SK, Jung K, Kumar N, Davis TP, Boyer C (2014) J Mater Chem B 2(31):5003–5011
100. Boyer C, Bousquet A, Rondolo J, Whittaker MR, Stenzel MH, Davis TP (2010) Macromolecules 43(8):3775–3784
101. Takara M, Toyoshima M, Seto H, Hoshino Y, Miura Y (2014) Polym Chem 5(3):931–939
102. Lu JW, Zhang WD, Richards SJ, Gibson MI, Chen GJ (2014) Polym Chem 5(7):2326–2332

103. Boyer C, Whittaker MR, Chuah K, Liu JQ, Davis TP (2010) Langmuir 26(4):2721–2730
104. Boyer C, Whittaker MR, Luzon M, Davis TP (2009) Macromolecules 42(18):6917–6926
105. Boyer C, Whittaker MR, Nouvel C, Davis TP (2010) Macromolecules 43(4):1792–1799
106. Rossner C, Ebeling B, Vana P (2013) ACS Macro Lett 2(12):1073–1076
107. Zhang T, Wu YP, Pan XM, Zheng ZH, Ding XB, Peng YX (2009) Eur Polym J 45(6): 1625–1633
108. Ebeling B, Vana P (2013) Macromolecules 46(12):4862–4871
109. Zhang T, Zheng ZH, Ding XB, Peng YX (2008) Macromol Rapid Commun 29(21): 1716–1720
110. Shan J, Nuopponen M, Jiang H, Kauppinen E, Tenhu H (2003) Macromolecules 36(12): 4526–4533
111. Beija M, Marty JD, Destarac M (2011) Chem Commun 47(10):2826–2828
112. Liu J, Detrembleur C, De Pauw-Gillet MC, Momet S, Duguet E, Jérôme C (2014) Polym Chem 5(3):799–813
113. Beija M, Palleau E, Sistach S, Zhao XG, Ressier L, Mingotaud C, Destarac M, Marty JD (2010) J Mater Chem 20(42):9433–9442
114. Gibson MI, Danial M, Klok HA (2011) ACS Comb Sci 13(3):286–297
115. Luo SZ, Xu J, Zhang YF, Liu SY, Wu C (2005) J Phys Chem B 109(47):22159–22166
116. Hotchkiss JW, Lowe AB, Boyes SG (2007) Chem Mater 19(1):6–13
117. Zhuang YY, Zhu Q, Tu CL, Wang DL, Wu JL, Xia YM, Tong GS, He L, Zhu BS, Yan DY (2012) J Mater Chem 22(45):23852–23860
118. Roy D, Semsarilar M, Guthrie JT, Perrier S (2009) Chem Soc Rev 38(7):2046–2064
119. Eichhorn SJ (2011) Soft Mater 7(2):303–315
120. Malmstrom E, Carlmark A (2012) Polym Chem 3(7):1702–1713
121. Carlmark A (2013) Macromol Chem Phys 214(14):1539–1544
122. Carlsson L, Fall A, Chaduc I, Wagberg L, Charleux B, Malmstrom E, D'Agosto F, Lansalot M, Carlmark A (2014) Polym Chem 5(20):6076–6086
123. Barsbay M, Guven G, Stenzel MH, Davis TP, Barner-Kowollik C, Barner L (2007) Macromolecules 40(20):7140–7147
124. Barsbay M, Kodama M, Guven O (2014) Cellulose 21(6):4067–4079
125. Goldmann AS, Tischer T, Barner L, Bruns M, Barner-Kowollik C (2011) Biomacromolecules 12(4):1137–1145
126. Demirci S, Celebioglu A, Uyar T (2014) Carbohydr Polym 113:200–207
127. Roy D, Knapp JS, Guthrie JT, Perrier S (2008) Biomacromolecules 9(1):91–99
128. Roy D, Guthrie JT, Perrier S (2008) Soft Mater 4(1):145–155
129. Roy D, Guthrie JT, Perrier S (2006) Aust J Chem 59(10):737–741
130. Xiao C, Xia C (2013) Int J Biol Macromol 52:349–352
131. Yuan J, Huang XB, Li PF, Li L, Shen J (2013) Polym Chem 4(19):5074–5085
132. Roy D, Guthrie JT, Perrier S (2005) Macromolecules 38(25):10363–10372
133. Barsbay M, Guven O, Davis TP, Barner-Kowollik C, Barner L (2009) Polymer 50(4): 973–982
134. Chen J, Yi J, Sun P, Liu ZT, Liu ZW (2009) Cellulose 16(6):1133–1145
135. Liu X, Chen J, Sun P, Liu ZW, Liu ZT (2010) React Funct Polym 70(12):972–979
136. Liu Y, Jin XS, Zhang XS, Han MM, Ji SX (2015) Carbohydr Polym 117:312–318
137. Kodama Y, Barsbay M, Guven O (2014) Radiat Phys Chem 94:98–104
138. Hiltunen M, Riihela S, Maunu SL (2009) J Polym Sci B Polym Phys 47(19):1869–1879
139. Hufendiek A, Trouillet V, Meier MAR, Barner-Kowollik C (2014) Biomacromolecules 15(7):2563–2572
140. Zeinali E, Haddadi-Asl V, Roghani-Mamaqani H (2014) RSC Adv 4(59):31428–31442
141. Novoselov K, Geim A, Morozov S, Jiang D, Zhang Y, Dubonos S, Grigorieva I, Firsov A (2004) Science 306(5696):666–669
142. Novoselov K, Geim A, Morozov S, Jiang D, Grigorieva M, Dubonos S, Firsov A (2005) Nature 438(7065):197–200

143. Stankovich S, Dikin D, Dommett G, Kohlhaas K, Zimney E, Stach E, Piner R, Nguyen S, Ruoff R (2006) Nature 442(7100):282–286
144. Dreyer DR, Park S, Bielawski CW, Ruoff RS (2010) Chem Soc Rev 39(1):228–240
145. Kim H, Abdala AA, Macosko CW (2010) Macromolecules 43(16):6515–6530
146. Badri A, Whittaker MR, Zetterlund PB (2012) J Polym Sci A Polym Chem 50(15): 2981–2992
147. Layek RK, Nandi AK (2013) Polymer 54(19):5087–5103
148. Thickett SC, Zetterlund PB (2013) Curr Org Chem 17(9):956–974
149. Li Y, Li X, Dogn CK, Qi JY, Han XJ (2010) Carbon 48(12):3427–3433
150. Layek RK, Kuila A, Chatterjee DP, Nandi AK (2013) J Mater Chem A 1(36):10863–10874
151. Ye YS, Chen YN, Wang JS, Rick J, Huang YJ, Chang FC, Hwang BJ (2012) Chem Mater 24(15):2987–2997
152. Peeters M, Kobben S, Jimenez-Monroy KL, Modesto L, Kraus M, Vandenryt T, Gaulke A, van Grinsven B, Ingebrandt S, Junkers T (2014) Sensor Actuat B Chem 203:527–535
153. Liu Y, Meng XG, Luo M, Meng MJ, Ni L, Qiu J, Hu ZY, Liu FF, Zhong GX, Liu ZC (2015) J Mater Chem A 3(3):1287–1297
154. Beckert F, Friedrich C, Thomann R, Mulhaupt R (2012) Macromolecules 45(17):7083–7090
155. Etmimi HM, Tonge MP, Sanderson RD (2011) J Polym Sci A Polym Chem 49(7):1621–1632
156. Gu RP, Xu WZ, Charpentier PA (2014) Polymer 55(21):5322–5331
157. Cui L, Liu JQ, Wang R, Liu Z, Yang WR (2012) J Polym Sci A Polym Chem 50(21): 4423–4432
158. Nikdel M, Salami-Kalajahi M, Hosseini MS (2014) RSC Adv 4(32):16743–16750
159. Gu R, Xu WZ, Charpentier PA (2013) J Polym Sci A Polym Chem 51(18):3941–3949
160. Liu ZZ, Lu GL, Li YJ, Li YS, Huang XY (2014) RSC Adv 4(105):60920–60928
161. Zhang B, Chen Y, Zhuang XD, Liu G, Yu B, Kang ET, Zhu JH, Li YX (2010) J Polym Sci A Polym Chem 48(12):2642–2649
162. Zhang B, Chen Y, Xu LQ, Zeng LJ, He Y, Kang ET, Zhang JJ (2011) J Polym Sci A Polym Chem 49(9):2043–2050
163. Zhang PP, Jiang K, Ye CN, Zhao YL (2011) Chem Commun 47(33):9504–9506
164. Jiang K, Ye CN, Zhang PP, Wang XS, Zhao YL (2012) Macromolecules 45(3):1346–1355
165. Nazir T, Afzal A, Siddiqi HM, Ahmad Z, Dumon M (2010) Prog Org Coat 69(1):100–106
166. Yan W, Han ZJ, Phung BT, Ostrikov KK (2012) ACS Appl Mater Interfaces 4(5):2637–2642
167. Guo SZ, Zhang C, Wang WZ, Liu TX (2010) Express Polym Lett 4(1):17–25
168. Salami-Kalajahi M, Haddadi-Asl V, Rahimi-Razin S, Behboodi-Sadabad F, Najafi M, Roghani-Mamaqani H (2012) J Polym Res 19(2):9793
169. Zhu LJ, Zhu LP, Jiang JH, Yi Z, Zhao YF, Zhu BK, Xu YY (2014) J Membr Sci 451:157–168
170. Zhu LJ, Zhu LP, Zhao YF, Zhu BK, Xu YY (2014) J Mater Chem A 2(37):15566–15574
171. Zhi SH, Deng R, Xu J, Wan LS, Xu ZK (2015) React Funct Polym 86:184–190
172. Zhang YF, Gu WY, Xu HX, Liu SY (2008) J Polym Sci A Polym Chem 46(7):2379–2389
173. Sun JT, Yu ZQ, Hong CY, Pan CY (2012) Macromol Rapid Commun 33(9):811–818
174. Majewski AP, Stahlschmidt U, Jerome V, Freitag R, Müller AHE, Schmalz H (2013) Biomacromolecules 14(9):3081–3090
175. Hong CY, Li X, Pan CY (2008) J Phys Chem C 112(39):15320–15324
176. Hong CY, Li X, Pan CY (2009) J Mater Chem 19(29):5155–5160
177. Zhou JM, Zhang WJ, Hong CY, Pan CY (2015) ACS Appl Mater Interfaces 7(6):3618–3625
178. Cui L, Wang R, Ji XQ, Hu M, Wang B, Liu JQ (2014) Mater Chem Phys 148(1-2):87–95
179. Müllner M, Schallon A, Walther A, Freitag R, Müller AHE (2010) Biomacromolecules 11(2):390–396
180. Wan XJ, Wang D, Liu SY (2010) Langmuir 26(19):15574–15579
181. Moraes J, Ohno K, Maschmeyer T, Perrier S (2013) Chem Mater 25(17):3522–3527
182. Ji WD, Li NJ, Chen DY, Qi XX, Sha WW, Jiao Y, Xu QF, Li JM (2013) J Mater Chem B 43(43):5942–5949
183. Hemstrom P, Szumski M, Irgum K (2006) Anal Chem 78(20):7098–7103

184. Ni CH, Wang WT, Zhu CP, Huang B, Yao BL (2010) Soft Mater 8(1):14–28
185. Roohi F, Titirici MM (2008) New J Chem 32(8):1409–1414
186. Roohi F, Antonietti M, Titirici MM (2008) J Chromatogr A 1203:160–167
187. Ali F, Cheong WJ, Alothman ZA, Almajid AM (2013) J Chromatogr A 1303:9–17
188. Ali F, Kim YS, Lee JW, Cheong WJ (2014) J Chromatogr A 1324:115–120
189. Ali F, Kim YS, Cheong WJ (2014) Bull Korean Chem Soc 35(2):539–545
190. Zhang Z, Chen ML, Cheng XD, Shi ZG, Yuan BF, Feng YQ (2014) J Chromatogr A 1351: 96–102
191. Yang XL, Zhu YH, Zhu MQ, Li CZ (2003) J Inorg Mater 18(6):1293–1298
192. Liu GY, Zhang H, Yang XL, Wang YM (2007) Polymer 48(20):5896–5904
193. Liu GY, Ji HF, Yang XL, Wang YM (2008) Langmuir 24(3):1019–1025
194. Liu GY, Yang XL, Wang YM (2008) Langmuir 24(10):5485–5491
195. Liu GY, Wang H, Yang XL (2009) Polymer 50(12):2578–2586
196. Zhang H, Yang XL (2010) Polym Chem 1(5):670–677
197. Ji M, Liu HL, Yang XL (2011) Polym Chem 2(1):148–156
198. Li GL, Xu LQ, Tang XZ, Neoh KG, Kang ET (2010) Macromolecules 43(13):5797–5803
199. Li GL, Wan D, Neoh KG, Kang ET (2010) Macromolecules 43(24):10275–10282
200. Wu T, Ge ZS, Liu SY (2011) Chem Mater 23(9):2370–2380
201. Rahman MM, Elaissari A (2012) J Mater Chem 22(3):1173–1179
202. Panahian P, Salami-Kalajahi M, Hosseini MS (2014) Ind Eng Chem Res 53(19):8079–8086
203. Bompart M, Haupt K (2009) Aust J Chem 62(8):751–761
204. Turiel E, Martin-Esteban A (2005) J Sep Sci 28(8):719–728
205. Uludag Y, Piletsky SA, Turner APF, Cooper MA (2007) FEBS J 274(21):5471–5480
206. Saridakis E, Chayen NE (2013) Trends Biotechnol 31(9):515–520
207. Wu XY (2012) Mikrochim Acta 176(1-2):23–47
208. Cervini P, Cavalheiro ETG (2012) Anal Lett 45(4):297–313
209. Zhang MS, Zeng JB, Wang YR, Chen X (2013) J Chromatogr Sci 51(7):577–586
210. Fuchs Y, Soppera O, Haupt K (2012) Anal Chim Acta 717:7–20
211. Lofgreen JE, Ozin GA (2014) Chem Soc Rev 43(3):911–933
212. Algieri C, Drioli E, Guzzo L, Donato L (2014) Sensors 14(8):13863–13912
213. Wackerlig J, Lieberzeit PA (2015) Sensor Actuat B Chem 207:144–157
214. Titirici MM, Sellergren B (2006) Chem Mater 18(7):1773–1779
215. Lu CH, Zhou WH, Han B, Yang HH, Chen X, Wang XR (2007) Anal Chem 79(14): 5457–5461
216. Li Y, Zhou WH, Yang HH, Wang XR (2009) Talanta 79(2):141–145
217. Xu SF, Li JH, Chen LX (2011) J Mater Chem 21(12):4346–4351
218. Halhalli MR, Aureliano CSA, Schillinger E, Sulitzky C, Titirici MM, Sellergren B (2012) Polym Chem 3(4):1033–1042
219. Halhalli MR, Schillinger E, Aureliano CSA, Sellergren B (2012) Chem Mater 24(15): 2909–2919

Adv Polym Sci (2016) 270: 107–122
DOI: 10.1007/12_2015_310

Published online: 18 April 2015

Surface-Initiated Living Radical Polymerizations Using Iodine, Organotellurium, and Organic Catalysts

Atsushi Goto and Yoshinobu Tsujii

Abstract This chapter reviews surface-initiated living radical polymerizations via iodine transfer polymerization (ITP), organotellurium-mediated radical polymerization (TERP), and reversible chain-transfer catalyzed polymerization (RTCP) using organic catalysts. The successful application of these polymerizations made it possible to graft various polymers with well-defined structures onto flat substrates and nanoparticles. Living radical polymerizations, including ITP, TERP, and RTCP, also lead to a striking increase in the graft density. Because of their unique advantages as synthetic tools, ITP, TERP, and RTCP can be used to expand the scope of controlled surface modification.

Keywords Iodine · Organic catalyst · Organotellurium · Polymer brush · Surface-initiated living radical polymerization

Contents

A. Goto (✉) and Y. Tsujii
Institute for Chemical Research, Kyoto University, Uji, Kyoto 611-0011, Japan
e-mail: agoto@scl.kyoto-u.ac.jp

Abbreviations

σ	Graft density
σ^*	Dimensionless reduced graft density
AT	Atom transfer
ATRP	Atom transfer radical polymerization
BHE	(2-Bromo-2-methyl)propionyloxyhexyltriethoxysilane
BzMA	Benzyl methacrylate
C_{ex}	Degenerative (exchange) chain transfer constant
DC	Dissociation-combination
DT	Degenerative (exchange) chain transfer
GMA	Glycidyl methacrylate
GPC	Gel permeation chromatography
HEA	2-Hydroxyethyl acrylate
ICAR	Initiators for continuous activator regeneration
IHE	(2-Iodo-2-methyl)propionyloxyhexyltriethoxysilane
ITP	Iodine transfer polymerization
L_e	Equilibrium thickness in a good solvent
LRP	Living radical polymerization
MMA	Methyl methacrylate
M_n	Number-average molecular weight
M_w	Weight-average molecular weight
N	Degree of polymerization
NIPAM	*N*-Isopropylacrylamide
NIS	*N*-Iodosuccinimide
NMP	Nitroxide-mediated polymerization
NVC	*N*-Vinylcarbazole
NVP	*N*-Vinylpyrrolidine
PEGA	Poly(ethyleneglycol)methylether acrylate
Polymer$^{\bullet}$	Polymer radical
Polymer-X	Dormant species
RAFT	Reversible addition-fragmentation chain transfer
RCMP	Reversible complexation mediated polymerization
RITP	Reverse iodine transfer polymerization
RT	Reversible chain transfer
RTCP	Reversible chain transfer catalyzed polymerization
SAM	Self-assembled monolayer
TeBE	4-(Triethoxysilyl)butyl 2-methyltellanyl-2-methylpropionate
TeMe	Methyltelluride
TEOS	Triethoxysilyl
TERP	Organotellurium-mediated radical polymerization
VAc	Vinyl acetate
VDF	Vinylidene fluoride
X	Capping agent

1 Introduction

The surface of a material plays a crucial role in its mechanical, thermodynamic, chemical, optical, and electrical properties. Grafting a polymer onto a surface can dramatically change these properties; therefore, the grafting technique is an important issue in many areas of science and technology [1–6]. In this chapter, we focus on "end-grafting" polymers onto solid surfaces. There are essentially two methods for preparing end-grafted polymers. One is the "grafting-to" technique, in which a preformed polymer is attached onto the surface. The other is the "grafting-from" technique, also referred to as surface-initiated polymerization, in which polymerization is conducted from the initiating groups bound to the surface. The grafting-from method potentially provides much higher graft densities than the grafting-to method, which is a clear advantage of the grafting-from method. This difference in graft density is because, in the grafting-to process, preformed polymers to be grafted on the surface have to diffuse against the concentration barrier formed by the already grafted polymers. The diffusion becomes more and more difficult as the density and chain length of the already grafted polymers increase, resulting in a limited graft density that sharply decreases with increasing chain length. In the grafting-from process, it is usually low-mass compounds such as monomers and catalysts that have to diffuse across the barrier of the grafted polymers. For this reason, chains can grow even on highly congested surfaces and to very high degrees of polymerization. The chain growth is especially effective when the polymerization proceeds in a living fashion. The graft chains can grow more or less simultaneously with their active chain ends, which are concentrated near the outermost surface of the graft layer.

The conformation of those polymers in a solvent can dramatically change with the graft density [1, 2, 7–9]. At low graft densities (i.e., in the "dilute" regime), the polymer chains assume a "mushroom" conformation (Fig. 1). With increasing graft density, the grafted chains are obliged to stretch away from the surface, forming a so-called "polymer brush". Polymer brushes can be categorized into two groups according to their graft density: "semidilute" and "concentrated" brushes (Fig. 1). In a semidilute brush, the polymer chains overlap each other, but their volume fraction is still so low that the free energy of interaction can be approximated by a binary interaction, and the elastic free energy can be approximated by that of a Gaussian chain. Scaling theoretical analysis [10–15] predicts that, in a good solvent, the equilibrium thickness (L_e) of the semidilute brush varies according to Eq. (1):

$$L_e \propto N\sigma^{1/3} \tag{1}$$

Here, N and σ are the degree of polymerization and the graft density (chains/nm^2), respectively. The 1/3 power dependence of L_e on σ is a characteristic feature of the semidilute brush. In a concentrated brush, the mentioned approximations are no longer valid and higher-order interactions should be taken into account. Therefore,

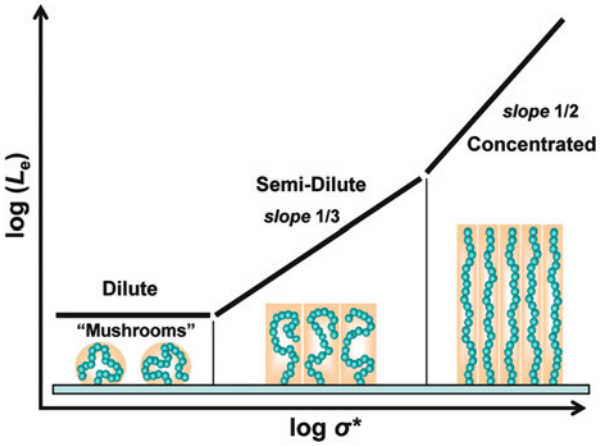

Fig. 1 Illustration of dilute, semidilute, and concentrated polymer brushes and the dependence of equilibrium thickness (L_e) on reduced graft density (σ^*) for these brushes

concentrated brushes are expected to exhibit properties that are different from those of semidilute brushes. The L_e of the concentrated brush is theoretically predicted by Eq. (2) [14, 15]:

$$L_e \sim N\sigma^{1/2} \tag{2}$$

L_e shows a 1/2 power dependence on σ. L_e steeply increases with the graft density and, hence, the polymer chains are significantly extended in this region. The boundary between the semidilute and concentrated brushes is located around a reduced graft density (surface occupancy) of $\sigma^* = 0.1$ (10% of surface) [2].

Until recently, the structures and properties of concentrated brushes had not been well studied experimentally because of the unavailability of well-defined concentrated brushes. The recent development of living polymerizations, including anionic, cationic, ring-opening, and radical methods, has opened up synthetic routes for producing well-defined concentrated brushes [1–4]. Among these methods, living radical polymerization (LRP) [16–29], which is tolerant to impurities and is versatile for a wide range of monomers, has been extensively applied to surface-initiated polymerization on various organic, inorganic, and metallic solids [1–6]. Surface-initiated LRP has brought about a dramatic increase in the graft density, allowing systematic studies of concentrated brushes. The surface occupancy reaches approximately 40% ($\sigma^* = 0.4$), at which point the polymer chains extend to as much as 80% of the all-*trans* conformation length in good solvents [2]. These studies have revealed that the structures and properties of the concentrated brushes are quite different from those of the semidilute brushes and, in some cases, even unpredictable [1, 2]. These unique properties of concentrated brushes may find useful application.

Several LRP techniques have been used to prepare well-defined end-grafted polymers in dilute, semidilute, and concentrated regions for different purposes. These LRP techniques include nitroxide-mediated polymerization (NMP), atom

transfer radical polymerization (ATRP), and reversible addition-fragmentation chain transfer (RAFT) polymerization. In this chapter, we review the use of iodine transfer polymerization (ITP), organotellurium-mediated radical polymerization (TERP), and reversible chain transfer catalyzed polymerization (RTCP) with organic catalysts for surface-initiated polymerization. These LRP techniques are robust, versatile for a variety of monomers, and/or inducible by photo-irradiation. These features make these LRP techniques attractive candidates for widening the scope of surface-initiated polymerization.

2 Reversible Activation

The basic concept of LRP is the reversible activation of a dormant species (Polymer-X) to a polymer radical (Polymer$^{\bullet}$) (Scheme 1a). A sufficiently large number of activation–deactivation cycles are required to yield a low-dispersity polymer [28, 29]. The reversible activation reactions include dissociation–combination (DC) (Scheme 1b), atom transfer (AT) (Scheme 1c), and degenerative (or exchange) chain transfer (DT) (Scheme 1d) mechanisms. NMP [18], ATRP [19–21], and RAFT [22] systems are based on DC, AT, and DT, respectively. ITP [23] uses iodine as a capping agent (X) and is based on DT. TERP [24] uses organotellurides such as methyl telluride (TeMe) as X. TERP involves both DC and DT, but DT is the main mechanism and DC becomes important at elevated temperatures. RTCP [30–35] uses iodine as capping agent X and organic molecules as catalysts for reversible activation. RTCP is based on a different reversible activation mechanism from these three mechanisms, as explained in Sect. 5.

LRP has been applied to surface-initiated graft polymerization by immobilizing either a dormant species (Fig. 2a) or a conventional radical initiator (Fig. 2b) on a surface. In the latter case, a capping agent is added to the solution phase (reverse LRP). The use of a surface-bound dormant species is promising for obtaining well-defined high-density polymer brushes (in reverse surface-initiated LRP, the efficiency and speed of attaching the capping agent can affect the graft density and dispersity). Because of immobilization of the dormant species on the surface, surface-initiated polymerization results in different situations from those in solution polymerization. A question is whether the polymerization is as controllable on the surface (within a graft layer) as it is in solution. The limited surface area of a substrate (e.g., a flat substrate) leads to a low overall concentration of the dormant species (capping agent), resulting in poor control of the polymerization, which must be circumvented. Thus, an unimmobilized free dormant species or a capping agent is often added to the solution to increase the overall concentration [1–6]. Tethering and crowding of polymers affect the local concentrations of the reactants and, hence, their reaction rates. This behavior has the most important effect on intermolecular reactions between graft chains, e.g., termination between two graft radicals and DT between a graft radical and a graft dormant species. For examining polymerization behavior in the graft layer, an interesting system is one

Scheme 1 (**a**) Reversible activation, (**b**) dissociation–combination, (**c**) atom transfer, and (**d**) degenerative chain transfer

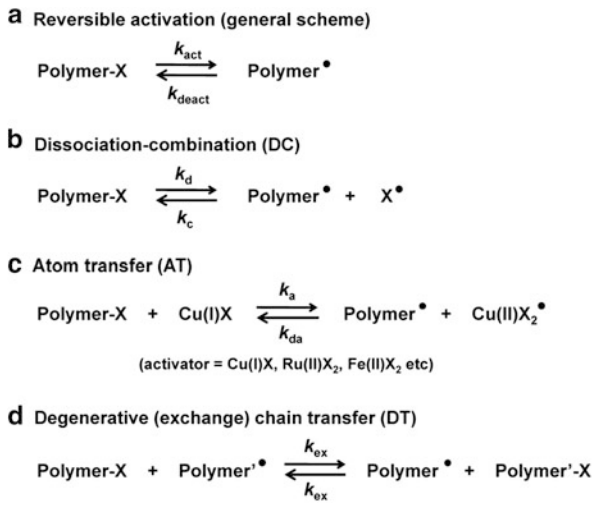

Fig. 2 (**a**) Surface-initiated LRP and (**b**) surface-initiated reverse LRP

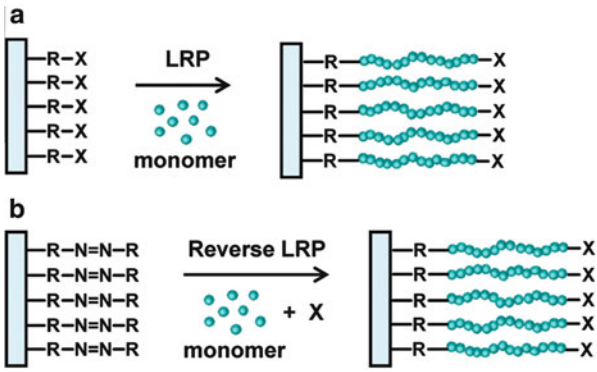

with an added free dormant species, because the polymerization simultaneously proceeds in both the graft and solution phases under the same conditions and we can compare the chain length and chain-length distribution between the graft and free polymers.

From a mechanistic point of view, a particularly interesting case is graft polymerization based on DT. Unlike DC and AT, DT can occur between graft chains (Fig. 3). Because the graft chains in a high-density brush are highly stretched in a good solvent, their chain ends are concentrated near the outermost surface of the graft layer. Thus, DT can occur effectively between the graft chains, and a sequence of DT processes can be viewed as migration or reaction–diffusion of the otherwise strictly localized graft radicals. This surface migration narrows the dispersity of the graft chains in DT systems such as RAFT, ITP, and TERP systems. Tsujii et al. studied surface-initiated RAFT polymerization of styrene on silica particles [36]. They used silica particles grafted with probe oligomeric polystyrene chains

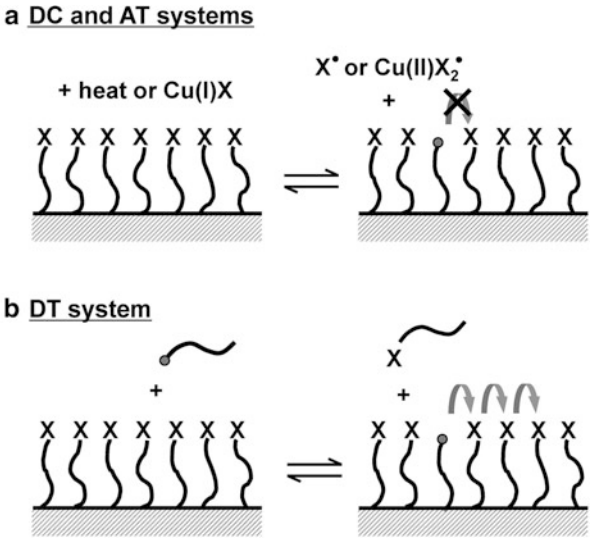

Fig. 3 Comparison of the key processes in (**a**) DC and AT systems and (**b**) the DT system

with a dithiobenzoate capping agent (X = SCSPh). After chain extension by styrene polymerization, the graft chains were cleaved from the silica particles using HF and characterized. Polystyryl radicals were predominantly terminated via recombination to give dead chains with doubled molecular weight. Gel permeation chromatography (GPC) analysis has shown two facts: First, the chain-length distribution of the main-peak component, which could be assigned to living or unterminated chains, was narrower than that of the free polymer. This suggests more frequent occurrence of DT on the surface than in solution. Second, this surface migration led to significant termination among the graft radicals. The minor-peak component, which could be assigned to the terminated chains with doubled molecular weight, was unusually large. This could occur when the surface migration is extremely fast, that is, when the degenerative (exchange) transfer constant (C_{ex}) is extremely large. The styrene/dithiobenzoate system is a well-known system with an extremely large C_{ex} value ($C_{ex} > 6{,}000$) [37]. This result clearly proves the occurrence of radical migration (chemical diffusion of radicals) on the surface. There was also observed a critical value of the graft density, below which migration of the graft radicals hardly occurred. Below this limit, the effects of migration are not expected and, thus, the migration is a characteristic kinetic feature of the "concentrated" regime.

3 Surface-Initiated ITP

The ITP system contain a monomer, an alkyl iodide dormant species, and a radical source such as an azo compound and a peroxide that supplies Polymer$^{\bullet}$ to induce DT and run the polymerization. ITP is one of the simplest and most technically

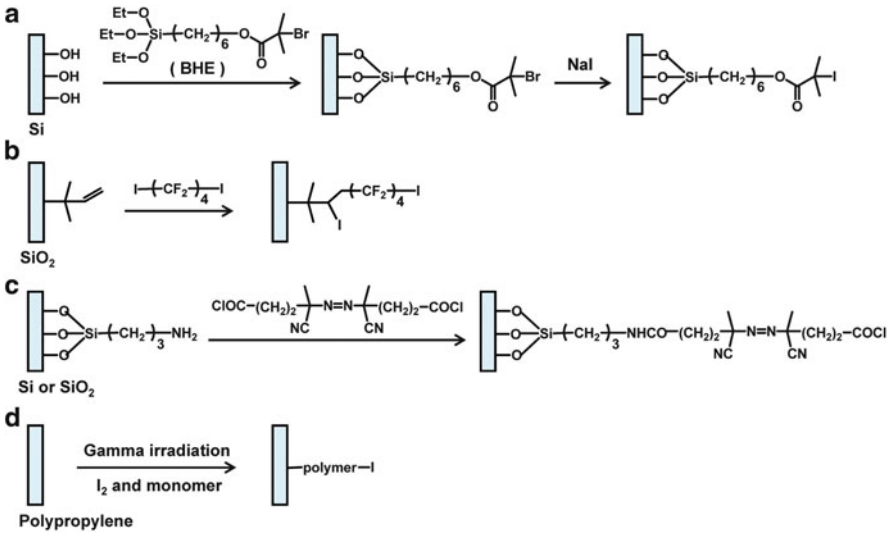

Scheme 2 Immobilization of ITP initiator onto a surface

robust LRP techniques [23, 38–44]. ITP has been applied to surface-initiated polymerization on flat substrates and fine particles.

The first example was reported by Takahara and coworkers, who prepared poly (vinyl acetate) brushes on a silicon wafer (flat substrate) [45]. Instead of using an "iodide" surface-immobilizable initiating dormant species, the authors used a "bromide" species, (2-bromo-2-methyl)propionyloxyhexyltriethoxysilane (BHE) (Scheme 2a), which consists of an alkyl bromide moiety and a triethoxysilyl (TEOS) group. BHE was covalently immobilized onto a silicon wafer via a chemical vapor adsorption method, whereby the TEOS group of BHE was coupled with the silanol group on the silicon surface. Then, on the surface of the wafer, bromine was converted to iodine via a halogen exchange reaction using NaI (Scheme 2a). The obtained "ITP initiator" immobilized wafer was immersed in a mixture of vinyl acetate (VAc), a radical source (an azo compound), and free ITP initiator (ethyl iodoisobutylate) that was structurally similar to the immobilized initiator. The system was then heated for the polymerization. Without the free initiator, the graft polymerization can be controlled only poorly because of the low overall concentration of the dormant species.

Although the graft polymer was not directly characterized in this work, we may, a priori, assume that the produced free polymer can be used as a useful measure of the chain length and chain-length distribution of the graft polymer. In other systems such as ATRP (and TERP, as described later), several research groups have directly characterized the graft polymers cleaved from the substrates and observed good agreement in the number-average molecular weight (M_n) and dispersity index (M_w/M_n) between the graft and free polymers [2] (M_w being the weight-average molecular weight). The thickness of the poly(vinyl acetate) brush, as determined using

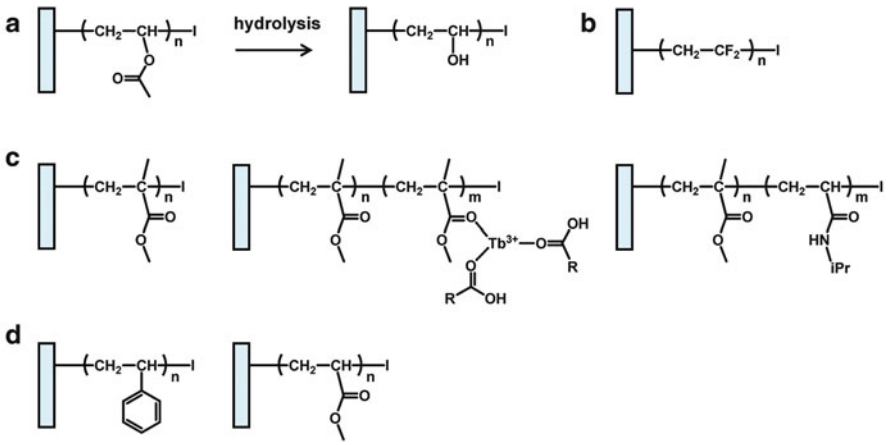

Fig. 4 Polymer brushes prepared by surface-initiated ITP

ellipsometry, increased with an increase in M_n of the free polymer. Assuming the same M_n for the graft and free polymers, the graft density σ was calculated to be 0.09 chains/nm^2 (i.e., the reduced graft density $\sigma^* = 0.04$). The M_w/M_n of the free polymer was 1.7–2.0. The M_w/M_n of the graft polymer in ITP might be smaller than that of the free polymer because of the radical migration mentioned above. The obtained poly(vinyl acetate) brushes were then converted to poly(vinyl alcohol) brushes via hydrolysis (Fig. 4a). These hydrophilic brushes were then subjected to tribology studies [46].

An advantage of ITP is that ITP is applicable to fluorinated vinyl monomers [38, 47, 48]. Améduri and coworkers conducted surface-initiated ITP of vinylidene fluoride (VDF) on silica particles (Fig. 4b) [49]. They used silica particles bearing vinyl groups on the surface (Scheme 2b). An ITP initiator, 1,4-diiodoperfluorobutane, was immobilized onto the surface through an addition reaction of 1,4-diiodoperfluorobutane to the double bonds on the surface. The ITP-initiator immobilized particles were mixed with VDF and a radical source (peroxide) and heated for the polymerization, without using a free ITP initiator. Elemental analysis, water contact angle measurement, and thermogravimetric analysis clearly showed successful grafting of poly(vinylidene fluoride) on the particles. Regarding VDF, other approaches (i.e., grafting-to) were also used for grafting poly (vinylidene fluoride) onto silica particles [50] and carbon black particles [51]. The free polymer was prepared by ITP, and the terminal iodine unit or the post-transformed terminal azido unit was used for grafting the polymer onto the surfaces.

Instead of a dormant species, a conventional radical initiator can be immobilized on the surface to conduct reverse LRP. Reverse iodine transfer polymerization (RITP) has been established in solution by Lacroix-Desmazes and colleagues [42–44] and Tatemoto and Nakagawa [38]. A conventional radical initiator such an azo compound (R–N=N–R) and molecular iodine (I_2) are used as starting compounds; then, the alkyl iodide (R–I) formed in situ is used for the polymerization. Wang

et al. immobilized an azo radical initiator onto silica particles (Scheme 2c) and successfully applied RITP to the graft polymerization of methyl methacrylate (MMA) [52]. Taking advantage of the living nature of ITP, these researchers also extended the graft chain with a second monomer (a terbium-complexed MMA) and obtained a block copolymer brush (Fig. 4c) [52]. The obtained silica/polymer/terbium hybrid material showed strong fluorescence due to terbium, suggesting successful block copolymerization. The same research group also applied this RITP approach to a flat silicon substrate and obtained an amphiphilic block copolymer brush using MMA and *N*-isopropyl acrylamide (NIPAM) (Fig. 4c) [53].

Besides inorganic substrates, Boyer and coworkers used a polypropylene film as a substrate (Scheme 2d) [54]. They conducted surface-initiated RITP using γ-irradiation to generate radicals on the film surface in the presence of I_2, obtaining brushes of styrene and methyl acrylate (Fig. 4d). The γ-irradiation approach is useful for directly forming polymer brushes on inert polymer films that lack functional groups for immobilizing initiators.

Photo-induced ITP has recently been developed in solution by Wolpers and Vana [55]. The polymer–iodine bond was directly cleaved by photo-irradiation (DC process in Scheme 1b), and accumulation of the iodine deactivator (generated by DC) was avoided by continuously supplying Polymer$^{\bullet}$ using a conventional radical initiator. It would be interesting to apply this photo-induced ITP to surface-initiated polymerization in the future.

4 Surface-Initiated TERP

The TERP system contains a monomer, an organotellurium dormant species, and a conventional radical initiator for inducing DT [24, 56–59]. Interestingly, TERP can also be conducted at elevated temperature [56, 57] or under photo-irradiation [59], even without adding a conventional radical initiator. High temperatures and photo-irradiation can induce thermal and photochemical dissociation of the organotellurium dormant species (DC in Scheme 1b), respectively, which can act as an alternative radical source; then, the polymerization is mainly controlled by DT. The most attractive advantage of TERP would its high monomer versatility. TERP is amenable to both conjugated and nonconjugated monomers and is also compatible with a variety of functional monomers. TERP can also provide high molecular weight polymers with low dispersities, which may be beneficial for obtaining thick polymer brushes. Photo-induced TERP could also be useful for surface-initiated polymerization. Thus, TERP could expand the synthetic scope of polymer brushes.

Yamago et al. [60] prepared a surface-immobilizing TERP initiator, 4-(triethoxysilyl)butyl 2-methyltellanyl-2-methylpropionate **2** (TeBE) (Scheme 3a). TeBE was immobilized on a silicon wafer and silica particles, and then heated with a monomer and a free TERP initiator. A conventional azo initiator was added in some cases, depending on the monomer and temperature. In the polymerization of styrene, in selected runs, the graft polymer was cleaved from the surface and

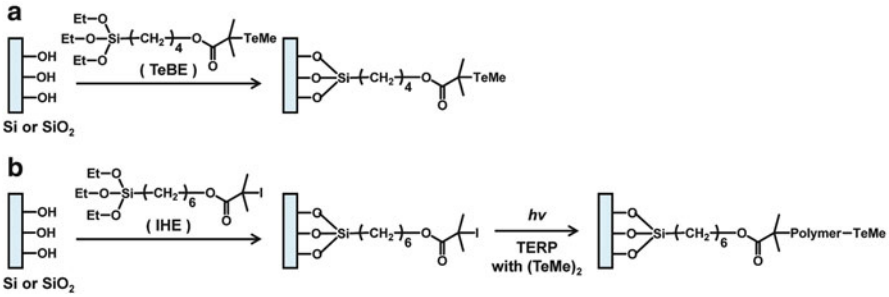

Scheme 3 Immobilization of TERP initiator onto a surface

analyzed by GPC. The M_n of the graft polymer was very similar to that of the free polymer (within a 5% difference) and agreed well with the theoretical M_n value up to $M_n = 58{,}000$. The M_w/M_n was also very similar for the free and graft polymers and was typically as low as 1.1–1.2. In some cases, the graft polymer had an even smaller M_w/M_n value than the free polymer, possibly because of the fast DT induced by radical migration on the surface as well as the effect of the polymers generated by autoinitiation of styrene in the solution phase. The termination product by the radical migration was not significant in TERP, in contrast to the mentioned RAFT system. The C_{ex} value ($C_{ex} > 6{,}000$) in the RAFT system [37] was extremely large and more than 300 times greater than that ($C_{ex} = 17$) in the TERP system [58, 61], explaining why significant termination was observed only in the RAFT system. The thickness of the graft layer increased proportionally to the M_n of the graft (and free) polymer, indicating that the graft density remained constant during polymerization. The reduced graft density σ^* was high (up to 0.48) and was located in the concentrated region. These results demonstrate the successful preparation of well-defined concentrated polymer brushes by TERP. Surface-initiated TERP was also applied to MMA, butyl acrylate, NIPAM, *N*-vinylcarbazole (NVC), and *N*-vinylpyrrolidine (NVP) (Fig. 5). The σ^* value was 0.32 for MMA, 0.30 for butyl acrylate, 0.36 for NIPAM, 0.53 for NVC, and 0.50 for NVP; M_w/M_n was small (<1.41) in all cases. NVC and NVP are nonconjugated monomers, and this result is the first preparation of concentrated brushes of nonconjugated monomers. Thus, a wide range of monomers can be used for surface-initiated TERP. Figure 5 also shows transmission electron microscope (TEM) images of silica nanoparticles fabricated with polystyrene brushes of two different molecular weights.

TERP can be photochemically induced, as mentioned. Photo-induced reactions do not require heat and thus are applicable to functional groups and materials that decompose at high temperatures. Photochemical stimuli can also be used as external stimuli to switch the reactions "on" and "off" and can trigger the reactions locally at specific positions. Thus, photo-induced LRP can expand the scope of monomers and substrates and offer temporal and spatial control in surface-initiated LRP. In this regard, Tsujii, Yamago and coworkers conducted photo-induced

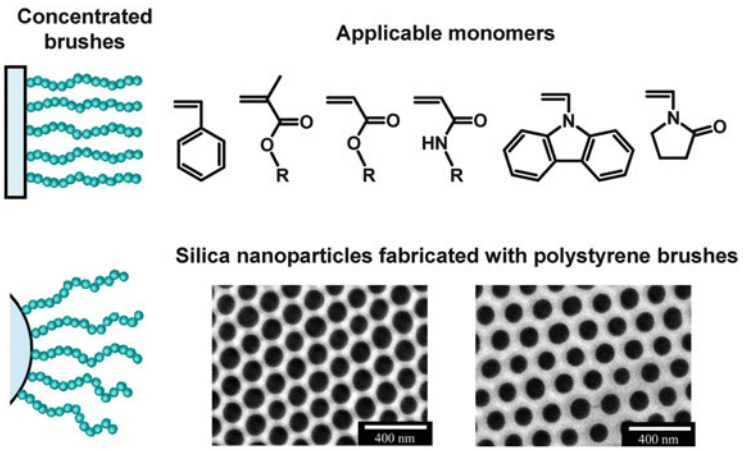

Fig. 5 Surface-initiated TERP. Applicable monomers and TEM images of silica nanoparticles fabricated with polystyrene brushes. The *black* and *white* parts correspond to silica particles and polystyrene, respectively. Reproduced with permission from Yamago et al. [60] (Copyright 2013 American Chemical Society)

surface-initiated TERP under photo-irradiation at $\lambda = 450$–530 nm [62]. They attached an iodide immobilizing initiator, (2-iodo-2-methyl)propionyloxyhexyltriethoxysilane **3** (IHE) (Scheme 3b), onto a silicon wafer and silica particles, instead of the telluride initiator (TeBE). After the immobilization, iodine was exchanged with a telluride group in situ during the polymerization. IHE is insensitive to oxygen and has the advantages that it is easy to prepare and handle, whereas TeBE is slightly sensitive to oxygen. The photo-induced TERP of 2-hydroxyethyl acrylate (HEA) and poly(ethyleneglycol)methylether acrylate (PEGA) successfully produced well-defined hydrophilic concentrated brushes. The σ^* value was 0.34 for HEA and 0.42 for PEGA, and the M_w/M_n value was 1.2–1.3 in both cases. These hydrophilic concentrated brushes exhibited superlubrication in aqueous solutions [62], which is a unique feature of concentrated brushes.

5 Surface-Initiated RTCP

The RTCP system contains a monomer, an alkyl iodide dormant species, a conventional radical initiator as radical source, and an organic catalyst [30–35]. The component is ITP including a catalyst. In ITP, the C_{ex} value is relatively small, and thus the dispersity control is limited in many case (e.g., $C_{ex} = 4.0$ for styrene at 60°C [63] and 1.6 for MMA at 90°C [64]). The addition of a catalyst in RTCP dramatically improves the control of dispersity.

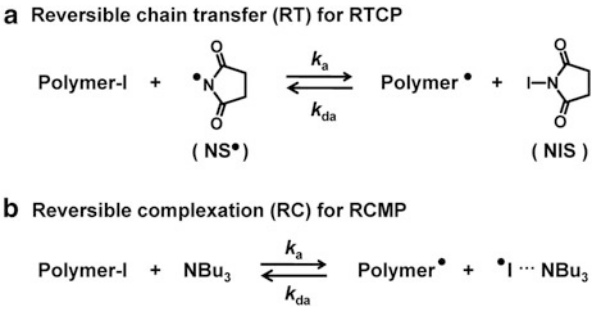

Scheme 4 (**a**) Reversible chain transfer for RTCP and (**b**) reversible complexation for RCMP

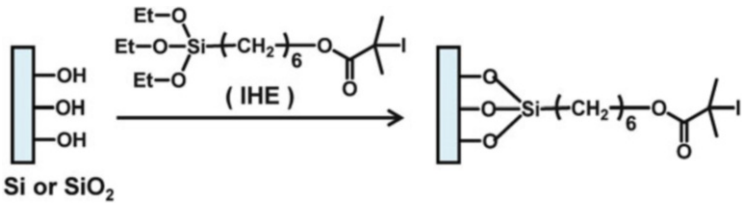

Scheme 5 Immobilization of RTCP initiator onto a surface

RTCP involves a reversible chain transfer (RT) process with a catalyst (Scheme 4a) that improves the dispersity control, as well as the mentioned small contribution of DT (Scheme 1d). The catalyst can be, e.g., *N*-iodosuccinimide (NIS) (Scheme 4a) [31], and works as a deactivator. Polymer$^{\bullet}$ (which is originally supplied by the conventional radical initiator) reacts with NIS to produce *N*-succinimide radical (NS$^{\bullet}$). NS$^{\bullet}$ works as an activator of Polymer-I to generate Polymer$^{\bullet}$ and NIS again. This cycle allows for frequent reversible activation of Polymer-I. This process is a reversible chain transfer of NIS that catalytically activates Polymer-I. Therefore, the polymerization was termed reversible chain transfer catalyzed polymerization (RTCP). Regarding the components used, RTCP is similar to initiators for continuous activator regeneration (ICAR)-ATRP [65]. Both systems use a monomer, a dormant species (alkyl iodide or alkyl bromide), a conventional radical initiator, and a deactivator [NIS or copper (II)] to regenerate a highly reactive activator [NS$^{\bullet}$ or copper (I)].

Goto and coworkers attached a surface-immobilizing initiator IHE onto a silicon wafer (Scheme 5) and prepared polymer brushes by RTCP [66]. The IHE-immobilized silicon wafer was immersed in a mixture of MMA, 2-cyanopropyl iodide (a free iodide initiator), azobis(isobutyronitrile) (a radical source), and NIS (a catalyst). The system was purged with an inert gas and heated at 70°C for 4 h to induce polymerization. The M_n and M_w/M_n values of the free polymer were 15,000 and 1.31, respectively. From the thickness of the graft polymer and the M_n of the free polymer, the σ^* value was calculated to be 0.28. This result indicates the successful controlled synthesis of a concentrated polymer brush by RTCP. Another example of the graft polymerization is depicted in Fig. 6,

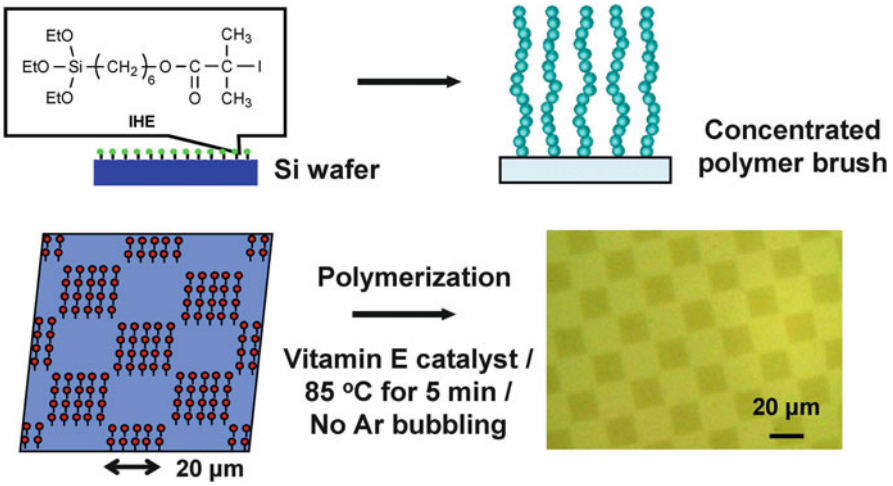

Fig. 6 Surface-initiated RTCP for preparing a patterned brush. Reproduced with permission from Tanishima et al. [66] (Copyright 2014 MDPI)

in which IHE was fixed onto the surface in a patterned manner. For demonstration purposes, Goto and colleagues carried out an RTCP of benzyl methacrylate (BzMA) for a short period of 5 min at 85°C, using a nontoxic catalyst (vitamin E) and without prior purge with an inert gas. After the polymerization, the polymer brushes were observed as black square spots (Fig. 6), demonstrating the robust and quick synthesis of a patterned polymer brush.

Regarding the use of RTCP, a grafting-to approach was also used for chemically attaching polystyrene onto silica particles. Afsharian-Moghaddam and Haddadi-Asl prepared a free polystyrene-iodide by RTCP [67]. They utilized a nucleophilic substitution reaction of the iodine end of the polymer with the hydroxyl groups on the inorganic surface. Using this method, the polymer can be directly attached to the surface, without requiring modification of the inorganic surfaces or functionalization of the polymers. The method could serve as a simple technique for end-grafting polymers.

In addition to RTCP, Goto and coworkers also developed another type of organo-catalyzed LRP, i.e., reversible complexation-mediated polymerization (RCMP) (Scheme 4b) [64, 68–70]. RCMP is mechanistically different from RTCP. The RCMP system contains a monomer, an alkyl iodide (dormant species), and a catalyst (activator), and is technically similar to "normal" ATRP. The RCMP catalysts include, e.g., tertiary amines (R_3N) [64] and quaternary ammonium iodide ($R_4N^+I^-$) [68]. The organic catalysts for both RTCP and RCMP are inexpensive and easy to handle and in many cases also have minor colors, smells, and toxicities. RTCP and RCMP are amenable to a variety of monomers, and RCMP can be induced by photo-irradiation [69] as well as thermal heating. These features of RTCP and RCMP make them attractive for a variety of brush designs.

6 Conclusions

ITP, TERP, and RTCP have successfully been applied to surface-initiated polymerizations of several monomers for preparing well-defined, dilute, semidilute, and concentrated polymer brushes on flat substrates and particles. These LRP techniques are attractive for their robustness, high monomer versatility, and inducibility by photo-irradiation, for example, and widen the scope of surface-initiated polymerization. Access to a range of macromolecular surface designs could be beneficial for a variety of applications.

References

1. Barbey R, Lavanant L, Paripovic D, Schüwer N, Sugnaux C, Tugulu S, Klok HA (2009) Chem Rev 109:5437
2. Tsujii Y, Ohno K, Yamamoto S, Goto A, Fukuda T (2006) Adv Polym Sci 197:1
3. Edmondson S, Osborne VL, Huck WTS (2004) Chem Soc Rev 33:14
4. Olivier A, Meyer F, Raquez JM, Damman P, Dubois P (2011) Prog Polym Sci 37:157
5. Chen T, Amin I, Jordan R (2012) Chem Soc Rev 41:3280
6. Ayres N (2010) Polym Chem 1:769
7. Israelachvili JN (1992) Intermolecular and surface forces, 2nd edn. Academic, London
8. Halperin A, Tirrell M, Lodge TP (1992) Adv Polym Sci 100:31
9. Kawaguchi M, Takahashi A (1992) Adv Colloid Interface Sci 37:219
10. Alexander S (1977) J Phys (Paris) 38:983
11. de Gennes PG (1980) Macromolecules 13:1069
12. Taunton HJ, Toprakcioglu C, Fetters LJ, Klein J (1990) Macromolecules 23:571
13. Courvoisier A, Isel F, Francois J, Maaloum M (1998) Langmuir 14:3727
14. Daoud M, Cotton JP (1982) J Phys (Paris) 43:531
15. Birstein TM, Zhulina EB (1984) Polymer 25:1453
16. Matyjaszewski K, Möller M (2012) Polymer science: a comprehensive reference. Elsevier, Amsterdam
17. Tsarevsky NV, Sumerlin BS (2013) Fundamentals of controlled/living radical polymerization. Royal Society of Chemistry, London
18. Nicolas J, Guillaneuf Y, Lefay C, Bertin D, Gigmes D, Charleux B (2013) Prog Polym Sci 38:63
19. Matyjaszewski K, Tsarevsky NV (2014) J Am Chem Soc 136:6513
20. Ouchi M, Terashima T, Sawamoto M (2009) Chem Rev 109:4963
21. Zhang N, Samanta SR, Rosen BM, Percec V (2014) Chem Rev 114:5848
22. Keddie DJ, Moad G, Rizzardo E, Thang SH (2012) Macromolecules 45:5321
23. David G, Boyer C, Tonnar J, Améduri B, Lacroix-Desmazes P, Boutevin B (2006) Chem Rev 106:3936
24. Yamago S (2009) Chem Rev 109:5051
25. Zetterlund PB, Kagawa Y, Okubo M (2008) Chem Rev 108:3747
26. Satoh K, Kamigaito M (2009) Chem Rev 109:5120
27. Monteiro MJ, Cunningham MF (2012) Macromolecules 45:4939
28. Fischer H (2011) Chem Rev 101:3581
29. Goto A, Fukuda T (2004) Prog Polym Sci 29:329
30. Goto A, Zushi H, Hirai N, Wakada T, Tsujii Y, Fukuda T (2007) J Am Chem Soc 129:13347
31. Goto A, Hirai N, Wakada T, Nagasawa K, Tsujii Y, Fukuda T (2008) Macromolecules 41:6261

32. Goto A, Tsujii Y, Fukuda T (2008) Polymer 49:5177
33. Vana P, Goto A (2010) Macromol Theory Simul 19:24
34. Yorizane M, Nagasuga T, Kitayama Y, Tanaka A, Minami H, Goto A, Fukuda T, Okubo M (2010) Macromolecules 43:8703
35. Goto A, Hirai N, Nagasawa K, Tsujii Y, Fukuda T, Kaji H (2010) Macromolecules 43:7971
36. Tsujii Y, Ejaz M, Sato K, Goto A, Fukuda T (2001) Macromolecules 34:8872
37. Goto A, Sato K, Tsujii Y, Fukuda T, Moad G, Rizzardo E, Thang SH (2001) Macromolecules 34:402
38. Tatemoto M, Nakagawa T (1978) DE2729671 (Chem Abstr 88:137374)
39. Yutani Y, Tatemoto M (1992) EP489370 A1
40. Matyjaszewski K, Gaynor S, Wang JS (1995) Macromolecules 28:2093
41. Kato M, Kamigaito M, Sawamoto M, Higashimura T (1995) Macromolecules 28:1721
42. Lacroix-Desmazes P, Severac R, Boutevin B (2005) Macromolecules 38:6299
43. Boyer C, Lacroix-Desmazes P, Robin JJ, Boutevin B (2006) Macromolecules 39:4044
44. Tonnar J, Lacroix-Desmazes P (2008) Angew Chem Int Ed 47:1294
45. Terayama Y, Kobayashi M, Takahara A (2007) Chem Lett 36:1280
46. Kobayashi M, Takahara A (2010) Chem Rec 10:208
47. Boyer C, Valade D, Sauguet L, Améduri B, Boutevin B (2005) Macromolecules 38:10353
48. Beuermann S, Imran-ul-haq M (2007) Macromol Symp 259:210
49. Durand N, Boutevin B, Silly G, Améduri B (2011) Macromolecules 44:8487
50. Durand N, Gaveau P, Silly G, Améduri B, Boutevin B (2011) Macromolecules 44:6249
51. Vukićević R, Hierzenberger P, Hild S, Beuermann S (2010) J Polym Sci A Polym Chem 48:4847
52. Wang LP, Dong LH, Hao JC, Lv XH, Li WZ, Li YC, Zhen JM, Hao YC, Ma F (2011) J Colloid Interface Sci 361:400
53. Wang LP, Lv XH, Li G, Li YC (2014) Polym Eng Sci 925
54. Foster O, Soeriyadi AH, Whittaker MR, Davis TP, Boyer C (2012) Polym Chem 3:2102
55. Wolpers A, Vana P (2014) Macromolecules 47:954
56. Yamago S, Iida K, Yoshida J (2002) J Am Chem Soc 124:2874
57. Yamago S, Iida K, Yoshida J (2002) J Am Chem Soc 124:13666
58. Goto A, Kwak Y, Fukuda T, Yamago S, Iida K, Nakajima M, Yoshida J (2003) J Am Chem Soc 125:8720
59. Yamago S, Ukai Y, Matsumoto A, Nakamura Y (2009) J Am Chem Soc 131:2100
60. Yamago S, Yahata Y, Nakanishi K, Konishi S, Kayahara E, Nomura A, Goto A, Tsujii Y (2013) Macromolecules 46:6777
61. Kwak Y, Tezuka M, Goto A, Fukuda T, Yamago S (2007) Macromolecules 40:1881
62. Nomura A, Goto A, Ohno K, Kayahara E, Yamago S, Tsujii Y (2011) J Polym Sci A Polym Chem 49:5284
63. Goto A, Ohno K, Fukuda T (1998) Macromolecules 31:2809
64. Goto A, Suzuki T, Ohfuji H, Tanishima M, Fukuda T, Tsujii Y, Kaji H (2011) Macromolecules 44:8709
65. Matyjaszewski K, Gaynor S, Wang JS (2006) Proc Natl Acad Sci U S A 103:15309
66. Tanishima M, Goto A, Lei L, Ohtsuki A, Kaji H, Nomura A, Tsujii Y, Yamaguchi Y, Komatsu H, Miyamoto M (2014) Polymers 6:311
67. Afsharian-Moghaddam H, Haddadi-Asl V (2013) Iran Polym J 22:757
68. Goto A, Ohtsuki A, Ohfuji H, Tanishima M, Kaji H (2013) J Am Chem Soc 135:11131
69. Ohtsuki A, Goto A, Kaji H (2013) Macromolecules 46:96
70. Lei L, Tanishima M, Goto A, Kaji H, Yamaguchi Y, Komatsu H, Jitsukawa T, Miyamoto M (2014) Macromolecules 47:6610

Adv Polym Sci (2016) 270: 123–162
DOI: 10.1007/12_2015_313

Published online: 17 May 2015

Synthesis of Nanocapsules and Polymer/Inorganic Nanoparticles Through Controlled Radical Polymerization At and Near Interfaces in Heterogeneous Media

Elodie Bourgeat-Lami, Franck D'Agosto, and Muriel Lansalot

Abstract This review describes recent advances in the synthesis of polymeric nanocapsules and polymer/inorganic hybrid nanoparticles where controlled radical polymerization (CRP) has been used in (mini)emulsion systems to restrict the location of polymerization to an interface. For the synthesis of nanocapsules, CRP polymers stabilize the initial miniemulsion droplet interface and are chain-extended mainly towards the center of the droplets, which contain an inert liquid core. For encapsulation of inorganic particles, CRP polymers adsorbed on their surface are chain-extended to form a polymer shell around the inorganic core. Precise control over the structure and composition of the polymers allows their location to be restricted to these interfaces. Polymerization in the subsequent (mini) emulsion system then commences from these specific locations, courtesy of the reactivatable functions. The developed strategies retain the advantages of traditional emulsion or miniemulsion systems, while greatly expanding their potential to generate novel nanostructured functional materials.

Keywords ATRP · Capsules · Composite materials · Controlled radical polymerization · Emulsion polymerization · Encapsulation · Inorganic particles · Miniemulsion polymerization · NMP · RAFT

Contents

E. Bourgeat-Lami, F. D'Agosto, and M. Lansalot (✉)
Laboratoire de Chimie, Université de Lyon, Univ. Lyon 1, CPE Lyon, CNRS UMR 5265, Catalyse, Polymères et Procédés (C2P2), LCPP group, 69616 Villeurbanne, France
e-mail: muriel.lansalot@univ-lyon1.fr

Abbreviations

AA	Acrylic acid
ACPA	4,4′-Azobis(4-cyanopentanoic acid)
AIBN	2,2′-Azobis(isobutyronitrile)
A(R)GET	Activator (re)generated by electron transfer
ATRP	Atom transfer radical polymerization
BA	*n*-Butyl acrylate
BAEDS	Bis-acryloyloxyethyl disulfide
BMA	*n*-Butyl methacrylate
CDPA	4-Cyano-4(dodecylsulfanylthiocarbonyl)sulfanylpentanoic acid
CdS	Cadmium sulfide
CRP	Controlled radical polymerization
Cryo-TEM	Cryogenic transmission electron microscopy
CTAB	Cetyl trimethylammonium bromide
$Đ$	Dispersity
DBTTC	Dibenzyl trithiocarbonate
DFA	Dodecafluoroheptyl acrylate
DIBTC	Dodecyl isobutyric acid trithiocarbonate
DLS	Dynamic light scattering
DMAEMA	2-Dimethylaminoethyl methacrylate
dNbPy	4,4′-Dinonyl-2,2′-bipyridine
DODAB	Dimethyldioctadecyl ammonium bromide
DSDMA	Bis(2-methacryloyloxyethyl)disulfide
DT	Degenerative transfer
DVB	Divinylbenzene
EBiB	Ethyl α-bromoisobutyrate
EGDMA	Ethylene glycol dimethacrylate
GO	Graphite oxide
HD	Hexadecane
IMEPP	Inverse miniemulsion periphery polymerization
KPS	Potassium persulfate
MA	Methyl acrylate

macroRAFT agent	Macromolecular RAFT agent
MAn	Maleic anhydride
MAA	Methacrylic acid
MBA	*N*,*N*′-Methylenebisacrylamide
MMA	Methyl methacrylate
MMT	Montmorillonite
M_n	Number-average molar mass
MNP	Magnetic nanoparticle
NMP	Nitroxide-mediated polymerization
NIPAM	*N*-Isopropylacrylamide
OA	Oleic acid
PAA	Poly(acrylic acid)
PAH	Poly(allylamine hydrochloride)
PBA	Poly(*n*-butyl acrylate)
PBMA	Poly(*n*-butyl methacrylate)
PDFA	Poly(dodecafluoroheptyl acrylate)
PDMAEMA	Poly(2-dimethylaminoethyl methacrylate)
PEOMA	Poly(ethylene oxide) methacrylate
PHPMA	Poly[*N*-(2-hydroxypropyl methacrylamide)]
PISA	Polymerization-induced self-assembly
PMAA	Poly(methacrylic acid)
PMMA	Poly(methyl methacrylate)
PNIPAM	Poly(*N*-isopropylacrylamide)
PPPDTA	Phenyl 2-propyl phenyldithioacetate
PS	Polystyrene
QD	Quantum dot
RAFT	Reversible addition-fragmentation chain transfer
REEP	MacroRAFT-mediated encapsulating emulsion polymerization
RDRP	Reversible-deactivation radical polymerization
(R)ITP	(Reverse) iodine-transfer polymerization
SAXS	Small-angle X-ray scattering
SDBS	Sodium dodecylbenzene sulfonate
SDS	Sodium dodecyl sulfate
SG1	*N*-*tert*-butyl-*N*-[1-diethylphosphono-(2,2-dimethylpropyl)] nitroxide
SR&NI	Simultaneous reverse and normal initiation
S	Styrene
t-BA	*tert*-Butyl acrylate
TEM	Transmission electron microscopy
TERP	Organotellurium-mediated living radical polymerization
TFA	Trifluoroacetic acid
T_g	Glass transition temperature
THF	Tetrahydrofuran
VBTMACl	Vinylbenzyl trimethylammonium chloride

1 Introduction

Free-radical polymerization is arguably the most important method for the production of synthetic polymers in view of its widespread industrial use and the large variety of applications for the resulting polymers. A wide range of functional monomers can be (co)polymerized by free-radical polymerization to produce a myriad of polymer compositions and properties [1], but the unavoidable occurrence of fast radical–radical termination reactions means that their molar masses, chain-end functionalities, and macromolecular architectures cannot be controlled. In the last two decades, the development of controlled radical polymerization (CRP) techniques (IUPAC recommended term: reversible-deactivation radical polymerization, RDRP) has impacted the polymer field tremendously by overcoming these limitations. CRP techniques can be subdivided into two categories: those based on a *reversible termination reaction* and those based on a *reversible chain transfer reaction*. In both cases, macromolecular radicals, called active species, undergo reversible deactivation under the influence of a controlling agent to form dormant chains (with the controlling functionalities at their termini). Only a very small fraction of the total number of chains are simultaneously active and therefore capable of propagation, but rapid interchange of the active centers between macromolecular chains means that all chains have an equal chance of propagating. CRP systems therefore display narrow molar mass distributions and a linear increase in the number-average molar mass (M_n) with monomer conversion, because the polymer chains grow concurrently. The production of block copolymers and more complex architectures is also possible because polymers produced by CRP bear the mediating function at the chain end and can thus be further extended with either the same or another monomer in a subsequent polymerization step.

Emulsion polymerization is an important industrial process for the production of latex paints, rubbers, coatings, and adhesives [2–4]. A "conventional" emulsion polymerization starts with the emulsification of an insoluble (or scarcely soluble) monomer in water with the aid of a surfactant. A hydrophilic initiator is also present in the aqueous phase. At this point, the monomer is primarily distributed between large emulsion droplets and small surfactant micelles, with a minor amount dissolved in the aqueous phase. Polymerization starts in the aqueous phase by the formation of free radicals from the initiator and the addition of the first monomer units. These oligomeric radical species are rapidly captured by the monomer-swollen micelles, leading to particle formation in the nucleation step. Their continued propagation is supported by the supply of monomer molecules diffusing through the aqueous phase from the large droplets. In surfactant-free emulsion polymerizations, the nucleation occurs by precipitation of the oligoradicals to form unstable nuclei, which fuse to form larger particles. Polymerization takes place mainly within these monomer-swollen particles, which grow in a similar fashion to those in a surfactant-containing system.

In the last 20 years, emulsion polymerization has proven highly suitable for the production of polymer/inorganic particles to generate a variety of composite

colloids. These can be further processed into films with improved mechanical, thermal, or barrier properties compared with their pure-polymer counterparts [5–7]. The encapsulation of inorganic nano-objects into polymer particles can be achieved either by physical adsorption of preformed polymer chains or particles onto the inorganic particles, or by encapsulation of inorganic objects within the polymer latex by using them as seeds in the emulsion polymerization process. To circumvent the lack of compatibility between the inorganic and organic parts, coupling agents such as silanes, titanates, or carboxylates and surfactants are usually employed to render the inorganic surface more hydrophobic.

Miniemulsion polymerization is another widely employed tool for the production of polymer/inorganic nanoparticles in dispersed systems [8–12]. In miniemulsion polymerization, high shear is initially applied to the suspension of monomer in a dispersing phase to produce small uniform monomer droplets. Stability is maintained by the presence of a surfactant and also by the use of a solvophobic species that suppresses molecular diffusion between droplets. These droplets then accept radicals produced in the initiation step and polymerize to form the final latex particles. In an ideal miniemulsion polymerization, every droplet is nucleated to produce a one-to-one particle copy. When performed in water, miniemulsion polymerization combines the features of an emulsion polymerization with the possibility of dispersing a hydrophobic species inside the monomer droplets. By avoiding the often complicated nucleation step observed in emulsion polymerization, the miniemulsion process is a powerful tool for encapsulating compatible components (including inert liquids and inorganic particles) into the latexes [13–18].

Regardless of the synthetic strategy, controlling the size and morphology of latex particles is key to modulating the properties of the final material. The use of CRP in emulsion and miniemulsion systems can enhance the possibilities for fine tuning the particle composition and morphology by controlling the polymer chains at the molecular level, thus opening the door to well-defined materials for a variety of new applications. The achievements of CRP in dispersed media have been covered in several excellent review articles [19–22]. The present work focuses more specifically on recent advances in the use of well-defined CRP polymers to generate nanocapsules and polymer/inorganic hybrid nanostructures in heterogeneous systems. Particular attention is placed on the use of CRP polymers as reactivatable precursors in the (mini)emulsion systems. Because CRP allows tuning of the physico-chemical properties of these polymers to precisely direct their location at the interface, reactivation of their dormant end groups permits resumption of the polymerization at these specific loci.

2 Controlled Radical Polymerization Techniques

CRP techniques are classed as either reversible termination processes or reversible chain transfer processes. Within the first category, nitroxide-mediated polymerization (NMP) [23] and atom transfer radical polymerization (ATRP) [24] are the two most commonly used methods. In NMP, control is induced by nitroxide derivatives, which are capable of reversibly capping active radicals to form dormant alkoxyamines. Although alkoxyamines are stable at low temperatures, their C–O bonds can undergo reversible homolytic cleavage at elevated temperatures, regenerating active radicals that can add a few monomer units before being once more capped by the nitroxide. This equilibrium between propagating radicals and dormant macroalkoxyamines governs NMP. In ATRP, an alkyl halide initiator is activated by a redox reaction with a transition metal complex. In this reaction, the alkyl halide is reduced to produce an active radical capable of propagation, while the transition metal is oxidized. In most ATRP systems, Cu(I) species complexed by multidentate amine ligands are used as activators. After the activation step, the propagating radical can add monomer for a short time before being deactivated again through the reverse process: oxidation of the propagating radical by the Cu (II) complex to regenerate an alkyl halide and the original Cu(I) activator. The activation step can be performed using different approaches, starting either from Cu (I) or from Cu(II). If Cu(I) is used, the process is called direct ATRP, and only the alkyl halide is employed as initiator. If Cu(II) is used, there are multiple initiation possibilities, including (i) the reverse ATRP process [24], which uses a classical radical initiator; (ii) the simultaneous reverse and normal initiation (SR&NI) method [25], which utilizes an alkyl halide in conjunction with a small fraction of a classical radical initiator to reduce Cu(II) to Cu(I); (iii) the activator (re)generated by electron transfer (A(R)GET) technique [26], which uses an alkyl halide initiator in combination with a reducing agent to turn Cu(II) into Cu(I); and (iv) e-ATRP [27], which utilizes the concept of ARGET ATRP via an electrochemical stimulus to provide enhanced polymerization control.

CRP methods that proceed according to a reversible transfer mechanism (also called degenerative transfer, DT, processes) rely on a conventional radical initiator to generate a small number of active radicals, with the presence of a reversible chain transfer agent in large excess allowing the active radicals to be continuously redistributed between a large number of chains. Chains that are not active contain the chain transfer agent as their end group. In (reverse) iodine-transfer polymerization, (R)ITP, an iodine atom is transferred between active chains [28–30]. Organotellurium-mediated living radical polymerization (TERP) follows a similar mechanism [31], with the exchange of a terminal $TeCH_3$ group. The most popular DT technique is reversible addition-fragmentation chain transfer (RAFT) polymerization [32, 33], which utilizes a thiocarbonyl (i.e., C=S based) compound – typically a dithioester, dithiocarbonate, dithiocarbamate, or trithiocarbonate – as chain transfer agent [denoted Z-C(=S)-SR]. A radical can add to the thiocarbonyl group to generate a tertiary carbon-based radical intermediate, which then

fragments to release a second radical (the "R group" of the RAFT agent) that is also capable of propagating. In this manner, the active radical functions are rapidly and continually transferred between all the growing chains. If the initial concentration of the radical initiator is low with respect to the initial concentration of the transfer agent, a large majority of macromolecules have the same RAFT agent-derived end groups and the concentration of growing macromolecular chains becomes constant and close to the initial concentration of the RAFT agent. Precise molar masses can therefore be targeted by simply adjusting the feed ratio of monomer to RAFT agent.

3 Synthesis of Polymeric Nanocapsules

Nanocapsules are latex particles with a hollow or non-polymeric core, and heterogeneous polymerization systems employing CRP polymers at an interface have proven particularly amenable to their synthesis. The first method for nanocapsule synthesis in dispersed media using CRP is to mix a compatible inert liquid (also called a templating liquid) with the monomer in a miniemulsion system stabilized by CRP polymers. The inert liquid is subsequently entrapped in the core of the latex particles after polymerization. Post-polymerization removal of this liquid generates hollow particles, which are interesting for a variety of applications including drug delivery [17, 11]. CRP (typically RAFT and ATRP) is central to this approach because carefully designed controlling agents allow the polymerization to be confined to the interface of the dispersed and continuous phases and, thereby, entrap the templating liquid in the particle core [34]. Most studies describing this approach employ oil-in-water miniemulsion (also called direct miniemulsion) systems, as detailed in Sect. 3.1. Inverse miniemulsion systems, in which hydrophilic monomer droplets swollen with water are polymerized in an organic dispersing phase, have also been successfully reported and are detailed in Sect. 3.2. An alternative approach to generation of nanocapsules by using vesicles rather than liquids as templates is described in Sect. 3.3. Here, CRP polymers are electrostatically adsorbed on the surface of the vesicles, and a hydrophobic polymer shell is grown from this locus via emulsion polymerization.

3.1 Direct Miniemulsion

3.1.1 Non-crosslinked Nanocapsules

The first example of the use of CRP in miniemulsion to produce nanocapsules was reported by van Zyl et al. [35], who employed a RAFT agent for the ab initio miniemulsion polymerization of styrene. It is important to note that, in this example, the dispersed phase was stabilized by a traditional surfactant (rather than a CRP polymer), with the CRP polymer generated in situ in the continuous phase before

joining the surfactant at the interface. More specifically, the starting miniemulsion was formed in presence of sodium dodecyl sulfate (SDS) as surfactant with iso-octane used as the templating liquid in the styrene droplets. Fine tuning of the polymerization kinetics and surface effects allowed the droplet-entering oligomeric species to be anchored at the surface of the particles, where polymerization continued. Systems employing phenyl 2-propyl dithiobenzoate and phenyl 2-propyl phenyldithioacetate (PPPDTA) as molecular chain transfer agents and potassium persulfate (KPS) or 2,2′-azobis(isobutyronitrile) (AIBN) as initiators were tested. The use of AIBN did not lead to surface-active oligomeric species and thus favored confinement of the formed chains inside the particles. However, PPPDTA used in conjunction with KPS generated surface-active oligomeric species that resided at the water–monomer droplet interface. A rapid increase in the molar mass of the chains was observed, leading to reduced mobility where they were formed and thereby discouraging any migration away from the interface. The confinement of RAFT polymerization close to the surface of the droplets successfully resulted in formation of nanocapsules.

Shortly after this first successful report, Luo and Gu envisaged the use of a macromolecular RAFT (macroRAFT) agent that could both act as a stabilizer of the droplets and help to localize the controlled polymerization at the surface of the monomer droplets. In a seminal work [36], they used a preformed RAFT copolymer of styrene and maleic anhydride (MAn) in the subsequent miniemulsion polymerization of styrene. The particularity of this comonomer pair is that strictly alternating copolymers are obtained when identical molar amounts of styrene and MAn are used. RAFT polymerization of styrene and MAn was thus conducted in bulk to give P(S-*alt*-MAn), which was then mixed with styrene and the templating liquid ($C_{19}H_{40}$). This organic phase was dispersed in water containing ammonia, which aminolyzed the MAn units to hydrophilic carboxylate and amide groups. The resulting polymer chains migrated to the surface of the miniemulsion droplets, where they assumed the role of reactive stabilizers capable of chain extension with the styrene units in the droplets. The localization of these reactive stabilizers at the surface and the presence of the core material maintained the polymerization loci at the interface with water and allowed the inward growth of PS chains to generate nanocapsules. It is worth mentioning that the system did not provide capsule morphology quantitatively and a certain fraction of solid particles were also formed. Detailed investigation showed the importance of the hydrophilicity and molar mass of the aminolyzed P(S-*alt*-MAn) chains in reducing the proportion of solid particles [37]. The minimum amount of solid particles was obtained when aminolysis of the prepolymer was performed using an ammonia-to-anhydride ratio of 0.9. Solid particles could be avoided under these conditions either by slightly increasing the M_n of the P(S-*alt*-MAn) chains (from 1,400 to 1,795 g mol^{-1}) or by the additional use of SDS as surfactant.

With the aim of producing capsules quantitatively, the same group further developed this interface-confined miniemulsion concept by employing poly(acrylic acid)-*block*-polystyrene (PAA-*b*-PS) block oligomers as reactive surfactants [38]. Miniemulsions of styrene were prepared in water under alkaline conditions

in the presence of a large amount of hexadecane (HD) as templating liquid. Although only very short block copolymers were attainable (containing on average only two AA units and from one to three styrene units per chain), surface tension measurements confirmed their surface activity, and stable miniemulsions could be formed. Polymerizations were carried out with KPS as initiator. Upon polymerization, capsules were formed by chain extension of these oligomers located and maintained at the surface of the HD-rich monomer droplets. Control of the RAFT-mediated polymerization occurring in most of the particles was demonstrated by a linear increase in molar mass with conversion. An uncontrolled high molar mass population was also observed, which the authors initially suspected corresponded to the small proportion of solid particles formed by homogeneous nucleation. The presence of these particles was attributed to the hydrolysis of some RAFT functionalities to produce chains that were no longer capable of chain extension, increasing the chance of homogeneous nucleation in which RAFT control is not imposed. This explanation was consistent with the higher-than-expected experimental molar mass values of the controlled polymer population, because fewer RAFT groups in the system would increase the average chain length at a given monomer conversion. The addition of SDS before sonication, keeping all else constant, suppressed formation of the high molar mass population. Surprisingly, however, solid particles were still present, suggesting that the high molar mass polymer in the SDS-free system does not originate from solid particles; further experiments are therefore required to explain its origin. The addition of a small fraction of SDS after miniemulsion formation was also studied and led to the generation of homogeneous capsules that could be separated by centrifugation from the unavoidable small amount of solid particles. In a similar study, the authors showed that homogeneous nucleation could be attributed to the escape of hydrophilic stabilizer-derived radicals from the surface of the droplets to the water phase [39].

3.1.2 Shell-Crosslinked Nanocapsules

On the strength of this new strategy to produce nanocapsules using RAFT-synthesized reactive stabilizers, Luo's group extended the interfacial RAFT miniemulsion polymerization idea to the synthesis of hollow nanoparticles exhibiting a crosslinked fluorinated shell [40]. Dodecafluoroheptyl acrylate (DFA) was miniemulsified in water in the presence of HD as hydrophobe, hexyl acetate as liquid core material, divinylbenzene (DVB) as crosslinker, and AIBN as initiator. To stabilize the resulting droplets, low molar mass (1,728 g mol^{-1}, $Đ = 1.07$) poly(methacrylic acid)-*block*-poly(dodecafluoroheptyl acrylate) (PMAA-*b*-PDFA) block copolymers were first synthesized by RAFT using 4-cyano-4(dodecylsulfanylthiocarbonyl)sulfanylpentanoic acid (CDPA) as chain transfer agent. The previous findings of the authors were used here to prevent the formation of solid particles: a low pH value (6.46) of the aqueous phase, use of a hydrophobic initiator (AIBN), addition of a radical scavenger in water ($NaNO_2$),

and post-emulsification addition of a small amount of SDS. More than 95% of the particles obtained were nanocapsules and the gel content was measured to be 99%, suggesting a high degree of crosslinking in the fluorinated shell. A control experiment was performed under the same conditions, but with PMAA-*b*-PDFA being replaced by a corresponding amount of methacrylic acid (MAA). Solid particles were obtained. This result strongly suggests that the interfacial RAFT miniemulsion polymerization overcomes not only the kinetic but also the thermodynamic barriers to form well-defined core–shell structures. Hollow nanoparticles were obtained after removing the liquid core material by displacing it with tetrahydrofuran (THF) and drying the resulting dispersion.

Although not targeting nanocapsules, Jiang and colleagues employed a similar strategy to obtain shell-crosslinked nanoparticles using RAFT in miniemulsion [41]. Poly(2-dimethylaminoethyl methacrylate) (PDMAEMA) was first synthesized by RAFT polymerization using CDPA as controlling agent. The presence of a long alkyl Z group in CDPA probably helped the resulting PDMAEMA-SC(=S)$SC_{12}H_{25}$ to be surface-active and to co-stabilize, together with cetyl trimethylammonium bromide (CTAB), a miniemulsion of styrene and bis-acryloyloxyethyl disulfide (BAEDS) as crosslinking comonomer. However, in this study, cyclohexane was used only as hydrophobe and, thus, in quantities lower than required for it to act as a liquid core material. The authors claimed that shell-crosslinked nanoparticles were successfully obtained after initiating the polymerization with AIBN, without clearly stating why the crosslinking reaction only occurred in the shell.

ATRP has also been employed to design nanocapsules using miniemulsion polymerization [42]. The strategy was again based on the design of amphiphilic block copolymers that could be reactivated, in this case for the miniemulsion polymerization of an *n*-butyl methacrylate (BMA) dispersed phase. The positioning of these block copolymers at the surface of the monomer droplets forced the growth of the hydrophobic PBMA chains inwards, while the use of templating liquid (anisole and HD) confined the chains to the monomer droplet–water interface. The additional use of a crosslinker [either ethylene glycol dimethacrylate (EGDMA) or bis(2-methacryloyloxyethyl)disulfide (DSDMA)] allowed crosslinking of the polymer chains to generate shell-crosslinked nanocapsules. The reactive stabilizers used in this system contained hydrophilic portions based on poly(ethylene oxide) (PEO): one portion in which PEO formed the main polymer chain, and one in which PEO formed the side chains. The latter was produced by polymerizing a PEO-based methacrylate monomer (PEOMA) using an azide-containing ATRP initiator, with the azide intended for post-functionalization of the final nanocapsules. Chain extension of both these PEO-based hydrophilic macroinitiators with BMA generated the reactive stabilizers denoted PEO-*b*-PBMA-Cl ($M_n = 12{,}000$ g mol^{-1} and dispersity $Đ = 1.15$) and N_3-P(POEMA)-*b*-PBMA-Cl [43] (molar mass characteristics not mentioned). Subsequent miniemulsion polymerization of BMA and the aforementioned crosslinkers using AGET ATRP produced several types of multifunctional

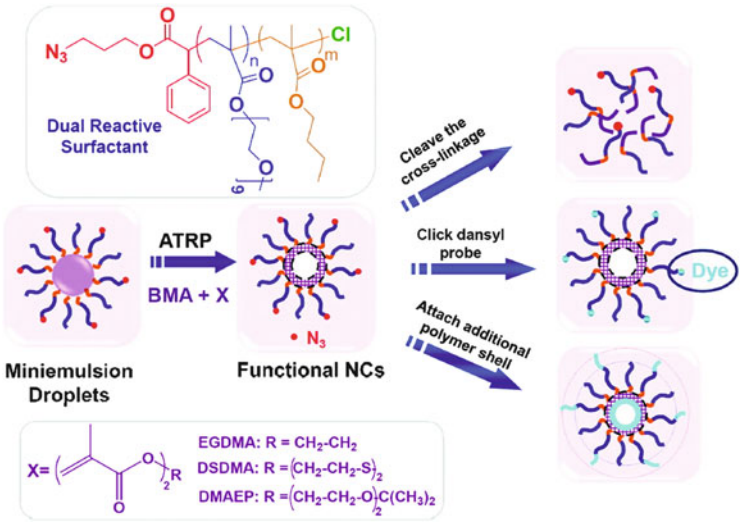

Fig. 1 Preparation of polymeric nanocapsules in miniemulsion using AGET ATRP and a mixture of dual and monofunctional reactive surfactants. Reproduced from [43] with permission from the American Chemical Society

capsules, including degradable nanocapsules to which probes or other polymers could be clicked, courtesy of their azide functionalities (Fig. 1).

3.2 Inverse Miniemulsion

The success of the RAFT-confined interfacial miniemulsion polymerizations described in the previous section was transposed to inverse miniemulsions with the aim of expanding the range of nanocapsules that could be synthesized. Lu et al. were the first in this pursuit, designing thermosensitive nanocapsules using a PEO-SC(=S)S-$C_{12}H_{25}$ trithiocarbonate as controlling agent [44]. *N*-Isopropylacrylamide (NIPAM) as hydrophilic monomer was mixed with water as templating liquid, PEO-SC(=S)S-$C_{12}H_{25}$ as reactive stabilizer, VA044 as initiator, and Na_2SO_4 as co-stabilizer. With the help of a nonionic commercial surfactant (B246SF from Uniquema), this solution formed a stable miniemulsion in cyclohexane, which was polymerized to form nanocapsules. Molar mass characterization of the polymer chains constituting these capsules confirmed successful chain extension of PEO-SC(=S)S-$C_{12}H_{25}$ with NIPAM under RAFT control. The same experiment was also conducted in the absence of PEO-SC(=S)S-$C_{12}H_{25}$. Transmission electron microscopy (TEM) of the nano-objects produced in the two experiments showed that only the PEO-SC(=S)S-$C_{12}H_{25}$ system induced interfacial miniemulsion polymerization to produce nanocapsules (Fig. 2). Dynamic light

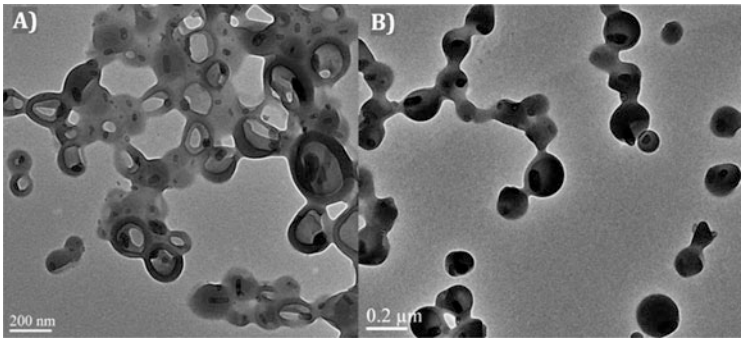

Fig. 2 TEM images of the latex obtained after (**a**) RAFT interfacial inverse miniemulsion polymerization of NIPAM and (**b**) free radical inverse miniemulsion polymerization of NIPAM. Reproduced from [44] with permission from the American Chemical Society

scattering (DLS) measurements performed at temperatures below and above the lower critical solution temperature of poly(*N*-isopropylacrylamide) (PNIPAM) demonstrated the thermosensitivity of the nanocapsules.

Wang et al. [45] demonstrated the versatility of the active stabilizer PDMAEMA-SC(=S)S-$C_{12}H_{25}$ used in their previous work [41] by employing it for the inverse miniemulsion polymerization of MAA and BAEDS (crosslinker) in cyclohexane to produce hydrophilic shell-crosslinked nanocapsules. Ammonium persulfate, MAA, and PDMAEMA-SC(=S)S-$C_{12}H_{25}$ dissolved in water were added to a continuous phase composed of cyclohexane, Span 80 as surfactant, and BAEDS as cleavable crosslinking comonomer. A stable miniemulsion was obtained after sonication, and polymerization generated shell-crosslinked nanocapsules. It is very interesting that successful crosslinking was achieved even when the crosslinker did not reside with the MAA monomer in the hydrophilic dispersed phase. This was made possible by the confinement of the PDMAEMA-SC (=S)S-$C_{12}H_{25}$ reactive stabilizers at the interface, which meant that the propagating species were generated very close to the interface and could therefore react with both MAA units from the water phase and crosslinker units from the continuous phase.

Utama et al. [46] recently proposed an alternative strategy for the preparation of nanocapsules using RAFT polymerization in an inverse miniemulsion system. In this approach, dispersed aqueous droplets (with RAFT-based active stabilizers at their interface) simply acted as templates, and chain extension (with hydrophobic monomers and crosslinkers contained in the surrounding continuous phase) yielded the nanocapsules. More specifically, methyl methacrylate (MMA) [46] or styrene [47], crosslinker (EGDMA or DVB, respectively), and initiator (AIBN) were dissolved in a toluene continuous phase. Water droplets containing sodium chloride as lipophobe were formed in these toluene solutions and stabilized with RAFT-synthesized poly[*N*-2-(hydroxypropyl methacrylamide)]-*block*-poly(methyl methacrylate) (PHPMA-*b*-PMMA) or PHPMA-*b*-PS block copolymers, where the PHPMA segment is hydrophilic. The subsequent polymerization was confined to

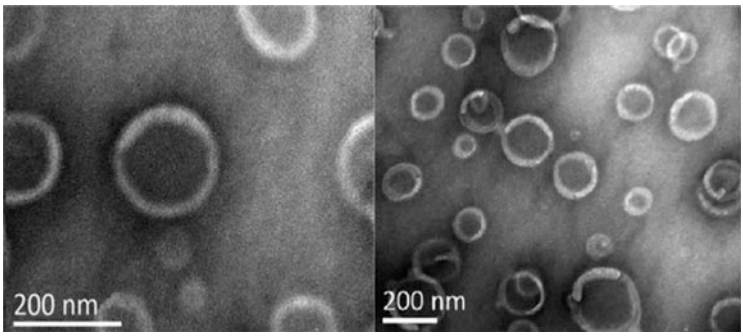

Fig. 3 TEM images of hollow nanoparticles synthesized via RAFT inverse miniemulsion periphery polymerization of MMA and EGDMA. Reproduced from [46] with permission from the Royal Society of Chemistry

the periphery of the water droplets, generating the nanocapsules. The styrene system (which attained 17% conversion in 24 h) was complicated by some coalescence and solid particle formation [47]. In the case of MMA [46, 47], conversion reached 51% in 7 h without any noticeable change in turbidity or viscosity, implying that the features of the original miniemulsion were preserved. Conversions higher than 51% led to an increase in viscosity associated with the onset of interparticle crosslinking. A good correlation between the starting water droplet size (170 nm) and the final capsules size (220 nm), observed by DLS, was as expected for a miniemulsion polymerization process. The desired shell-crosslinked hollow nanoparticles were clearly revealed by TEM (Fig. 3), confirming the effectiveness of the synthetic strategy. The successful encapsulation of bovine serum albumin in the aqueous core and its subsequent release were also demonstrated, with no detrimental denaturation of the protein occurring during the synthesis.

This novel strategy, named inverse miniemulsion periphery polymerization (IMEPP), based on previous works of Wang and colleagues [48], is a valuable one-pot alternative to the nanocapsule syntheses described earlier. One of its significant advantages is the location of the RAFT functionality at the periphery of the final objects, which can be taken advantage of to perform further functionalization. This was evaluated when the same authors targeted pH-responsive nanocapsules by IMEPP [49].

3.3 Vesicle-Templated Controlled Radical Polymerization: An Alternative to Miniemulsion

Colloidal templating is an alternative route for the synthesis of nanocapsules and one in which CRP also plays a pivotal role. The technique involves electrostatic deposition of charged RAFT polymers onto vesicles (which display the opposite

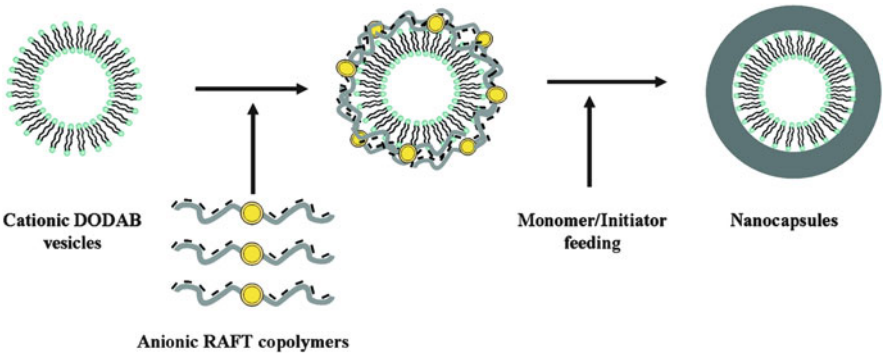

Fig. 4 Synthesis of vesicle-templated nanocapsules by aqueous starve–feed emulsion polymerization using RAFT copolymers as stabilizers. Reproduced from [50] with permission from the American Chemical Society

charge), followed by emulsion polymerization to generate a hydrophobic polymer shell (Fig. 4). This approach, first reported by Ali et al. [50], is conceptually identical to Hawkett's strategy for encapsulating charged inorganic particles [51], as described in Sect. 4.2.

Ali et al. [50] investigated the adsorption of P(AA-*co*-BA) obtained by dibenzyl trithiocarbonate (DBTTC)-mediated RAFT copolymerization onto cationic vesicles formed from the double-chain cationic surfactant dimethyldioctadecyl ammonium bromide (DODAB). To obtain large unilamellar vesicles, a membrane extrusion method was employed, giving vesicles of around 130 nm. Three negatively charged copolymers with varying AA/BA compositions (9:6, 10:3, 4:6) were then adsorbed onto the positively charged vesicles. A careful study using zeta potential measurements and size analyses showed that the adsorption can be controlled in the range above the charge inversion of the starting vesicles.

Encapsulations were performed by starve–feed emulsion polymerization of a MMA/BA monomer mixture (molar ratio of 10:1). Polymerization commenced at the vesicle surface, courtesy of the active RAFT end groups of the adsorbed polymer chains, generating a hydrophobic polymer shell. The strategy was extended to the design of pH-responsive polymeric capsules by incorporating a crosslinker (EGDMA, 3–10 mol%) into the MMA/*tert*-butyl acrylate (*t*-BA) monomer feed [52]. The high stability of the crosslinked nanocapsules was confirmed by surfactant lysis experiments using Triton X-100, a nonionic surfactant known for its excellent membrane destabilizing properties, using turbidity measurements. Increasing the crosslinker content in the monomer feed led to polymer segregation (as shown by TEM in Fig. 5d, left) rather than a uniform polymer shell. A high concentration of crosslinker increased the likelihood of forming highly branched polymer at a very early stage of the polymerization, restricting the diffusion of both the polymer chains and the monomer on the polymerization locus. Selective cleavage of the *tert*-butyl ester groups in the final nanocapsules using anhydrous trifluoroacetic acid (TFA) in dioxane converted the *t*-BA units to AA units,

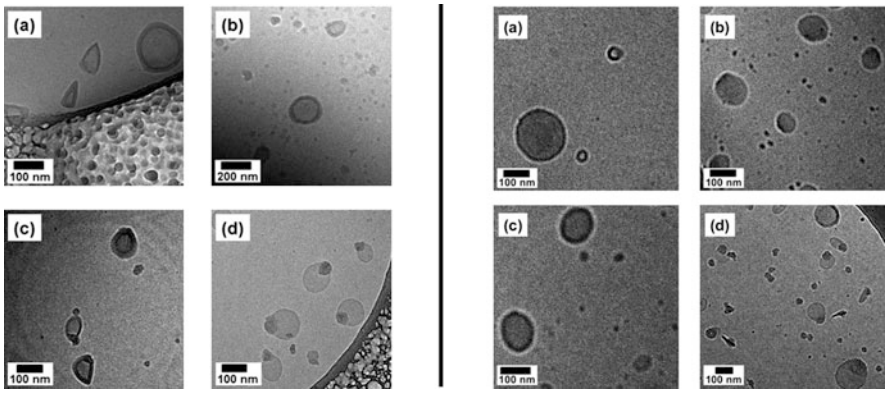

Fig. 5 Cryo-TEM micrographs of crosslinked nanocapsules. *Left*: Nanocapsules obtained by encapsulating DODAB vesicles (obtained by extrusion through 100 nm pore size filters) using RAFT copolymer P(BA_6-*co*-AA_9) and MMA:*t*-BA:EGDMA monomer at molar feed ratios of (**a**) 2:1:0.14, (**b**) 1:2:0.1, (**c**) 1:2:0.16, and (**d**) 1:2:0.33. *Right*: Crosslinked P(MMA-*co*-AA) nanocapsules obtained after acid hydrolysis of the same four crosslinked P(MMA-*co*-*t*-BA) nanocapsules shown on the *left*. Sample vitrification was performed at pH 7.2 in liquid ethane. Reproduced from [52] with permission from the Royal Society of Chemistry

affording pH-responsive particles with smoother surfaces than the pristine nanocapsules (as shown by TEM in Fig. 5, right). The pH responsiveness of these capsules was demonstrated by their swelling or contraction upon variation of the pH value.

4 Synthesis of Polymer/Inorganic Composite Particles

(Mini)emulsion polymerizations have naturally emerged as methods of choice for generating a broad range of composite organic/inorganic colloids that, depending on the field of application, can be either used directly as dispersions or further processed into films with improved mechanical, thermal, or barrier properties compared with the corresponding films without an inorganic component. In this regard, mastering the size, shape, and morphology of composite particles is key in controlling the final material properties. In that respect, CRP appears to be a very powerful tool for increasing the design range of such particles. Section 4.1 details the most recent works relying on the use of CRP in miniemulsion polymerization for the preparation of composite colloids; emulsion polymerization-based strategies are described in Sect. 4.2. In many cases, CRP enables access to morphologies that could not be attained using conventional free radical polymerization. CRP also brings the additional advantage of carrying out emulsion polymerization in the absence of a molecular surfactant that could have a detrimental effect on the properties of the final material.

4.1 Miniemulsion Polymerization Approaches

As mentioned in the "Introduction," the intrinsic features of miniemulsions can be taken advantage of for the incorporation of inorganic materials [14–17, 12, 18], the success of the reaction relying on good dispersibility of the inorganic particles in the monomer droplets before the beginning of the polymerization. Indeed, in most cases, these particles typically tend to be hydrophilic, whereas the monomer droplets (and later on the polymer particles) are hydrophobic, which prevents direct interaction and makes pretreatment of their surface with compatibilizers indispensible. CRP techniques can be efficient tools in the development of successful miniemulsion polymerization approaches for the synthesis of polymer/inorganic composite particles. Various strategies can be envisioned. The first strategy consists in the modification of the inorganic particle, either with inactive hydrophobization species or with molecules involved in the CRP process (i.e., immobilized monomers or controlling agents). These surface-active particles can then be used in bulk or solution polymerization to grow polymer chains from their surface. The resulting polymer-decorated inorganics can then be used in miniemulsion polymerization. A more straightforward method, however, consists in directly using the surface-active particles (if organosoluble) in the miniemulsion process. These different approaches have been explored using the main CRP techniques (i.e., NMP, ATRP and RAFT) and are detailed in the following sections, arranged according to the type of inorganic particle used.

4.1.1 Silica

NMP, (AGET) ATRP, and RAFT have all been used for the synthesis of silica-based composite latexes. Bailly et al. [53] were the first to report the use of CRP to grow PS chains from the surface of 80 nm silica particles previously modified by the adsorption of an alkoxyamine derived from *N*-*tert*-butyl-*N*-[1-diethylphosphono-(2,2-dimethylpropyldimethylpropyl)] nitroxide (SG1). The obtained PS-covered silica particles were then efficiently dispersed in styrene droplets to yield silica/PS core–shell particles after miniemulsion NMP. In a later experiment, Bombalski et al. successfully implemented AGET ATRP for the miniemulsion polymerization of BA droplets containing 20 nm silica particles modified by 1-(chlorodimethylsilyl)propyl 2-bromoisobutyrate [54]. Hereby, $CuBr_2$ and the amino ligand bis(2-pyridylmethyl)octadecylamine were first mixed with silica and BA to generate the Cu(II) complexes. After addition of Brij 98 (surfactant), HD (costabilizer), and water, the miniemulsion was generated by sonication. Ascorbic acid (reducing agent) was added to start the polymerization. A conversion of 70% was reached in 20 h, providing a stable latex composed of composite particles with diameters of approximately 220 nm, each one incorporating an average of 75 silica particles. Control of polymerization was satisfactory, with a relatively good agreement between theoretical and experimental molar

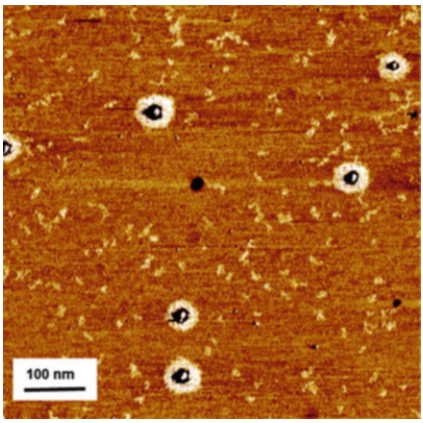

Fig. 6 AFM image of silica/PBA nanoparticles prepared by AGET ATRP in miniemulsion. The hybrid nanoparticles were collected by re-dispersing the dried miniemulsion samples in THF before subjecting the dispersion to AFM characterization. Reproduced from [54] with permission from the American Chemical Society

masses indicating high initiation efficiency. Atomic force microscopy (AFM) of the hybrid particles after drying and re-dispersing in THF showed formation of the expected silica/poly(*n*-butyl acrylate) (PBA) core–shell particles (Fig. 6). Compared with the analog bulk experiment, the miniemulsion process allowed the preparation of such hybrid materials with a higher yield (because of a higher conversion) and a higher polymerization rate, without the macroscopic gelation associated with interparticle coupling that is usually observed in bulk polymerizations.

In both the NMP and the AGET ATRP studies, CRP was used to grow polymer chains from the silica surface and thus to provide good compatibility of these modified particles with the monomer phase for subsequent miniemulsion polymerization. In the next example describing the formation of silica/PMMA composite particles by RAFT-mediated miniemulsion polymerization [55], the pursued strategy was different. After modification of the silica surface with a polymerizable silane (3-methacryloxypropyl trimethoxysilane), MMA miniemulsion polymerization was performed in the presence of an organosoluble trithiocarbonate RAFT agent, namely 2-{[(*tert*-butylsulfanyl)carbonothioyl]sulfanyl} propanoic acid. The good agreement between theoretical and experimental molar masses and the low dispersities indicated good control of the polymerization. Increasing the silica content led to decreased monomer conversions (and consequently to lower molar masses). Despite thermal analyses indicating the positive effects of silica on the thermal stability of the formed nanocomposites, TEM images did not clearly show the final particle morphologies. Not even the presence of silica particles could be proven with this method. The very same study was then performed without preceding surface modification of the silica [56]. The overall conclusions were basically the same. The authors mentioned in this second work that the silica nanoparticles were possibly located at the PMMA particle–water interface, but without providing clear explanations. In both studies, there was no comment on the initial state of the systems that could clarify whether the polymerization actually proceeded according to a miniemulsion process.

4.1.2 Montmorillonite

Following an NMP-based approach similar to that used by Bailly et al. for silica [53], Mičušík et al. [57] prepared montmorillonite (MMT)/P(BA-*co*-MMA) composite latexes (Fig. 7). A cationic macroalkoxyamine based on vinylbenzyl trimethylammonium chloride (VBTMACl), MMA, and styrene [P(VBTMACl-*co*-MMA_7-*co*-S_4); N^+M in Fig. 7] was prepared using the BlocBuilder alkoxyamine, and then exchanged with the sodium cations of MMT ($C–N^+M$ in Fig. 7). Copolymerization of BA and MMA was then performed in bulk in the presence of the modified MMT with a limited control over the molar masses, nevertheless leading to the formation of exfoliated clay sheets decorated with polymer chains. This polymer/clay composite was then dispersed in BA/MMA droplets using stearyl acrylate as a hydrophobe and Dowfax 2A1 (alkyldiphenyloxide disulfonate) as a surfactant. Miniemulsion polymerization was then initiated by addition of KPS, yielding a stable latex able to form nanocomposite films that incorporated exfoliated clay platelets and showed improved adhesive properties compared with the neat polymer. In comparison, the use of MMT that had been only modified by the cationic macroalkoxyamine and without prepolymerization did not lead to a stable latex, showing the crucial role of the grafted P(BA-*co*-MMA) chains in ensuring a good dispersibility and compatibility of MMT with the polymer matrix.

Khezri et al. [58] used AGET ATRP to prepare P(S-*co*-MMA)/MMT nanocomposites. The commercial organomodified MMT was dispersed in monomer droplets with a diameter of approximately 200 nm. The system also contained

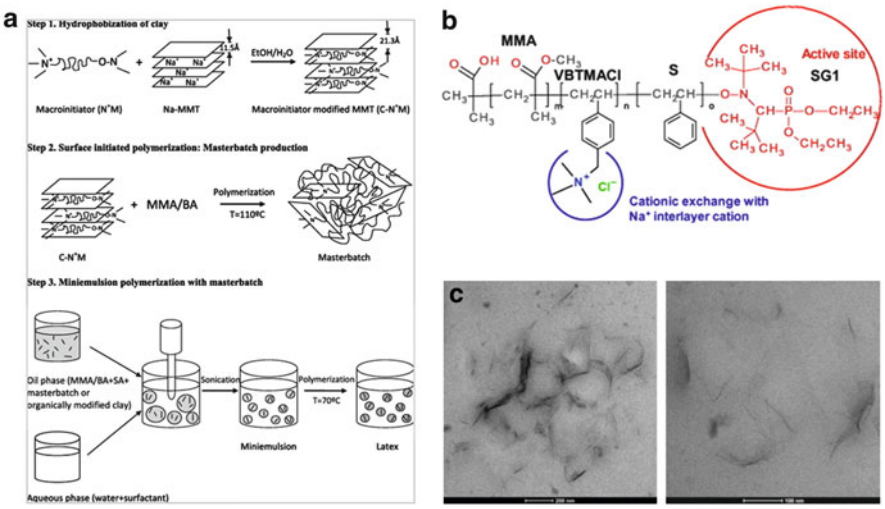

Fig. 7 Synthesis of MMT/P(BA-*co*-MMA) composite latexes. (**a**) Synthetic procedure followed to produce waterborne acrylic/clay nanocomposites. (**b**) Chemical structure of the macroinitiator containing a quaternary ammonium salt (N^+M) used to modify Na–MMT. (**c**) TEM images of a film prepared with P(BA-*co*-MMA)/$C–N^+M$ masterbatch and KPS. Reproduced from [57] with permission from Elsevier

ethyl α-bromoisobutyrate (EBiB), the ligand 4,4′-dinonyl-2,2′-bipyridine (dNbPy), $CuBr_2$, HD, and CTAB as the stabilizer (less temperature-sensitive than the commonly used Brij 98). The polymerization was started by addition of ascorbic acid and led to the formation of polymer/MMT composite particles. Increasing the amount of clay (from 0 to 2 wt%) induced a decrease in both conversion and molar masses and yielded broader molar mass distributions. According to the authors, this could be ascribed to the partitioning of $CuBr_2$ (deactivator) between the different phases and a high concentration of ascorbic acid. In addition, the clay platelets could also hinder diffusion of the monomer, initiator, and metal complex, and promote irreversible chain transfer and termination reactions. Nevertheless, the presence of clay improved the thermal stability of the nanocomposites. Exfoliated platelets were found well dispersed in the polymer matrix. In a very similar study conducted by the same authors using reverse ATRP [59], comparable nanocomposites were obtained. The strategy was later repeated for styrene with reverse ATRP [60], and for MMA with SR&NI ATRP [61]. The same team also prepared P(S-*co*-BA)/MMT composite latexes by both miniemulsion AGET ATRP [62] and miniemulsion reverse ATRP [63]. On the whole, they noticed the same effect of clay content on conversion, molar masses, and thermal stability, even if the clay sheets were in some cases only partially delaminated as a result of the lower molar masses of the polymer chains [62]. A deeper kinetic and mechanistic investigation of this AGET ATRP system was later reported [64]. It is worth noting that, in all these works, ATRP was used to grow polymer chains in the vicinity of the MMT platelets but not from their surface, because the platelets did not carry any functionalities that could participate in the ATRP process.

The first report on the use of the RAFT technique for the preparation of composite latexes in a miniemulsion system can be attributed to Samakande et al., who described the encapsulation of MMT clay inside PS [65] or P(S-*co*-BA) [66] particles. Similar observations were made for both systems, in which MMT platelets modified with anchored cationic (ammonium bromide-type) RAFT agents (dithiobenzoate or trithiocarbonate, respectively) were readily dispersed in the monomer droplets. SDS and HD were used to stabilize the system and AIBN used as initiator. Monomer conversion decreased with increasing clay loading. As expected, as a result of the compartmentalization effect, the conversion was systematically higher than that obtained in analogous bulk experiments [67]. Although control over the molar masses of the produced polymers was reasonably good in both systems, the trithiocarbonate-based system provided better polymerization control. Molar masses and dispersities both decreased as the amount of clay increased, as a result of the higher concentration of RAFT agent. The discrepancy between theoretical and experimental molar masses was attributed to the lower controlling ability of anchored RAFT agents compared with RAFT agents in solution. The sizes of the droplets were not reported, but the diameter of the final clay-loaded particles increased with the amount of clay. The platelets could only be visualized with conventional TEM after being embedded in an epoxy resin. Small-angle X-ray scattering (SAXS) analyses also confirmed their presence. The platelets showed a partially exfoliated morphology that evolved into an intercalated

morphology as the clay loading increased, in accordance with the simultaneously growing molar masses of the polymer chains. The thermo-mechanical properties of the resulting nanocomposites depended on the molar masses and dispersities of the polymer chains, the clay loading, and the platelet morphology (i.e., partially exfoliated versus intercalated).

4.1.3 Quantum Dots

A system similar to that developed for silica by Bombalski et al. [54] (see above) was used by Esteves et al. [68] to form cadmium sulfide (CdS) quantum dot (QD)/PBA composite particles by miniemulsion AGET ATRP (Fig. 8, left). The QDs were first functionalized with trialkylphosphine ligand molecules carrying chlorine-based ATRP initiator groups. This step slightly affected the size and, consequently, the optical properties of the QDs. After 24 h of miniemulsion polymerization, a stable latex was obtained. The size of the resulting latex particles was not mentioned, but the diameter of the core–shell QD/PBA particles observed by AFM after dispersion in THF was estimated to be close to 100 nm. Good control over the growth of the PBA chains was achieved. This approach allowed preservation of the optical properties of the QDs by avoiding the use of conventional radical initiators,

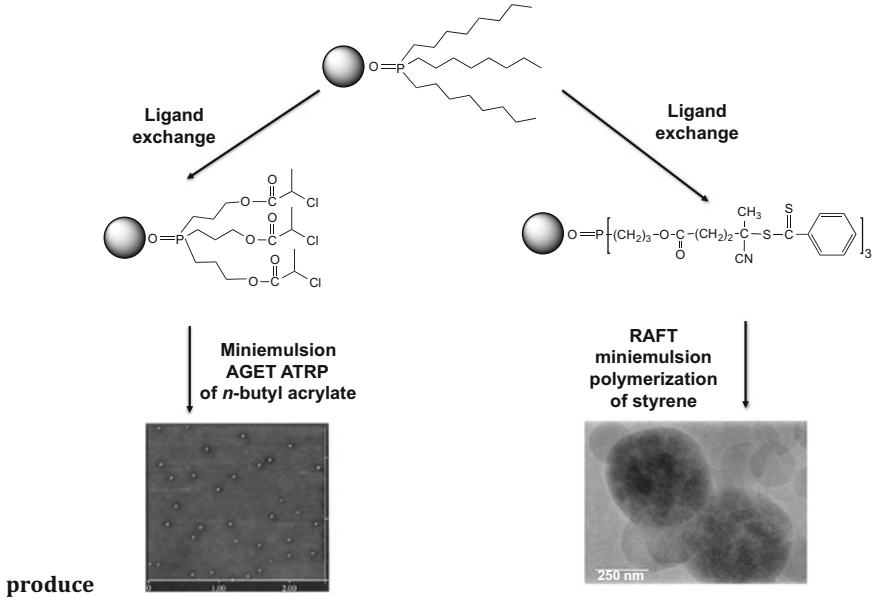

Fig. 8 Synthesis of QD/polymer composite latexes. Synthetic procedures followed to produce either (*left*) QD/PBA latexes through AGET ATRP in miniemulsion [68] (tapping-mode AFM image, 2.5 × 2.5 μm) or (*right*) QD/PS latexes through RAFT miniemulsion polymerization [69] (TEM image). Reproduced and adapted from [68] and from [69] with permission from Wiley-VCH

which can lead to extensive degradation of QDs. Following on from this study, Esteves et al. [69] prepared CdS or CdSe QD/PS nanocomposites using the RAFT technique (Fig. 8, right). The QD surface was first functionalized with a trialkylphosphine oxide bearing the RAFT-active 4-cyano-4-(thio-benzoylsulfanyl) pentanoic acid moieties. The resulting hydrophobic nanoparticles could be well dispersed in styrene. Miniemulsion polymerization resulted in the formation of QD-tagged PS particles (along with an unquantified, but minor fraction of free PS particles). The QDs, encapsulated in the PS particles as small clusters, preserved their optical properties (except for a slight blue shift of the onset of the absorption signal), proving that the integrity of the nanocrystals had been maintained.

4.1.4 Magnetic Nanoparticles

Despite the widespread interest in the synthesis of magnetic polymer latexes, Chakraborty et al. have recently been the first to report a RAFT-mediated miniemulsion polymerization approach [70] (Fig. 9) involving magnetic nanoparticles (MNPs) of iron oxide. In addition, their study was also the first work describing the use of amphiphilic ionic liquids (1-*N*-alkyl-3-methylimidazolium bromide-type) as surfactants. In spite of the known incompatibility of oleic acid (OA) and PS, OA-coated MNPs were used in this study. The employment of these MNPs in a conventional miniemulsion polymerization systematically led to phase separation between PS and the MNPs inside the particles (Janus-type morphology, Fig. 9b), mostly accompanied by low stability of the resulting latexes and formation of empty PS particles. Capitalizing on the known affinity of carboxylic acid groups for the surface of MNPs, another series of miniemulsion experiments was then undertaken using an organosoluble symmetrical trithiocarbonate RAFT agent that carried carboxylic acid groups, 2,2′-[carbonothiobis(thio)]bis (2-methylpropionic acid). Fine tuning of the molar ratio of AIBN and the RAFT agent and varying the final conversion allowed the formation of relatively stable PS particles incorporating up to 27 wt% (with respect to polymer) of MNPs, which imparted their special magnetic properties to the composite products (saturation magnetization M_s of 16.6 emu g^{-1} for the sample with the highest value). The molar ratio of AIBN and RAFT agent also strongly impacted the final particle morphology, which was either a homogeneous distribution of the MNPs within the PS particles (Fig. 9c) or a Janus-type morphology (Fig. 9d). In all cases, no empty PS particles were found. The synthesis of magnetic composite particles was also recently reported by Gu et al. [71]. Taking advantage of their recent Fe(0)-mediated RAFT technique [72], crosslinked P(MMA-*co*-EGDMA) particles incorporating Fe (0) nanoparticles were obtained. The magnetic properties of the final particles were, however, only very weak (M_s lower than 0.1 emu g^{-1}).

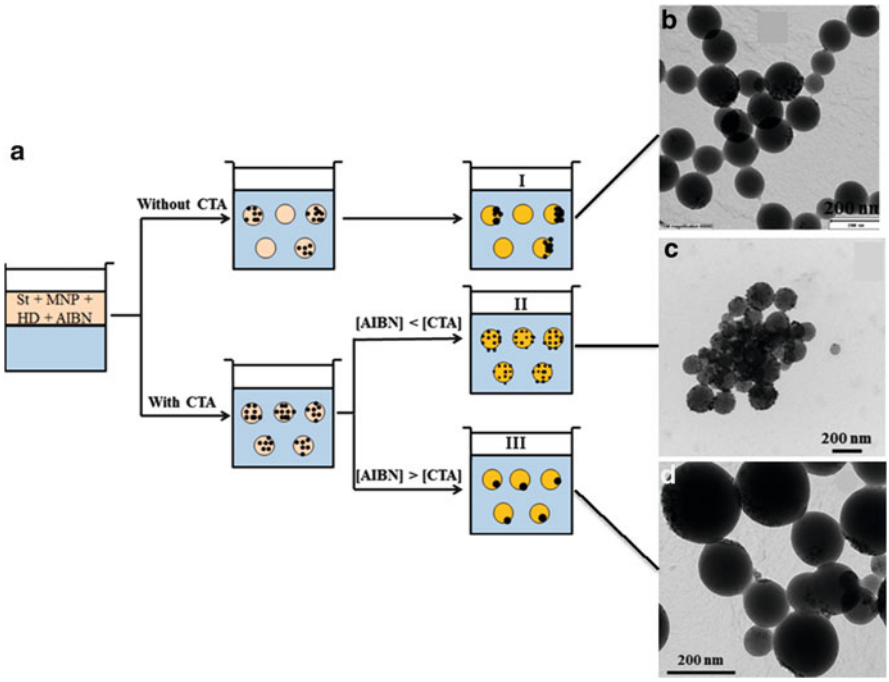

Fig. 9 Synthesis of PS particles containing magnetic iron oxide nanoparticles via polymerization in a miniemulsion system stabilized by amphiphilic ionic liquids. (**a**) Different accessible morphologies and the corresponding synthesis pathways. (**b**) TEM image of the particles formed using conventional miniemulsion polymerization. (**c**) TEM image of the particles obtained by RAFT-mediated miniemulsion polymerization, showing homogeneous distribution of the MNPs within the PS particles. (**d**) TEM image of the particles obtained by RAFT-mediated miniemulsion polymerization with a significantly higher amount of initiator, leading to an anisotropic distribution of MNPs (Janus-like morphology). Reproduced from [70] with permission from the American Chemical Society

4.1.5 Graphite Oxide

In another study that should be included here, PS particles containing graphite oxide (GO) sheets were prepared via RAFT-mediated miniemulsion polymerization [73]. As a matter of fact, GO is technically not an inorganic compound, but its encapsulation involves concepts similar to those described above. The carboxyl-group-bearing RAFT agent dodecyl isobutyric acid trithiocarbonate (DIBTC) was first attached to the GO sheets via the esterification reaction to their hydroxyl groups. To enable dispersion of the GO-DIBTC nanoplatelets in styrene and the formation of stable miniemulsions, several experimental steps were required: (i) dispersion of DIBTC-decorated GO in water under sonication; (ii) addition of styrene, AIBN, and HD followed by stirring and sonication of the mixture; and (iii) addition of an aqueous solution of sodium dodecylbenzene sulfonate (SDBS) followed by stirring and sonication of the mixture. Different miniemulsion

polymerizations were then performed using various amounts of DIBTC-covered GO (up to 7 wt% per monomer). Stable latexes were obtained, the particle diameter increasing with the GO content from 125 to 160 nm (as measured by DLS). As expected, an increase in the grafting density of DIBTC on the GO (i.e., an increasing RAFT agent concentration) led to lower molar masses of the resulting polymer chains, with narrower distributions. The GO sheets could not be visualized directly via TEM of the obtained particles but could be identified after embedding the dried latex in an epoxy resin. Most of the graphite nanoplatelets were of exfoliated morphology, with a few intercalated nanosheets. This structure was additionally confirmed by X-ray diffraction measurements. In the final analyses, the GO/PS nanocomposites showed enhanced mechanical properties and thermal stability compared with neat PS.

4.2 Emulsion Polymerization Approaches

Emulsion polymerization has several advantages over miniemulsion polymerization. In particular, it requires neither any energy-consuming high shear devices to create the miniemulsion droplets nor the presence of additional additives such as hydrophobic costabilizers. Among the most important features of emulsion polymerization is the ability to control the particle morphology (e.g., formation of core–shell particles and other equilibrium morphologies) by successive addition of different monomers in the presence of preformed organic or inorganic particles. In the last 20 years, there has been an increasing interest in the synthesis of polymeric/inorganic materials by emulsion polymerization and the reader is referred to a number of recent comprehensive reviews [5–7].

As mentioned in the "Introduction," physical or chemical methods can be employed to encapsulate inorganic particles in emulsion polymerization. Although the chemical approach has been successful in a number of cases, it frequently entails inherent experimental problems such as loss of colloidal stability, formation of secondary nucleated particles devoid of inorganic component, incomplete encapsulation of the inorganic particles accompanied by the formation of hemispherical or other anisotropic structures, and lack of reproducibility. In addition, this strategy often requires time-consuming chemical modification of the particle surfaces, which does not always lead to the desired morphology. With recent developments in the field of CRP techniques in aqueous media, new approaches for obtaining hybrid latexes with different particle morphologies have been made feasible, opening up new and promising pathways for the synthesis of colloidal nanocomposites. An overview of these methods is given in the following sections. It should be noted that, of the various CRP techniques, RAFT-mediated processes have been almost exclusively reported until now, with the exception of one example involving NMP.

4.2.1 MacroRAFT-Assisted Encapsulating Emulsion Polymerization

In the last two decades, CRP techniques have been extensively used to generate a large variety of organic/inorganic hybrid morphologies such as Janus, core–corona, and core–shell nanoparticles as well as several types of anisotropic particles. This could be achieved using grafting-from, grafting-to, or self-assembly techniques [74–78]. These techniques usually involve surface modification (by covalent linking or via physisorption) of preformed inorganic particles with copolymers (synthesized by CRP) in organic solvents, and subsequent solvent evaporation or solvent displacement to recover the hybrid particles prior to their application (for which water-based systems are often needed). However, since January 2000, the use of volatile organic compounds has been severely restricted by law and coating formulators are progressively switching from solvent-borne processes or products to safer waterborne alternatives. In parallel, striking progress has been made in the development of CRP in dispersed systems and an extensive range of monomers can now be polymerized using CRP methods in aqueous systems. Controlled and well-defined polymer particles can thus be obtained [79]. Taking advantage of these advances, the implementation of CRP in emulsion polymerization has been developed as an innovative route for the generation of a variety of organic/inorganic composite particles [80]. Among them, core–shell particles where the core is an inorganic particle and the shell is composed of a polymer have attracted particular attention [81]. The shell can protect the core from extraneous physical or chemical changes and can enhance the compatibility between the inorganic filler and the polymer matrix. Alternatively, the core could be an organic pigment. Core–shell particles are currently of interest for a wide variety of applications, including emulsion paints, optics, and various biological applications.

The first reports of macroRAFT-assisted encapsulating emulsion polymerization (REEP) were published almost simultaneously by Nguyen et al. [51] and Daigle et al. [82]. These authors developed a simple and versatile method allowing the efficient encapsulation of both organic and inorganic particulate materials via free-radical polymerization in aqueous dispersed media. In short, the method uses living amphiphilic random copolymers, which can adsorb on the core particles and lead the emulsion polymerization to occur at their surface (as illustrated schematically in Fig. 10). These copolymers are synthesized via RAFT polymerization and thus possess a RAFT functionality on one extremity, which is able to be reactivated for the polymerization of hydrophobic monomers. In addition, the relatively high hydrophilicity of the macroRAFT agent provides stability for the aqueous dispersion of nanoparticles before the polymerization, and contributes to the stability of the final encapsulated particles. The overall process involves two steps: (i) macroRAFT agent adsorption on the surface of the inorganic particles in aqueous suspensions, and (ii) emulsion polymerization of hydrophobic monomers in batch or under starve–feed conditions, whereby the macroRAFT-functionalized particles act as seeds for the nucleation process. The presence of the living copolymers on the particle surface facilitates rapid transfer of hydrophobic polymer

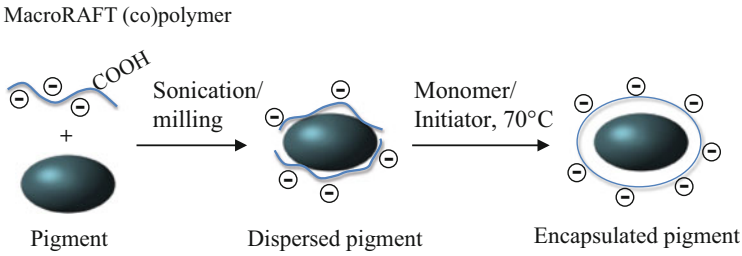

Fig. 10 MacroRAFT-assisted encapsulating emulsion polymerization (REEP) technique. Reproduced from [51] with permission from the American Chemical Society

growth between the chains, allowing homogeneous growth over the entire particle surface. The orderly extension of each polymer chain results in an even build-up of the polymer, which forms a layer surrounding the particles and leads to their encapsulation.

Nguyen et al. [51] first applied this strategy to encapsulate both hydrophilic (zirconia- and alumina-coated titanium dioxide) and hydrophobic (phthalocyanine blue) pigments with poly(methyl methacrylate-*co*-*n*-butyl acrylate), P(MMA-*co*-BA). The particulate materials were first mixed with short-chain random copolymers composed of AA and BA (M_n lower than 2,000 g mol^{-1}), which readily adsorbed on their surface. Encapsulation polymerization was then performed at 70°C by slowly feeding the dispersed system with the hydrophobic monomers using 4,4′-azobis(4-cyanopentanoic acid) (ACPA) as a water-soluble initiator. The pH value and the copolymer composition were optimized to promote macroRAFT adsorption: the higher the hydrophobicity of the macroRAFT agent and the lower the pH value, the better the interaction with the particle surface. At the same time, the BA units were incorporated into the polymer chains to increase the affinity of the hydrophobic monomer molecules for the particle environment, which was a key requirement for efficient encapsulation. Lastly, the random nature of the copolymer prevented the macroRAFT (co)polymers from self-assembling into micelles, which would have inevitably led to the unwanted formation of new particles via micellar nucleation. As shown in Fig. 11, a very uniform encapsulation was achieved for both substrates. As expected, there was only a minor fraction of free secondary particles and the entire amount of pigment introduced was encapsulated.

Unexpectedly, careful examination of the events taking place in water revealed that despite the presence of a high initial amount of free non-adsorbing macroRAFT agent and a constant supply of monomer and free radicals, only a small fraction of the macroRAFT agent (∼19 %) participated in the chain extension process. In other words, the macroRAFT agent could only add hydrophobic monomers when adsorbed onto the surface of the pigment. Growth of the labile macroRAFT copolymer remaining in the aqueous phase was comparatively less favored. SEC analyses performed on the polymer chains formed during the encapsulation reaction, after selective dissolution of the polymer in a mixture of THF and TFA to remove the inorganic part, showed good control of the polymerization (*Đ* ranging

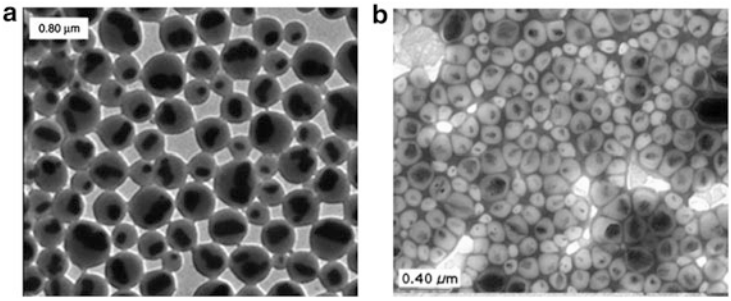

Fig. 11 TEM images of encapsulated (**a**) TiO_2 and (**b**) phthalocyanine pigment particles with P(MMA-*co*-BA) shell using P(AA_{10}-*co*-BA_5) and P(AA_5-*co*-BA_5) macroRAFT agents as dispersants, respectively. Reprinted from [51] with permission from the American Chemical Society

from 1.2 to 1.7 and good agreement between theoretical and experimental M_n), with better control being attained at low conversions. As shown in [82], the formation of very well-defined diblock copolymers is, in many cases. not mandatory for successful encapsulation. It is therefore clear that the key feature of this technique is not necessarily the use of CRP as a tool to precisely control the molar masses of the produced polymers, but instead the main merit of the CRP process is the fact that the living polymer chains can be reactivated during the emulsion polymerization.

In the same period, Daigle et al. reported a similar approach for encapsulation of a range of inorganic compounds such as oxides ($BaTiO_3$, TiO_2 [rutile and anatase], Al_2O_3, CuO, ZrO_2), metals (Zn, Mo), and nitrides (Si_3N_4) employing SDS as an additional surfactant [82]. Unlike Nguyen and coworkers, the authors used a macroRAFT agent composed purely of AA units. In addition, the monomer (styrene and/or BA) was introduced at the beginning of the reaction while a solution of initiator was fed over 4 h. Although, as stated above, low hydrophobicity of the macroRAFT agent is unfavorable according to Nguyen et al., TEM analysis showed the successful formation of a thin polymer shell around the inorganic particles, with an absence of aggregation. Concurrently, polymer particles devoid of inorganic cores were also formed. This new population of particles probably originated from the self-assembly of block copolymers formed in the water phase via chain extension of the free macroRAFT agent and secondary nucleation. The success of encapsulation was attributed to the large amount of inorganic particles (20 wt%) and to the strong macroRAFT adsorption, leading to very slow exchange between the adsorbed and free polymer chains, enabling the efficient growth of polymer chains at the particle surface. Indeed, while the adsorbed polymer is growing, it becomes more and more hydrophobic, which favors shell formation. In contrast, the free polymer becomes amphiphilic and eventually segregates into a second population of particles. According to the authors, however, macroRAFT agents displaying only weak adsorption also become more and more hydrophobic upon chain extension, and the situation is therefore analogous to the case of strong adsorption. In contrast to the results of Nguyen et al. [51], SEC analyses of the soluble polymer in THF indicated only a poor level of control, which supports the

idea that the key role of the RAFT agent is its provision of many active sites for re-initiation of chain growth, with its ability to control the polymerization being less important.

The REEP strategy was further expanded to the encapsulation of cadmium sulfide (CdS) [83] and lead sulfide (PbS) [84] QDs, still in the presence of SDS. The CdS particles were first dispersed in an aqueous solution of PAA or P(AA-*co*-BA) macroRAFT agents with the help of ultrasound at pH 6 and mixed with styrene and surfactant. The polymerization was then conducted by slowly feeding an initiator solution at 80°C over 4 h and stirring for another 2 h. In accordance with the earlier work of Nguyen et al. [51], successful encapsulation was only achieved when the random macroRAFT copolymer was employed. However, in this case, the composite particles contained a large number of aggregated QDs instead of a single-particle core. Because the CdS particles had not aggregated after macroRAFT adsorption, this was attributed to the small particle size and the large number of encapsulated QDs formed in the early stages of the polymerization. These core–shell particles would be colloidally unstable and therefore agglomerate to larger particles. PbS particles were encapsulated in a similar manner. Depending on monomer, dispersant, and PbS concentration, particles containing a single core (for low PbS concentrations) or multiple cores (for higher PbS concentrations) were successfully obtained.

With the aim of forming anisotropic polymer/inorganic composite latex particles and controlling the orientation of the inorganic filler within the polymer film formed after deposition, Ali et al. used Gibbsite clay sheets as a model for platelet-like colloidal substrates [85]. Gibbsite platelets were coated with P(AA-*co*-BA) macroRAFT agents similar to those used by Nguyen and colleagues by dropwise addition of the Gibbsite suspension to the macroRAFT solution at pH 7 until charge inversion was reached. For the polymerization experiments, the amount of macroRAFT agent was then kept at almost twice the isoelectric-point concentration to ensure that a sufficient amount of RAFT copolymer was present in the aqueous phase to adsorb onto the growing surface during encapsulation, providing the required stabilization. As mentioned above for the earlier work of Nguyen et al. [51], the random nature of the copolymers prevented them from self-assembling in the aqueous phase at the beginning of the polymerization, reducing the probability of secondary nucleation. However, the formation of a second population of empty particles could not be fully avoided. The authors noticed that raising the hydrophobicity of the macroRAFT copolymer by increasing the number of BA units resulted in appreciable growth of polymer particles in the aqueous phase, arguably as a result of the reduced solubility of the RAFT polymers, which are more likely to cause secondary nucleation. On the contrary, a decreasing BA content indeed resulted in more hydrophilic macroRAFT agents and a lower fraction of secondary particles. However, the macroRAFT agent also exerts a lower stabilizing effect on the Gibbsite particles, inevitably leading to a higher degree of nanoparticle aggregation. The best compromise was found using a P(AA_{10}-*co*-BA_5) macroRAFT agent. It is also worth mentioning the tremendous impact of the monomer feed composition. Although core–shell particles with individual platelets

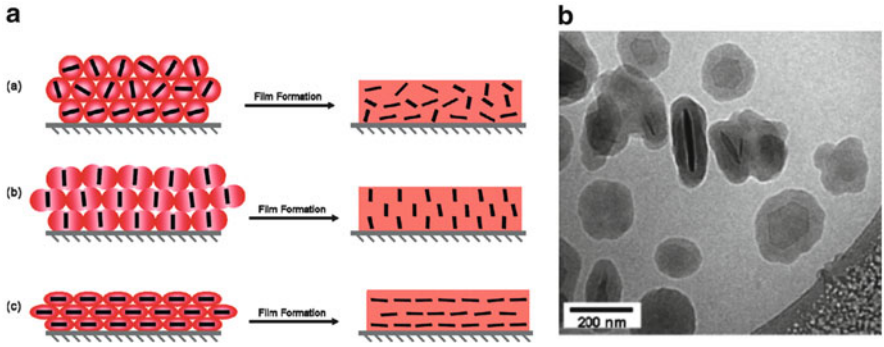

Fig. 12 (**a**) Expected orientation of the Gibbsite platelets in the formed films for different composite latex morphologies, (**b**) Cryo-TEM image of the encapsulated Gibbsite particles with a P(MMA-*co*-BA) (MMA:BA = 10:1 weight ratio) shell using a P(AA_5-*co*-BA_{10}) macroRAFT agent. Reproduced from [85] with permission from the American Chemical Society

evenly surrounded by a thin polymer shell were successfully obtained using a 10:1 (in weight) feed of MMA and BA (Fig. 12b), the use of a MMA to BA weight ratio of 7:3 led to a loss of control over the platelet encapsulation, and additional armored morphologies were obtained as a consequence. This morphological trend was attributed to the increased hydrophobicity and higher chain mobility of the polymer shell, possibly allowing migration of the inorganic particles to the polymer–water interface to minimize interfacial energy. An even encapsulation is, however, crucial for the envisaged application of the formation of polymer films incorporating oriented platelets after deposition of the composite latex (Fig. 12a).

A similar approach was used by the same group to encapsulate MMT platelets using cationic RAFT copolymers composed of randomly distributed BA and quaternized units of 2-dimethylaminoethyl methacrylate (DMAEMA) and a MMA:BA (10:1 weight ratio) monomer feed [86]. Despite the successful formation of flat, cornflake-like composite particles, Brownian motion prevented them from adopting a specific orientation after deposition on a substrate.

Inspired by the seminal work of Nguyen and coworkers, our group also reported the successful encapsulation of cerium dioxide (CeO_2) particles using the REEP technique [87]. CeO_2 possesses valuable properties such as catalytic oxidation activity, UV light absorption, and high scratch resistance that make it an attractive candidate for coating applications. As a result of the well-known affinity of carboxylic acid groups for CeO_2, a statistical macroRAFT copolymer composed of 11 AA and 11 BA units [P(AA_{11}-*co*-BA_{11}); $M_n = 25{,}000$ g mol^{-1}, $Đ = 1.08$] was used. Adsorption was conducted by slowly adding the macroRAFT solution (pH 6.5) to the CeO_2 suspension (pH ~ 2), which resulted in massive precipitation of the CeO_2 particles due to screening of the surface charges that originally ensured the stability of the sol. Increasing the pH value to 8 in order to deprotonate the AA units allowed redispersion of the CeO_2 in the form of finitely sized clusters with diameters of about 100 nm. Encapsulation was finally performed by slowly feeding

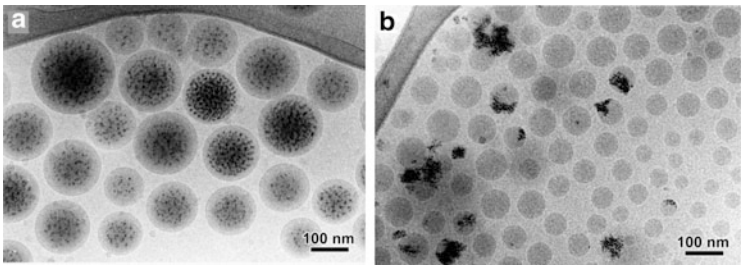

Fig. 13 Cryo-TEM images of composite latex particles obtained after emulsion polymerization of (**a**) MMA:BA (50:50 weight ratio) and (**b**) BA in the presence of CeO_2 nanoclusters coated with a P(AA_{11}-*co*-BA_{11}) macroRAFT agent. Reproduced from [87] with permission from the Royal Society of Chemistry

a mixture of MMA and BA at 70°C using ACPA as water-soluble initiator. Cryo-TEM showed the successful formation of a polymer shell around the CeO_2 nanoclusters, resulting in complete encapsulation without any appreciable free polymer particles (Fig. 13a). Similar to the work of Ali and coworkers, no encapsulation was observed when BA replaced the MMA/BA mixture. This was attributed to the higher surface energy and the lower T_g of the polymer shell driving the more hydrophilic CeO_2 nanoclusters towards the polymer–water interface (Fig. 13b).

The works of Zhong et al. [88] and Nguyen et al. [89] on the encapsulation of carbon nanotubes using the REEP technique are also noteworthy. Zhong et al. used various types of macroRAFT agents [i.e., PAA_{40}, P(AA_{10}-*co*-BA_5), and P(AA_3-*co*-S_3)], which all enabled successful encapsulation of single-wall and multiwall carbon nanotubes upon chain extension with MMA or styrene, despite their poor affinity for the nanotube surface. The carbon nanotubes were coated with a thin and regular polymer shell, forming kinetically trapped morphologies as long as the monomer feed rate was maintained sufficiently low to avoid formation of phase-separated domains. To increase the adsorption efficiency of the negatively charged macroRAFT agent, Nguyen and coworkers introduced positive groups on the nanotube surface using poly(allylamine hydrochloride) (PAH) as cationic polyelectrolyte. Subsequent adsorption of poly(4-vinylbenzenesulfonic acid-*co*-BA) RAFT copolymer on the surface of the cationic nanotubes and chain extension with MMA/BA (10:1 weight ratio) resulted in a uniform polymer coating with complete coverage (including the tips), provided that the amount of PAH introduced in the first step was sufficiently large. Varying the amount of monomer introduced during the reaction enabled control of the shell thickness from a few nanometers to several tens of nanometers.

The potential of the REEP technique goes beyond the encapsulation of organic or inorganic particulate materials and includes the design of more elaborate systems such as the synthesis of TiO_2/polymer hybrid "nanorattles" [90]. In this work, TiO_2 pigments were first encapsulated in a water-swellable polymer shell composed of MMA, BA, and MAA using a poly(4-vinylbenzenesulfonic acid-*co*-AA-*co*-BA) macroRAFT agent at a low pH value (pH~4). The shell was subsequently coated

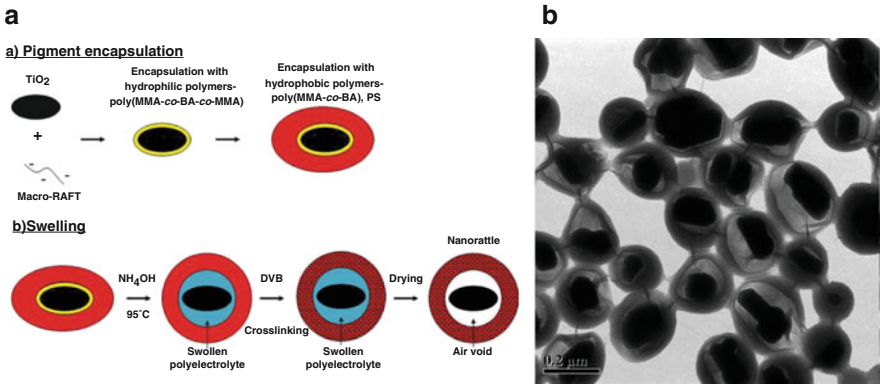

Fig. 14 (**a**) Nanorattle synthesis using amphiphilic macroRAFT copolymers as stabilizers. (**b**) TEM of nanorattles formed after swelling at pH 11 and 95°C and crosslinking of the outer shell. Reproduced from [90] with permission from Wiley InterScience

with a hard hydrophobic layer. Hybrid nanorattles were then produced by swelling the hydrophilic layer in a basic solution at elevated temperatures, followed by crosslinking of the outer polymer shell to consolidate the hollow morphology and withstand the compressive forces that develop during the drying step (Fig. 14). Air voids were shown to be controlled by the swelling time, temperature, and thickness of the hydrophilic polymer layer. The final TiO_2-filled hollow spheres are expected to be more efficient opacifiers than either traditional or encapsulated titanium dioxide pigments and could find applications in both the paper and architectural coatings market.

As described above, many parameters in the REEP process can influence the particle morphology, such as the pH of the suspension, the feeding process (batch or semi-batch), and the macroRAFT agent and hydrophobic monomer compositions. In some cases, the inorganic particles are not encapsulated and different morphologies are formed. For instance, Garnier et al. [91] attempted to encapsulate nanoceria into poly(styrene-*co*-methyl acrylate), P(S-*co*-MA), latex particles using P(AA-*co*-BA) RAFT copolymers similar to those used by Ali et al. [85] for the encapsulation of Gibbsite platelets. However, the presence of adsorbed citric acid on the nanoceria particle surface limited macroRAFT adsorption and prevented effective encapsulation. Instead, the CeO_2 particles were located on the latex surface (Fig. 15a). The use of a sulfonated macroRAFT agent with the aim of increasing latex stability and decreasing latex particle size did not result in hybrid particles at all, with the nanoceria instead remaining free in solution (Fig. 15b) [92]. This was attributed to the poor affinity of this macroRAFT agent for the CeO_2 surface, again highlighting the importance of the surface properties of the macroRAFT-coated inorganic particles in determining hybrid particle morphology. The work of Warnant et al. [93] on the synthesis of CeO_2/poly(vinylidene chloride-*co*-methyl acrylate) hybrid latexes mediated by a phosphonated poly(vinylbenzyl-phosphonic acid-*co*-styrene) RAFT copolymer also highlights this effect. Cryo-

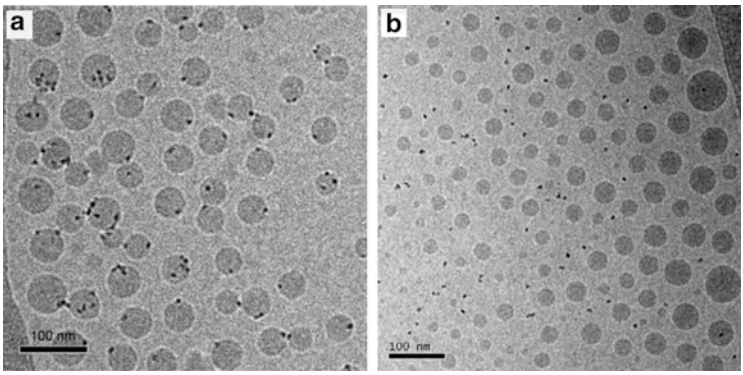

Fig. 15 Cryo-TEM images of the CeO_2/P(S-*co*-MA) hybrid latexes obtained employing (**a**) P($BA_{7.5}$-*co*-AA_{10}), and (**b**) P($BA_{7.2}$-*co*-$AMPS_{7.6}$) macroRAFT copolymers. Reprinted with permission from [91] and [92]. Copyright 2012 Wiley-VCH and Copyright 2013 Elsevier Inc, respectively

TEM showed composite particles decorated by several ceria particles, which were once again located at the polymer–water interface in an armored morphology.

The transposition of CRP techniques from homogeneous systems to aqueous dispersed media, particularly ab initio emulsion polymerization, is not straightforward because of partitioning of the controlling agent between the different phases, leading to transport issues from the droplets to the polymerization sites. Such issues are generally circumvented by using the polymerization-induced self-assembly (PISA) technique. However, there are still situations where the PISA process struggles to achieve a good level of control, notably when using PEO-based macroRAFT agents as the hydrophilic block. Indeed, the latter are still hydrophobic enough to partition to some extent to the monomer phase, resulting in poor colloidal stability, low reaction rates, and high molar mass dispersities.

With the aim of designing polymer/clay hybrid latexes, a novel strategy for well-controlled RAFT ab initio emulsion polymerization of styrene with PEO-based macroRAFT agents was developed by Rodrigues Guimarães et al. [94] in which Laponite clay platelets were used to "support" the controlling agents. Adsorption isotherms exhibited Langmuir-type profiles, indicating high affinity of the macroRAFT agent for the clay surface. Immobilization of the macroRAFT agent on the clay surface minimized its partitioning between the monomer droplets and the water phase during the subsequent polymerization. Immobilization significantly improved the latex colloidal stability and the living character of the polymerization. The best level of control was achieved for intermediate macroRAFT concentrations (Fig. 16a), which were high enough to promote colloidal stability of the latex particles while avoiding any partitioning of free non-adsorbing macroRAFT agent. The resulting composite particles exhibited an armored morphology (with the Laponite clay sheets located at the particle surface), with embedded PEO domains originating from heterocoagulation of the self-assembled block

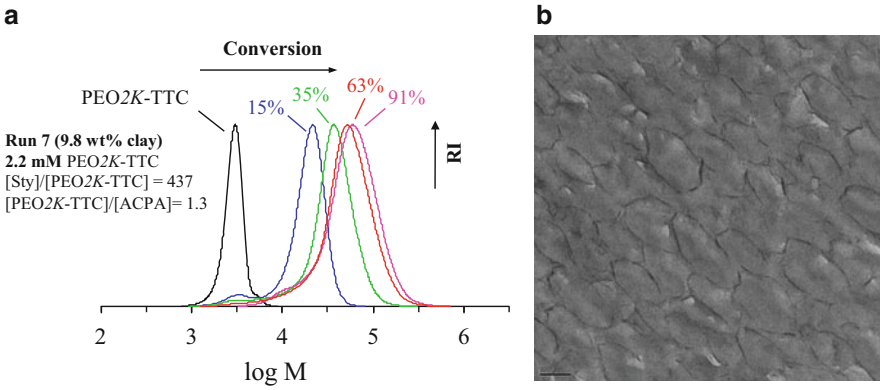

Fig. 16 (**a**) Evolution of the size-exclusion chromatograms with monomer conversion (SEC THF, PS calibration) showing the good control of the polymerization. (**b**) TEM image of an ultrathin cross-section of epoxy-embedded Laponite/PS composite latex particles synthesized by macroRAFT-mediated ab initio emulsion polymerization of styrene. Reproduced from [94] with permission from the Royal Society of Chemistry

copolymers formed in the aqueous phase with the copolymers nucleated on the Laponite clay discs (Fig. 16b).

4.2.2 Synthesis of Organic/Inorganic Hybrid Particles by Nitroxide-Mediated Emulsion Polymerization

Although most CRP-mediated syntheses of colloidal nanocomposites use RAFT polymerization to control the polymer architecture and particle morphology, NMP has also been successfully employed for the same purpose. As reviewed elsewhere, NMP has been successfully conducted in aqueous dispersed media for the PISA technique (which was pioneered using RAFT polymerization) [79]. NMP is less versatile than RAFT polymerization in terms of monomer choice because it is generally incompatible with methacrylates [95] except when some specific nitroxides are employed [96]. However, the applicability of NMP has been expanded to methacrylate systems through a technique developed by Charleux et al. [97], in which a small amount of styrene is added to the monomer feed when preparing the macroalkoxyamine. This enhances the reversible deactivation process and forms stable alkoxyamines.

Qiao et al. [98] recently exploited this approach to synthesize water-soluble P(PEOMA-*co*-S)-SG1 brush-type macroalkoxyamine initiators, which were adsorbed onto colloidal silica and subsequently used to initiate the growth of BMA in aqueous emulsion and form sterically stabilized self-assembled block copolymers. The resulting particle morphology was shown to be pH-sensitive, which was interpreted in terms of a salting-out effect induced by the concomitant increase in ionic strength upon neutralization of the alkoxyamine initiator. In a

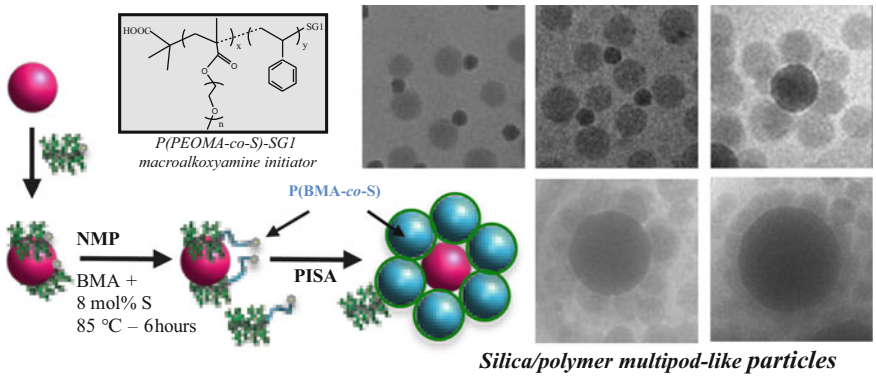

Fig. 17 Synthesis of multipod-like silica/polymer particles by NMP-mediated polymerization-induced self-assembly (PISA) of block copolymers by means of a PEO-based brush-type macroalkoxyamine initiator previously adsorbed at the surface of colloidal silica nanoparticles. Reproduced from [99] with permission from the American Chemical Society

subsequent work, these PEO-based macroalkoxyamine initiators were adsorbed onto colloidal silica and chain-extended with BMA in ab initio emulsion polymerization. This resulted for the very first time in the formation of multipod-like silica/self-assembled block copolymer hybrid particles with dumbbell-, raspberry-, and daisy-shaped morphologies, depending on the silica particle size and macroinitiator concentration [99] (see Fig. 17).

This example and the previous examples of RAFT-mediated polymerization highlight the great potential of aqueous CRP emulsion polymerization techniques for the synthesis of organic/inorganic colloids of controllable shape, morphology, and surface functionality, thus opening the door to microstructured particles and coatings with great promise in many areas of materials science.

5 Conclusions

Emulsion polymerization systems are powerful, industrially relevant tools for the production of polymeric latexes. Although not yet widely transposed to industry, controlled radical polymerization in dispersed media should confer even greater flexibility to these systems. Although the primary aim in the initial application of CRP to dispersed media was control over molar masses in latexes, the recent developments discussed in this review focus on the ability to recommence the polymerization process from specific interfaces, either a liquid–liquid interface or the surface of added (inorganic) particles. This is permitted by the ability of CRP to precisely tailor the affinity of preformed polymers for the desired interface, and to resume polymerization from the retained mediating groups. Confining the CRP to the interface combines the advantages offered by both CRP and heterogeneous polymerization systems, providing elegant pathways to new colloidal structures and

morphologies. We have highlighted examples showing the innovative synthesis of nanocapsules by incorporating an inert "templating liquid" in the dispersed monomer phase, which is retained as a removable particle core after chain extension of the stabilizing polymers at the interface. Other original strategies in which dispersed aqueous droplets or vesicles are used as templates for nanocapsule synthesis have also been discussed. In addition, significant advances in the integration of different types of inorganic particles into latexes facilitated by CRP polymers adsorbed onto the inorganic surfaces have been highlighted. Along with the capability to chain-extend, the precisely controlled composition of CRP polymers is key to their affinity for the inorganic surfaces in both aqueous miniemulsion and emulsion systems. We can envisage continual refinement of these systems to overcome some of the challenges in attaining pure populations of the desired nanocapsule structures and polymer/inorganic nanoparticle morphologies. We expect that some of the exotic structures (e.g., "nanorattles") already produced will inspire the development of even more sophisticated motifs for new functional material applications.

Acknowledgements Drs Bastian Ebeling and Samuel Pearson (C2P2) are gratefully acknowledged for fruitful discussions.

References

1. Matyjaszewski K, Davis TP (eds)(2002) Handbook of radical polymerization. Wiley, Hoboken
2. Gilbert RG (1995) Emulsion polymerization: a mechanistic approach. Academic, London
3. Lovell PA, El-Aasser MS (eds) (1997) Emulsion polymerization and emulsion polymers. Wiley, Hoboken
4. Pichot C, Daniel JC (eds) (2006) Les latex synthétiques: elaboration, propriétés, applications. Lavoisier, Paris
5. Bourgeat-Lami E, Lansalot M (2010) Organic/inorganic composite latexes: the marriage of emulsion polymerization and inorganic chemistry. Adv Polym Sci 233:53–123
6. Rahman MM, Elaissari A (2010) Organic–inorganic hybrid magnetic latex. Adv Polym Sci 233:237–281
7. Ladj R, Bitar A, Eissa MM, Fessi H, Mugnier Y, Le Dantec R, Elaissari A (2013) Polymer encapsulation of inorganic nanoparticles for biomedical applications. Int J Pharm 458: 230–241
8. Antonietti M, Landfester K (2002) Polyreactions in miniemulsions. Prog Polym Sci 27: 689–757
9. Asua JM (2002) Miniemulsion polymerization. Prog Polym Sci 27:1283–1346
10. Schork FJ, Luo Y, Smulders W, Russum JP, Butté A, Fontenot K (2005) Miniemulsion polymerization. Adv Polym Sci 175:129–255
11. Cao ZH, Ziener U (2013) A versatile technique to fabricate capsules: miniemulsion. Curr Org Chem 17:30–38
12. Asua JM (2014) Challenges for industrialization of miniemulsion polymerization. Prog Polym Sci 39:1797–1826
13. Guyot A, Landfester K, Schork FJ, Wang C (2007) Hybrid polymer latexes. Prog Polym Sci 32:1439–1461

14. Landfester K (2009) Miniemulsion polymerization and the structure of polymer and hybrid nanoparticles. Angew Chem Int Ed 48:2–22
15. Weiss C, Landfester K (2010) Miniemulsion polymerization as a means to encapsulate organic and inorganic materials. Adv Polym Sci 233:185–236
16. Hu J, Chen M, Wu L (2011) Organic-inorganic nanocomposites synthesized via miniemulsion polymerization. Polym Chem 2:760–772
17. Cao Z, Ziener U (2013) Synthesis of nanostructured materials in inverse miniemulsions and their applications. Nanoscale 5:10093–10107
18. Qi D, Cao Z, Ziener U (2014) Recent advances in the preparation of hybrid nanoparticles in miniemulsions. Adv Colloid Interface Sci 211:47–62
19. Zetterlund PB, Kagawa Y, Okubo M (2008) Controlled/living radical polymerization in dispersed systems. Chem Rev 108:3747–3794
20. Charleux B, Delaittre G, Rieger J, D'Agosto F (2012) Polymerization-induced self-assembly: from soluble macromolecules to block copolymer nano-objects in one step. Macromolecules 45:6753–6765
21. Monteiro MJ, Cunningham MF (2012) Polymer nanoparticles via living radical polymerization in aqueous dispersions: design and applications. Macromolecules 45:4939–4957
22. Warren NJ, Armes SP (2014) Polymerization-induced self-assembly of block copolymer nano-objects via RAFT aqueous dispersion polymerization. J Am Chem Soc 136:10174–10185
23. Nicolas J, Guillaneuf Y, Lefay C, Bertin D, Gigmes D, Charleux B (2013) Nitroxide-mediated polymerization. Prog Polym Sci 38:63–235
24. Matyjaszewski K (2012) Atom transfer radical polymerization (ATRP): current status and future perspectives. Macromolecules 45:4015–4039
25. Gromada J, Matyjaszewski K (2001) Simultaneous reverse and normal initiation in atom transfer radical polymerization. Macromolecules 34:7664–7671
26. Jakubowski W, Matyjaszewski K (2005) Activator generated by electron transfer for atom transfer radical polymerization. Macromolecules 38:4139–4146
27. Magenau AJD, Strandwitz NC, Gennaro A, Matyjaszewski K (2011) Electrochemically mediated atom transfer radical polymerization. Science 332:81–84
28. Matyjaszewski K, Gaynor S, Wang J-S (1995) Controlled radical polymerizations: the use of alkyl iodides in degenerative transfer. Macromolecules 28:2093–2095
29. Tatemoto M, Nakagawa T (1978) German Patent DE2729671 (Daikin Kogyo Co., Ltd)
30. Tonnar J, Lacroix-Desmazes P (2008) Use of sodium iodide as the precursor to the control agent in ab initio emulsion polymerization. Angew Chem Int Ed 47:1294–1297
31. Yamago S (2009) Precision polymer synthesis by degenerative transfer controlled/living radical polymerization using organotellurium, organostibine, and organobismuthine chain-transfer agents. Chem Rev 109:5051–5068
32. Keddie DJ, Moad G, Rizzardo E, Thang SH (2012) RAFT agent design and synthesis. Macromolecules 45:5321–5342
33. Moad G, Rizzardo E, Thang SH (2008) Radical addition–fragmentation chemistry in polymer synthesis. Polymer 49:1079–1131
34. Lefay C, Nicolas J (2010) Controlled/living radical polymerization in aqueous miniemulsion. In: Mittal V (ed) Miniemulsion polymerization technology. Wiley, Hoboken, pp 173–210
35. van Zyl AJP, Bosch RFP, McLeary JB, Sanderson RD, Klumperman B (2005) Synthesis of styrene based liquid-filled polymeric nanocapsules by the use of RAFT-mediated polymerization in miniemulsion. Polymer 46:3607–3615
36. Luo Y, Gu H (2006) A general strategy for nano-encapsulation via interfacially confined living/controlled radical miniemulsion polymerization. Macromol Rapid Commun 27:21–25
37. Luo Y, Gu H (2007) Nanoencapsulation via interfacially confined reversible addition fragmentation transfer (RAFT) miniemulsion polymerization. Polymer 48:3262–3272
38. Lu F, Luo Y, Li B (2007) A facile route to synthesize highly uniform nanocapsules: use of amphiphilic poly(acrylic acid)-*block*-polystyrene RAFT agents to interfacially confine miniemulsion polymerization. Macromol Rapid Commun 28:868–874

39. Lu F, Luo Y, Li B (2010) pH Effects on the synthesis of nanocapsules via interfacial miniemulsion polymerization mediated by amphiphilic RAFT agent with the R group of poly(methyl acrylic acid-*ran*-styrene). Ind Eng Chem Res 49:2206–2212
40. Chen H, Luo Y (2011) Facile synthesis of nanocapsules and hollow nanoparticles consisting of fluorinated polymer shells by interfacial RAFT miniemulsion polymerization. Macromol Chem Phys 212:737–743
41. Wang Y, Jiang G, Sun X, Ding M, Hu H, Chen W (2010) Preparation of shell cross-linked nanoparticles via miniemulsion RAFT polymerization. Polym Chem 1:1638–1643
42. Li W, Matyjaszewski K, Albrecht K, Möller M (2009) Reactive surfactants for polymeric nanocapsules via interfacially confined miniemulsion ATRP. Macromolecules 42:8228–8233
43. Li W, Yoon JA, Matyjaszewski K (2010) Dual-reactive surfactant used for synthesis of functional nanocapsules in miniemulsion. J Am Chem Soc 132:7823–7825
44. Lu F, Luo Y, Li B, Zhao Q, Schork FJ (2010) Synthesis of thermo-sensitive nanocapsules via inverse miniemulsion polymerization using a PEO−RAFT agent. Macromolecules 43: 568–571
45. Wang Y, Jiang G, Zhang M, Wang L, Wang R, Sun X (2011) Facile one-pot preparation of novel shell cross-linked nanocapsules: inverse miniemulsion RAFT polymerization as an alternative approach. Soft Matter 7:5348–5352
46. Utama RH, Guo Y, Zetterlund PB, Stenzel MH (2012) Synthesis of hollow polymeric nanoparticles for protein delivery via inverse miniemulsion periphery RAFT polymerization. Chem Commun 48:11103–11105
47. Utama RH, Stenzel MH, Zetterlund PB (2013) Inverse miniemulsion periphery RAFT polymerization: a convenient route to hollow polymeric nanoparticles with an aqueous core. Macromolecules 46:2118–2127
48. Liang G, Xu J, Wang X (2009) Synthesis and characterization of organometallic coordination polymer nanoshells of prussian blue using miniemulsion periphery polymerization (MEPP). J Am Chem Soc 131:5378–5379
49. Utama RH, Drechsler M, Förster S, Zetterlund PB, Stenzel MH (2014) Synthesis of pH-responsive nanocapsules via inverse miniemulsion periphery RAFT polymerization and post-polymerization reaction. ACS Macro Lett 3:935–939
50. Ali SI, Heuts JPA, van Herk AM (2010) Controlled synthesis of polymeric nanocapsules by RAFT-based vesicle templating. Langmuir 26:7848–7858
51. Nguyen D, Zondanos HS, Farrugia JM, Serelis AK, Such CH, Hawkett BS (2008) Pigment encapsulation by emulsion polymerization using macro-RAFT copolymers. Langmuir 24:2140–2150
52. Ali SI, Heuts JPA, van Herk AM (2011) Vesicle-templated pH-responsive polymeric nanocapsules. Soft Matter 7:5382–5390
53. Bailly B, Donnenwirth A-C, Bartholome C, Beyou E, Bourgeat-Lami E (2006) Silica-polystyrene nanocomposite particles synthesized by nitroxide-mediated polymerization and their encapsulation through miniemulsion polymerization. J Nanomater 2006:76371. doi: 10.1155/JNM/2006/76371
54. Bombalski L, Min K, Dong H, Tang C, Matyjaszewski K (2007) Preparation of well-defined hybrid materials by ATRP in miniemulsion. Macromolecules 40:7429–7432
55. Ma J, Lu M, Cao C, Zhang H (2013) Synthesis and characterization of PMMA/SiO_2 organic–inorganic hybrid materials via RAFT-mediated miniemulsion polymerization. Polym Comp 34:626–633
56. Ma J, Zhang H (2014) Preparation and characterization of poly(methyl methacrylate)/SiO_2 organic–inorganic hybrid materials via RAFT-mediated miniemulsion Polymerization. J Polym Res 21:1–9
57. Mičušík M, Bonnefond A, Paulis M, Leiza JR (2012) Synthesis of waterborne acrylic/clay nanocomposites by controlled surface initiation from macroinitiator modified montmorillonite. Eur Polym J 48:896–905

58. Khezri K, Haddadi-Asl V, Roghani-Mamaqani H, Salami-Kalajahi M (2011) Synthesis and characterization of exfoliated poly(styrene-*co*-methyl methacrylate) nanocomposite via miniemulsion atom transfer radical polymerization: an activators generated by electron transfer approach. Polym Comp 32:1979–1987
59. Khezri K, Haddadi-Asl V, Roghani-Mamaqani H, Salami-Kalajahi M (2012) Synthesis of clay-dispersed poly(styrene-*co*-methyl methacrylate) nanocomposite via miniemulsion atom transfer radical polymerization: a reverse approach. J Appl Polym Sci 124:2278–2286
60. Khezri K, Haddadi-Asl V, Roghani-Mamaqani H, Salami-Kalajahi M (2012) Nanoclay-encapsulated polystyrene microspheres by reverse atom transfer radical polymerization. Polym Comp 33:990–998
61. Khezri K, Haddadi-Asl V, Roghani-Mamaqani H, Salami-Kalajahi M (2012) Encapsulation of organomodified montmorillonite with PMMA via in situ SR&NI ATRP in miniemulsion. J Polym Res 19:1–10
62. Hatami L, Haddadi-Asl V, Roghani-Mamaqani H, Ahmadian-Alam L, Salami-Kalajahi M (2011) Synthesis and characterization of poly(styrene-*co*-butyl acrylate)/clay nanocomposite latexes in miniemulsion by AGET ATRP. Polym Comp 32:967–975
63. Khezri K, Haddadi-Asl V, Roghani-Mamaqani H, Salami-Kalajahi M (2012) Synthesis of well-defined clay encapsulated poly(styrene-*co*-butyl acrylate) nanocomposite latexes via reverse atom transfer radical polymerization in miniemulsion. J Polym Eng 32:111–119
64. Hatami L, Haddadi-Asl V, Ahmadian-Alam L, Roghani-Mamaqani H, Salami-Kalajahi M (2013) Effect of nanoclay on styrene and butyl acrylate AGET ATRP in miniemulsion: study of nucleation type, kinetics, and polymerization control. Int J Chem Kinet 45:221–235
65. Samakande A, Sanderson RD, Hartmann PC (2008) Encapsulated clay particles in polystyrene by RAFT mediated miniemulsion polymerization. J Polym Sci Part A: Polym Chem 46: 7114–7126
66. Samakande A, Sanderson RD, Hartmann PC (2009) Rheological properties of RAFT-mediated poly(styrene-*co*-butyl acrylate)-clay nanocomposites [P(S-*co*-BA)-PCNs]: emphasis on the effect of structural parameters on thermo-mechanical and melt flow behaviors. Polymer 50: 42–49
67. Samakande A, Juodaityte JJ, Sanderson RD, Hartmann PC (2008) Novel cationic RAFT-mediated polystyrene/clay nanocomposites: synthesis, characterization, and thermal stability. Macromol Mater Eng 293:428–437
68. Esteves ACC, Bombalski L, Trindade T, Matyjaszewski K, Barros-Timmons A (2007) Polymer grafting from CdS quantum dots via AGET ATRP in miniemulsion. Small 3:1230–1236
69. Esteves ACC, Hodge P, Trindade T, Barros-Timmons AMMV (2009) Preparation of nanocomposites by reversible addition-fragmentation chain transfer polymerization from the surface of quantum dots in miniemulsion. J Polym Sci Part A Polym Chem 47:5367–5377
70. Chakraborty S, Jähnichen K, Komber H, Basfar AA, Voit B (2014) Synthesis of magnetic polystyrene nanoparticles using amphiphilic ionic liquid stabilized RAFT mediated miniemulsion polymerization. Macromolecules 47:4186–4198
71. Gu Y, Zhao J, Liu Q, Zhou N, Zhang Z, Zhu X (2014) Zero-valent iron (Fe(0)) mediated RAFT miniemulsion polymerization: a facile approach for the fabrication of Fe(0)-encapsulated polymeric nanoparticles. Polym Chem 5:4215–4218
72. Zhang Z, Wang W, Cheng Z, Zhu J, Zhou N, Yang Y, Tu Y, Zhu X (2010) Zero-valent iron/RAFT agent-mediated polymerization of methyl methacrylate at ambient temperature. Macromolecules 43:7979–7984
73. Etmimi HM, Tonge MP, Sanderson RD (2011) Synthesis and characterization of polystyrene-graphite nanocomposites via surface RAFT-mediated miniemulsion polymerization. J Polym Sci Part A Polym Chem 49:1621–1632
74. Kang Y, Taton TA (2005) Core/Shell gold nanoparticles by self-assembly and crosslinking of micellar, block-copolymer shells. Angew Chem Int Ed 44:409–412

75. Hickey RJ, Haynes AS, Kikkawa JM, Park SJ (2011) Controlling the self-assembly structure of magnetic nanoparticles and amphiphilic block-copolymers: from micelles to vesicles. J Am Chem Soc 133:1517–1525
76. Mai YEA (2012) Selective localization of preformed nanoparticles in morphologically controllable block copolymer aggregates in solution. Accounts Chem Res 45:1657–1666
77. Wang J, Li W, Zhu J (2014) Encapsulation of inorganic nanoparticles into block copolymer micellar aggregates: strategies and precise localization of nanoparticles. Polymer 55:1079–1096
78. Liang R, Xu J, Li W, Liao Y, Wang K, You J, Zhu J, Jiang W (2015) Precise localization of inorganic nanoparticles in block copolymer micellar aggregates: from center to interface. Macromolecules 48:256–263
79. Zetterlund PB, Kagawa Y, Okubo M (2008) Controlled/living radical polymerization in dispersed systems. Chem Rev 108:3747–3794. doi:10.1021/cr800242x
80. Charleux B, D'Agosto F, Delaittre G (2010) Preparation of hybrid latex particles and core-shell particles through the use of controlled radical polymerization techniques in aqueous media. Adv Polym Sci 233:125–183
81. Cenacchi-Pereira A, Grant E, D'Agosto F, Lansalot M, Bourgeat-Lami E (2014) Encapsulation with the use of controlled radical polymerization. In: Kobayashi S, Müllen K (eds) Encyclopedia of polymeric nanomaterials. Springer, Berlin Heidelberg. doi:10.1007/978-3-642-36199-9_347-1
82. Daigle J-C, Claverie JP (2008) A simple method for forming hybrid core-shell nanoparticles suspended in water. J Nanomater 2008:609184. doi: 10.1155/2008/609184
83. Das P, Zhong W, Claverie J (2011) Copolymer nanosphere encapsulated CdS quantum dots prepared by RAFT copolymerization: synthesis, characterization and mechanism of formation. Colloid Polym Sci 289:1519–1533
84. Das P, Claverie JP (2012) Synthesis of single-core and multiple-core core-shell nanoparticles by RAFT emulsion polymerization: Lead sulfide-copolymer nanocomposites. J Polym Sci Part A Polym Chem 50:2802–2808
85. Ali SI, Heuts JPA, Hawkett BS, van Herk AM (2009) Polymer encapsulated gibbsite nanoparticles: efficient preparation of anisotropic composite latex particles by RAFT-based starved feed emulsion polymerization. Langmuir 25:10523–10533
86. Mballa Mballa MA, Ali SI, Heuts JPA, van Herk AM (2012) Control of the anisotropic morphology of latex nanocomposites containing single montmorillonite clay particles prepared by conventional and reversible addition-fragmentation chain transfer based emulsion polymerization. Polym Int 61:861–865
87. Zgheib N, Putaux J-L, Thill A, Bourgeat-Lami E, D'Agosto F, Lansalot M (2013) Cerium oxide encapsulation by emulsion polymerization using hydrophilic macroRAFT agents. Polym Chem 4:607–614
88. Zhong W, Zeuna JN, Claverie JP (2012) A versatile encapsulation method of noncovalently modified carbon nanotubes by RAFT polymerization. J Polym Sci Part A Polym Chem 50: 4403–4407
89. Nguyen D, Such CH, Hawkett BS (2013) Polymer coating of carboxylic acid functionalized multiwalled carbon nanotubes via reversible addition-fragmentation chain transfer mediated emulsion polymerization. J Polym Sci Part A Polym Chem 51:250–257
90. Nguyen D, Such C, Hawkett B (2012) Polymer-TiO_2 composite nanorattles via RAFT-mediated emulsion polymerization. J Polym Sci Part A Polym Chem 50:346–352
91. Garnier J, Warnant J, Lacroix-Desmazes P, Dufils P-E, Vinas J, Vanderveken Y, van Herk AM (2012) An emulsifier-free RAFT-mediated process for the efficient synthesis of cerium oxide/polymer hybrid latexes. Macromol Rapid Commun 33:1388–1392
92. Garnier J, Warnant J, Lacroix-Desmazes P, Dufils P-E, Vinas J, van Herk A (2013) Sulfonated macro-RAFT agents for the surfactant-free synthesis of cerium oxide-based hybrid latexes. J Colloid Interface Sci 407:273–281

93. Warnant J, Garnier J, van Herk A, Dufils P-E, Vinas J, Lacroix-Desmazes P (2013) A CeO_2/PVDC hybrid latex mediated by a phosphonated macro-RAFT agent. Polym Chem 4: 5656–5663
94. Rodrigues Guimarães T, de Camargo CT, D'Agosto F, Lansalot M, Martins Dos Santos A, Bourgeat-Lami E (2014) Synthesis of multi-hollow clay-armored latexes by surfactant-free emulsion polymerization of styrene mediated by poly(ethylene oxide)-based macroRAFT/Laponite complexes. Polym Chem 5:6611–6622
95. McHale R, Aldabbagh F, Zetterlund PB (2007) The role of excess nitroxide in the SG1 (*N*-tert-butyl-*N*-[1-diethylphosphono-(2,2-dimethylpropyl)] nitroxide)-mediated polymerization of methyl methacrylate. J Polym Sci Part A Polym Chem 45:2194–2203
96. Detrembleur C, Jerome C, Winter JD, Gerbaux P, Clement J-L, Guillaneuf Y, Gigmes D (2014) Nitroxide mediated polymerization of methacrylates at moderate temperature. Polym Chem 5:335–340
97. Charleux B, Nicolas J, Guerret O (2005) Theoretical expression of the average activation-deactivation equilibrium constant in controlled/living free-radical copolymerization operating via reversible termination. Application to a strongly improved control in nitroxide-mediated polymerization of methyl methacrylate. Macromolecules 38:5485–5492
98. Qiao XG, Lansalot M, Bourgeat-Lami E, Charleux B (2013) Nitroxide-mediated polymerization-induced self-assembly of poly(poly(ethylene oxide) methyl ether methacrylate-*co*-styrene)-*b*-poly(*n*-butyl methacrylate-*co*-styrene) amphiphilic block copolymers. Macromolecules 46:4285–4295
99. Qiao XG, Dugas PY, Charleux B, Lansalot M, Bourgeat-Lami E (2015) Synthesis of multipod-like silica/polymer latex particles via nitroxide-mediated polymerization-induced self-assembly of amphiphilic block copolymers. Macromolecules 48:545–556

Adv Polym Sci (2016) 270: 163–192
DOI: 10.1007/12_2015_315

Published online: 3 June 2015

Post-polymerization Modification of Surface-Bound Polymers

Hanju Jo and Patrick Theato

Abstract Surfaces that have been intricately functionalized with reactive polymers have attracted scientific attention recently because of their potential use in a broad range of applications. Polymers containing chemically reactive functional groups can be utilized for subsequent modification of various surfaces. Reactive polymeric surfaces can be produced by surface-initiated polymerization, such as atom transfer radical polymerization, nitroxide-mediated polymerization, and ring-opening metathesis polymerization. Such surfaces can subsequently undergo post-polymerization modification to alter their physicochemical properties. Post-polymerization modification has a number of advantages, including the fact that diverse polymer structures are rapidly accessible without individual synthesis; polymerization of new functional monomers can produce a variety of surfaces and interfaces; and other materials can be easily modified, which would be difficult using conventional direct polymerization. In addition, the libraries of chemical reactions and materials that can be used in post-polymerization modifications are abundant. Therefore, post-polymerization modification opens up new platforms for the facile and versatile modification of various surfaces. This chapter focuses on a discussion of post-polymerization modification of various surface-bound polymers, from planar surfaces to three-dimensional objects, and on the extended applications of the reactive surfaces.

Keywords Click chemistry • Functionalized surfaces • Multifunctionalization • Post-polymerization modification • Surface-initiated polymerization

H. Jo and P. Theato (✉)
Institute for Technical and Macromolecular Chemistry, University of Hamburg, Bundesstrasse 45, 20146 Hamburg, Germany
e-mail: theato@chemie.uni-hamburg.de

Contents

1 Introduction

Surface-initiated polymerization has been developed as a compelling method for modification of a broad range of surfaces with the desired polymer brushes and can be used in many applications, such as nonbiofouling surfaces, antibacterial coatings, and stimuli-responsive surfaces [1–3]. Reactive polymeric surfaces can be produced by surface-initiated polymerization, such as atom transfer radical polymerization (ATRP), nitroxide-mediated polymerization (NMP), and ring-opening metathesis polymerization (ROMP) [4–12]. Such surfaces can subsequently undergo post-polymerization modification to alter their physicochemical properties [13–16]. The formation of polymer brushes on surfaces can be achieved either by physical deposition of a thin film (physisorption) or by covalent attachment (chemisorption) [17, 18]. In physisorbed polymers, only weak intermolecular forces exist between the polymer brushes and the substrate; therefore, complications such as dewetting, delamination, or desorption can occur. In contrast, covalently attached polymer brushes provide enhanced stability, which is necessary for subsequent post-polymerization modification. Covalently attached polymer brushes can be formed in two ways: The "grafting-to" approach involves synthesizing a polymer that has a reactive functional group at one end of the chain, which reacts with a complementary functional group on the surface. The "grafting-from" approach involves direct polymerization from an immobilized initiator on the surface [19–21]. Both methods have various benefits [22], especially the "grafting-from" approach, which results in a high grafting density and a high volume of functional groups, enabling effective post-polymerization modification [23, 24].

Conventional polymerizations require specific conditions (e.g., organic solvents, UV light, or high temperature) that affect the reactive functionalities. However, post-polymerization modification using polymers with sophisticated chemical

reactive groups can be used to avoid these problems [25]. To conduct a post-polymerization modification of a reactive polymer, a monomer containing a reactive group is first polymerized from a surface-immobilized initiator. Then, a functional group, usually a small molecule, that is complementary to the reactive group of the polymer chain is covalently attached to the polymer brush. The range of chemical reactions and materials that can be involved in the post-polymerization modification is extremely broad. As common reactions, thiol–ene/yne addition [26], activated ester coupling [2, 16, 27], ring opening reactions of succinic anhydrides and azlactones [28–31], Michael addition [32], and Cu(I)-catalyzed alkyne–azide [2 + 3] cycloadditions (CuAACs) [33] have been intensively studied, among others. Details of all post-polymerization modification reactions are not covered in this chapter and the reader is invited to refer to the numerous reviews on this topic [18]. Instead, selected reactions that have been applied to surface modifications are discussed in detail in the following sections. Note that post-polymerization modifications have been conducted on diverse surfaces, ranging from simple planar surfaces to highly complex surfaces. The following sections introduce post-polymerization modification of various surface-bound polymers and are organized according to the type of surface.

2 Post-polymerization Modifications on Planar Surfaces

2.1 Reactive Polymer Brushes

Surface-initiated controlled radical polymerization techniques have been intensively used to generate polymer brushes because of their precise control over the growth of brushes (i.e., their thickness and grafting density) [4, 12, 34]. Controlled radical polymerizations, including ATRP and NMP, as well as ROMP reactions [4–11, 35] have been mostly utilized. All of these controlled polymerizations allow the polymerization of functionalized monomers (i.e., those featuring a reactive epoxide, azide, azlactone, isocyanate, active ester, or alkyne) from the surface [36–46]. Gopalan and coworkers, for instance, reported the surface-initiated ATRP of 2-vinyl-4,4-dimethylazlactone (VDMA) on silicon surfaces with a silane initiator. The resulting polymer brushes were post-modified with aminated proteins [40]. In similar studies, *N*-hydroxysuccinimide 4-vinyl benzoate (NHS4VB) was polymerized via surface-initiated ATRP by Locklin and coworkers [46]. In a subsequent step, the poly(NHS4VB) brushes were post-modified with primary amines.

Polymers containing activated ester functional groups have also been frequently employed for post-polymerization modifications [47–49]. Poly(pentafluorophenyl methacrylate) (PPFPMA) is a particularly attractive activated ester polymer because it has a high reactivity towards amines, hydrolytic stability, and good solubility in a variety of common organic solvents [50, 51]. Moreover, the

corresponding monomer, pentafluorophenyl methacrylate (PFPMA) can easily be prepared with high yields via a one-step reaction [52]. Using PFPMA or pentafluorophenyl acrylate (PFPA), the groups of Klok and Theato prepared activated ester-containing polymer brushes via direct polymerization or via reversible addition–fragmentation chain transfer polymerization (RAFT), respectively [53–55], and investigated the feasibility and versatility of these polymer brushes during post-polymerization modification with various amines [47]. With primary amines, post-polymerization modification proceeded with quantitative conversion, unlike with secondary amines. The modified surfaces showed different film thicknesses and water contact angles, depending on the amine used.

Mostly, post-polymerization modifications were conducted on the "grafting-from" surfaces as mentioned above; however, in some cases, immobilization of the initiator and subsequent polymerization of the desired monomers was not possible. Theato and coworkers introduced an alternative, yet convenient, method for fabrication of reactive polymer brushes on surfaces by simply spin-coating a precursor hybrid reactive copolymer. For this purpose, poly (methylsilsesquioxane)–poly(pentafluorophenyl acrylate) (PMSSQ-PPFPA) hybrid polymers were comprehensively investigated by the group [56, 57]. PMSSQ-PPFPA hybrid polymers were synthesized by RAFT polymerization using a PMSSQ-based inorganic chain transfer agent. Polymer films could then be formed on various substrates, such as silicon, glass, gold, PMMA, PDMS, and steel by either spin- or dip-coating, followed by a short thermal annealing step (Fig. 1) [49]. Subsequently, these crosslinked polymer films were dipped into solutions of a particular amine to functionalize the polymer brush films. As an example, the converted amine-functionalized films showed changes in surface wettability towards either hydrophilic or hydrophobic behavior, depending on the amine used. In addition, films based on the common temperature-responsive polymer poly(*N*-isopropyl acrylamide) (PNIPAM) were easily produced by modification of PMSSQ-PPFPA films with isopropylamine. The obtained temperature-responsive films showed a switching of the contact angle induced by the lower critical solution temperature (LCST) of PNIPAM [58, 59].

Furthermore, a study of light-reactive surface coatings based on PMSSQ-PPFPA hybrid polymers was also conducted by Theato's group. The PMSSQ-PPFPA films were converted to photoswitchable films featuring photochromic moieties such as

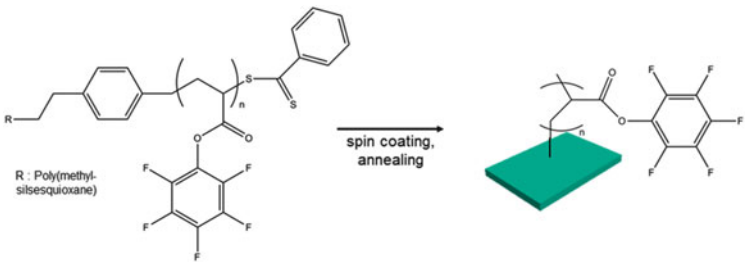

Fig. 1 Fabrication of poly(pentafluorophenyl acrylate) (PPFPA) polymer thin films

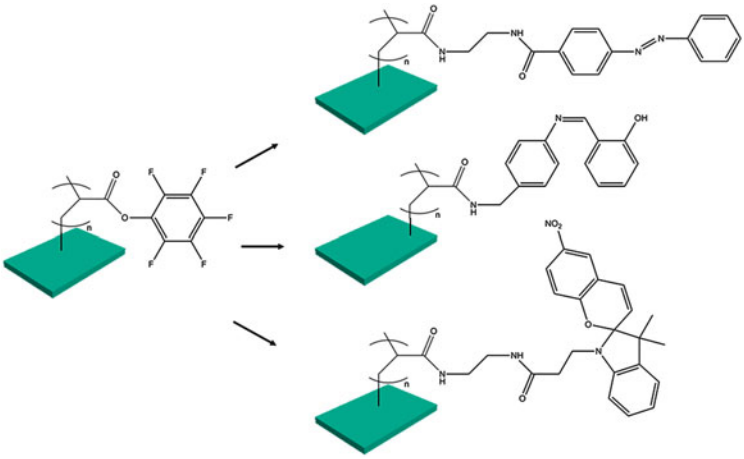

Fig. 2 Reaction for the fabrication of photoswitchable surface coatings

N-salicylidene aniline or spiropyran [48]. The salicylidene aniline group isomerizes from the enol form into the keto form under UV irradiation, and spiropyran isomerizes by ring-opening reaction into a zwitterionic merocyanine structure, resulting in a strong change in the dipole moment, consequently influencing the surface wetting properties [60–65]. Amino-functionalized spiropyrans and azobenzenes were also synthesized and used to functionalize PMSSQ-PPFPA films [66]. The surface of PMSSQ-PPFPA films could be successfully modified in a short time, and reversible changes in color and water contact angle were observed, which could be altered by switching the wavelength of the light irradiating the surfaces (Fig. 2). Moreover, a significant difference in the water contact angles was realized for the two isomeric states.

2.2 *Reactive Layer-by-Layer Assembly of Thin Polymer Multilayers*

The layer-by-layer (LbL) assembly of charged polyelectrolytes has been intensively investigated for the design of new materials and functional interfaces [67, 68]. Conventional polyelectrolyte multilayers can be fabricated by stepwise and alternating deposition of oppositely charged polymers on a substrate. The method is technically straightforward and inexpensive; however, the LbL assembly of charged polyelectrolytes only involves weak intramolecular interactions within the ionically crosslinked multilayers. To improve the system, Lynn and coworkers developed "reactive" LbL assembly of thin polymer multilayers containing azlactones [67, 69–73]. Azlactone-functionalized polymers can react with polymers containing primary amines through ring-opening reactions [70]. Consequently,

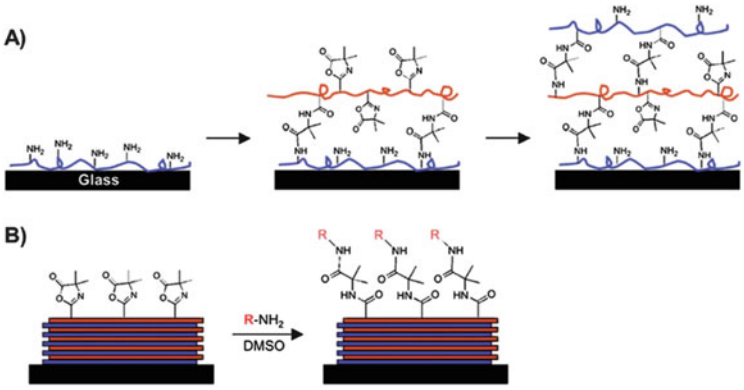

Fig. 3 "Reactive" layer-by-layer assembly (**a**) and subsequent chemical functionalization (**b**) of polymer multilayers fabricated using azlactone-functionalized polymers. (**a**) Branched poly(ethylene imine) is first adsorbed onto a substrate followed by treatment with a solution of an azlactone-containing polymer. Repetition of this process results in layer-by-layer buildup of covalently crosslinked multilayers containing residual azlactone functionality. (**b**) A broad range of surface functionality can be imparted to the films post-fabrication by treatment of residual azlactone functionality with primary amine-containing nucleophiles. Reproduced with permission from Buck et al. [75]. Copyright 2012 Royal Society of Chemistry

reactive LbL assembly leads to the formation of covalently crosslinked multilayers and induces robustness against organic solvents.

The group of Lynn focused mostly on films constituted of poly(2-vinyl-4,4-dimethylazlactone) (PVDMA) and poly(ethylene imine) (PEI) for reactive LbL assembly [3, 74–82]. On a variety of surfaces, such as silicon/glass substrates and other topographically more complex surfaces (e.g., hair, paper, cotton, thread, and commercial wound dressings), reactive LbL assembly of PEI and PVDMA was conducted. First, branched or linear PEI was adsorbed onto the desired substrate, followed by immersion of the substrate in a solution of the azlactone-containing polymer (Fig. 3a). Repetition of the process produced covalently crosslinked multilayers. Furthermore, the post-polymerization modification proceeded by treatment of residual azlactone functionality exposed on top of the surface with primary amine-containing nucleophiles (Fig. 3b). Both flat LbL thin films and covalently crosslinked and amine-reactive hollow microcapsules were fabricated by reactive LbL assembly [82]. Branched PEI and PVDMA were adsorbed alternately on the surfaces of calcium carbonate or glass microparticle templates. Elimination of the calcium carbonate or glass microparticle sacrificial core resulted in the formation of amine-reactive microcapsules. These microcapsules were used for encapsulation of a model macromolecule (FITC-dextran) and were stable for at least 22 h under several critical conditions.

Covalent LbL assembly based on click chemistry, especially CuAAC, has also been exploited comprehensively [83–95]. Caruso and coworkers built up covalently crosslinked multilayers on silicon, quartz, or gold-coated substrates by alkyne- and azide-functionalized poly(acrylic acid) (PAA) copolymers [83]. The results showed

that linear film growth was found during assembly and that these covalently crosslinked PAA-based films were physically stable under varying solution conditions (e.g., salt concentration, pH). Several other groups also investigated the azide/alkyne coupling reactions for covalent LbL assembly. Chance and coworkers reported the fabrication of covalently crosslinked multilayers using azide- and alkyne-functionalized poly(*N*-isopropylacrylamide) (PNIPAM) derivatives [87], and Boulmedais and coworkers used bifunctionalized poly(ethylene glycol) (PEG) spacer and azide- or alkyne-modified PAA for their experiments [90]. Covalently bonded LbL multifunctional thin films based on activated esters were also investigated by the group of Theato [96]. Poly(pentafluorophenyl-4-vinylbenzoate) (PPFPVB) or PFPA were used to fabricate LbL multilayer films with poly(allyl amine) (PAAm). Activated ester side groups formed amide bonds with amine groups in PAAm, and stable covalently bonded LbL layers were obtained during the LbL deposition. Subsequently, the activated ester groups remaining inside the LbL polymer film or as the outermost layer were functionalized with fluorescent dyes, 5-[(2-aminoethyl)amino]naphthalene-1-sulfonic acid (EDANS) or poly (allylamine hydrochloride) labeled with Rhodamine B isothiocyanate (PAH-rho), respectively, which was documented by taking fluorescence images. Furthermore, surface patterning was conducted using microcontact printing with PAH-rho, followed by functionalization with EDANS during post-treatment of the whole film. Note that the LbL films could be separated from the substrate under mild acidic conditions, resulting in free-standing films that showed excellent physiochemical stability and functionality. These films could be useful for development of flexible and multifunctional thin films for various chemical and biological applications.

2.3 Complex Reactive Surfaces

Post-polymerization modification of reactive polymer films provides the possibility to design complex coatings associated with intricate structure and morphology [1, 4, 97, 98]. Using a simple procedure, two or more types of chemical functionalities can be applied onto substrates that are contained in covalently grafted polymer films. Multifunctional surfaces can be fabricated by sequential click reactions or simultaneous multiple click reactions in one-pot. “Click-like” reactions such as thiol-based additions, activated ester coupling, and azide–alkyne cycloadditions are those most used for post-polymerization modification, because these reactions yield orthogonal reactive polymer brushes rapidly and quantitatively [17].

Locklin and coworkers have intensively researched post-polymerization modification via click chemistry for the design of complex surfaces [41, 99–106]. The patterning of polymer-grafted planar surfaces was carried out by consecutive functionalization using the same click-type reaction or multiple click-type reactions. One example is a spatially patterned polymer brush surface fabricated by the combination of surface-initiated free-radical polymerization (SI-FRP) and

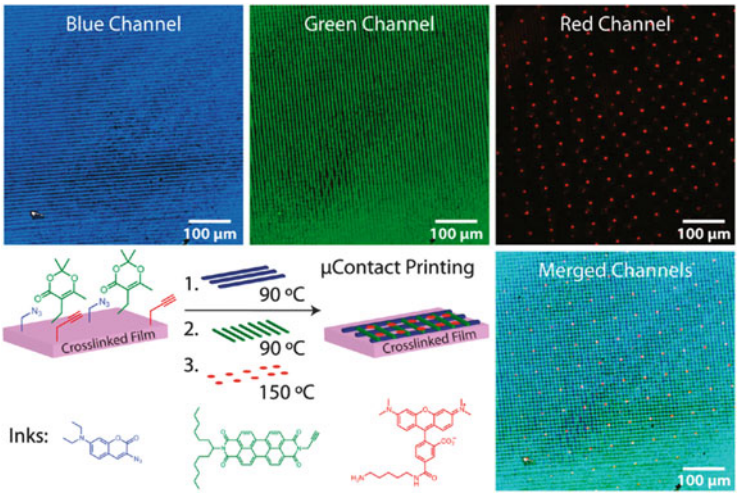

Fig. 4 Trifunctional polymer films that were functionalized in a three-step process with *blue*, *green*, and *red* dyes orthogonally using thermal microcontact printing. Reproduced with permission from Spruell et al. [105]. Copyright 2011 American Chemical Society

sequential area-selective thiol–alkyne post-polymerization modification [102]. A poly(propargyl methacrylate-trimethylsilane), poly(PgMA-TMS), brush was prepared via surface-initiated photopolymerization. Subsequently, various commercially available thiols were reacted with the brush via thiol–yne click reactions after deprotection of the brush. To pattern the surfaces, a photomask was placed directly on to the brush surface, and the first photo thiol–yne click reaction was conducted with 3-mercaptopropionic acid (MPA) on the exposed area of poly(PgMA) brush. Afterwards, the photomask was removed and the remaining area, which had been previously protected by the photomask, was modified with 1-dodecanethiol (DDT) to afford a micropatterned and multicomponent surface by the same click-type reaction.

Trifunctional polymers containing azide, alkyne, and acyl ketene functional groups, which can be used for further multiple click-type reactions, were reported by Hawker and coworkers [105]. The crosslinked trifunctional polymer thin films were patterned through stepwise thermal microcontact printing to address each of the alkyne, azide, and acyl ketene functionalizations selectively [99, 105, 106]. The polymer was synthesized by copolymerization of an acyl ketene styrenic precursor with styrene, vinylbenzyl azide, and TMS-protected propargyloxy-styrene; the alkyne was deprotected afterwards. The trifunctional polymer was then spin-coated and thermally crosslinked. Fluorescent amine-containing dyes were printed on the films in different patterns via stepwise microcontact printing to separately address each of the click reactions. First, the line pattern of blue azido-coumarin dye was printed and then the same pattern of green alkyne-perylene dye was printed in a perpendicular direction. After the activation of ketene by heating the substrate to

150°C, red amine dye in a dot pattern was then printed on this substrate to produce the trifunctional surface, as shown in Fig. 4.

Recently, a new one-pot dual functionalization method was reported by Locklin and coworkers [101]. PPFPA was directly grafted to silicon oxide and the polymer brush patterned via a reactive microcapillary printing method for a one-pot, self-sorting, post-polymerization modification [10, 81, 100, 107]. A PDMS stamp was placed onto the PPFPA film and 1 μL of an amine-containing dibenzocyclooctyne (DIBO) derivative solution was dropped at one edge of the stamp. As a result of capillary force, the solution was sucked into the channels and reacted with the exposed area of the PPFPA surface. After elimination of the stamp, the substrate was dipped into a solution containing an azido-Texas Red dye and an amino-fluorescein dye for a one-pot reaction. The results showed that a self-sorting reaction proceeded in one-pot. The surface-bound DIBO moieties formed a triazole with azido-Texas Red dye through strain-promoted alkyne–azide cycloaddition, and the PPFPA underwent aminolysis with the amino-fluorescein dye. The fluorescence images of patterned surfaces showed high-fidelity patterns without cross-contamination.

3 Post-polymerization Modifications on Hollow Surfaces

3.1 Polymeric Monolithic Columns

In situ post-polymerization modification of monolithic columns has been developed for a decade and such columns are commonly used as scavenger resins [108–111]. Macroporous monoliths are amenable to flow-through processes and can be used as reactive filters to remove specific reagents [112–115]. Tripp and coworkers reported the fabrication of reactive polymeric monoliths grafted with PVDMA by surface-initiated polymerization of VDMA (Fig. 5) [101, 113]. These azlactone-functionalized monoliths were able to scavenge ~75% of primary amine nucleophiles and ~90% of secondary amines. Fontaine and coworkers have also reported the preparation of azlactone-functionalized polymer columns for reactive filtration and nucleophile scavenging [112, 115–117]. VDMA was polymerized via ATRP and the resulting PVDMA scavenged benzylamine effectively.

Various click chemistries, building the foundation for most post-polymerization modifications, have also been applied for fabrication of reactive porous polymer monoliths [118–125]. Click reactions include alkyne–azide, thiol–ene, and thiol–yne reactions, and these reactions can be conducted under mild conditions, unlike many other polymer graft reactions. Svec and coworkers used the thiol–ene reaction to functionalize porous polymer monoliths [121]. Monoliths were thiolated with cysteamine, followed by cleavage of the disulfide bonds using tri(2-carboxylethyl) phosphine to expose the desired thiol groups. Then, lauryl methacrylate monomers were clicked onto the monoliths using either heat or UV initiation. Thiol–yne and

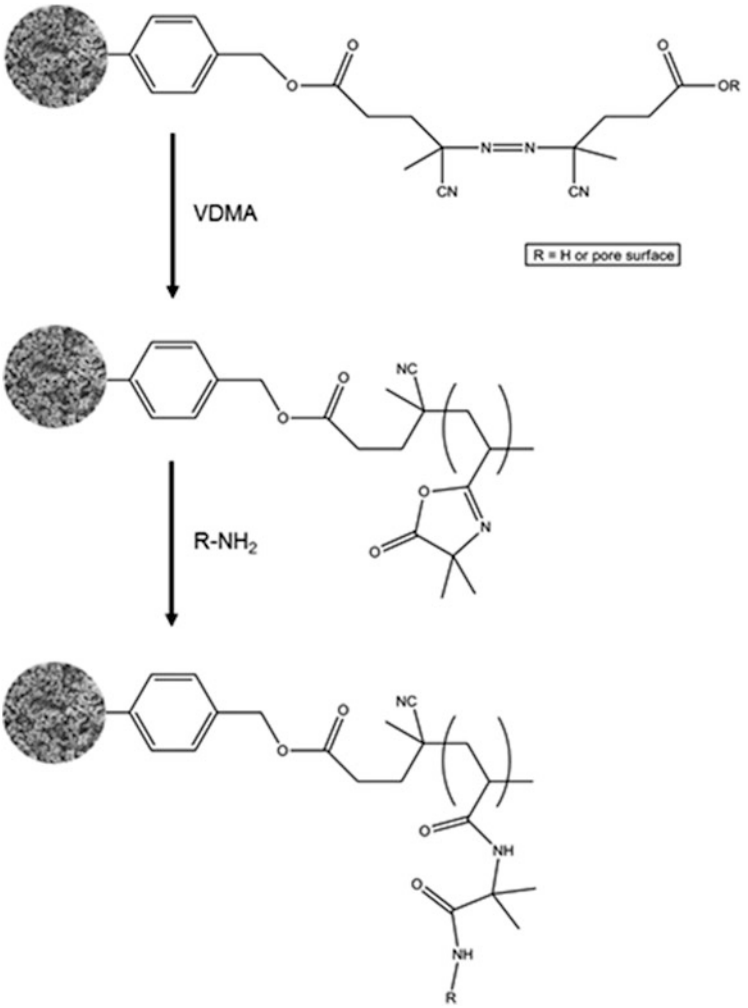

Fig. 5 Preparation of polymeric monoliths by surface-initiated polymerization of 2-vinyl-4,4-dimethylazlactone (VDMA) and post-polymerization modification with amines

CuAAC reactions were also utilized to achieve reactive porous polymer monoliths [8, 124]. Zhang and coworkers produced poly(glycidyl methacrylate-*co*-divinylbenzene), poly(GMA-*co*-DVB), and poly(vinylbenzyl chloride-*co*-divinylbenzene), (poly(VBC-*co*-DVB), monoliths to provide the reactive sites for click chemistry [29]. 1-Decyne was clicked via the CuAAC reaction.

The reactive porous polymer monoliths can be used as bioreactors to immobilize specific enzymes, proteins, and DNA [29, 126–135]. Svec, Frechet and colleagues reported a patterned polymer monolith column containing reactive vinylazlactone, which reacts with amines, through post-polymerization modification [130]. The

patterned region with vinylazlactone could spatially immobilize a variety of enzymes that include a reactive amine group.

In a joint study, the groups of Theato and Cameron fabricated highly porous polymers incorporating activated esters via the high internal phase emulsions (HIPEs) technique [18, 136]. PolyHIPEs were prepared by photopolymerization of HIPEs containing PFPA in the monomer phase. The resulting PFPA-polyHIPEs featured high porosity and well-defined pore morphology, with average diameters of 30–50 μm. It is worth noting that PFPA-polyHIPEs containing reactive groups were prepared without using surface-initiated polymerization. The PFP groups within the polyHIPEs were post-functionalized with different amines, such as tris-(2-aminoethyl)amine, benzylamine, and Rhodamine 123, and the complete modification was confirmed by ^{19}F NMR spectroscopy.

3.2 Cellulosic Honeycomb Films

Bioactive paper has recently attracted attention as a new field with applications in global issues such as scarcity of food and water safety [137, 138]. The fabrication of inexpensive bioactive packaging, assays, and sensors is urgently required for these issues. Cellulose, the most abundant biopolymer, is a superior candidate for fabrication of bioactive papers because of its biocompatibility and the accumulated knowledge about the material. Cellulose has been used as an ideal support material for bioactive systems, which utilize the pores of the cellulosic matrix to entrap biomolecules [139–143]. The internal surface of pores can be chemically modified, and the functionalized surfaces offer a high selectivity and reactivity for molecular recognition of pathogens.

Kadla and coworkers recently prepared micropatterned honeycomb films with ordered pore structures using an amphiphilic regioselective cellulose derivative, 3-*O*-poly(ethylene glycol)-2,6-di-*O*-thexyldimethylsilyl (3-N_3EG-2,6-TDMS) cellulose [144]. As a further demonstration, the site-specific functionalization of cellulosic micropatterned films through post-polymerization modification was conducted [145]. The CuAAC reaction was chosen because of its reproducibility and high degree of specificity. In addition, the azide–alkyne cycloaddition is adaptable to water; therefore, it is suitable for a variety of in vivo and in vitro applications [146–149]. The azide-functionalized cellulosic honeycomb films were produced by the simple “breath-figure” method and immersed in a solution of alkynated biotin. The alkynated biotin was covalently linked with 3-N_3EG-2,6-TDMS cellulose via CuAAC, and the successful reaction was proven by ATR-FTIR (Fig. 6). The results indicate that this concept has great potential for the development of biosensors in the future.

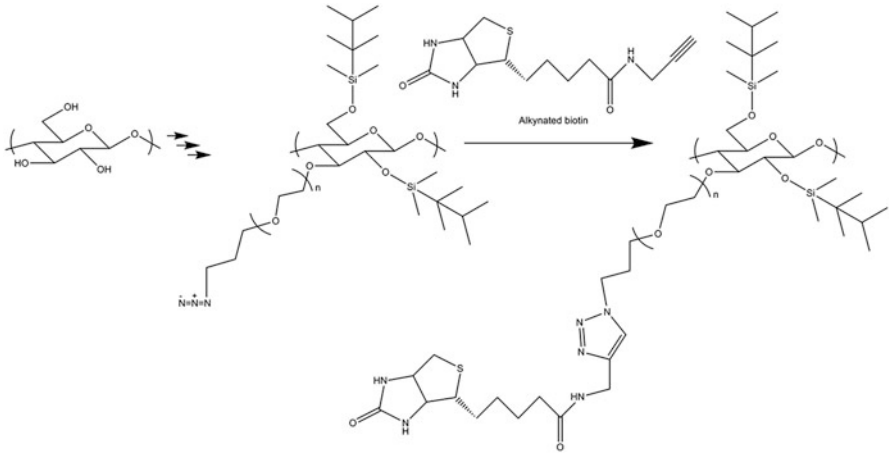

Fig. 6 Synthetic scheme for reaction of 3-N_3EG-2,6-TDMS cellulose via Cu-catalyzed [2 + 3] cycloaddition reaction

3.3 Alumina Hybrid Membranes

Anodized aluminum oxide (AAO) membranes, which have well-ordered hexagonally packed pores on the surface, have been extensively used for a variety of applications because of their considerable internal surface area that is ideal for sensing, recognition, and the controlled release of biologically relevant molecules [150]. The pore dimensions can be easily tuned by the anodization conditions. Furthermore, the facile fabrication of various length scales of membranes with diameters from 20 to 200 nm and length up to several hundred micrometers extends the range of fields in which they can be applied. The surface properties of porous AAO can be modified with appropriate molecules, providing a chance to control the hydrophilicity/hydrophobicity, surface charge, and selectivity of AAO membranes.

So far, most studies of surface modification of porous AAO membranes have been conducted using silanization, with organosilane compounds covalently bound to the oxide surfaces of AAO membranes. Organosilanes on AAO surfaces can be used to immobilize polymers, proteins, and other molecules for additional functionalization [151, 152].

Polymer brushes can be grafted onto the pore wall of porous AAO membranes to improve the binding capacity, stability, and selectivity of the membranes. To initiate radical polymerization on the wall, surfaces need to be modified with an appropriate initiator or chain-transfer agent. Generally, a chlorosilane- or alkoxysilane-modified initiator/chain-transfer agent is used; however, the use of silanes requires anhydrous reaction conditions, which can be restrictive in some cases. Therefore, Klok and coworkers utilized catechol as an alternative anchoring moiety for surface-initiated polymerization [153]. The advantage of catechol-based initiators is that they can be immobilized in aqueous solution, without the need for

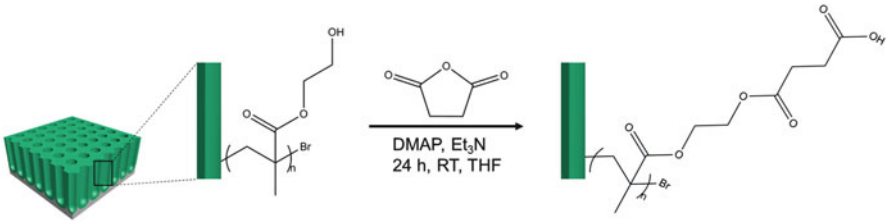

Fig. 7 Post-polymerization modification of poly(2-hydroxyethyl methacrylate) (PHEMA)-brush-modified alumina membranes

extreme anhydrous conditions. ATRP initiators based on salicyclic acid, catechol, phthalic acid, and *m*- and *p*-benzoic acid were immobilized on alumina membranes. Hydrophilic poly(2-hydroxyethyl methacrylate) (PHEMA) and poly[poly(ethylene glycol)methacrylate] ($PPEGMA_6$) brushes were then grown on the resulting initiator-modified alumina membranes. Interestingly, only polymer brushes derived from salicylate or catechol initiators achieved comparable thicknesses of the brushes, whereas initiators based on phthalic acid and benzoic acid resulted in thin brushes or no brush growth at all. Of the various ATRP initiators investigated in this study, 2-bromoisobutyrate derivatives and the salicylate-based initiator showed promising results; therefore, further polymerizations were conducted on alumina membranes that had been functionalized with a 5-(2-bromo-2-methylpropanamido)-2-hydroxybenzoic acid initiator. After immobilization of the initiator, PHEMA brushes were grown from the surface via ATRP. By post-polymerization modification of the corresponding PHEMA brushes with succinic anhydride, a pH-responsive carboxylic acid-functionalized brush was obtained on the internal surface of the alumina membranes (Fig. 7). The water permeation of polymer-brush-modified alumina hybrid membranes can be regulated by pH, which controls the thickness of carboxylic acid-functionalized brushes by swelling/deswelling. The results showed that the carboxylic acid-modified alumina membrane is strongly pH-dependent and that the mass flux of water dramatically decreased under basic conditions

4 Post-polymerization Modification of Nano-Objects

4.1 Reactive Polymeric Nanorods

Organic nano-objects such as rods, tubes, and wires have been widely applied in many fields [154–159]. One of the most commonly used methods for fabrication of organic nanostructures is the hard-template method using AAO templates [160–163]. Porous AAO templates can be prepared by conventional two-step anodization [164, 165], yielding pores of defined size that can be used as shape-defined molds for infiltration of organic materials. The infiltration of desired monomers or

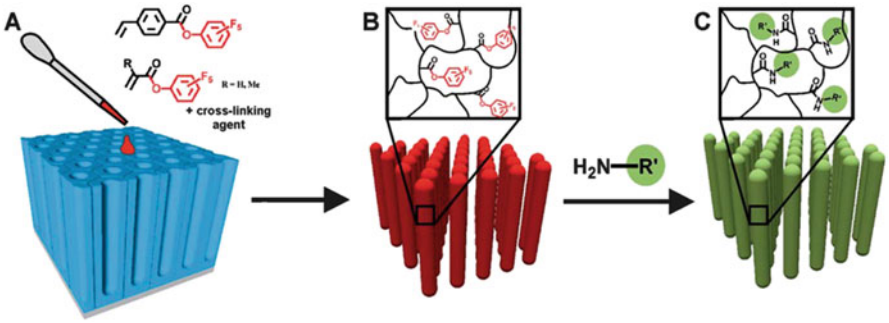

Fig. 8 Template-assisted fabrication of reactive nanorods and their post-functionalization. Reproduced with permission from Haberkorn et al. [172]. Copyright 2011 Royal Society of Chemistry

polymers into the pores can be achieved by template wetting with melts or solutions of the correspondent materials or precursors. Martin and coworkers have intensively investigated the template wetting technique for preparation of functional nano-objects [166–171].

Theato and coworkers introduced a new route for the template-based fabrication of reactive nanorods via post-polymerization modification using AAO membranes as templates (Fig. 8) [172]. For template wetting, highly concentrated solutions containing activated ester monomers, crosslinker, and initiator were prepared and drop-casted onto the AAO templates. Activated ester monomers, in this casePFPA, PFPMA, or PFPVB with proper crosslinkers, were infiltrated into the AAO pores and crosslinked thermally or photochemically with azobisisobutyronitrile (AIBN) or Lucirin TPO as initiators, respectively. Subsequently, the sacrificial AAO template was etched with phosphoric acid to obtain the corresponding polymeric nanorods, which were trapped in the AAO template. Note that the AAO template removal must be conducted under acidic conditions and not basic conditions in order to prevent hydrolysis of the ester. Bundles of activated ester polymeric nanorods were successfully produced and subjected to subsequent post-modification with amine-functionalized reagents. In particular, the activated ester polymeric nanorods were modified with isopropylamine to generate temperature-responsive PNIPAM nanorods, based on the fact that PNIPAM features a lower critical solution temperature (LCST) in water.

It is well known that PNIPAM shows a reversible phase transition from a swollen hydrated state to a collapsed dehydrated form, depending on whether the temperature of the solution of PNIPAM is below or above its LCST. Optical micrographs of fully converted PNIPAM nanorods confirmed that the nanorods respond to temperature and that the transition is reversible (Fig. 9). These promising results show that the reactive nanorods can be used in various applications, such as drug delivery systems in which an efficient reversible phase transition is desired.

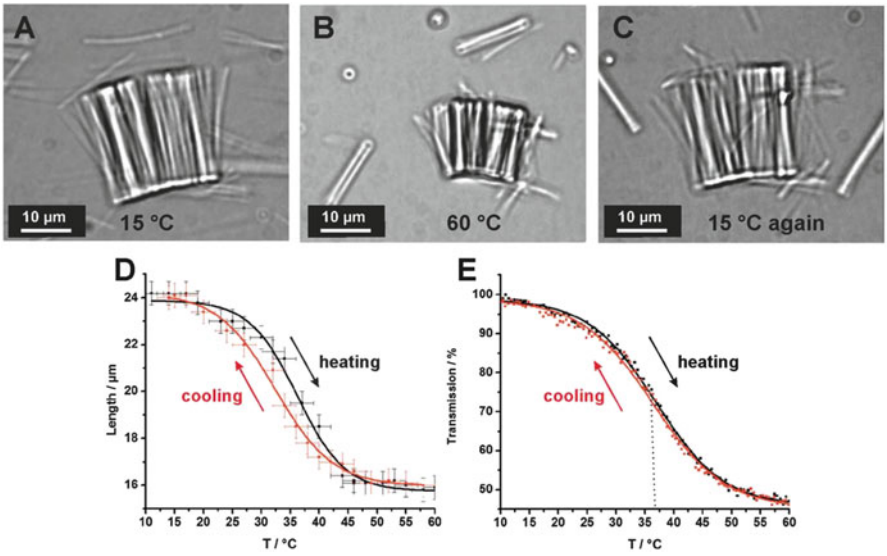

Fig. 9 (**a**–**c**) Optical micrographs of a bundle of crosslinked poly(pentafluorophenyl acrylate) (PPFPA) nanorods after conversion into poly(*N*-isopropyl acrylamide) (PNIPAM) nanorods, showing reversible response to temperature. (**d**) Plot of the length variation (along the axis of the nanorods) of PNIPAM nanorods dispersed in water versus temperature (heating rate $10°C\ min^{-1}$). (**e**) Temperature-dependent turbidity measurement curve of an aqueous dispersion of PNIPAM nanorods. Reproduced with permission from Haberkorn et al. [172]. Copyright 2011 Royal Society of Chemistry

4.2 Functionalized Nanoparticles

Nanocarriers have been intensively studied because of their superior properties, such as accessible surface, interaction with cells and proteins, and higher mobility. To improve the versatility of nanocarriers, many researchers have investigated nano-objects, which possess an easily tunable architecture. One valuable approach is the use of nanoparticles that can be tailored with polymer brushes for the design of single-cored hybrid structures [173–180]. The desired polymer brushes can be densely formed on the surface of nanoparticles using the "grafting-to" method to achieve a brush–shell architecture.

As one example, Schmidt and coworkers reported single-cored hybrid magnetic core–shell particles, which can be applied for bioseparation and catalysis [181]. The activated ester-functionalized magnetic particles were fabricated by copolymerization of succinimidyl methacrylate (SIMA) and oligo(ethylene glycol) methyl ether methacrylate (OEGMA) via surface-initiated ATRP (Fig. 10). The ATRP initiator used was [4-(chloromethyl)phenyl]-trimethoxysilane. Further modification with trypsin was conducted to fabricate the magnetic biocatalysts [182]. Trypsin was immobilized on the shell of poly(OEGMA-*co*-SIMA)$_{15}$ magnetic nanoparticles and used to cleave specific peptide bonds. The results showed that *N*-benzoyl-D,L-

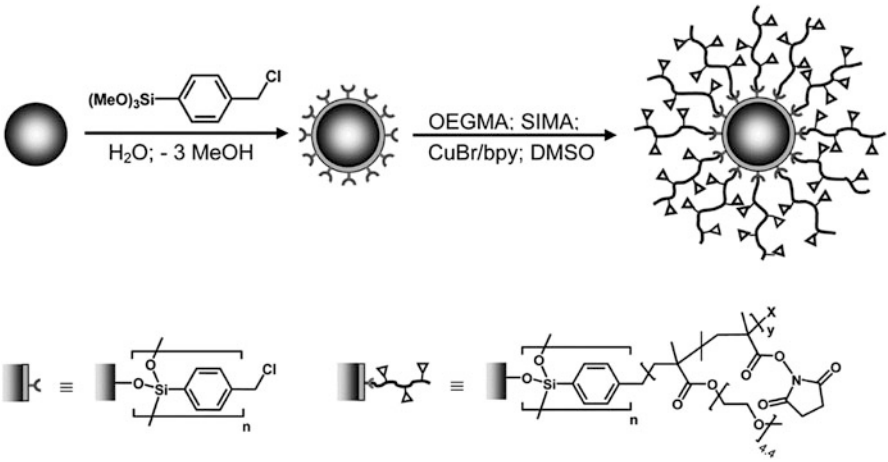

Fig. 10 Synthesis of FeOx–P(OEGMA-*co*-SIMA) magnetic polymer brush particles by surface-initiated ATRP. Reproduced with permission from Gelbrich et al. [181]. Copyright 2010 American Chemical Society

arginine-4-nitroanilide was cleaved by the trypsin-mediated scission and that *p*-nitroaniline was released.

Theato and coworkers reported functionalized gold nanoparticles (AuNPs) suitable for post-modification with amine. AuNPs were prepared by two-phase reduction in ethyl acetate and water. Various disulfides were used as stabilizing ligands for the synthesis of AuNPs and, among the library of ligands, bis(6-hydroxyhexyl) disulfide bis(2-bromoisobutyl) ester and bis(5-carboxypentyl) disulfide bis (pentafluorophenyl) ester resulted in small, narrowly distributed AuNPs [183]. Although AuNPs prepared from the bis(6-hydroxyhexyl) disulfide bis (2-bromoisobutyl) ester allowed grafting-from ATRP, the use of bis (5-carboxypentyl) disulfide bis(pentafluorophenyl) ester resulted in functional AuNPs suitable for post-modification. Key to the successful installation of PFP esters was the two-phase reduction method in ethyl acetate and water, which allowed rapid reduction in water and immediate separation of the formed AuNPs from the reduction media by transfer into the ethyl acetate phase. Amino end-functionalized poly(ethylene oxide) ($M_n = 550$ g/mol) was grafted onto the PFP ester-functionalized AuNPs. Successful grafting could be observed with the naked eye by a complete transfer of the AuNPs from the organic phase into the water phase. With the same method, benzophenone-stabilized gold nanoparticles (Bph-AuNPs) were synthesized by employing a benzophenone-functionalized disulfide [184]. Benzophenone allowed the functionalized AuNPs to react with material containing C–H bonds, under the influence of UV irradiation. Using this technique, polycarbonate–gold core–shell particles were easily prepared by grafting polycarbonate onto AuNPs. Furthermore, Bph-AuNPs could be covalently attached to alkylated silica microspheres or cellulose paper and used for photolithographic surface patterning by selective UV irradiation.

4.3 Functionalized Carbon Nanotubes

Carbon nanotubes (CNTs) have been functionalized frequently and have, for example, found application in DNA detection. Detection of DNA hybridization has received great attention for application in the diagnosis of pathogenic and genetic diseases [185–187]. The rapid recognition of genes expressing a congenital disease is highly demanded. The electrochemical sensing method has been improved to monitor in situ hybridization of DNA in conjunction with various biosensor techniques [188–199]. Nanostructured materials, such as quantum dots, nanoparticles, nanowires, and CNTs have also been extensively researched for biosensing [200–203]. As a new approach for rapid label-free DNA detection, field-effect transistors based on semiconductor CNTs have been introduced [204–207]. A specific DNA molecule can be bound on the surface of a single CNT performing as a conducting channel in transistors, and this binding can perturb the current flow, resulting in a change in the electronic characteristics.

Bokor and coworkers fabricated a CNT transistor array for label-free DNA biosensors [208]. To support specific adsorption between CNTs and DNA, a copolymer containing an activated ester functionality, poly[methyl methacrylate-*co*-poly(ethyleneglycol)methyl methacrylate-*co*-*N*-succinimidyl methacrylate] (abbreviated as NO6), was synthesized and electrostatically immobilized on the CNT transistor array. *N*-Succinimidyl ester groups that composed one part of the copolymer allowed the aminated single-strand DNA sequences to bind covalently onto the surface of CNTs (Fig. 11). After the attachment of DNA, the hysteresis of the I_d–V_g curve was significantly increased as a result of the increase in the charge traps on the CNTs. By measurement of the I_d–V_g curve, DNA hybridization can be easily and rapidly detected.

An alternative approach to functionalized CNTs is direct surface functionalization of CNTs with reactive groups. For example, Theato and coworkers used partly oxidized multiwall CNTs to install PFP esters on the surface, which could be used for further surface functionalization or for use in the reactive LbL assembly of multilayer polymer films. It is worth noting that the obtained thin films were transparent and conductive, making them suitable candidates for solution-processed transparent electrodes [209].

4.4 Functionalized Electrospun Polymer Fibers

Electrospinning is a versatile technique for the preparation of various nanofibers with different morphologies [210]. Various synthetic methodologies, such as in situ polymerization, surface modification, plasma-induced grafting, graft polymerization, blending, and polymer–inorganic composite formation were used to produce nanofibers suitable for numerous applications [211–216]. Recently, surface

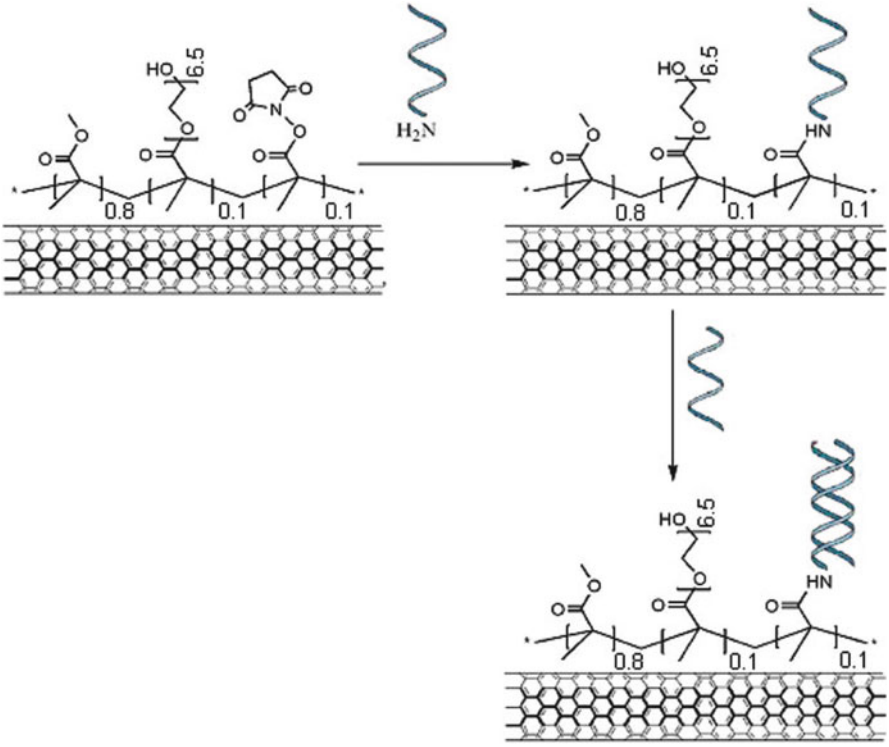

Fig. 11 Bonding of the polymer to single-walled carbon nanotubes (*top right* and *left*) and DNA hybridization (*lower right*). Reproduced with permission from Martinez et al. [208]. Copyright 2009 American Chemical Society

modification by grafting or interfacial polymerization of nanofibers has been explored as a facile method for controlling surface properties.

Theato and coworkers reported a thiol–ene modification of electrospun polybutadiene fibers [217]. A solution of polybutadiene rubber (BR) , in a tetrahydrofuran/*N*,*N*-dimethylformamide solvent mixture containing photo-initiator and crosslinker, was electrospun into a methanol solution containing 1% sodium chloride, with in situ UV irradiation to induce crosslinking. The resulting BR fibers were collected from the methanol bath and washed to remove excess salt. Afterwards, the BR fibers containing carbon double bonds were modified with 2-mercaptoethanol or thioglycolic acid via thiol–ene click reaction. The contact angles of modified BR fiber mats changed dramatically from 135° to 0° after modification, which confirmed that the modification was successfully conducted.

5 Conclusions and Outlook

Post-polymerization modification methods are facile and efficient ways to produce diverse multifunctional surfaces. They allow the modification of complex surfaces that are not adaptable with conventional polymerization techniques and can improve the complexity of multifunctional surfaces, which can in turn improve technologies for a broad area of study. In this chapter, various types of post-polymerization modification of miscellaneous surfaces were introduced and highlighted by selected examples. We clearly show that the post-polymerization modification approach is rapidly developing and will expand in future. Active research on the fabrication of highly complex structures and the reactivity of post-polymerization modifications are ongoing and will contribute to the development of new applications for which precisely defined functional surfaces are required.

References

1. Azzaroni O (2012) Polymer brushes here, there, and everywhere: recent advances in their practical applications and emerging opportunities in multiple research fields. J Polym Sci A Polym Chem 50:3225–3258
2. Tsujii Y, Ohno K, Yamamoto S, Goto A, Fukuda T (2006) Structure and properties of high-density polymer brushes prepared by surface-initiated living radical polymerization. Adv Polym Sci 197:1–45
3. Olivier A, Meyer F, Raquez JM, Damman P, Dubois P (2012) Surface-initiated controlled polymerization as a convenient method for designing functional polymer brushes: from self-assembled monolayers to patterned surfaces. Prog Polym Sci 37:157–181
4. Barbey R, Lavanant L, Paripovic D, Schuwer N, Sugnaux C, Tugulu S, Klok HA (2009) Polymer brushes via surface-initiated controlled radical polymerization: synthesis, characterization, properties, and applications. Chem Rev 109:5437–5527
5. Chen K, Liang D, Tian J, Shi L, Zhao H (2008) In-situ polymerization at the interfaces of micelles: a "grafting from" method to prepare micelles with mixed coronal chains. J Phys Chem B 112:12612–12617
6. Liu X, Guo S, Mirkin CA (2003) Surface and site-specific ring-opening metathesis polymerization initiated by dip-pen nanolithography. Angew Chem Int Ed Engl 42:4785–4789
7. Senkovskyy V, Khanduyeva N, Komber H, Oertel U, Stamm M, Kuckling D, Kiriy A (2007) Conductive polymer brushes of regioregular head-to-tail poly(3-alkylthiophenes) via catalyst-transfer surface-initiated polycondensation. J Am Chem Soc 129:6626–6632
8. Sontag SK, Marshall N, Locklin J (2009) Formation of conjugated polymer brushes by surface-initiated catalyst-transfer polycondensation. Chem Commun 2009(23):3354–3356. doi: 10.1039/B907264K
9. Tomlinson MR, Genzer J (2003) Formation of surface-grafted copolymer brushes with continuous composition gradients. Chem Commun 2003(12):1350–1351 doi: 10.1039/B303823H
10. Wang X, Tu H, Braun PV, Bohn PW (2006) Length scale heterogeneity in lateral gradients of poly(N-isopropylacrylamide) polymer brushes prepared by surface-initiated atom transfer radical polymerization coupled with in-plane electrochemical potential gradients. Langmuir 22:817–823

11. Zhao B (2004) A combinatorial approach to study solvent-induced self-assembly of mixed poly(methyl methacrylate)/polystyrene brushes on planar silica substrates: effect of relative grafting density. Langmuir 20:11748–11755
12. Edmondson S, Osborne VL, Huck WT (2004) Polymer brushes via surface-initiated polymerizations. Chem Soc Rev 33:14–22
13. Gauthier MA, Gibson MI, Klok HA (2009) Synthesis of functional polymers by post-polymerization modification. Angew Chem Int Ed Engl 48:48–58
14. Boaen NK, Hillmyer MA (2005) Post-polymerization functionalization of polyolefins. Chem Soc Rev 34:267–275
15. Theato P (2008) Synthesis of well-defined polymeric activated esters. J Polym Sci A Polym Chem 46:6677–6687
16. Evans RA (2007) The rise of azide-alkyne 1,3-dipolar 'click' cycloaddition and its application to polymer science and surface modification. Aust J Chem 60:384–395
17. Arnold RM, Patton DL, Popik VV, Locklin J (2014) A dynamic duo: pairing click chemistry and postpolymerization modification to design complex surfaces. Acc Chem Res 47:2999–3008
18. Theato P, Klok H-A (2013) Functional polymers by post-polymerization modification : concepts, guidelines, and applications. Wiley-VCH, Weinheim
19. Milner ST (1991) Polymer brushes. Science 251:905–914
20. Ionov L, Zdyrko B, Sidorenko A, Minko S, Klep V, Luzinov I, Stamm M (2004) Gradient polymer layers by "grafting to" approach. Macromol Rapid Commun 25:360–365
21. Minko S, Patil S, Datsyuk V, Simon F, Eichhorn KJ, Motornov M, Usov D, Tokarev I, Stamm M (2002) Synthesis of adaptive polymer brushes via "grafting to" approach from melt. Langmuir 18:289–296
22. Advincula RC (2004) Polymer brushes: synthesis, characterization, applications. Wiley-VCH, Weinheim
23. Zhao B, Brittain WJ (2000) Polymer brushes: surface-immobilized macromolecules. Prog Polym Sci 25:677–710
24. Brittain WJ, Minko S (2007) A structural definition of polymer brushes. J Polym Sci A Polym Chem 45:3505–3512
25. Iwakura Y, Kurosaki T, Nakabayashi N (1961) Reactive fiber.1. Copolymerization and copolymer of acrylonitrile with glycidyl methacrylate and with glycidyl acrylate. Macromol Chem 44–6:570–590
26. Wong LJ, Sevimli S, Zareie HM, Davis TP, Bulmus V (2010) PEGylated functional nanoparticles from a reactive homopolymer scaffold modified by thiol addition chemistry. Macromolecules 43:5365–5375
27. Henry SM, El-Sayed MEH, Pirie CM, Hoffman AS, Stayton PS (2006) pH-responsive poly (styrene-alt-maleic anhydride) alkylamide copolymers for intracellular drug delivery. Biomacromolecules 7:2407–2414
28. Mansfeld U, Pietsch C, Hoogenboom R, Becer CR, Schubert US (2010) Clickable initiators, monomers and polymers in controlled radical polymerizations – a prospective combination in polymer science. Polym Chem 1:1560–1598
29. Heilmann SM, Rasmussen JK, Krepski LR (2001) Chemistry and technology of 2-alkenyl azlactones. J Polym Sci A Polym Chem 39:3655–3677
30. Kolb HC, Finn MG, Sharpless KB (2001) Click chemistry: diverse chemical function from a few good reactions. Angew Chem Int Ed 40:2004–2021
31. Barner-Kowollik C, Du Prez FE, Espeel P, Hawker CJ, Junkers T, Schlaad H, Van Camp W (2011) "Clicking" polymers or just efficient linking: what is the difference? Angew Chem Int Ed 50:60–62
32. Yang SK, Weck M (2009) Covalent and orthogonal multi-functionalization of terpolymers. Soft Matter 5:582–585
33. Xu JW, Prifti F, Song J (2011) A versatile monomer for preparing well-defined functional polycarbonates and poly(ester-carbonates). Macromolecules 44:2660–2667

34. Pyun J, Kowalewski T, Matyjaszewski K (2003) Synthesis of polymer brushes using atom transfer radical polymerization. Macromol Rapid Commun 24:1043–1059
35. Wu T, Gong P, Szleifer I, Vlcek P, Subr V, Genzer J (2007) Behavior of surface-anchored poly(acrylic acid) brushes with grafting density gradients on solid substrates: 1. Experiment. Macromolecules 40:8756–8764
36. Edmondson S, Huck WTS (2004) Controlled growth and subsequent chemical modification of poly(glycidyl methacrylate) brushes on silicon wafers. J Mater Chem 14:730–734
37. Xu FJ, Zhong SP, Yung LY, Tong YW, Kang ET, Neoh KG (2006) Thermoresponsive comb-shaped copolymer-Si(100) hybrids for accelerated temperature-dependent cell detachment. Biomaterials 27:1236–1245
38. Barbey R, Klok HA (2010) Room temperature, aqueous post-polymerization modification of glycidyl methacrylate-containing polymer brushes prepared via surface-initiated atom transfer radical polymerization. Langmuir 26:18219–18230
39. Li Y, Benicewicz BC (2008) Functionalization of silica nanoparticles via the combination of surface-initiated RAFT polymerization and click reactions. Macromolecules 41:7986–7992
40. Cullen SP, Mandel IC, Gopalan P (2008) Surface-anchored poly(2-vinyl-4,4-dimethyl azlactone) brushes as templates for enzyme immobilization. Langmuir 24:13701–13709
41. Hensarling RM, Rahane SB, LeBlanc AP, Sparks BJ, White EM, Locklin J, Patton DL (2011) Thiol-isocyanate "click" reactions: rapid development of functional polymeric surfaces. Polym Chem 2:88–90
42. Cai T, Neoh KG, Kang ET (2011) Poly(vinylidene fluoride) graft copolymer membranes with "clickable" surfaces and their functionalization. Macromolecules 44:4258–4268
43. Nozaki K, Sato N, Tonomura Y, Yasutomi M, Takaya H, Hiyama T, Matsubara T, Koga N (1997) Mechanistic aspects of the alternating copolymerization of propene with carbon monoxide catalyzed by Pd(II) complexes of unsymmetrical phosphine-phosphite ligands. J Am Chem Soc 119:12779–12795
44. Angiolini L, Caretti D, Mazzocchetti L, Salatelli E, Willem R, Biesemans M (2006) Cross-linked polystyrene resins containing triorganotin-4-vinylbenzoates: assessment of their catalytic activity in transesterification reactions. J Organomet Chem 691:3043–3052
45. Aamer KA, Tew GN (2007) RAFT polymerization of a novel activated ester monomer and conversion to a terpyridine-containing homopolymer. J Polym Sci A Polym Chem 45:5618–5625
46. Orski SV, Fries KH, Sheppard GR, Locklin J (2010) High density scaffolding of functional polymer brushes: surface initiated atom transfer radical polymerization of active esters. Langmuir 26:2136–2143
47. Gunay KA, Schuwer N, Klok HA (2012) Synthesis and post-polymerization modification of poly(pentafluorophenyl methacrylate) brushes. Polym Chem 3:2186–2192
48. Kessler D, Jochum FD, Choi J, Char K, Theato P (2011) Reactive surface coatings based on polysilsesquioxanes: universal method toward light-responsive surfaces. ACS Appl Mater Interfaces 3:124–128
49. Kessler D, Theato P (2009) Reactive surface coatings based on polysilsesquioxanes: defined adjustment of surface wettability. Langmuir 25:14200–14206
50. Eberhardt M, Theato P (2005) RAFT polymerization of pentafluorophenyl methacrylate: preparation of reactive linear diblock copolymer. Macromol Rapid Commun 26:1488–1493
51. Gibson MI, Frohlich E, Klok HA (2009) Postpolymerization modification of poly (pentafluorophenyl methacrylate): synthesis of a diverse water-soluble polymer library. J Polym Sci A Polym Chem 47:4332–4345
52. Eberhardt M, Mruk R, Zentel R, Theato P (2005) Synthesis of pentafluorophenyl(meth) acrylate polymers: new precursor polymers for the synthesis of multifunctional materials. Eur Polym J 41:1569–1575
53. Li CZ, Benicewicz BC (2005) Synthesis of well-defined polymer brushes grafted onto silica nanoparticles via surface reversible addition-fragmentation chain transfer polymerization. Macromolecules 38:5929–5936

54. Ranjan R, Brittain WJ (2008) Synthesis of high density polymer brushes on nanoparticles by combined RAFT polymerization and click chemistry. Macromol Rapid Commun 29:1104–1110
55. De P, Li M, Gondi SR, Sumerlin BS (2008) Temperature-regulated activity of responsive polymer-protein conjugates prepared by grafting-from via RAFT polymerization. J Am Chem Soc 130:11288–11289
56. Kessler D, Teutsch C, Theato P (2008) Synthesis of processable inorganic-organic hybrid polymers based on poly(silsesquioxanes): grafting from polymerization using ATRP. Macromol Chem Phys 209:1437–1446
57. Kessler D, Theato P (2008) Synthesis of functional inorganic-organic hybrid polymers based on poly(silsesquioxanes) and their thin film properties. Macromolecules 41:5237–5244
58. Tiktopulo EI, Bychkova VE, Ricka J, Ptitsyn OB (1994) Cooperativity of the coil-globule transition in a homopolymer – microcalorimetric study of poly(N-isopropylacrylamide). Macromolecules 27:2879–2882
59. Fujishige S, Kubota K, Ando I (1989) Phase-transition of aqueous-solutions of poly (N-isopropylacrylamide) and poly(N-isopropylmethacrylamide). J Phys Chem 93:3311–3313
60. Barbara PF, Rentzepis PM, Brus LE (1980) Photochemical kinetics of salicylidenaniline. J Am Chem Soc 102:2786–2791
61. Thompson BC, Abboud KA, Reynolds JR, Nakatani K, Audebert P (2005) Electrochromic conjugated N-salicylidene-aniline (anil) functionalized pyrrole and 2,5-dithienylpyrrole-based polymers. New J Chem 29:1128–1134
62. Ledbette JW (1966) Spectroscopic evidence for enol imine-keto enamine tautomerism of N-(O- and P-hydroxybenzylidene) anils in solution. J Phys Chem 70:2245
63. Rissing C, Son DY (2009) Application of thiol-Ene chemistry to the preparation of carbosilane-thioether dendrimers. Organometallics 28:3167–3172
64. Samanta S, Locklin J (2008) Formation of photochromic spiropyran polymer brushes via surface-initiated, ring-opening metathesis polymerization: reversible photocontrol of wetting behavior and solvent dependent morphology changes. Langmuir 24:9558–9565
65. Fries K, Samanta S, Orski S, Locklin J (2008) Reversible colorimetric ion sensors based on surface initiated polymerization of photochromic polymers. Chem Commun 2008 (47):6288–6290 doi: 10.1039/B818042C
66. Jochum FD, Theato P (2009) Temperature and light sensitive copolymers containing azobenzene moieties prepared via a polymer analogous reaction. Polymer 50:3079–3085
67. Decher G (1997) Fuzzy nanoassemblies: toward layered polymeric multicomposites. Science 277:1232–1237
68. Bertrand P, Jonas A, Laschewsky A, Legras R (2000) Ultrathin polymer coatings by complexation of polyelectrolytes at interfaces: suitable materials, structure and properties. Macromol Rapid Commun 21:319–348
69. Bergbreiter DE, Liao KS (2009) Covalent layer-by-layer assembly-an effective, forgiving way to construct functional robust ultrathin films and nanocomposites. Soft Matter 5:23–28
70. Buck ME, Zhang J, Lynn DM (2007) Layer-by-layer assembly of reactive ultrathin films mediated by click-type reactions of poly(2-alkenyl azlactone)s. Adv Mater 19:3951–3955
71. Peyratout CS, Dahne L (2004) Tailor-made polyelectrolyte microcapsules: from multilayers to smart containers. Angew Chem Int Ed 43:3762–3783
72. Tang ZY, Wang Y, Podsiadlo P, Kotov NA (2006) Biomedical applications of layer-by-layer assembly: from biomimetics to tissue engineering. Adv Mater 18:3203–3224
73. Boudou T, Crouzier T, Ren KF, Blin G, Picart C (2010) Multiple functionalities of polyelectrolyte multilayer films: new biomedical applications. Adv Mater 22:441–467
74. Buck ME, Lynn DM (2011) Layer-by-layer fabrication of covalently crosslinked and reactive polymer multilayers using azlactone-functionalized copolymers: a platform for the design of functional biointerfaces. Adv Eng Mater 13:B343–B352
75. Buck ME, Breitbach AS, Belgrade SK, Blackwell HE, Lynn DM (2009) Chemical modification of reactive multilayered films fabricated from poly(2-alkenyl azlactone)s: design of

surfaces that prevent or promote mammalian cell adhesion and bacterial biofilm growth. Biomacromolecules 10:1564–1574
76. Buck ME, Lynn DM (2010) Reactive layer-by-layer assembly of suspended thin films and semipermeable membranes at interfaces created between aqueous and organic phases. Adv Mater 22:994–998
77. Buck ME, Lynn DM (2010) Functionalization of fibers using azlactone-containing polymers: layer-by-layer fabrication of reactive thin films on the surfaces of hair and cellulose-based materials. ACS Appl Mater Interfaces 2:1421–1429
78. Buck ME, Lynn DM (2010) Free-standing and reactive thin films fabricated by covalent layer-by-layer assembly and subsequent lift-off of azlactone-containing polymer multilayers. Langmuir 26:16134–16140
79. Buck ME, Schwartz SC, Lynn DM (2010) Superhydrophobic thin films fabricated by reactive layer-by-layer assembly of azlactone-functionalized polymers. Chem Mater 22:6319–6327
80. Kinsinger MI, Buck ME, Abbott NL, Lynn DM (2010) Immobilization of polymer-decorated liquid crystal droplets on chemically tailored surfaces. Langmuir 26:10234–10242
81. Broderick AH, Azarin SM, Buck ME, Palecek SP, Lynn DM (2011) Fabrication and selective functionalization of amine-reactive polymer multi layers on topographically patterned microwell cell culture arrays. Biomacromolecules 12:1998–2007
82. Saurer EM, Flessner RM, Buck ME, Lynn DM (2011) Fabrication of covalently crosslinked and amine-reactive microcapsules by reactive layer-by-layer assembly of azlactone-containing polymer multilayers on sacrificial microparticle templates. J Mater Chem 21:1736–1745
83. Such GK, Quinn JF, Quinn A, Tjipto E, Caruso F (2006) Assembly of ultrathin polymer multilayer films by click chemistry. J Am Chem Soc 128:9318–9319
84. Kinnane CR, Such GK, Caruso F (2011) Tuning the properties of layer-by-layer assembled poly(acrylic acid) click films and capsules. Macromolecules 44:1194–1202
85. Tang YC, Liu GM, Yu CQ, Wei XL, Zhang GZ (2008) Chemical oscillation induced periodic swelling and shrinking of a polymeric multilayer investigated with a quartz crystal microbalance. Langmuir 24:8929–8933
86. Such GK, Tjipto E, Postma A, Johnston APR, Caruso F (2007) Ultrathin, responsive polymer click capsules. Nano Lett 7:1706–1710
87. Bergbreiter DE, Chance BS (2007) "Click"-based covalent layer-by-layer assembly on polyethylene using water-soluble polymeric reagents. Macromolecules 40:5337–5343
88. Huang CJ, Chang FC (2009) Using click chemistry to fabricate ultrathin thermoresponsive microcapsules through direct covalent layer-by-layer assembly. Macromolecules 42:5155–5166
89. Vestberg R, Malkoch M, Kade M, Wu P, Fokin VV, Sharpless KB, Drockenmuller E, Hawker CJ (2007) Role of architecture and molecular weight in the formation of tailor-made ultrathin multilayers using dendritic macromolecules and click chemistry. J Polym Sci A Polym Chem 45:2835–2846
90. El Haitami AE, Thomann JS, Jierry L, Parat A, Voegel JC, Schaaf P, Senger B, Boulmedais F, Frisch B (2010) Covalent layer-by-layer assemblies of polyelectrolytes and homobifunctional spacers. Langmuir 26:12351–12357
91. Jierry L, Ben Ameur N, Thomann JS, Frisch B, Gonthier E, Voegel JC, Senger B, Decher G, Felix O, Schaaf P, Mesini P, Boulmedais F (2010) Influence of Cu(I)-alkyne pi-complex charge on the step-by-step film buildup through sharpless click reaction. Macromolecules 43:3994–3997
92. De Geest BG, Van Camp W, Du Prez FE, De Smedt SC, Demeester J, Hennink WE (2008) Degradable multilayer films and hollow capsules via a 'click' strategy. Macromol Rapid Commun 29:1111–1118
93. Ochs CJ, Such GK, Stadler B, Caruso F (2008) Low-fouling, biofunctionalized, and biodegradable click capsules. Biomacromolecules 9:3389–3396

94. Zhang Y, He H, Gao C, Wu JY (2009) Covalent layer-by-layer functionalization of multiwalled carbon nanotubes by click chemistry. Langmuir 25:5814–5824
95. Rydzek G, Thomann JS, Ben Ameur N, Jierry L, Mesini P, Ponche A, Contal C, El Haitami AE, Voegel JC, Senger B, Schaaf P, Frisch B, Boulmedais F (2010) Polymer multilayer films obtained by electrochemically catalyzed click chemistry. Langmuir 26:2816–2824
96. Seo J, Schattling P, Lang T, Jochum F, Nilles K, Theato P, Char K (2010) Covalently bonded layer-by-layer assembly of multifunctional thin films based on activated esters. Langmuir 26:1830–1836
97. Arnold RM, Huddleston NE, Locklin J (2012) Utilizing click chemistry to design functional interfaces through post-polymerization modification. J Mater Chem 22:19357–19365
98. Orski SV, Fries KH, Sontag SK, Locklin J (2011) Fabrication of nanostructures using polymer brushes. J Mater Chem 21:14135–14149
99. Orski SV, Poloukhtine AA, Arumugam S, Mao LD, Popik VV, Locklin J (2010) High density orthogonal surface immobilization via photoactivated copper-free click chemistry. J Am Chem Soc 132:11024–11026
100. Arnold RM, Locklin J (2013) Self-sorting click reactions that generate spatially controlled chemical functionality on surfaces. Langmuir 29:5920–5926
101. Arnold RM, McNitt CD, Popik VV, Locklin J (2014) Direct grafting of poly (pentafluorophenyl acrylate) onto oxides: versatile substrates for reactive microcapillary printing and self-sorting modification. Chem Commun 50:5307–5309
102. Hensarling RM, Doughty VA, Chan JW, Patton DL (2009) "Clicking" polymer brushes with thiol-yne chemistry: indoors and out. J Am Chem Soc 131:14673–14675
103. Hensarling RM, Hoff EA, LeBlanc AP, Guo W, Rahane SB, Patton DL (2013) Photocaged pendent thiol polymer brush surfaces for postpolymerization modifications via thiol-click chemistry. J Polym Sci A Polym Chem 51:1079–1090
104. Bally F, Cheng K, Nandivada H, Deng XP, Ross AM, Panades A, Lahann J (2013) Co-immobilization of biomolecules on ultrathin reactive chemical vapor deposition coatings using multiple click chemistry strategies. ACS Appl Mater Interfaces 5:9262–9268
105. Spruell JM, Wolffs M, Leibfarth FA, Stahl BC, Heo JH, Connal LA, Hu J, Hawker CJ (2011) Reactive, multifunctional polymer films through thermal cross-linking of orthogonal click groups. J Am Chem Soc 133:16698–16706
106. Rahane SB, Hensarling RM, Sparks BJ, Stafford CM, Patton DL (2012) Synthesis of multifunctional polymer brush surfaces via sequential and orthogonal thiol-click reactions. J Mater Chem 22:932–943
107. Diamanti S, Arifuzzaman S, Elsen A, Genzer J, Vaia RA (2008) Reactive patterning via post-functionalization of polymer brushes utilizing disuccinimidyl carbonate activation to couple primary amines. Polymer 49:3770–3779
108. Slater MD, Frechet JMJ, Svec F (2009) In-column preparation of a brush-type chiral stationary phase using click chemistry and a silica monolith. J Sep Sci 32:21–28
109. Chen Y, Wu M, Wang K, Chen B, Yao S, Zou H, Nie L (2011) Vinyl functionalized silica hybrid monolith-based trypsin microreactor for on line digestion and separation via thiol-ene "click" strategy. J Chromatogr A 1218:7982–7988
110. Wang K, Chen Y, Yang H, Li Y, Nie L, Yao S (2012) Modification of VTMS hybrid monolith via thiol-ene click chemistry for capillary electrochromatography. Talanta 91:52–59
111. Yang HH, Chen YZ, Liu YX, Nie LH, Yao SZ (2013) One-pot synthesis of (3-sulfopropyl methacrylate potassium)-silica hybrid monolith via thiol-ene click chemistry for CEC. Electrophoresis 34:510–517
112. Fournier D, Pascual S, Montembault V, Haddleton DM, Fontaine L (2006) Well-defined azlactone-functionalized (Co)polymers on a solid support: synthesis via supported living radical polymerization and application as nucleophile scavengers. J Comb Chem 8:522–530
113. Tripp JA, Stein JA, Svec F, Frechet JMJ (2000) "Reactive filtration": use of functionalized porous polymer monoliths as scavengers in solution-phase synthesis. Org Lett 2:195–198

114. Tripp JA, Svec F, Frechet JMJ (2001) Grafted macroporous polymer monolithic disks: a new format of scavengers for solution-phase combinatorial chemistry. J Comb Chem 3:216–223
115. Lucchesi C, Pascual S, Dujardin G, Fontaine L (2008) New functionalized polyHIPE materials used as amine scavengers in batch and flow-through processes. React Funct Polym 68:97–102
116. Guyomard A, Fournier D, Pascual S, Fontaine L, Bardeau JF (2004) Preparation and characterization of azlactone functionalized polymer supports and their application as scavengers. Eur Polym J 40:2343–2348
117. Lucchesi C, Pascual S, Jouanneaux A, Dujardin G, Fontaine L (2007) Tuning the parameters of the suspension polymerization of styrene, divinylbenzene, and N-(p-vinylbenzyl)-4,4-dimethylazlactone. J Polym Sci A Polym Chem 45:3677–3686
118. Dao TTH, Guerrouache M, Carbonnier B (2012) Thiol-yne click adamantane monolithic stationary phase for capillary electrochromatography. Chin J Chem 30:2281–2284
119. Preinerstorfer B, Bicker W, Lindner W, Lammerhofer M (2004) Development of reactive thiol-modified monolithic capillaries and in-column surface functionalization by radical addition of a chromatographic ligand for capillary electrochromatography. J Chromatogr A 1044:187–199
120. Lv Y, Hughes TC, Hao X, Hart NK, Littler SW, Zhang X, Tan T (2010) A novel route to prepare highly reactive and versatile chromatographic monoliths. Macromol Rapid Commun 31:1785–1790
121. Lv Y, Lin Z, Svec F (2012) "Thiol-ene" click chemistry: a facile and versatile route for the functionalization of porous polymer monoliths. Analyst 137:4114–4118
122. Tijunelyte I, Babinot J, Guerrouache M, Valincius G, Carbonnier B (2012) Hydrophilic monolith with ethylene glycol-based grafts prepared via surface confined thiol-ene click photoaddition. Polymer 53:29–36
123. Sun XL, Lin D, He XW, Chen LX, Zhang YK (2010) A facile and efficient strategy for one-step in situ preparation of hydrophobic organic monolithic stationary phases by click chemistry and its application on protein separation. Talanta 82:404–408
124. Sun XL, He XW, Chen LX, Zhang YK (2011) In-column "click" preparation of hydrophobic organic monolithic stationary phases for protein separation. Anal Bioanal Chem 399:3407–3413
125. Salwinski A, Roy V, Agrofoglio LA, Delepee R (2011) In situ one-step method for synthesis of "click"-functionalized monolithic stationary phase for capillary electrochromatography. Macromol Chem Phys 212:2700–2707
126. Xie SF, Svec F, Frechet JMJ (1999) Design of reactive porous polymer supports for high throughput bioreactors: poly(2-vinyl-4,4-dimethylazlactone-co-acrylamide-co-ethyl dimethacrylate) monoliths. Biotechnol Bioeng 62:30–35
127. Peterson DS, Rohr T, Svec F, Frechet JMJ (2002) Enzymatic microreactor-on-a-chip: protein mapping using trypsin immobilized on porous polymer monoliths molded in channels of microfluidic devices. Anal Chem 74:4081–4088
128. Peterson DS, Rohr T, Svec F, Frechet JMJ (2003) Dual-function microanalytical device by in situ photolithographic grafting of porous polymer monolith: integrating solid-phase extraction and enzymatic digestion for peptide mass mapping. Anal Chem 75:5328–5335
129. Geiser L, Eeltink S, Svec F, Frechet JMJ (2008) In-line system containing porous polymer monoliths for protein digestion with immobilized pepsin, peptide preconcentration and nano-liquid chromatography separation coupled to electrospray ionization mass spectroscopy. J Chromatogr A 1188:88–96
130. Logan TC, Clark DS, Stachowiak TB, Svec F, Frechet JMJ (2007) Photopatterning enzymes on polymer monoliths in microfluidic devices for steady-state kinetic analysis and spatially separated multi-enzyme reactions. Anal Chem 79:6592–6598
131. Ekstrom S, Onnerfjord P, Nilsson J, Bengtsson M, Laurell T, Marko-Varga G (2000) Integrated microanalytical technology enabling rapid and automated protein identification. Anal Chem 72:286–293

132. Lazar IM, Ramsey RS, Ramsey JM (2001) On-chip proteolytic digestion and analysis using "wrong-way-round" electrospray time-of-flight mass spectrometry. Anal Chem 73:1733–1739
133. Krenkova J, Svec F (2009) Less common applications of monoliths: IV. Recent developments in immobilized enzyme reactors for proteomics and biotechnology. J Sep Sci 32:706–718
134. Chen HX, Huang T, Zhang XX (2009) Immunoaffinity extraction of testosterone by antibody immobilized monolithic capillary with on-line laser-induced fluorescence detection. Talanta 78:259–264
135. Connolly D, O'Shea V, Clark P, O'Connor B, Paull B (2007) Evaluation of photografted charged sites within polymer monoliths in capillary columns using contactless conductivity detection. J Sep Sci 30:3060–3068
136. Kircher L, Theato P, Cameron NR (2013) Reactive thiol-ene emulsion-templated porous polymers incorporating pentafluorophenyl acrylate. Polymer 54:1755–1761
137. Pelton R (2009) Bioactive paper provides a low-cost platform for diagnostics. Trends Analyt Chem 28:925–942
138. Martinez AW, Phillips ST, Butte MJ, Whitesides GM (2007) Patterned paper as a platform for inexpensive, low-volume, portable bioassays. Angew Chem Int Ed 46:1318–1320
139. Tiller JC, Rieseler R, Berlin P, Klemm D (2002) Stabilization of activity of oxidoreductases by their immobilization onto special functionalized glass and novel aminocellulose film using different coupling reagents. Biomacromolecules 3:1021–1029
140. Turner MB, Spear SK, Holbrey JD, Daly DT, Rogers RD (2005) Ionic liquid-reconstituted cellulose composites as solid support matrices for biocatalyst immobilization. Biomacromolecules 6:2497–2502
141. Boese BJ, Breaker RR (2007) In vitro selection and characterization of cellulose-binding DNA aptamers. Nucleic Acids Res 35:6378–6388
142. Pelegrin M, Marin M, Noel D, Del Rio M, Saller R, Stange J, Mitzner S, Gunzburg WH, Piechaczyk M (1998) Systemic long-term delivery of antibodies in immunocompetent animals using cellulose sulphate capsules containing antibody-producing cells. Gene Ther 5:828–834
143. Ali MM, Aguirre SD, Xu YQ, Filipe CDM, Pelton R, Li YF (2009) Detection of DNA using bioactive paper strips. Chem Commun 2009(43):6640–6642 doi: 10.1039/B911559E
144. Kadla JF, Asfour FH, Bar-Nir B (2007) Micropatterned thin film honeycomb materials from regiospecifically modified cellulose. Biomacromolecules 8:161–165
145. Xu WZ, Zhang X, Kadla JF (2012) Design of functionalized cellulosic honeycomb films: site-specific biomolecule modification via "click chemistry". Biomacromolecules 13:350–357
146. Kolb HC, Sharpless KB (2003) The growing impact of click chemistry on drug discovery. Drug Discov Today 8:1128–1137
147. Bryan MC, Fazio F, Lee HK, Huang CY, Chang A, Best MD, Calarese DA, Blixt O, Paulson JC, Burton D, Wilson IA, Wong CH (2004) Covalent display of oligosaccharide arrays in microtiter plates. J Am Chem Soc 126:8640–8641
148. Wang Q, Chan TR, Hilgraf R, Fokin VV, Sharpless KB, Finn MG (2003) Bioconjugation by copper(I)-catalyzed azide-alkyne [3 + 2] cycloaddition. J Am Chem Soc 125:3192–3193
149. Link AJ, Tirrell DA (2003) Cell surface labeling of Escherichia coli via copper(I)-catalyzed [3 + 2] cycloaddition. J Am Chem Soc 125:11164–11165
150. Lee W, Park SJ (2014) Porous anodic aluminum oxide: anodization and templated synthesis of functional nanostructures. Chem Rev 114:7487–7556
151. Liakos IL, Newman RC, McAlpine E, Alexander MR (2004) Comparative study of self-assembly of a range of monofunctional aliphatic molecules on magnetron-sputtered aluminium. Surf Interface Anal 36:347–354
152. Chen YF, Hu YH, Chou YI, Lai SM, Wang CC (2010) Surface modification of nano-porous anodic alumina membranes and its use in electroosmotic flow. Sens Actuat B Chem 145:575–582

153. Sugnaux C, Lavanant L, Klok HA (2013) Aqueous fabrication of pH-gated, polymer-brush-modified alumina hybrid membranes. Langmuir 29:7325–7333
154. Aryal M, Trivedi K, Hu WW (2009) Nano-confinement induced chain alignment in ordered P3HT nanostructures defined by nanoimprint lithography. ACS Nano 3:3085–3090
155. Haberkorn N, Lechmann MC, Sohn BH, Char K, Gutmann JS, Theato P (2009) Templated organic and hybrid materials for optoelectronic applications. Macromol Rapid Commun 30:1146–1166
156. Gitsas A, Yameen B, Lazzara TD, Steinhart M, Duran H, Knoll W (2010) Polycyanurate nanorod arrays for optical-waveguide-based biosensing. Nano Lett 10:2173–2177
157. Steinhart M, Jia ZH, Schaper AK, Wehrspohn RB, Gosele U, Wendorff JH (2003) Palladium nanotubes with tailored wall morphologies. Adv Mater 15:706–709
158. Dersch R, Steinhart M, Boudriot U, Greiner A, Wendorff JH (2005) Nanoprocessing of polymers: applications in medicine, sensors, catalysis, photonics. Polym Adv Technol 16:276–282
159. Greiner A, Wendorff JH, Yarin AL, Zussman E (2006) Biohybrid nanosystems with polymer nanofibers and nanotubes. Appl Microbiol Biotechnol 71:387–393
160. Hulteen JC, Martin CR (1997) A general template-based method for the preparation of nanomaterials. J Mater Chem 7:1075–1087
161. Huczko A (2000) Template-based synthesis of nanomaterials. Appl Phys A Mater Sci Process 70:365–376
162. Li AP, Muller F, Birner A, Nielsch K, Gosele U (1998) Hexagonal pore arrays with a 50–420 nm interpore distance formed by self-organization in anodic alumina. J Appl Phys 84:6023–6026
163. Ono S, Saito M, Ishiguro M, Asoh H (2004) Controlling factor of self-ordering of anodic porous alumina. J Electrochem Soc 151:B473–B478
164. Masuda H, Fukuda K (1995) Ordered metal nanohole arrays made by a 2-step replication of honeycomb structures of anodic alumina. Science 268:1466–1468
165. Masuda H, Yamada H, Satoh M, Asoh H, Nakao M, Tamamura T (1997) Highly ordered nanochannel-array architecture in anodic alumina. Appl Phys Lett 71:2770–2772
166. Cepak VM, Martin CR (1999) Preparation of polymeric micro- and nanostructures using a template-based deposition method. Chem Mater 11:1363–1367
167. Steinhart M, Wehrspohn RB, Gosele U, Wendorff JH (2004) Nanotubes by template wetting: a modular assembly system. Angew Chem Int Ed 43:1334–1344
168. Steinhart M, Wendorff JH, Wehrspohn RB (2003) Nanotubes a la carte: wetting of porous templates. ChemPhysChem 4:1171–1176
169. Schlitt S, Greiner A, Wendorff JH (2008) Cylindrical polymer nanostructures by solution template wetting. Macromolecules 41:3228–3234
170. Al-Kaysi RO, Ghaddar TH, Guirado G (2009) Fabrication of one-dimensional organic nanostructures using anodic aluminum oxide templates. J Nanomater 2009:1–4
171. Zhang MF, Dobriyal P, Chen JT, Russell TP, Olmo J, Merry A (2006) Wetting transition in cylindrical alumina nanopores with polymer melts. Nano Lett 6:1075–1079
172. Haberkorn N, Nilles K, Schattling P, Theato P (2011) Reactive nanorods based on activated ester polymers: a versatile template-assisted approach for the fabrication of functional nanorods. Polym Chem 2:645–650
173. Lai JJ, Hoffman JM, Ebara M, Hoffman AS, Estournes C, Wattiaux A, Stayton PS (2007) Dual magnetic-/temperature-responsive nanoparticles for microfluidic separations and assays. Langmuir 23:7385–7391
174. Perruchot C, Khan MA, Kamitsi A, Armes SP, von Werne T, Patten TE (2001) Synthesis of well-defined, polymer-grafted silica particles by aqueous ATRP. Langmuir 17:4479–4481
175. Chen XY, Randall DP, Perruchot C, Watts JF, Patten TE, von Werne T, Armes SP (2003) Synthesis and aqueous solution properties of polyelectrolyte-grafted silica particles prepared by surface-initiated atom transfer radical polymerization. J Colloid Interface Sci 257:56–64

176. Li DJ, Sheng X, Zhao B (2005) Environmentally responsive "Hairy" nanoparticles: mixed homopolymer brushes on silica nanoparticles synthesized by living radical polymerization techniques. J Am Chem Soc 127:6248–6256
177. Li DJ, Jones GL, Dunlap JR, Hua FJ, Zhao B (2006) Thermosensitive hairy hybrid nanoparticles synthesized by surface-initiated atom transfer radical polymerization. Langmuir 22:3344–3351
178. Schmidt AM (2005) The synthesis of magnetic core-shell nanoparticles by surface-initiatied ring-opening polymerization of epsilon-Caprolactone. Macromol Rapid Commun 26:93–97
179. Gelbrich T, Feyen M, Schmidt AM (2006) Magnetic thermoresponsive core-shell nanoparticles. Macromolecules 39:3469–3472
180. Kaiser A, Gelbrich T, Schmidt AM (2006) Thermosensitive magnetic fluids. J Phys Condens Matter 18:S2563–S2580
181. Gelbrich T, Reinartz M, Schmidt AM (2010) Active ester functional single core magnetic nanostructures as a versatile immobilization matrix for effective bioseparation and catalysis. Biomacromolecules 11:635–642
182. Erlanger BF, Kokowsky N, Cohen W (1961) The preparation and properties of two new chromogenic substrates of trypsin. Arch Biochem Biophys 95:271–278
183. Roth PJ, Theato P (2008) Versatile synthesis of functional gold nanoparticles: grafting polymers from and onto. Chem Mater 20:1614–1621
184. Roth PJ, Theato P (2012) Covalent attachment of gold nanoparticles to surfaces and polymeric substrates using UV light. Macromol Chem Phys 213:2550–2556
185. Castaneda MT, Merkoci A, Pumera M, Alegret S (2007) Electrochemical genosensors for biomedical applications based on gold nanoparticles. Biosens Bioelectron 22:1961–1967
186. Palecek E, Jelen F (2002) Electrochemistry of nucleic acids and development of DNA sensors. Crit Rev Anal Chem 32:261–270
187. Wang J, Polsky R, Merkoci A, Turner KL (2003) "Electroactive beads" for ultrasensitive DNA detection. Langmuir 19:989–991
188. Grieshaber D, MacKenzie R, Voros J, Reimhult E (2008) Electrochemical biosensors - sensor principles and architectures. Sensors 8:1400–1458
189. Bearinger JP, Voros J, Hubbell JA, Textor M (2003) Electrochemical optical waveguide lightmode spectroscopy (EC-OWLS): a pilot study using evanescent-field optical sensing under voltage control to monitor polycationic polymer adsorption onto indium tin oxide (ITO)-coated waveguide chips. Biotechnol Bioeng 82:465–473
190. Brusatori MA, Van Tassel PR (2003) Biosensing under an applied voltage using optical waveguide lightmode spectroscopy. Biosens Bioelectron 18:1269–1277
191. Yu Y, Jin G (2005) Influence of electrostatic interaction on fibrinogen adsorption on gold studied by imaging ellipsometry combined with electrochemical methods. J Colloid Interface Sci 283:477–481
192. Sun P, Laforge FO, Mirkin MV (2007) Scanning electrochemical microscopy in the 21st century. Phys Chem Chem Phys 9:802–823
193. Edwards MA, Martin S, Whitworth AL, Macpherson JV, Unwin PR (2006) Scanning electrochemical microscopy: principles and applications to biophysical systems. Physiol Meas 27:R63–R108
194. Fortin E, Defontaine Y, Mailley P, Livache T, Szunerits S (2005) Micro-imprinting of oligonucleotides and oligonucleotide gradients on gold surfaces: a new approach based on the combination of scanning electrochemical microscopy and surface plasmon resonance imaging (SECM/SPR-i). Electroanalysis 17:495–503
195. Xiang CH, Xie QJ, Hu JM, Yao S (2005) Symmetric current oscillations at tip and substrate electrodes of scanning electrochemical microscope during silver deposition/stripping. J Electroanal Chem 584:201–209
196. Boldt FM, Heinze J, Diez M, Petersen J, Borsch M (2004) Real-time pH microscopy down to the molecular level by combined scanning electrochemical microscopy/single-molecule fluorescence spectroscopy. Anal Chem 76:3473–3481

197. Shi GD, Garfias-Mesias LF, Smyrl WH (1998) Preparation of a gold-sputtered optical fiber as a microelectrode for electrochemical microscopy. J Electrochem Soc 145:2011–2016
198. Fan FRF, Cliffel D, Bard AJ (1998) Scanning electrochemical microscopy. 37. Light emission by electrogenerated chemiluminescence at SECM tips and their application to scanning optical microscopy. Anal Chem 70:2941–2948
199. Amemiya S, Guo JD, Xiong H, Gross DA (2006) Biological applications of scanning electrochemical microscopy: chemical imaging of single living cells and beyond. Anal Bioanal Chem 386:458–471
200. Michalet X, Pinaud FF, Bentolila LA, Tsay JM, Doose S, Li JJ, Sundaresan G, Wu AM, Gambhir SS, Weiss S (2005) Quantum dots for live cells, in vivo imaging, and diagnostics. Science 307:538–544
201. Reinhard BM, Siu M, Agarwal H, Alivisatos AP, Liphardt J (2005) Calibration of dynamic molecular rule based on plasmon coupling between gold nanoparticles. Nano Lett 5:2246–2252
202. Bunimovich YL, Shin YS, Yeo WS, Amori M, Kwong G, Heath JR (2006) Quantitative real-time measurements of DNA hybridization with alkylated nonoxidized silicon nanowires in electrolyte solution. J Am Chem Soc 128:16323–16331
203. Tans SJ, Verschueren ARM, Dekker C (1998) Room-temperature transistor based on a single carbon nanotube. Nature 393:49–52
204. Avouris P (2004) Carbon nanotube electronics and optoelectronics. MRS Bull 29:403–410
205. Martel R, Schmidt T, Shea HR, Hertel T, Avouris P (1998) Single- and multi-wall carbon nanotube field-effect transistors. Appl Phys Lett 73:2447–2449
206. Chen ZH, Appenzeller J, Lin YM, Sippel-Oakley J, Rinzler AG, Tang JY, Wind SJ, Solomon PM, Avouris P (2006) An integrated logic circuit assembled on a single carbon nanotube. Science 311:1735
207. Yang WR, Thordarson P, Gooding JJ, Ringer SP, Braet F (2007) Carbon nanotubes for biological and biomedical applications. Nanotechnology 18:1–12
208. Martinez MT, Tseng YC, Ormategui N, Loinaz I, Eritja R, Bokor J (2009) Label-free DNA biosensors based on functionalized carbon nanotube field effect transistors. Nano Lett 9:530–536
209. Park HJ, Kim J, Chang JY, Theato P (2008) Preparation of transparent conductive multilayered films using active pentafluorophenyl ester modified multiwalled carbon nanotubes. Langmuir 24:10467–10473
210. Nasreen SA, Sundarrajan S, Nizar SA, Balamurugan R, Ramakrishna S (2013) Advancement in electrospun nanofibrous membranes modification and their application in water treatment. Membranes (Basel) 3:266–284
211. Li LC, Wang BG, Tan HM, Chen TL, Xu JP (2006) A novel nanofiltration membrane prepared with PAMAM and TMC by in situ interfacial polymerization on PEK-C ultrafiltration membrane. J Membr Sci 269:84–93
212. You H, Li X, Yang Y, Wang BY, Li ZX, Wang XF, Zhu MF, Hsiao BS (2013) High flux low pressure thin film nanocomposite ultrafiltration membranes based on nanofibrous substrates. Sep Purif Technol 108:143–151
213. Aerts S, Vanhulsel A, Buekenhoudt A, Weyten H, Kuypers S, Chen H, Bryjak M, Gevers LEM, Vankelecom IFJ, Jacobs PA (2006) Plasma-treated PDMS-membranes in solvent resistant nanofiltration: characterization and study of transport mechanism. J Membr Sci 275:212–219
214. Deng B, Yang XX, Xie LD, Li JY, Hou ZC, Yao S, Liang GM, Sheng KL, Huang Q (2009) Microfiltration membranes with pH dependent property prepared from poly(methacrylic acid) grafted polyethersulfone powder. J Membr Sci 330:363–368
215. Zhang PY, Xu ZL, Yang H, Wei YM, Wu WZ, Chen DG (2013) Preparation and characterization of PVDF-P(PEGMA-r-MMA) ultrafiltration blend membranes via simplified blend method. Desalination 319:47–59

216. Kango S, Kalia S, Celli A, Njuguna J, Habibi Y, Kumar R (2013) Surface modification of inorganic nanoparticles for development of organic-inorganic nanocomposites – a review. Prog Polym Sci 38:1232–1261
217. Thielke MW, Bruckner EP, Wong DL, Theato P (2014) Thiol-ene modification of electrospun polybutadiene fibers crosslinked by UV irradiation. Polymer 55:5596–5599

Adv Polym Sci (2016) 270: 193–220
DOI: 10.1007/12_2015_314

Published online: 6 May 2015

Nanocomposites and Self-Assembled Structures via Controlled Radical Polymerization

Christian Rossner and Philipp Vana

Abstract We report recent findings on the formation of nanocomposites and self-assembled hybrid nanoarchitectures, in which controlled radical polymerization plays a key role. Specifically, we address how macromolecular design via these controlled methods can be used to flexibly guide the formation of hybrid nanoarchitectures in a rational and predetermined fashion. To this end, the role of polymeric architecture in tuning polymer/inorganic nanocomposite structures is examined.

Keywords Nanoparticles · Phase separation · Polymeric architecture · Reversible-deactivation radical polymerization · Self-assembly

Contents

C. Rossner and P. Vana (✉)
Institut für Physikalische Chemie, Georg-August-Universität Göttingen, Tammannstrasse 6, 37077 Göttingen, Germany
e-mail: pvana@uni-goettingen.de

Abbreviations

AFM	Atomic force microscopy
AgNP	Silver nanoparticle
ATRP	Atom-transfer radical polymerization
AuNP	Gold nanoparticle
CPB	Concentrated polymer brush
DC	Daoud−Cotton
DEGEMA	Diethyleneglycol ethylmethacrylate
DEGMMA	Diethylenegylcol methylmethacrylate
DLS	Dynamic light scattering
DMAEMA	*N*,*N*-Diemthylaminoethyl methacrylate
DMF	*N*,*N*-Dimethylformamide
DMSO	Dimethylsulfoxide
GMA	Glycidyl methacrylate
HBP	Hyperbranched polymer
IONP	Iron oxide nanoparticle
LAMP	Lipoic acid 2-hydroxy-3-(methacryloyloxy)-propyl ester
LCST	Lower critical solution temperature
MPC	2-(Methacryloyloxy)ethyl phosphorylcholine
NMR	Nuclear magnetic resonance
NMRP	Nitroxide-mediated radical polymerization
NP	Nanoparticle
PDMAEMA	Poly(*N*,*N*-diemthylaminoethyl methacrylate)
PdNP	Palladium nanoparticle
PEG	Poly(ethylene glycol)
PEO	Poly(ethylene oxide)
PGMA	Poly(glycidyl methacrylate)
PMAA	Poly(methacrylic acid)
PMMA	Poly(methyl methacrylate)
PMPC	Poly(2-(methacryloyloxy)ethyl phosphorylcholine)
PN^{i}PAAM	Poly(*N*-isopropylacrylamide)
POEGMA	Poly(oligo(ethylene glycol) methacrylate)
PS	Polystyrene
PVP	Poly(vinylpyridine)
RAFT	Reversible addition−fragmentation chain transfer
RDRP	Reversible-deactivation radical polymerization
SAXS	Small-angle X-ray scattering
SDPB	Semidilute polymer brush
SEC	Size-exclusion chromatography
SI	Surface-initiated
SiNP	Silica nanoparticle
stat	Statistical
TEM	Transmission electron microscopy

THF	Tetrahydrofuran
TTC	Trithiocarbonate

1 Introduction

Inorganic nanoparticles (NPs) have been recognized as building units for the construction of materials that take advantage of the specific properties of NPs [1]. In order to obtain particles that are compatible for incorporation into such materials, it is necessary to shield their reactive surfaces with stabilizing ligands. To this end, functionalization of NPs with a polymer shell is an attractive way to introduce colloidal stability and at the same time modulate the properties of the resulting nanomaterial and equip it with stimuli-responsiveness [2–4]. The functionalization of particles with polymer can be undertaken by two different approaches: Using the so-called in-situ functionalization, it is possible to induce NP formation in the presence of polymers, which act as stabilizers for the growing particles. This strategy can, for example, be implemented using water-soluble reversible addition−fragmentation chain transfer (RAFT) polymers with dithiobenzoate termini, which can be reduced to thiol groups in the presence of a gold or silver salt precursor, leading to stable nanocomposites [5]. Alternatively, NPs can be functionalized ex-situ after their synthesis and work-up, either directly with polymers ("grafting-to") or with an initiator/chain transfer agent for surface-initiated (SI) polymerizations ("grafting-from"). The types of inorganic particles most often used in nanocomposites, and therefore considered in this chapter, are noble metal NPs, metal oxide NPs, and quantum dots. Metal NPs are particularly interesting because of their unique optical properties, which stem from surface plasmon resonance [6]. As a result of their chemical stability and facile surface modification, gold nanoparticles (AuNPs) are extensively studied representatives of this class. They are also particularly interesting in the realm of controlled radical polymerization, as RAFT polymers inherently contain anchor groups for gold surfaces. It has been shown that trithiocarbonate (TTC) and dithiobenzoate groups attach to gold [7]. Although a value of 36 kJ mol^{-1} has been determined for the free energy of adsorption of phenyldithioesters on a particular type of AuNP [8], another recent study [9] suggested that polymers with TTC and dithioester end groups can form even denser layers than thiol-terminated (the functional group most often encountered for the coating of gold surfaces) [10] polymers. Metal oxide NPs can also be readily conjugated with polymers via established anchor moieties [11], while the choice of anchor group might also influence the structure of the resulting nanocomposites [12]. Their incorporation into hybrid materials with polymers could lead to modulation of mechanical properties and also to cost reduction.

Controlled radical polymerizations (also called reversible-deactivation radical polymerization, RDRP, according to IUPAC recommendations) offer a unique way to modulate polymeric materials at the molecular level. By exploiting a dormant state of the propagating macroradical, the fraction of irreversibly terminated species

among the produced macromolecules can be reduced to a small number, which imparts "living" characteristics to the system and therefore enables the formation of complex macromolecular architectures, such as block copolymers and star polymers. Under typical conditions, the macromolecular species are rapidly switched between the dormant and active state, which leads to an equal distribution of growth probabilities for all chains and can result in narrow molecular weight distributions. It is thus possible to produce uniform polymers with defined molecular characteristics. These characteristics are defined by a large parameter space (monomer composition, degree of polymerization, degree of branching, distribution of special functional groups, etc.), which opens a huge operational window for macromolecular engineers to design polymers to meet specific requirements. In this chapter, we examine the literature of the past 10 years to evaluate if and how macromolecular design by means of controlled radical polymerization can be used to prepare polymer/inorganic nanocomposite materials with controlled architectures (location of NPs in polymer matrices, interparticle spatial relations, etc.) and properties.

2 Linear Homopolymers

We consider in this section the simplest case of homopolymers attached to a solid substrate with one end group. The polymer is thus composed of exactly one particular monomeric repeating unit; the average degree of polymerization of which can be controlled via living radical polymerization techniques. Hence, this type of polymer contains two sorts of information: (i) the functional group that is repeatedly expressed in the polymeric side chain or at the chain end remote from the NP surface, and (ii) the average size of one macromolecule. Both features influence the properties of composite materials of inorganic particles with polymers on their surfaces.

Homopolymers with distinct side chain functionalities can be obtained directly through homopolymerization or after post-polymerization modification of a polymer with reactive functional groups in its backbone, which can act as a platform for the preparation of a library of homopolymers with defined side chain moieties [13, 14]. The polymeric backbone can be chosen such that stable nanocomposites with NPs in the respective solvent can be obtained. Such stabilizing polymers can, for example, be applied in NP functionalization together with destabilizing molecules in varying molar ratios in order to control the aggregation of NPs in colloidal dispersion [15]. Regarding the chemistry in the polymer side chains, it is particularly interesting to study homopolymer brushes in cases where the monomeric repeating unit is capable of undergoing specific interactions that are rather weak individually, but significantly enhanced in the case of multivalent interactions [16]. As a result of such multivalent interactions, materials with fundamentally new properties are obtained when homopolymers bearing weakly interacting repeating units are assembled on a solid support. An illustrative example of this

principle is the so-called glyco-cluster effect, which is the reason why nanocomposites with glycopolymers have been investigated extensively in recent years.

RAFT polymerization is arguably tolerant to functional groups present in the monomer to be polymerized and also provides end groups that can be used as surface attachment points with or without additional post-polymerization modification. Therefore, monomers bearing unprotected glucosamine [17], glucoseamido and lactobioamido [18], mannose [19], or galactose [20] moieties can be polymerized in a RAFT process and their polymers grafted to NP surfaces. As an alternative to the direct polymerization of glycomonomers, the sugar moiety can be clicked to the polymeric backbone in a tandem polymerization [3+2]-cycloaddition reaction [21]. Nanocomposites of glycopolymers with AuNPs form complexes with lectins, which can lead to AuNP clustering and result in a plasmon band red shift [17, 19]. This recognition through complex formation may even be glycopolymer-specific [17, 20]. Complex formation with lectins can be further exploited in developing cancer theranostics [22]: RAFT homopolymers with glucosamine in their side chains can also be used to prepare nanocomposites with iron oxide nanoparticles (IONPs) of different shapes. The authors demonstrated that these nanohybrids attached to cell membranes of HeLa carcinoma cells expressing glucose transporters on their membranes. Also, the internalization of IONPs coated with glycopolymer was significantly increased compared with unmodified IONPs. Furthermore, cubic shaped IONPs showed a higher probability of cellular uptake than spindle-shaped particles in two different cell lines [22].

It should be noted, however, that substrate recognition through gold nanocomposites with a homopolymer layer is indeed a broad concept not limited to glycochemistry: Recognition can also lead to quantitative and cation-specific detection [23]. AuNPs covered with poly(methacrylic acid) (PMAA) were shown to aggregate upon exposure to Cr^{3+} cations. This led to a concentration-dependent shift of the localized surface plasmon resonance absorption band. After exposure to analyte solution, the sensor could be recovered by removal of Cr^{3+} using EDTA. When the recognition element implemented into the polymer brushes is self-complementary, nanohybrids with a tendency to form assembled network structures are formed [24]. This can be realized by decorating RAFT polymers with the ureidopyrimidone moiety at the α-chain end and grafting those polymers to AuNPs with a sulfur-containing ω-end. Therefore, the functionality that acts as recognition element does not need to be incorporated into the polymeric backbone, but can instead be located at the dangling end of the polymer brush that is remote from the particle surface, as the monomeric repeating units act as spacers.

RDRP techniques allow the preparation of macromolecules with predetermined degree of polymerization and narrow molar mass distribution. When such macromolecules are grafted onto the surface of NPs, it is interesting to investigate whether this size information can be used to organize inorganic particles in ordered assemblies. Following this idea and using surface-initiated atom-transfer radical polymerization (SI-ATRP), Fukuda and coworkers assembled nanocomposites of AuNPs [25] and SiNPs [26] with a poly(methyl methacrylate) (PMMA) shell in a

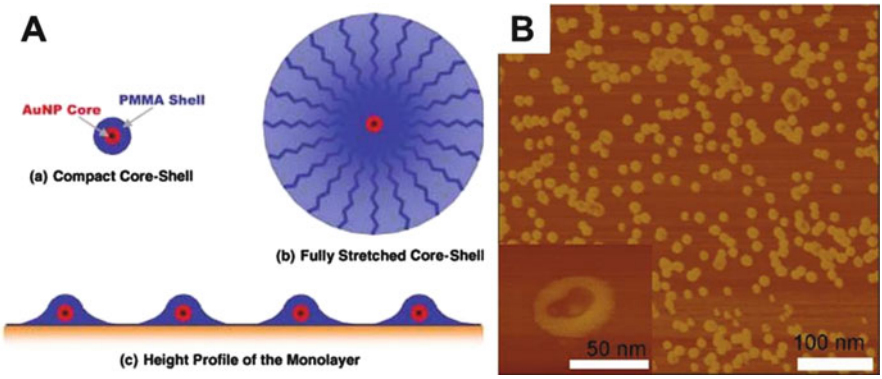

Fig. 1 (**a**) Structural model for a monolayer of hybrid particles, developed based on AFM measurements. Adapted with permission from [25]. Copyright 2003 Wiley-VCH Verlag GmbH & Co. KGaA, Weinheim. (**b**) Phase contrast AFM image showing a soft layer of polymer assembled around a hard gold particle core. Adapted with permission from [27]. Copyright 2009 American Chemical Society

two-dimensional array using Langmuir–Blodgett deposition. The authors found that the PMMA shell keeps the AuNP cores at certain distances, which increase with increasing graft chain length. Using atomic force microscopy (AFM), it was demonstrated that the PMMA forms a compact shell on top of AuNPs and a stretched shell around AuNPs, which causes the AuNP core spacings [25]. Analogous shell morphology in gold nanocomposites was also revealed by Davis and colleagues, who observed a soft shell assembled around a hard core in phase contrast AFM images of hybrid particles deposited on a solid substrate [27]. This indicates that the brushes on top of a particle were pulled downwards during the solvent evaporation process (Fig. 1).

When polymers are terminally grafted onto a surface at a high density, the surface-bound polymer adopts an extended conformation and stretches away from the surface; thus, the grafted polymer is in the concentrated polymer brush (CPB) regime. A unique feature of particle surfaces is that, as a result of their curvature, the concentration of polymer segments decreases in regions remote from the surface. This can lead to surface-bound polymer eventually going into the semidilute polymer brush (SDPB) regime, as a result of decreasing packing constraints [28, 29]. Dynamic light scattering (DLS) measurements of polymer brush height on individual nanohybrid particles [28, 30] and confocal laser scanning microscopy of three-dimensional colloidal crystals [28–31] confirm this behavior. The scaling of polymer brush height can be understood roughly in terms of a simple blob model pioneered by Daoud and Cotton [32]. This model was originally developed to describe star polymer conformations, but can also be applied to polymer brushes attached to a solid core. When the number of branches (i.e., the grafting density) is high, the individual branches adopt a stretched conformation in regions close to the core. Farther away from the core, the individual branches begin to relax because of the increased volume available for the chains, leading to a

different scaling of star radius with the number of repeat units in a branch N. For large N, the Daoud–Cotton (DC) model predicts a scaling of star radius (polymer brush height) of $\sim N^{0.6}$. This scaling is in agreement with polymer brush height measured by DLS in this regime [33]. However, the simple DC model fails to describe the behavior of brushes for smaller brush heights (i.e., when the chains are in the CPB regime). In this case, brush height was shown experimentally to scale with $\sim N^{0.8}$, an intermediate scaling between $\sim N^{0.6}$ and $\sim N^{1.0}$, the latter being the limit for highest grafting density and minimum surface curvature (i.e., dense polymer brushes on flat surfaces) [33]. Fukuda and coworkers applied the DC model to polymer brushes grafted onto a large core to investigate at what distance from the center of the particle the crossover from CPB to SDPB takes place [28]. This critical distance r_c was found to be given by:

$$r_c = r_o \times \sigma^{*1/2} \left((4\pi)^{1/2} \nu \right)^{-1}, \quad (1)$$

where r_o is the radius of the inorganic core, σ^* the dimensionless grafting density, and ν the excluded volume parameter. It follows that for small enough grafting densities, r_c is smaller than r_o and the whole polymer brush thus shows SDPB behavior. For large enough values of σ^* and small polymer brush heights, the entire brush shows CPB behavior. At a critical brush height, the CPB-to-SDPB transition occurs. Thus, the height of a polymer brush on an inorganic particle clearly scales with the degree of polymerization of the grafted chains, and the scaling behavior can provide information about whether the polymer is in the concentrated brush regime or not. This is valuable information, as it was recognized that the mechanical properties of self-assembled structures from hybrid particles are strongly influenced by the CPB–SDPB transition because more interparticle chain entanglements can occur in the SDPB case [34, 35]. The toughness of the hybrid materials of silica NPs with polystyrene (PS) and PMMA brushes was found to increase as the polymer brush height increased beyond the CPB–SDPB crossover [35]. On the other hand, material properties that do not depend much on polymer entanglements (i.e., the elastic modulus and hardness of the material) were shown to increase with increasing polymer brush molar mass and level off before the CPB–SDPB transition (Fig. 2) [35].

The state of the polymer brushes also affects the order formation in two-dimensional nanohybrid assemblies, because the SDPBs do not add significantly to the interparticle repulsive potential and act to dilute the array structure, resulting in decreased assembly order as the system goes far into the SDPB regime [36]. However, this behavior can be exploited intentionally by grafting bimodal polymer brushes, one of which is short and of high grafting density to shield the particle surface and one that is long with low grafting density, to achieve nanohybrids that can be more regularly dispersed in a polymer matrix [37], preventing particle assembly and structuring [38]. In such a molten state or blend, growing interparticle distances with increasing molecular weight of the surface-

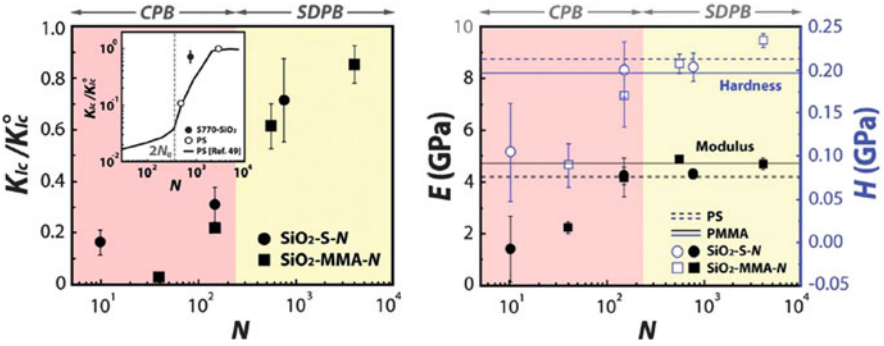

Fig. 2 Mechanical properties of nanocomposites of silica NPs with PS and PMMA. *Left*: Development of material toughness with increasing average number of monomeric repeat units per brush (N). *Right*: Dependence of elastic modulus E and hardness H on N. Adapted from [35] with permission of The Royal Society of Chemistry

bound polymer can also be observed by small-angle X-ray scattering (SAXS), and it was found that the interparticle distances can be further swollen by blending the hybrid particles with free polymer [39]. In the case of AuNPs, the gold core spacing results in unique optical responses, which stem from surface plasmon coupling [40] or, when the spacing is of the order of the wavelength of visible light, from Bragg diffraction [28, 31, 41].

Nanocomposites with a tailored polymer shell thickness can also be obtained through RAFT polymerization surface-initiated from silica [42, 43] and IONP surfaces [42], or via grafting-to approaches [44, 45]. The grafting-to strategy is particularly interesting because it can allow precise control of the polymer properties independently of the NP, prior to immobilization on a surface. For such an attachment of polymer chains, it is necessary that the enthalpy gain from the interaction of the anchor moiety with the surface balances the loss of entropy of the polymer chain. This entropy loss is reflected in a decrease in polymer grafting density with increasing average molecular weight of the employed polymer, which was verified for two types of AuNPs [45]. This behavior is logical, since the increased entropy loss (resulting from the conical confinement of longer polymer chains) can only be counterbalanced by more relaxed conformations as a result of their confinement in a larger space (i.e., by reducing the grafting density). When homopolymers are grafted to NPs with one end group, the question of whether they form brushes on the surface can be answered by determining the polymer shell thickness as a function of polymer molecular weight. This shell thickness can be quantified by systematically measuring the edge-to-edge distance between inorganic NP cores in self-assembled monolayers (Fig. 3) [44].

The data points obtained from the analysis of several TEM images can be fitted to a function describing the increase in interparticle distance with the increase in mean molar mass of grafted polymer. A simple yet suitable function can be chosen of the following form:

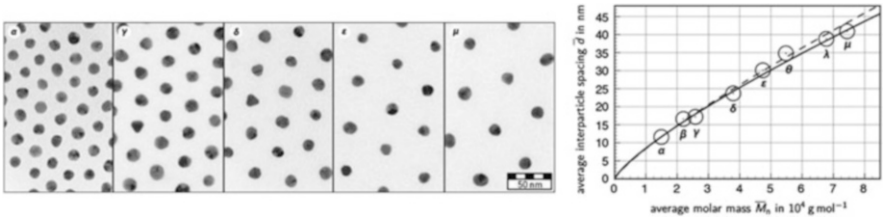

Fig. 3 *Left*: TEM images showing self-assembled monolayers from nanohybrid particles with gold cores and PN^{i}PAAM shells. The average degree of polymerization of N^{i}PAAM increases from *left* to *right*. *Right:* Dependence of interparticle spacing on the average degree of polymerization. Adapted with permission from [44]. Copyright 2013 American Chemical Society

$$\overline{d} = k \times \left[\overline{M}_n\right]^{1/l}. \tag{2}$$

A fit of (2) to the data yields $k = 6.02 \times 10^{-12}$ m and $1/l = 0.79$. When k is identified to be twice the contour length of the polymer and set fixed to this value (4.4×10^{-12} m), a value of 0.82 is obtained for the exponent $1/l$. Taking into consideration how the molar mass of surface-bound polymer translates to polymer shell thickness, this value obtained for $1/l$ might reflect densely grafted polymer brushes on the NP surface, provided that interparticle spacing in self-assembled monolayers can indeed be used as a measure of polymer shell thickness. That is, the information that is included in the scaling of interparticle distance with molar mass can be used to draw conclusions about the conformational state of the surface-anchored polymer chains.

3 Mixed Brushes of Two Different Linear Polymers

When two chemically different types of polymer are grafted to NPs, the situation becomes much more complex because the properties of both species influence the behavior of the resulting nanocomposites, depending on the individual chain lengths, grafting densities, and chemical properties of the two different brushes. Also, the different polymers might be grafted independently of each other, leading to a statistical distribution of both polymers on the surface, or they might be grafted as diblock copolymers at their block junction. Because the outcome of the latter results in mixed polymer brushes, we discuss this special case here and not in Sect. 3, which deals with copolymers in a more general sense. The behavior of nanocomposites with mixed brushes can reflect the properties of both polymeric species at the same time or it can be intermediate between those of NPs with uniform polymer brushes. Grafting of brushes with different solubility characteristics can lead to amphiphilic nanocomposites with a tendency to phase-separate on the surfaces. The phase separation of immobilized macromolecules into different domains is a unique feature of mixed brushes and is particularly interesting

because, unlike micelle formation in solutions containing free amphiphilic (macro) molecules, the outcome of the assembly is not influenced by the dilution of the system. Also, as shown in this section, phase separation in mixed brushes on NP surfaces and its modulation can prove useful in tuning nanocomposite properties and directing particle assembly.

Different surface morphologies (including rippled structures, different island structures with varying number of islands, and layered structures) resulting from microphase separation of two anchored polymer species can be predicted from a theoretical model, depending on the chain lengths and composition of mixed brushes on NP surfaces [46]. It can be predicted theoretically that lateral phase separation of two different polymer brushes on surfaces occurs in a marginally good nonselective solvent if both chains are of nearly equal or only slightly asymmetric in length. If one polymer species becomes larger, the smaller polymers form domains in a bottom layer close to the surface and the top layer is composed exclusively of the longer stretched polymer [47]. This predicted behavior has been confirmed experimentally [48].

Because the topology of separated polymer brushes on surfaces depends so strongly on the architecture of the polymeric species (i.e., the grafting density of both brushes and their degree of polymerization), the formation of well-defined mixed brushes on NP surfaces requires polymerization techniques that allow precise control over macromolecular properties. To this end, the use of macroRAFT agents for the formation of diblock copolymers with gold-binding TTC groups at the block junction has been suggested [49]. This approach is interesting because it implies that the ratio of grafting densities for the different blocks is always equal to one. Alternatively, the different brushes can be grafted to the NP surface as individual homopolymers through specific reactions between the homopolymer end groups and functional groups on the particle surface [50]. This could offer a handle for tuning the ratio of the two grafting densities by adjusting the polymer feed ratio. Another elegant and much-adapted method for preparing precisely tailored mixed polymer brushes is SI-ATRP followed by nitroxide-mediated radical polymerization (NMRP) from an asymmetric initiator that can be grafted to a surface of the particle and comprises initiation sites for both types of controlled radical polymerization techniques [51]. The two successive polymerizations lead to block copolymers grafted through their block junction. The resulting NPs show chain reorganization in response to a selective solvent environment that can lead to mobile and collapsed phases [51]. Employing this SI polymerization technique with asymmetric initiator, it can be shown by TEM that lateral microphase separation occurs in nonselective good solvents when the polymer molecular weight reaches a certain threshold value, and that a selective solvent leads to collapsed domains of the polymer species interacting unfavorably with the solvent [52, 53]. A systematic experimental study showed, from the analysis of TEM images, that the domain sizes grow strictly with the molecular weight of the grafted brushes, although the exact scaling behavior was dependent on whether the particles were drop-cast from a (nonselective) good or bad solvent [54]. A lower grafting density of mixed brushes also leads to larger domain sizes, until the grafting density reaches a

lower threshold value, below which no phase separation can be observed [55]. Lateral phase separation apparently leads to wedge-shaped separated domains if the curvature of the solid particles becomes large enough [56]. Phase separation is different in isolated nanohybrids compared with nanohybrids in self-assembled monolayers. For isolated hybrid particles, phase separation only occurs at the bottom close to the substrate, whereas interparticle brush interactions lead to extended phase-separated regions between neighboring particles [57].

The influence of the mode of attachment of different brushes was also investigated. Mixed brushes of PMMA and PS were grown from a flat silica surface by either SI conventional radical polymerization or successive ATRP (PMMA brush) and NMRP (PS brush) from a common asymmetric initiator for both techniques, attached to the surface with one grafting point. Conformational changes in grafted polymer chains were studied theoretically and experimentally by investigation of microphase separation after solvent exchange cycles with toluene and acetone. It was found that microphase-separated areas were larger for individually anchored PMMA and PS brushes. This effect was explained by density fluctuations of the different polymer species, which occur using this approach. Also, the memory measure (the probability that a specific domain re-forms after one cycle) was smaller for diblock copolymers grafted at their block junction. This was an indication that local fluctuations in grafted polymer chains act as nuclei in the domain structure formation [58].

Randomly distributed mixed brushes of PS and PN^{i}PAAM on AuNPs can be obtained by in-situ reduction of a gold salt precursor in the presence of RAFT homopolymers [59]. The presence of both types of polymers on the AuNPs can be demonstrated using NMR and infrared spectroscopy. When thin films of the composite material are prepared via hydrophilic Langmuir–Blodgett transfer, a more hydrophobic surface is obtained than with hydrophobic transfer, as shown from contact angle measurements after depositing a water drop on both surfaces. The authors concluded that this phenomenon might be indicative of phase separation of the two distinct polymer species on the NP surface during Langmuir–Blodgett assembly [59]. Detailed investigations into the behavior of mixed brushes can be undertaken when the polymers are grafted to a flat surface, which allows investigation via AFM [60]. Again, conformational changes in the polymer brushes allow the surface to adapt to its solvent environment, but it is interesting to notice that these conformational transitions can be kinetically locked when long enough chains cover shorter ones and thus prevent their swelling by a selective solvent [60].

For both cases where mixed brushes are randomly distributed over the surface or grafted as diblock copolymers at their block junctions, it was shown that the chain conformations can flexibly adapt to global changes in the environment. These observations were made by studying mixed brushes on NPs and lead to the question of whether such phenomena can be made useful for NP assembly [61]. When mixed brushes of thiol-terminated poly(ethylene glycol) (PEG) and PMMA from SI-ATRP are present on large (42 nm) gold nanocrystals, the hybrid particles proved stable as unimers in common solvents for both brushes (DMF, chloroform, DMSO). However, when the solvent was changed by addition of water and

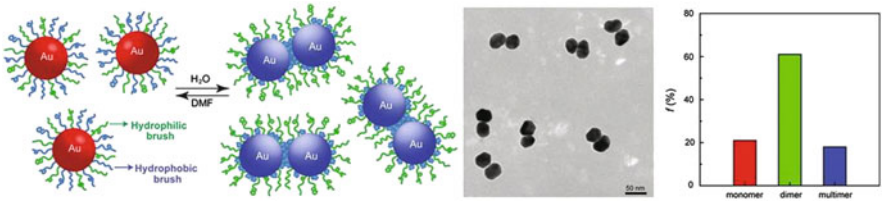

Fig. 4 *Left*: Proposed mechanism of dimerization upon solvent exchange to a selective solvent. *Center*: TEM image showing AuNP dimer structures. *Right*: Histogram showing the fraction of monomeric, dimeric, and multimeric AuNP species. Adapted with permission from [61]. Copyright 2011 American Chemical Society

subsequent dialysis, these nanohybrids aggregated, probably as a result of formation of hydrophobic domains of collapsed PMMA chains that act as contacting areas for different particles. Interestingly, NP assembly led to a huge proportion (>60%) of NP dimers. It was speculated that this is caused by depletion of PEG brushes from the dimer junction. The resulting accumulation of PEG brushes in the noncontacting areas leads to stabilization of the dimer structures (Fig. 4). This explanation is consistent with the observation that an increase in the PMMA fraction (PMMA:PEG ratio increase from 4:3 to >5:1) results in the formation of larger multimers upon addition of the selective solvent water [61].

Assemblies of nanocomposites into larger vesicular structures comprising several particles with mixed brushes can also be realized: AuNPs (14 nm) and nanorods (aspect ratio 4:1) were covered with thiol-terminated PEG (grafting-to) and thiol-terminated ATRP initiator, which allowed the growth of PMMA and PMMA-*stat*-poly(vinylpyridine) (PVP). Film rehydration of these nanocomposites led to vesicular structures. These structures were shown to decompose under heat or decreased pH, since vinylpyridine renders the system pH-responsive. In the case of nanorods, decomposition can be triggered with near-infrared radiation [62]. These features render this system promising for delivery and controlled release of therapeutic agents [63, 64].

4 Linear Diblock Copolymers and Random Copolymers

As a result of the general immiscibility of different homopolymers, diblock copolymers exhibit an inherent tendency to phase-separate and can therefore form a range of ordered structures in solution and in the molten state. Thus, there has been a lot of research using diblock copolymers in conjuncture with NPs and aiming to use these polymers as templates to form tailored NP arrangements. Block copolymers are attractive in the realm of nanocomposites because each of the two blocks can be employed for distinct functions. For example, for block copolymers grafted to IONPs, the inner block can be used as an attachment site for the incorporation of chemical tags, while the outer block provides solubility in the respective dispersant

[65]. Alternatively, block copolymers can be designed such that one entire block induces NP formation through gold salt reduction and shielding of the formed NP surface, and the second block provides colloidal stability. Following this idea, block copolymers of *N*,*N*-diemthylaminoethyl methacrylate (DMAEMA) and 2-(methacryloyloxy)ethyl phosphorylcholine (MPC) were prepared by ATRP. Addition of $HAuCl_4$ resulted in the accumulation of gold close to the DMAEMA repeating units as a result of formation of salt bridges. The (unprotonated) tertiary amine then acts as a reduction agent, which induces AuNP formation. Nanohybrids with an inner shell of PDMAEMA and an outer shell of PMPC are thus formed. Away from its isoelectric point, the PMPC layer imparts solubility to the nanocomposites. It was also shown that there is an optimum PDMAEMA block length for obtaining well-defined spherical AuNPs with reasonably narrow particle size distributions [66].

A more recent work employed the concept of gold salt reduction by one entire block of a block copolymer in an even more sophisticated fashion. Polymers comprising hydrophilic and hydrophobic blocks were used to coat AuNPs, which allowed growth of a gold nanoshell around these hybrid particles [67]. This became possible by introducing phenol side chain moieties into the hydrophilic block, which at basic pH were effective reducing agents for $KAuCl_4$, producing the gold shells. The hydrophobic blocks act as spacers in this case, which allows tuning of the thickness of the obtained nanogap between the gold core and shell, and also permits introduction of Raman tags by copolymerization with a functional monomer. The block that interacts with the NP surface is not necessarily chemically bound; adsorption of copolymers on NPs can lead to uniform polymer films [68]. It was demonstrated that hydrophobically functionalized AuNPs can be incorporated into micelles from polystyrene-*block*-poly(acrylic acid) (PS-*b*-PAA) copolymers by inducing micelle formation through addition of a selective solvent (water) and subsequent crosslinking of the outer shell of the micelle [69], or by cooling the solution to slowly decrease the critical micelle concentration [70]. In general, large excess of diblock copolymer (which can be separated after NP encapsulation) and a relatively large diameter of the NP ($>$10 nm) are necessary to avoid the incorporation of multiple NPs into one micelle. This has been observed for small NPs ($<$10 nm), which act as solutes swelling the micelle core [71]. In fact, the number of small NPs contained in a micelle can be controlled by adjusting the ratio of particles and block copolymers, with a higher average number of incorporated NPs being obtained as their relative proportion in the reaction mixture increases [72].

Triggered assembly of temperature-responsive diblock copolymers was used by McCormick and coworkers for colloidosome formation [73]. Block copolymers of DMAEMA and N^{i}PAAM were prepared by RAFT polymerization. Heating of a block copolymer solution induced reversible vesicle formation as a result of the collapse of the PN^{i}PAAM block. Addition of $NaAuCl_4$ to the assembled block copolymer solution at a fixed ratio at 50°C led to incorporation of gold salt in the vesicles. The tertiary amine group of the DMAEMA repeating unit triggered gold reduction and AuNP formation. Interestingly, the vesicular structure was fixed after cooling and did not dissociate into monomeric block copolymers, as observed

before AuNP formation [73]. In addition, the morphology of the self-assembled structures can be varied from simple micelles, mixtures of worm-like micelles and spherical micelles, and vesicles by adjusting the degree of polymerization of the temperature-responsive PN^{i}PAAM block in the preceding RAFT polymerization [74]. Preformed NPs can be incorporated into self-assembled solution structures of block copolymers depending on the specific interactions between the NP surface and both blocks. The NP–block copolymer interaction can, for example, lead to NPs being incorporated into micelle cores, although the constituting block copolymer alone forms vesicles. This is so because NP incorporation into the solvophobic phase can reduce the polymer stretching penalty in the self-assembled structures formed [75]. This point is further illustrated in a study by Park and coworkers [76], which showed that PS-coated quantum dots were incorporated into the PS domain of micelles formed from PS-*b*-PAA polymers. On the other hand, when alkyl-coated particles were employed, they formed a layer between the PS–PS interface [77]. This was shown to occur because the alkyl–PS interaction is the least unfavorable interaction and the incorporation of a NP layer reduces polymer stretching [76]. Thus, two NPs with different surface chemistries can be incorporated at different positions in the polymer matrix. The NP–copolymer interaction can also be tuned such that the NPs assemble at the PS–PAA interface of the micelles formed (by carefully choosing the surface chemistry of the NP) [78]. Hence, layered co-assemblies can be obtained with two types of particles located at the PS–PS and PS–PAA interfaces, resulting in different radial positions for the individual NPs (Fig. 5).

We have seen so far that enthalpic interaction parameters are often crucial in controlling the position of NPs in block copolymer assemblies [69–72, 74–78]. Nevertheless, it has been shown impressively that the contribution of entropy to the free energy can become important in controlling the position of NPs in vesicular structures [79]. The co-assembly of NPs decorated with polystyrene-*block*-poly (ethylene oxide) (PS-*b*-PEO) copolymers and free (not surface-bound) block copolymers of the same type leads to vesicles with the NPs being incorporated in the (solvophobic) PS domain. Interestingly, depending on the number of monomeric

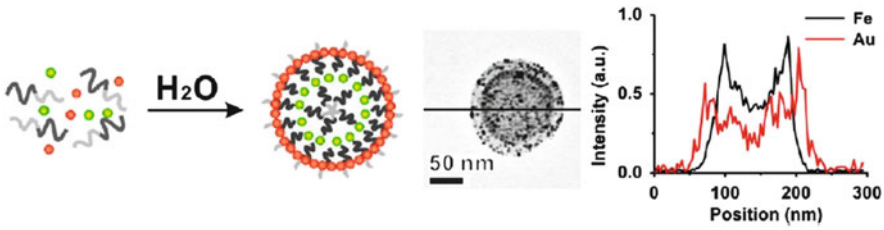

Fig. 5 Solvent-induced formation of layered assemblies from block copolymers of PAA and PS and AuNPs functionalized with mercaptoundecanol as well as IONPs functionalized with oleic acid. The AuNPs (*red*) are located at the PS–PAA interface, while the IONPs (*green and yellow*) are located at the PS–PS interface. The *graph* shows two different radial positions for the distinct NP species. Adapted with permission from [78]. Copyright 2013 American Chemical Society

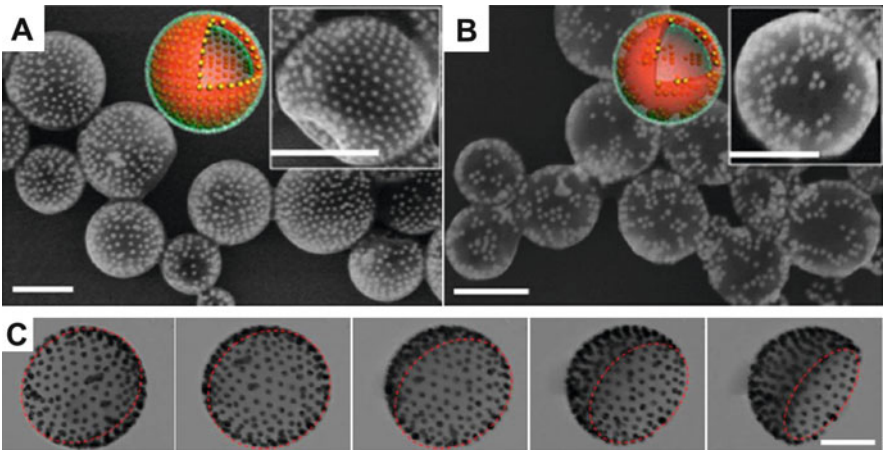

Fig. 6 (**a**, **b**) SEM images showing AuNPs grafted with block copolymers incorporated in vesicles and evenly distributed in one layer (**a**) or partly separated in clusters in this layer (**b**). (**c**) TEM images at different tilt angles revealing fully separated AuNPs in one hemisphere of the vesicle. *Scale bars*: 200 nm (**a**, **b**) and 100 nm (**c**). Adapted with permission from [79]. Copyright 2014 American Chemical Society

repeating units in the two blocks for both free and bound block copolymers, the NPs were either evenly distributed over the entire PS layer or they were separated. This separation led to an accumulation of NPs in some areas, leading to "patchy" vesicles, or – in cases of strong separation – to an accumulation on one hemisphere (and depletion on the other), leading to Janus-type structures (Fig. 6).

The concept of block copolymers acting as templates that can host NPs at defined locations can also be adopted to produce thin films. Thus, block copolymers, which show phase separation in the molten state, can be used as matrices for selective incorporation of particles. Depending on the block composition, and the temperature-dependent block interaction, phase separation can lead to different nanostructured morphologies [80]. However, we restrain ourselves here to discussion of the most common type of phase separation, lamellar phase separation, as an illustrative example. The lamellar type of phase separation has the advantage that, as a result of its symmetry, it facilitates computations towards the prediction of NP localization in diblock copolymer hosts. A theoretical study evaluating NP distribution in copolymer melts found that neutral NPs lead to a Gaussian distribution centered at the lamellar interfaces, whereas strongly selective NPs are incorporated in the preferred domain, with a Gaussian distribution centered at the middle of this domain [81]. There could also be intermediate situations in which Gaussian distributions with distinct shoulders are observed. Generally, large degrees of polymerization in the diblock copolymer, and therefore a high degree of domain segregation, were shown to lead to narrow particle distributions in this theoretical work [81], a finding that is, however, contrary to an experimental study investigating this effect [82].

Depending on the wetting behavior of the two blocks of the block copolymer with the surface, thin films can show phase separation that is either parallel or perpendicular to the surface. If the surface comprises equal wettability for both blocks, this usually results in perpendicular phase separation. This effect can be nicely demonstrated by comparing two types of NPs, one of which is selective and one of which is neutral for a common block copolymer of PS and PMMA. It can be demonstrated experimentally that selective AuNPs locate inside the favorable block domain, whereas neutral NPs are located at the domain interfaces (see Fig. 7) [83], fully consistent with theory [81] and other experimental studies [84, 85]. It was furthermore shown by cross-sectional TEM that selective NPs are distributed throughout the respective domain, but within the entire film thickness, whereas neutral NPs reside preferentially close to the surface–air interface for entropic reasons [83]. The attraction of NPs to the surface of the substrate thus induces a change in the surface wettability properties and results in conversion from parallel to perpendicular phase separation when the amount of neutral NPs is high enough. A similar transition of block copolymer orientation after addition of NPs to the system has also been observed by others, employing a different system comprising PS-*b*-PVP copolymer together with alkyl-coated CdSe particles [86, 87]. To take full advantage of the periodical features present on the surface of phase-separated thin films, one could also choose to further swell specific domains with selective solvents prior to the addition of particles [88] or to permanently fix the phase separation by photo-crosslinking [89].

By adding NPs to phase-separating block copolymer systems, one may also face phenomena resulting from interparticle interactions, which are often neglected by theory: When lamellar phase separation is used to introduce magnetic NPs

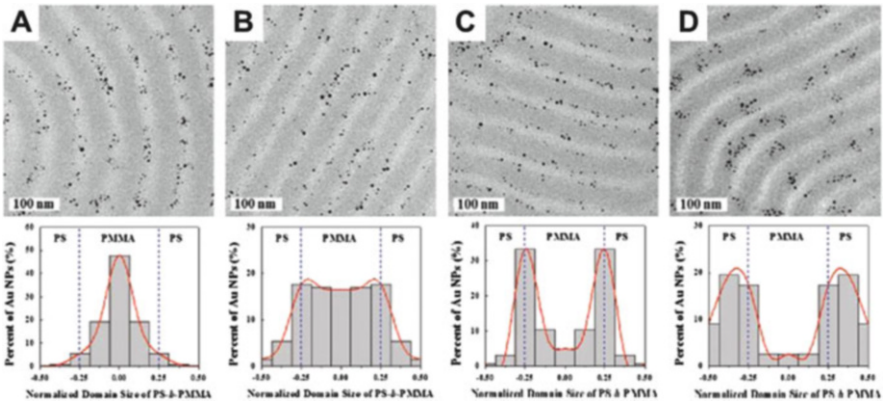

Fig. 7 *Top row*: TEM images showing the lamellar phase separation of a PS-*b*-PMMA polymer perpendicular to the substrate surface (PS domains were stained with RuO_4 and appear darker) and the distribution of AuNPs modified with four different polymeric ligands. The fraction of styrene increases from **a** to **d**. *Bottom row*: Particle distribution in the block copolymer domains for AuNPs coated with the four different polymers. Adapted with permission from [83]. Copyright 2011 American Chemical Society

functionalized with PMMA into the PMMA domain of a PS-*b*-PMMA copolymer, the incorporation can occur only at small NP concentrations. When the NP concentration is high enough, the polymer-coated NPs tend to form particle aggregates that are too large to be taken up inside one block domain, and therefore block copolymer assembly around these aggregates is observed [90]. A different scenario that can be observed upon increasing the NP concentration is an NP-induced phase transition. An interesting mechanism leading to phase transition in block copolymers has been described by Kramer and coworkers [91]. When NPs, which prefer to locate at block interfaces, were added with increasing concentration, the authors found that initially the domain size in lamellar phase-separated block copolymers decreased. This behavior was rationalized by strong segregation theory, predicting a scaling of domain thickness proportional to the block copolymer interfacial energy, which is decreased by addition of neutral NPs locating at the copolymer interfaces. Further increase in the NP concentration led to a lamellar-to-bicontinous transition, as shown for AuNPs selective for an interface with two different surface coatings. The effect of the molecular weight of the block copolymer matrix on the phase transition was also studied and it was found that matrices with higher molar masses required smaller NP concentrations for phase transition [91].

5 Linear Triblock Polymers

By applying triblock terpolymers as templates for the in situ formation of NPs, it is possible to introduce even more information into a linear polymer by using the different blocks for distinct functions. For example, two outer blocks can be chosen such that the resulting polymer has a tendency to self-assemble into specific solution structures, while the inner block can comprise binding sites for NPs [92, 93]; alternatively, one outer block can provide these binding sites and the other two blocks can provide amphiphilicity [94, 95]. Such triblock terpolymers are, for example, accessible through consecutive RAFT [92, 93] or ATR [94, 95] polymerizations. When an inner block of either PMAA [92] (providing attachment sites for the complexation of an iron salt precursor) or PDMAEMA [93] (providing attachment sites for tetrachloroauric acid) is sandwiched between outer blocks of PS and poly[oligo(ethylene glycol) methacrylate] (POEGMA), the polymers can be used to organize inorganic NPs into different patterns. Polymerization-induced self-assembly was employed in both of these studies; that is, the respective block copolymer precursors were used as macroRAFT agents in chain extension polymerizations with styrene in methanol, under which conditions polymeric NPs were formed. The two different inorganic precursor salts could then be introduced into the respective middle block of the triblock terpolymers, and inorganic particle formation could be triggered by adding base to form IONPs [92] or reduction agent to form AuNPs [93]. Depending on the degree of polymerization of styrene, this system can be tuned to form micelles, rods, and vesicles as hosts for inorganic NPs [92]. The polymers therefore encode these different solution structures and at the same time

carry information about where the inorganic NPs will be placed in the resulting nanohybrid assembly structures.

The studies mentioned above first assemble specifically designed polymers and then induce NP formation after assembly formation. In principle, however, it should be possible to first decorate inorganic NPs with a polymer to create amphiphilic hybrid particles, which can then assemble into a variety of structures. This has been realized by Eisenberg and coworkers [96]. Their approach used triblock polymers made by two successive ATR polymerizations of first styrene and then vinylpyridine, starting from a chloride-terminated PEG macroinitiator. The resulting PEG-*b*-PS-*b*-PVP polymers were used to cover AuNPs and PdNPs via attachment through the PVP block. The obtained hybrid particles had amphiphilic character and tended to assemble into micellar structures after addition of water to their dispersions in THF. The self-assembled structures revealed (by TEM characterization) NPs with defined location at the surface of the micellar core, which occurred in darker contrast as a result of the high electron density in the PS block. The defined NP position resulted from the covalent attachment of the separating blocks. The hydrophilic PEG block could effectively stabilize these micellar structures in the hydrophilic environment at high enough grafting densities [96].

Even higher precision in the formation of nanocomposites can be achieved by the ambitious procedure of NP monofunctionalization [97]. Liu and coworkers indeed found that small AuNPs can be functionalized with only a single macromolecule, a triblock terpolymer [98]. The authors used a macroRAFT agent with PEO in its RAFT leaving group ("R group") to successively polymerize glycidyl methacrylate (GMA) and styrene. The middle PGMA block was used to introduce lipoic acid, which acts as an anchor for gold surfaces via its dithiolane moiety. By analyzing the nanohybrids of this polymer with AuNPs via size-exclusion chromatography (SEC) and thermogravimetric analysis (TGA), it was concluded that indeed only one macromolecule attaches to AuNPs with diameters of ~2.0, ~2.9, and ~3.8 nm. Monofunctionalization was, however, not observed for AuNPs of ~4.9 nm, strongly suggesting a size selectivity for this stoichiometric functionalization. The nanocomposites with one macromolecule per inorganic particle were decorated with a PEO and a PS chain (the outer blocks of the initial triblock polymer) and can therefore be considered as true amphiphilic particles. The assembly of these nanohybrid particles into vesicles and micelles, depending on the packing parameter (which can be controlled by macromolecular design), has been demonstrated (Fig. 8) [98].

In addition to the above-discussed cases of triblock terpolymers, linear triblock polymers can also take the form of ABA copolymers. A recent study [99] employed a symmetric ATRP macroinitiator with a PEG linker between the two initiation sites. ATR copolymerization of diethylenegylcol methylmethacrylate (DEGMMA) and diethyleneglycol ethylmethacrylate (DEGEMA), together with a comonomer for fluorescent labeling, permitted the formation of outer blocks with defined lower critical solution temperature (LCST). Silica NPs were surface-functionalized by SI-ATRP with polymers of different compositions of DEGMMA and DEGEMA to tune the LCST of the surface-grafted polymer and another comonomer as

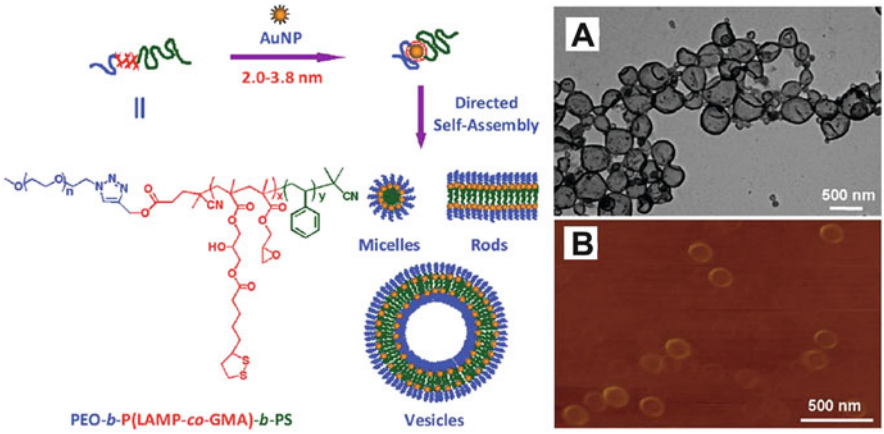

Fig. 8 *Left*: Strategy employed for the monofunctionalization of AuNPs with one macromolecule. *Right*: High resolution TEM (**a**) and AFM (**b**) images of the vesicular assembly structures obtained from these nanohybrids. Adapted with permission from [98]. Copyright 2012 American Chemical Society

fluorescent tag. The fluorescent labels were introduced to study the spatial relation of the surface-modified SiNPs with the outer blocks of the triblock ABA copolymer. When the polymer immobilized on the SiNP surface had a similar LCST as the outer blocks of the triblock copolymer, mixtures of both species formed gels at a temperature above their common LCST. In these gels, the NPs were localized in micellar compartments of the collapsed outer A blocks of the ABA copolymer. Gel formation was a result of the bridging of (soluble) PEG chains (B block of the ABA copolymer) between the collapsed entities. When the SiNPs were modified with a polymer of higher LCST than that of the outer block of the triblock copolymer, gels were formed at temperatures intermediate between the two LCSTs and SiNPs were not incorporated into the collapsed micelles. Careful manipulation of the properties of the surface-bound polymers therefore allows control of the location of inorganic NPs in organic polymer gels [99].

6 Linear Multiblock Polymers

RAFT polymerization is unique among the most prominent RDRP techniques because the inherently bifunctional TTC group can be employed in RAFT-type chain transfer agents. As a result of this bifunctional nature, the TTC moiety can be easily incorporated into the backbone of linear multifunctional RAFT agents [100, 101] or cyclic RAFT agents [102], both of which permit the formation of multiblock polymers with narrowly distributed block lengths. In such systems, the RAFT mechanism causes a continuous redistribution of all blocks and RAFT

groups during polymerization and this results in remarkably narrow ideal block distributions [103]. Consequently, such macromolecules are relatively well defined and can thus be used as the tailored organic part of nanohybrids with inorganic particles. For AuNPs, this polymer comprises TTC groups as gold attachment points in its backbone [104]. Another advantage of these systems is that multiblock copolymers can be obtained by only two successive polymerizations. Such multiblock copolymers can be useful, as shown by Du et al., who suggested that amphiphilic RAFT multiblock copolymers of styrene and vinylpyridine can be used for the interfacial assembly of AuNPs, gold nanorods, and AgNPs at liquid–liquid interfaces [105]. The authors did not show, however, whether the TTC groups are maintained in the multiblock copolymers after treating them with $NaBH_4$ during the in situ synthesis of AuNPs and AgNPs.

When the covalently linked blocks of a multiblock polymer are made of N^{i}PAAM monomer, the resulting polymeric material is water soluble and can therefore be brought directly into contact with AuNPs from the citrate reduction. Nanohybrids produced by this method were analyzed by TEM, which showed particles that assembled in hexagonal two-dimensional patterns with constant minimum spacing between the gold cores; absolutely no particle stacking was observed [44]. This indicates that the gold cores were not crosslinked by the multifunctional RAFT polymer, a result that was confirmed by SEC analysis. The binding mode of this polymer on the surface of this type of AuNP could be revealed in even more detail: The spacing between the gold cores was analyzed systematically for different multiblock polymers of N^{i}PAAM and compared with the data (see Sect. 1, Fig. 3) obtained for linear polymers of N^{i}PAAM with only one TTC group on the ω-end of the polymeric chain. It was found that gold core spacings were distinctively smaller and almost constant when multifunctional RAFT polymers with varying block numbers and degrees of polymerization were employed for surface functionalization reactions with these AuNPs. This leads to the conclusion that this type of polymer attaches to AuNPs from citrate reduction in a multivalent fashion via its multiple TTC groups, meaning that these macromolecules wrap around the AuNPs and form polymer loops on the NP surface [44].

Disclosing the binding motif of multiblock RAFT polymers on AuNPs from citrate reduction raises the question of whether the polymer binding can vary for different types of AuNPs. It is known that AuNPs from the two-phase Brust–Schiffrin synthesis can assemble into spherical particle networks when treated with low molecular weight crosslinking agent [106, 107]. When tetraoctylammonium bromide-capped AuNPs from this two-phase method are functionalized in toluene dispersion with multiblock RAFT polymers of styrene, the formation of spherical AuNP assemblies can be observed by TEM (Fig. 9) [108]. It can be concluded from these TEM images that the particle density inside

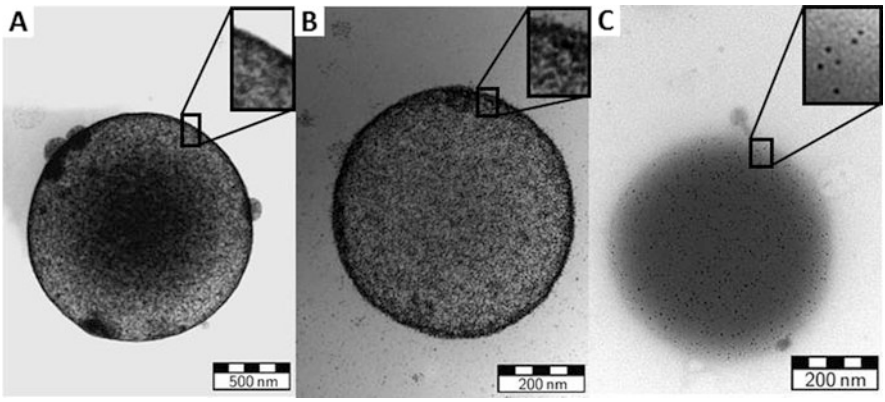

Fig. 9 (**a**–**c**) TEM images of AuNP networks obtained by treating TOAB-capped AuNPs in toluene with multifunctional RAFT polymers of styrene. The degree of polymerization of the polymeric particle linker increases from **a** to **c**. Adapted with permission from [108]. Copyright 2013 American Chemical Society

these assemblies decreases when polymers with increasing degree of polymerization are employed in NP functionalization reactions. By AFM characterization, it was possible to determine the three-dimensional shape of these structures after drop-casting from dispersion and solvent evaporation. It was found that these objects partly preserve a globular structure, which is indicative of NP crosslinking, as bonded particles are prevented from slipping when interconnected. The spherical superstructures can be further agglomerated into chain-like structures by addition of a non-solvent [104].

7 Branched Polymeric Architectures

Branched polymers are fundamentally different from linear polymers, which were discussed in previous sections: Polymers of linear topology contain two end groups, whereas multiple end groups are present in branched architectures, which allows incorporation of multiple functional groups into macromolecules of globular shape. Branched polymers can therefore be considered as promising macromolecular NP linkers. The branching points can be statistically distributed over the macromolecules (hyperbranched polymers, HBPs), occur strictly regularly leading to generational structures (dendrimers), or branches can be joined at a common core (star polymers).

Branched polymers can still attach to surfaces via one or multiple branches. It is possible to attach an HBP to an inorganic particle with only one of its branches if an ATRP initiator is immobilized on a surface, followed by polymerization of an initiator–monomer [109]. HBP with multiple anchor sites for NPs was prepared by Fredericks and coworkers [110], who produced hyberbranched RAFT polymer by copolymerization with a difunctional monomer. The RAFT agent was of the TTC type and also contained an alkyne moiety in its RAFT leaving group; both functional groups are known to attach to gold surfaces. Addition of these polymers to AuNPs from citrate reduction resulted in the formation of nanohybrid particles with unbound TTC and alkyne groups on their surfaces. These available functional groups could be used for the attachment of citrate-capped AuNPs, resulting in crosslinked AuNP nanoassemblies. In a subsequent study [111] by the same authors, it was shown that the structure of these nanoassemblies varies with the macromolecular architecture of the HBP: With low numbers of branches (and consequently a low number of anchoring sites for gold), the nanoassemblies showed a plate-like morphology, whereas for a higher number of branches, globular assemblies with densely packed AuNPs were found. Because the approach introduced in these studies allows the attachment of further particles to a scaffold of nanohybrid particles, it could also allow the attachment of particles of a different type to this scaffold architecture, leading to hierarchical multicomponent nanostructures. Such nanostructures can be realized using this approach by treating larger (48 nm) citrate-stabilized AuNPs with HBP to create nanohybrids acting as the scaffold, and then adding smaller (15 nm) citrate-capped AuNPs after purification of the initial nanohybrids [112]. The approach resulted in the formation of planet–satellite nanostructures; varying the stoichiometric ratio of the two types of inorganic particles employed could control the average number of satellite particles in these arrangements.

Another key parameter of such multicomponent particle architectures is the average interparticle distance. This parameter can be tightly controlled if RAFT star polymers with TTC groups on their exterior are used to interconnect two different types of AuNPs, as shown by Rossner and Vana [113]. In this study, particles from citrate reduction (14 nm) were treated with four-arm star polymers of N^{i}PAAM of varying molecular weight to form nanohybrid scaffold architectures. It was shown by TEM analysis that the thickness of the coating polymer shell increased strictly with increasing star polymer molecular weight. The purified star polymer nanocomposites could then be treated with AuNPs from the two-phase Brust–Schiffrin method to obtain planet–satellite arrangements with set planet–satellite distances (Fig. 10).

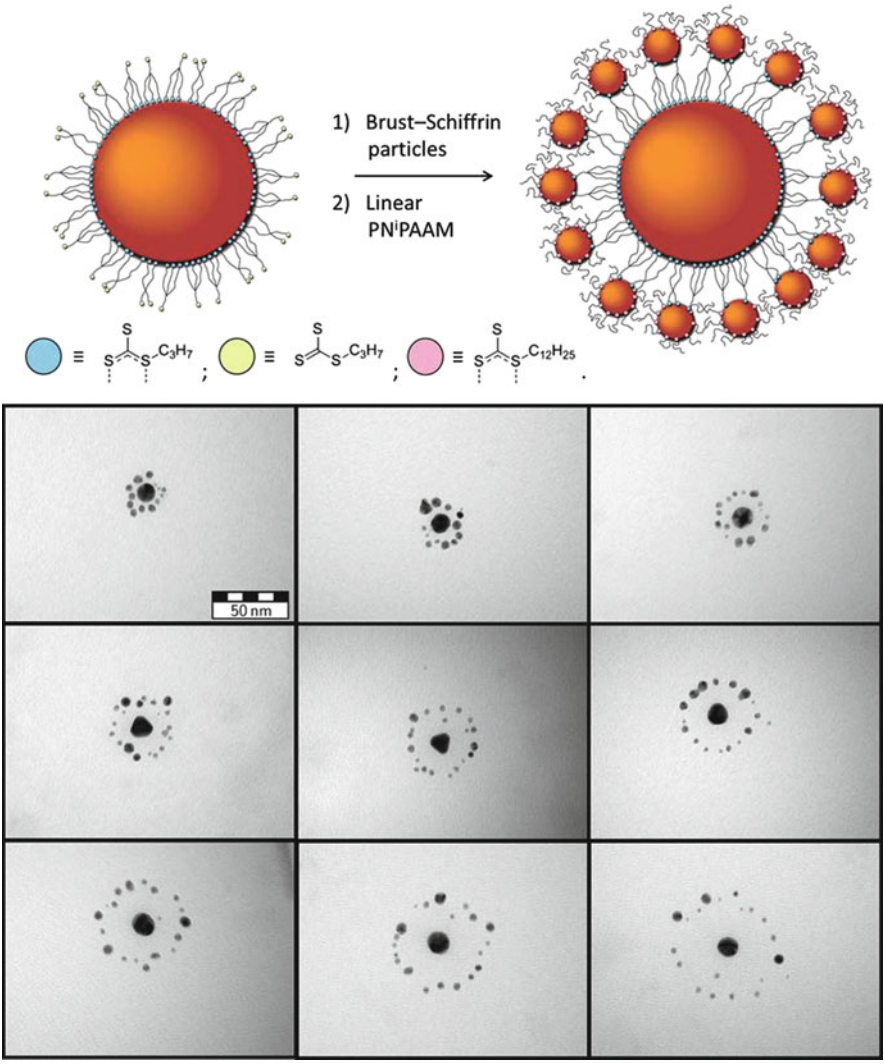

Fig. 10 *Top*: Synthetic scheme for the fabrication of planet–satellite nanostructures with star polymers acting as particle linkers, and linear polymers to provide colloidal stability. *Bottom*: TEM images of planet–satellite nanostructures. The average molecular weight of the linking star polymers increases from *left* to *right* and from *top* to *bottom*. Adapted with permission from [113]. Copyright 2014 Wiley-VCH Verlag GmbH & Co. KGaA, Weinheim

8 Conclusion

As indicated by the title of the chapter, we have restricted ourselves to a discussion of polymeric systems realized via controlled radical polymerization. There is a plethora of articles closely related to the research presented in this chapter; however, different techniques were employed to produce the polymers used for these studies. In order to stick with the idea of this chapter, we have not discussed such papers. One example that illustrates this point is work from Shenhar, Müller, and coworkers [114, 115]. These authors used anionic polymerization to prepare phase-separating block copolymers of PS and PMMA for incorporation of NPs into thin films. They employed interparticle interactions intentionally to achieve even more control of particle structuring in block copolymer thin films than in the examples given in Sect. 3: When NPs are used that interact unfavorably with both block copolymer domains, but less unfavorably with one domain, the NPs are incorporated into this domain but still have a tendency to separate, leading to hexagonally close-packed assemblies of NPs inside a specific host domain. It can be shown that the average distance between particles in these hexagonal arrangements can be controlled by tuning the length of the ligand attached to the NPs, a principle which we know from the discussion in Sect. 1.

We have seen in Sect. 1 that nanocomposites with distinct functional groups repeatedly presented on the surface can be used for specific interactions, which can lead to applications such as targeting of carcinoma cells. The length of the surface-bound polymer can be used to encode interparticle spacing in two- and three-dimensional assemblies, with possible applications in material science. Also, the scaling of interparticle distance with the molar mass of surface-anchored polymer contains information about the conformational state of the polymer at the surface. The set of parameters, which determines the architecture of polymers in nanocomposites, can be drastically expanded when two types of linear homopolymers are used instead of one (Sect. 2). In such situations, phase separation phenomena can be observed on the surfaces of colloidal particles, and we have seen how this phase separation can be modulated by the design of the employed macromolecules. The tendency of two different polymers to separate can also be exploited by covalently linking two immiscible homopolymers (i.e., by preparing diblock copolymers, as described in Sect. 3). By carefully adjusting its architecture, this type of polymer can be used to precisely control the location of inorganic NPs in a molten or solution state. Related to this is the case of triblock polymers presented in Sect. 4, whereby additional functionality can be imparted to the macromolecules through introduction of the third block. By further increasing the block number (i.e., creating multifunctional polymers, as discussed in Sect. 5), it is possible to encode polymer loops at surfaces and also to achieve NP crosslinking. The branched polymeric architectures presented in Sect. 6 can also be considered as multifunctional polymers, but with a different topology from linear multiblock polymers. It was shown that it is possible to accurately tune the distances between

two different types of NPs by adjusting the size of the branched polymeric linker through controlled radical polymerization.

The work done during the last decade and reflected in the literature summarized in this review therefore suggests that specifically designed macromolecules contain information that can be translated to the structure of nanohybrids and self-assembled structures. The encoding of this information with macromolecules becomes possible through macromolecular design by means of controlled radical polymerization. Thus, macromolecular design via controlled radical polymerization can be considered as a versatile programming language [116, 117] to guide nanocomposite formation and assembly.

The huge variety of defined nanostructures and materials that can be fabricated via controlled radical polymerization techniques will probably find applications in a wide field of different research directions. The possibility of combining several building units in one device will enable materials scientists to implement multiple levels of stimuli-responsiveness for the construction of smart materials. Research in biomedicine can be expected to benefit from the ability to generate defined nanopatterned surfaces that can play a central role in biophysical investigations. Also, the potential to create precisely defined confined environments could lead to nanocontainers as delivery vehicles, theranostic agents, or artificial enzymes.

References

1. Velev OD, Gupta S (2009) Adv Mater 21:1897–1905
2. Li D, Jones GL, Dunlap JR, Hua F, Zhao B (2006) Langmuir 22:3344–3351
3. Takara M, Toyoshima M, Seto H, Hoshino Y, Miura Y (2014) Polym Chem 5:931–939
4. Richards S-J, Gibson MI (2014) ACS Macro Lett 3:1004–1008
5. Lowe AB, Sumerlin BS, Donovan MS, McCormick CL (2002) J Am Chem Soc 124:11562–11563
6. Garcia MA (2011) J Phys D Appl Phys 44:283001
7. Duwez A-S, Guillet P, Colard C, Gohy J-F, Fustin C-A (2006) Macromolecules 39:2729–2731
8. Blakey I, Schiller TL, Merican Z, Fredericks PM (2010) Langmuir 26:692–701
9. Slavin S, Soeriyadi AH, Voorhaar L, Whittaker MR, Becer CR, Boyer C, Davis TP, Haddleton DM (2012) Soft Matter 8:118–128
10. Ulman A (1996) Chem Rev 96:1533–1554
11. Pujari SP, Scheres L, Marcelis ATM, Zuilhof H (2014) Angew Chem Int Ed 53:6322–6356
12. Huebner D, Koch V, Ebeling B, Mechau J, Steinhoff JE, Vana P (2015) J Polym Sci Part A Polym Chem 53:103–113
13. Gibson MI, Danial M, Klok H-A (2011) ACS Comb Sci 13:286–297
14. Freese C, Gibson MI, Klok H-A, Unger RE, Kirkpatrick CJ (2012) Biomacromoleules 13:1533–1543
15. Blakey I, Merican Z, Thurecht KJ (2013) Langmuir 29:8266–8274
16. Fasting C, Schalley CA, Weber M, Seitz O, Hecht S, Koksch B, Dernedde J, Graf C, Knapp E-W, Haag R (2012) Angew Chem Int Ed 51:10472–10498
17. Álvarez-Paino M, Bordegé V, Cuervo-Rodríguez R, Muñoz-Bonilla A, Fernández-García M (2014) Macromol Chem Phys 215:1915–1924
18. Housni A, Cai H, Liu S, Pun SH, Narain R (2007) Langmuir 23:5056–5061

19. Toyoshima M, Miura Y (2009) J Polym Sci Part A Polym Chem 47:1412–1421
20. Spain SG, Albertin L, Cameron NR (2006) Chem Commun 2006(40):4198–4200
21. Lu J, Zhang W, Richards S-J, Gibson MI, Chen G (2014) Polym Chem 5:2326–2332
22. Li X, Bao M, Weng Y, Yang K, Zhang W, Chen G (2014) J Mater Chem B 2:5569–5575
23. Li J, Han C, Wu W, Zhang S, Guo J, Zhou H (2014) New J Chem 38:717–722
24. Celiz AD, Lee T-C, Scherman OA (2009) Adv Mater 21:3937–3940
25. Ohno K, Koh K, Tsujii Y, Fukuda T (2003) Angew Chem Int Ed 42:2751–2754
26. Ohno K, Morinaga T, Koh K, Tsujii Y, Fukuda T (2005) Macromolecules 38:2137–2142
27. Boyer C, Whittaker MR, Luzon M, Davis TP (2009) Macromolecules 42:6917–6926
28. Ohno K, Morinaga T, Takeno S, Tsujii Y, Fukuda T (2007) Macromolecules 40:9143–9150
29. Morinaga T, Ohno K, Tsujii Y, Fukuda T (2008) Macromolecules 41:3620–3626
30. Ohno K, Akashi T, Huang Y, Tsujii Y (2010) Macromolecules 43:8805–8812
31. Ohno K, Morinaga T, Takeno S, Tsujii Y, Fukuda T (2006) Macromolecules 39:1245–1249
32. Daoud M, Cotton JP (1982) J Phys (Paris) 43:531–538
33. Dukes D, Li Y, Lewis S, Benicewicz B, Schadler L, Kumar SK (2010) Macromolecules 43:1564–1570
34. Choi J, Dong H, Matyjaszewski K, Bockstaller MR (2010) J Am Chem Soc 132:12537–12539
35. Choi J, Hui CM, Pietrasik J, Dong H, Matyjaszewski K, Bockstaller MR (2012) Soft Matter 8:4072–4082
36. Choi J, Hui CM, Schmitt M, Pietrasik J, Margel S, Matyjazsewski K, Bockstaller MR (2013) Langmuir 29:6452–6459
37. Rungta A, Natarajan B, Neely T, Dukes D, Schadler LS, Benicewicz BC (2012) Macromolecules 45:9303–9311
38. Akcora P, Liu H, Kumar SK, Moll J, Li Y, Benicewicz BC, Schadler LS, Acehan D, Panagiotopoulos AZ, Pryamitsyn V, Ganesan V, Ilavsky J, Thiyagarajan P, Colby RH, Douglas JF (2009) Nat Mater 8:354–359
39. Goel V, Pietrasik J, Dong H, Sharma J, Matyjaszewski K, Krishnamoorti R (2011) Macromolecules 44:8129–8135
40. Yockell-Lelièvre H, Gingras D, Vallée R, Ritcey AM (2009) J Phys Chem C 113:21293–21302
41. Karg M, Hellweg T, Mulvaney P (2011) Adv Funct Mater 21:4668–4676
42. Ohno K, Ma Y, Huang Y, Mori C, Yahata Y, Tsujii Y, Maschmeyer T, Moraes J, Perrier S (2011) Macromolecules 44:8944–8953
43. Moraes J, Ohno K, Gody G, Maschmeyer T, Perrier S (2013) Beilstein J Org Chem 9:1226–1234
44. Ebeling B, Vana P (2013) Macromolecules 46:4862–4871
45. Yockell-Lelièvre H, Desbiens J, Ritcey AM (2007) Langmuir 23:2843–2850
46. Wang Y, Yang G, Tang P, Qiu F, Yang Y, Zhu L (2011) J Chem Phys 134:134903
47. Wang J, Müller M (2009) J Phys Chem B 113:11384–11402
48. Jiang X, Zhong G, Horton JM, Jin N, Zhu L, Zhao B (2010) Macromolecules 43:5387–5395
49. Wang Z-L, Xu J-T, Du B-Y, Fan Z-Q (2011) J Colloid Interface Sci 360:350–354
50. Kotsuchibashi Y, Ebara M, Aoyagi T, Narain R (2012) Polym Chem 3:2545–2550
51. Li D, Sheng X, Zhao B (2005) J Am Chem Soc 127:6248–6256
52. Zhu L, Zhao B (2008) J Phys Chem B 112:11529–11536
53. Zhao B, Zhu L (2006) J Am Chem Soc 128:4574–4575
54. Bao C, Tang S, Wright RAE, Tang P, Qiu F, Zhu L, Zhao B (2014) Macromolecules 47:6824–6835
55. Bao C, Tang S, Horton JM, Jiang X, Tang P, Qiu F, Zhu L, Zhao B (2012) Macromolecules 45:8027–8036
56. Horton JM, Tang S, Bao C, Tang P, Qiu F, Zhu L, Zhao B (2012) ACS Macro Lett 1:1061–1065

57. Tang S, Lo T-Y, Horton JM, Bao C, Tang P, Qiu F, Ho R-M, Zhao B, Zhu L (2013) Macromolecules 46:6575–6584
58. Santer S, Kopyshev A, Donges J, Rühe J, Jiang X, Zhao B, Müller M (2007) Langmuir 23:279–285
59. Shan J, Nuopponen M, Jiang H, Viitala T, Kauppinen E, Kontturi K, Tenhu H (2005) Macromolecules 38:2918–2926
60. Ionov L, Minko S (2012) ACS Appl Mater Interfaces 4:483–489
61. Cheng L, Song J, Yin J, Duan H (2011) J Phys Chem Lett 2:2258–2262
62. Song J, Cheng L, Liu A, Yin J, Kuang M, Duan H (2011) J Am Chem Soc 133:10760–10763
63. Song J, Zhou J, Duan H (2012) J Am Chem Soc 134:13458–13469
64. Song J, Pu L, Zhou J, Duan B, Duan H (2013) ACS Nano 7:9947–9960
65. Basuki JS, Duong HTT, Macmillan A, Whan R, Boyer C, Davis TP (2013) Macromolecules 46:7043–7054
66. Yuan J-J, Schmid A, Armes SP, Lewis AL (2006) Langmuir 22:11022–11027
67. Song J, Duan B, Wang C, Zhou J, Pu L, Fang Z, Wang P, Lim TT, Duan H (2014) J Am Chem Soc 136:6838–6841
68. Marcelo G, Martinho JMG, Farinha JPS (2013) J Phys Chem B 117:3416–3427
69. Kang Y, Taton TA (2005) Angew Chem Int Ed 44:409–412
70. Chen HY, Abraham S, Mendenhall J, Delamarre SC, Smith K, Kim I, Batt CA (2008) ChemPhysChem 9:388–392
71. Kang Y, Taton TA (2005) Macromolecules 38:6115–6121
72. Kim B-S, Qiu J-M, Wang J-P, Taton TA (2005) Nano Lett 5:1987–1991
73. Li Y, Smith AE, Lokitz BS, McCormick CL (2007) Macromolecules 40:8524–8526
74. Smith AE, Xu X, Abell TU, Kirkland SE, Hensarling RM, McCormick CL (2009) Macromolecules 42:2958–2964
75. Hickey RJ, Haynes AS, Kikkawa JM, Park S-J (2011) J Am Chem Soc 133:1517–1525
76. Kamps AC, Sanchez-Gaytan BL, Hickey RJ, Clarke N, Fryd M, Park S-J (2010) Langmuir 26:14345–14350
77. Sanchez-Gaytan BL, Cui W, Kim Y, Mendez-Polanco MA, Duncan TV, Fryd M, Wayland BB, Park S-J (2007) Angew Chem Int Ed 46:9235–9238
78. Luo Q, Hickey RJ, Park S-J (2013) ACS Macro Lett 2:107–111
79. Liu Y, Li Y, He J, Duelge KJ, Lu Z, Nie Z (2014) J Am Chem Soc 136:2602–2610
80. Mai Y, Eisenberg A (2012) Chem Soc Rev 41:5969–5985
81. Matsen MW, Thompson RB (2008) Macromolecules 41:1853–1860
82. Chiu JJ, Kim BJ, Yi G-R, Bang J, Kramer EJ, Pine DJ (2007) Macromolecules 40:3361–3365
83. Yoo M, Kim S, Jang SG, Choi S-H, Yang H, Kramer EJ, Lee WB, Kim BJ, Bang J (2011) Macromolecules 44:9356–9365
84. Chiu JJ, Kim BJ, Kramer EJ, Pine DJ (2005) J Am Chem Soc 127:5036–5037
85. Li Q, He J, Glogowski E, Li X, Wang J, Emrick T, Russell TP (2008) Adv Mater 20:1462–1466
86. Lin Y, Böker A, He J, Sill K, Xiang H, Abetz C, Li X, Wang J, Emrick T, Long S, Wang Q, Balazs A, Russell TP (2005) Nature 434:55–59
87. He J, Tangirala R, Emrick T, Russell TP, Böker A, Li X, Wang J (2007) Adv Mater 19:381–385
88. Son JG, Bae WK, Kang H, Nealey PF, Char K (2009) ACS Nano 3:3927–3934
89. Tietz K, Finkhäuser S, Samwer K, Vana P (2014) Macromol Chem Phys 215:1563–1572
90. Xu C, Ohno K, Ladmiral V, Milkie DE, Kikkawa JM, Composto RJ (2009) Macromolecules 42:1219–1228
91. Kim BJ, Fredrickson GH, Hawker CJ, Kramer EJ (2007) Langmuir 23:7804–7809
92. Karagoz B, Yeow J, Esser L, Prakash SM, Kuchel RP, Davis TP, Boyer C (2014) Langmuir 30:10493–10502
93. Bleach R, Karagoz B, Prakash SM, Davis TP, Boyer C (2014) ACS Macro Lett 3:591–596
94. Duxin N, Liu F, Vali H, Eisenberg A (2005) J Am Chem Soc 127:10063–10069

95. Niu H, Zhang L, Gao M, Chen Y (2005) Langmuir 21:4205–4210
96. Azzam T, Bronstein L, Eisenberg A (2008) Langmuir 24:6521–6529
97. Krüger C, Agarwal S, Greiner A (2008) J Am Chem Soc 130:2710–2711
98. Hu J, Wu T, Zhang G, Liu S (2012) J Am Chem Soc 134:7624–7627
99. Hu B, Henn DM, Wright RAE, Zhao B (2014) Langmuir 30:11212–11224
100. Ebeling B, Vana P (2011) Polymers (Basel) 3:719–739
101. You Y-Z, Hong C-Y, Pan C-Y (2002) Chem Commun 2002(23):2800–280.1
102. Hong J, Wang Q, Fan Z (2006) Macromol Rapid Commun 27:57–62
103. Ebeling B, Eggers M, Vana P (2010) Macromolecules 43:10283–10290
104. Rossner C, Ebeling B, Vana P (2015) Design strategies for the fabrication of tailored nanocomposites via RAFT polymerization. In: Matyjaszewski K (ed) ACS symposium series. American Chemical Society, Washington, DC
105. Du B, Chen X, Zhao B, Mei A, Wang Q, Xu J, Fan Z (2010) Nanoscale 2:1684–1689
106. Hussain I, Wang Z, Cooper AI, Brust M (2006) Langmuir 22:2938–2941
107. Maye MM, Lim I-IS, Luo J, Rab Z, Rabinovich D, Liu T, Zhong C-J (2005) J Am Chem Soc 127:1519–1529
108. Rossner C, Ebeling B, Vana P (2013) ACS Macro Lett 2:1073–1076
109. Mori H, Seng DC, Zhang M, Müller AHE (2002) Langmuir 18:3682–3693
110. Dey P, Blakey I, Thurecht KJ, Fredericks PM (2013) Langmuir 29:525–533
111. Dey P, Blakey I, Thurecht KJ, Fredericks PM (2014) Langmuir 30:2249–2258
112. Dey P, Zhu S, Thurecht KJ, Fredericks PM, Blakey I (2014) J Mater Chem B 2:2827–2837
113. Rossner C, Vana P (2014) Angew Chem Int Ed 53:12639–12642
114. Ploshnik E, Langner KM, Halevi A, Ben-Lulu M, Müller AHE, Fraaije JGEM, Sevink GJA, Shenhar R (2013) Adv Funct Mater 23:4215–4226
115. Halevi A, Halivni S, Oded M, Müller AHE, Banin U, Shenhar R (2014) Macromolecules 47:3022–3032
116. Jiang W, Schalley CA (2009) Proc Natl Acad Sci USA 106:10425–10429
117. Jiang W, Schäfer A, Mohr PC, Schalley CA (2010) J Am Chem Soc 132:2309–2320

Index